AN ABSTRACT OF THE THESIS OF

Tobias Stefan Siller for the degree of Master of Science in Wood Science presented on April 12, 2002.

Title: EVALUATION OF THE TORSION TEST AS A METHOD TO DETERMINE THE SHEAR STRENGTH OF STRUCTURAL COMPOSITE LUMBER.

Redacted for Privacy

Abstract approved: _____
Rakesh Gupta

Torsion test was evaluated as a method to determine the shear strength parallel to grain of full-size structural composite lumber (SCL). Experimental results of eighty-five rectangular (44 x 140 mm^2) specimens were verified by finite element analysis. Laminated strand lumber (LSL), laminated veneer lumber (LVL) and parallel strand lumber (PSL) were tested using torsion. For comparison, ASTM shear block tests were performed in joist (LR-plane) as well as in plank (LT-plane) orientation with a shear plane of 2600 mm^2.

In torsion, a different failure behavior was observed for the three wood composites. LSL failed abruptly, in a brittle manner, on the center of the short side along the strands (LT-plane). LVL and PSL, on the contrary, failed gradually, in a more ductile manner, mostly on the center of the long side across the strands or veneers (LR-plane). LVL and especially PSL displayed a distinct decrease in torsional rigidity with increasing torque, while LSL showed a more linear torque-twist relationship. LSL was able to bear a much higher torque than LVL and PSL. Checks, like lathe checks (rotary peeling), internal checks (drying),

or not properly glued veneer or strand interfaces, as well as void areas, possibly decrease the shear resistance of LVL and PSL.

Due to the different failure behavior of the wood composites, orthotropic theory was applied to evaluate shear stresses in torsion. The ratio of shear moduli in the two longitudinal planes (G_{LT} and G_{LR}) had a significant influence on the orthotropic shear stresses. The following mean shear stresses were defined as shear strength in torsion, depending on the failure plane: LSL in plank orientation τ_{LR} = 6.43 MPa; LVL in joist orientation τ_{LT} = 7.96 MPa; PSL in joist orientation τ_{LT} = 6.82 MPa. The shear strength of LSL in joist orientation could not be determined, since the shear plane coincided for all specimens with the LT-plane. However, it must definitely be higher than the concomitant shear stress of τ_{LT} = 12.7 MPa.

Shear strength of SCL was found to be much higher in joist orientation, where failure occurs across the veneers or strands, compared to plank orientation ($\tau_{TL} > \tau_{RL}$), for both test methods, torsion and ASTM block. ASTM shear blocks of joist oriented LSL failed rather in compression parallel to grain (crushing), or a combined failure mode of crushing and shear, than in pure shear. In joist orientation, LSL has much higher shear strength (τ_{TL}) than LVL and PSL, while in plank orientation all three composites show similar shear strengths (τ_{RL}). In torsion, LVL showed a slightly higher shear strength than PSL, whereas the ASTM block test indicated the reverse. Shear strength of SCL based on torsion is much lower than shear strength based on shear block ($\tau_T/\tau_{ASTM} < 1$), as opposed to what has been observed earlier for solid-sawn lumber (SSL).

Shear strength based on tests of small ASTM shear blocks is not representative of the shear strength of full-size specimens. Torsion test is recommended as standard test method to determine the pure shear strength of full-size SCL, since it is the only test method that imposes a state of pure shear stress on the specimen. This will complement the way other stresses are determined, i.e., pure tensile, compressive and bending strength.

EVALUATION OF THE TORSION TEST AS A METHOD TO DETERMINE THE SHEAR STRENGTH OF STRUCTURAL COMPOSITE LUMBER

by

Tobias Stefan Siller

A THESIS

submitted to

Oregon State University

in partial fulfillment of
the requirements for the
degree of

Master of Science

Presented April 12, 2002
Commencement June, 2002

Master of Science thesis of Tobias Stefan Siller presented on April 12, 2002.

APPROVED:

Redacted for Privacy 19 April 2002

Major Professor, representing Wood Science

Redacted for Privacy 19 April 2002

Head of the Department of Wood Science and Engineering

Redacted for Privacy

Dean of the Graduate School

I understand that my thesis will become part of the permanent collection of Oregon State University libraries. My signature below authorizes release of my thesis to any reader upon request.

Redacted for Privacy

Tobias Stefan Siller, Author

ACKNOWLEDGEMENT

The author would like to thank Trus Joist – A Weyerhaeuser Company for providing the test material for this study; especially, Bruce Craig, who shared his knowledge and experience on the proprietary and newly designed wood composites with me.

In addition, the author would like to express his gratefulness to the department of Wood Science and Engineering at Oregon State University for providing the funding for this project.

Also, I am very grateful to my committee members for their guidance and support during the project. The innumerable contributions and advice of my major advisor, Dr. Gupta, as well as Dr. Leichti and Dr. Kennedy, are hereby acknowledged.

Further thanks go to:

... Milo Clauson for his support during the experimental testing.

... Rand Sether for an incredible accurateness in preparing the shear block samples.

... Dr. Blass from the University of Karlsruhe (TH) for his support and agreement to this research project.

... my family for their emotional and financial support.

TABLE OF CONTENTS

TABLE OF CONTENTS (Continued)

LIST OF FIGURES

Figure Page

LIST OF TABLES

Table Page

LIST OF TABLES (Continued)

Table | Page

EVALUATION OF THE TORSION TEST AS A METHOD TO DETERMINE THE SHEAR STRENGTH OF STRUCTURAL COMPOSITE LUMBER

1. Introduction

1.1 Background

Wood is one of the oldest building materials, because it has been easily available for centuries. Its natural origin is reflected in a complex anisotropic structure. But for practical reasons it is considered orthotropic with different properties in three mutually perpendicular planes. Wood is inhomogeneous due to discontinuities like knots, but it is still considered homogeneous in practical applications. Still, wood presents a challenge for any engineer when designing. Wood is, according to Bodig and Jayne (1982), the most highly orthotropic material known to man due to its very high ratio of longitudinal to tangential modulus of elasticity (E_L/E_T) of about 24. Wood is renewable, sustainable and known as light, but strong material. The strength to weight ratio of wood – based on axial tension – is about equal to the one of steel and superior to other construction materials (Tsoumis 1991), especially concrete.

The challenge that manufacturers of wood products are facing recently is an increasing demand for high quality timber while the supply of structural lumber is decreasing in quality and size. Engineered wood products (EWP) are destined to supplement solid-sawn lumber (SSL) to help overcome the shortage and reduce the immense costs, especially of high quality lumber in bigger sizes. Structural composite lumber (SCL) is a generic name for a subdivision of the

EWP family. SCL includes materials like laminated veneer lumber (LVL), parallel strand lumber (PSL) and laminated strand lumber (LSL). SCL is composed of either wood veneers or strands that are mainly oriented longitudinally, dried to a low moisture content, and bonded by an exterior, structural resin, i.e., a waterproof and heatproof, thermosetting adhesive. As a result of the manufacturing process, defects are either eliminated or at least dispersed. SCL is more homogeneous than SSL and shows less variability in measured properties, resulting in higher design values. Furthermore, SCL is resource efficient, because it offers a higher volume recovery of the individual log. SCL can be manufactured from fast growing, low density, small diameter trees. The major advantage of SCL is availability of relatively large sizes in combination with high strength, uniformity and straightness. Certain mechanical properties like strength, or stiffness can be enhanced during design mainly by strand or veneer orientation and densification, depending on the intended end use. In general, allowable stresses are highest for SCL, followed by glued-laminated timber and solid-sawn lumber. Typical structural applications of SCL are headers, beams, columns, posts, and scaffold planks. Also, rim boards specifically for LSL and I-joist flanges made of LVL.

Mechanical properties of wood used to be determined by tests on small, clear, straight-grained specimens. The advent of reliability based design philosophy was one major factor that caused a shift from testing small specimens to structural-size members. Since 1991, the tabulated values in the National Design Specification® for Wood Construction (NDS) for bending, compressive and tensile strengths, all parallel to the grain, are based on tests of full-size members. On the other hand, the design values for strength in compression perpendicular to the grain and shear are still based on tests of small, clear specimens. The current standard method of testing small, clear timber, ASTM D 143, does not define the orientation of the shear plane for SSL. In contrast, ASTM D 5456 for the evaluation of SCL requires two separate test series to induce shear failure in the LX-plane (LT) and LY-plane (LR). Note the different

orientations between the standard, where x refers to the tangential direction and y to the radial direction, and the current study, where x indicates the radial direction and y the tangential direction. Besides, the small shear block test, there are two common test methods to induce shear failure in full-size members, bending tests on short, deep beams or torsion tests on any size beams. Currently, the NDS does not apply a size factor on design values of shear strength. But, research has indicated that shear strength of wood products decreases with increasing member size in bending (Rammer et al. 1994 and 1996) as well as in torsion (Möhler and Hemmer 1977).

Shear strength (τ) of wood is defined as the maximum load per unit shear area and is, according to the *Wood Handbook* (1999), a measure of its ability to resist internal slipping of one plane relative to another along the grain. It is one of the mechanical properties and especially of interest for the design of short, deep beams of materials with relatively low shear strength (τ) compared to bending strength (σ), i.e., low τ/σ ratios. SCL (7 – 12 %) is therefore more susceptible to shear failure than glulams (13 – 23 %) and SSL (20 – 30 %) are, since the design of the engineered wood products is focused on the optimization of bending strength and not shear strength. The τ/σ ratios given in brackets are derived from chapter 2. Transverse shear strength of wood is about three to four times greater than longitudinal shear strength (Kollmann 1951). For this reason, transverse shear strength is of no practical importance, since wood will fail first in another mode. Kollmann (1951) reported that shear strength of pine was lowest and showed highest variation, if the shear plane coincided with the LT-plane, higher in the LR plane, and highest at an angle of about 45 degrees to the annual rings ($\tau_{LR} < \tau_{LT} < \tau_{45}$). Ylinen (1963) reported that for Finnish pine (*Pinus silvestris*) shear strength obtained via cube, ASTM block, torsion and tension test is lower, if the failure plane coincides with the LT-plane than with the LR-plane ($\tau_{LR} < \tau_{LT}$). According to Tsoumis (1991), shear strength of clear wood is comparatively very low and counts for only 6 – 10 % of the axial tensile strength. Typical values for

longitudinal shear strength, or shear strength parallel to grain, from here on referred to just as shear strength, range from 5 to 20 MPa (725 – 2,900 psi) for various wood species (Tsoumis 1991), based on small, clear samples.

In comparison, the bending strength, usually expressed as modulus of rupture (MOR), is much higher and varies between 55 and 160 MPa (8,000 – 23,200 psi), which is similar to the strength in axial tension for European and tropical species (Tsoumis 1991). Wangaard (1979) on the other hand, reported of higher tensile strength (100 – 120 MPa) compared to bending strength (75 MPa), whereas compressive strength (50 MPa) and shear strength (10 MPa) – all parallel to grain – are lower for moderately strong, clear North American softwoods. Shear strength of wood is proportional to density and the influence of moisture content (MC) on shear strength is less pronounced (Kollmann 1951) than it is on tensile or compressive strength. Moreover, it seems like strengths in shear and tension are much more sensitive to the orthotropic structure of wood than is compression.

The shear modulus (G), or modulus of rigidity, is a material constant, expressing the relation between shear stress and shear strain. It indicates the resistance to shear deformation. The softer a material, the smaller its shear modulus. To depict shear modulus, it can be defined as a shear stress that causes a unit shear strain of one radian or 57.3 degrees (Bodig and Jayne 1982). Although, this definition violates the restraint to small strains and most materials will fail long before reaching such a large distortion. Isotropic materials usually show a shear modulus of approximately 60 % of the modulus of elasticity (E/G = 1.67), while solid wood has an E/G ratio of 14 (Bodig and Jayne 1982). The E/G ratio is generally smaller for hardwoods compared to softwoods. Orthotropic materials like wood possess three shear moduli (G_{LR}, G_{LT}, G_{RT}), where the subscripts denote the plane of deformation. For instance, G_{LR} is the shear modulus based on shear strains in the LR plane, resulting from shear stresses τ_{LR} and τ_{RL} in the RT and LT planes. Considering shear stresses, the first subscript indicates the direction normal to the plane on which the stress acts.

The second subscript designates the direction of the stress component. As a consequence of this definition, shear failure in the LT plane is caused by shear stress τ_{LR}. For both, shear moduli and shear stresses, the subscripts may be interchanged (e.g., $G_{LR} = G_{RL}$ and $\tau_{LR} = \tau_{RL}$).

The torsional modulus (G_T) is different from any shear modulus (G) for orthotropic materials, like wood. In the case of torsion parallel to grain, the torsional modulus depends on the shear moduli G_{LT} and G_{LR} in the two longitudinal planes. These two shear moduli are within a narrow range for some wood species, resembling isotropic behavior. Ylinen (1963) reported that only for very few species of wood the ratio $g = G_{LT}/G_{LR}$ is about equal to unity, like, Douglas-fir, spruce, Sitka spruce, yellow-poplar, yellow birch, and maple. Other wood species and especially SCL might yet offer a higher degree of orthotropicity. The complexity concerning shear moduli is quite evident regarding Douglas-fir. A higher shear modulus is obtained in the LT plane from the elastic constant ratios given in the *Wood Handbook* (1999), whereas (Kollmann 1951) and Bodig and Jayne (1982) report a higher shear modulus in the LR plane.

Torsional strength (τ_T) is a measure of the resistance to rotation about a longitudinal axis and may be taken as shear strength parallel to grain for solid wood members (*Wood Handbook* 1999). The torsion test is the one and only test method that induces a state of pure shear stresses, whereas other tests have a combination of stresses. Stress concentrations and material inhomogeneity, especially internal checks are further factors that cause a complex state of stress and mask a clear picture of the shear phenomenon (Kollmann 1951). Shear strength obtained via bending or block tests is not representative of shear strength of wood and always remarkably lower than shear strength based on torsion tests (Kollmann 1951). The *Wood Handbook* (1999) suggests that two-thirds of the value for torsional shear strength may be used as an estimate of the torsional shear stress at the proportional limit. Shear modulus, torsional stress at proportional limit and torsional strength depend on MC (Trayer and March 1930) in a manner similar to other static mechanical properties. Torsional

strength and torsional modulus increase with increasing density (Möhler and Hemmer 1977). The same authors reported a size effect in torsion. Torsional strength (τ_T) and torsional modulus (G_T) increase with increasing aspect, or side (h/b) ratio for glulams and clear wood, while the effect of aspect ratio was less pronounced, or covered by wood texture, for SSL containing defects. Heck (1997) found no size effect in solid-sawn Douglas-fir. Aicher (1990) reported a distinct size or volume effect in vertically laminated glulams. Torsional shear strength and modulus decreased with increasing size and increasing number of sawn-up edge joints in the outer laminations. Torsion is present in every unsymmetric connection, for instance if purlins are jointed one-sided to rafters by means of purlin hangers. Furthermore, torsional rigidity might influence the design of structures considering lateral stability and the spacing of bracings.

1.2 Objectives

The objectives of the current study are:

- to evaluate the torsion test as a method to determine the shear strength of structural composite lumber (SCL).
- to perform a finite element analysis to enhance the understanding of the shear stress distribution within the torsion specimens.
- to compare shear strength obtained by torsion tests with shear strength obtained by ASTM shear block tests that were performed in two different setups.

2. Literature Review

This literature review was focused on shear strength of solid-sawn lumber (SSL) and structural composite lumber (SCL). The historical development of the evaluation of the shear strength of lumber was very well described by Ethington et al. (1979). The shear research conducted at Oregon State University was performed by Riyanto (1996) and Heck (1997). The interested reader is invited to consult these references for further information. Riyanto also visualized the different test setups referred to in this chapter.

2.1 Solid-Sawn Lumber (SSL)

Leicester and Breitinger (1992) investigated the in-service beam shear strength of softwood timber with a high shear/bending strength ratio (τ/σ). Three different bending test configurations were used. Three-point, five-point, and cantilever tests using a span/depth (L/d) ratio of 6 were performed. A relatively knotty Radiata pine machine stress-graded building grade (F5) was loaded in edgewise bending as a joist. An overhang of one times the specimen depth was applied. Failure occurred after $3-5$ minutes. About $30-40$ % of the 35×90 mm^2 specimens failed in shear and a uniform spread of the strength distribution was perceived. However, the authors remarked that the measured shear stresses at failure represent the lower tail of the true shear strength, since roughly two thirds of the samples failed in a bending mode. The mean shear stresses at failure [MPa] with the corresponding coefficients of variation [%] in brackets were the following: center-point 8.3 (20), cantilever 7.3 (28) and five-point 6.7 (31). A L/d ratio of 3 was applied for the three-point setup since the

percentage of shear failure and the shear stress at failure decreased drastically with increasing L/d. For example, the proportion of shear failure decreased from 42 to 12 [%] and the mean shear stress at failure from 8.3 to 5.2 [MPa] when the span was increased from 3d to 6d. The authors concluded that for a given L/d ratio the five-point test provided the critical simulation of an in-service loading configuration, because it yielded about twice the τ/σ ratio of the three-point test. Consequently, the probability of shear failure is higher for the five-point test.

Breitinger et al. (1994) published a follow up study on five Australian wood species. Three more pine species were tested in five-point bending, whereas Mountain ash was tested in three-point loading, since the hardwood was believed to be relatively weak in shear. Only 10 % of the latter failed in shear. However, the authors commented that, "even if all failures occur in a bending mode, the nominal shear stress at failure will be a useful lower bound since no higher shear stress/bending moment ratio can occur in practice". An intensive in-grade study including about 9000 Radiata pine test specimens of different size and grade showed a distinct size effect on shear strength. The characteristic (5^{th}-percentile) shear strength was found to be 20 to 30 % of the characteristic bending strength and roughly half the specimens failed in shear.

Asselin (1995) evaluated the five-point bending test to determine the shear strength of solid-sawn beams of Engelmann spruce (*Picea engelmannii*) and Southern pine (*Pinus taeda*). All samples were graded as No. 2 or better and showed a moisture content of approximately 25 %. Beams of five different sizes were tested using a constant span/depth ratio (L/d) of 5. For the Engelmann spruce 31.6 % failed in shear, and so did 53.0 % of the Southern pine. The results Asselin obtained correlated well to those of Rammer and Soltis (1994) on glued-laminated beams that are presented in section 2.2. Asselin suggested the use of shear volume as size parameter, because the regression analysis he performed showed that member depth was also closely correlated to the decrease in shear strength with increasing beam size. Therefore, he proposed an alternative equation to relate the shear strengths obtained from small, clear shear

blocks to those of structural-size members, based on shear volume. However, Asselin concluded that based on his regression analysis shear area best described the effect of beam size on shear strength. Full-size beam to small block shear strength ratios (τ_5/τ_{ASTM}) are presented in Table 2-1. The ratios decrease for each species and width category with less deep beams showing ratios larger than unity. Full-size member shear strength was based only on those specimens that failed in shear and no adjustments for MC or SG were considered.

Table 2-1: Shear Strength Ratios obtained by Asselin (1995) on SSL

L/d = 5	Engelmann spruce	Southern pine
Size [mm^2]	τ_5/τ_{ASTM}	τ_5/τ_{ASTM}
40 x 90	1.35	1.29
40 x 191	0.88	0.91
90 x 191	1.15	1.12
90 x 292	0.90	1.07
90 x 343	0.84	0.89

Peterson (1995) evaluated the effects of member size as well as natural and artificial defects, like saw kerfs on the shear strength of solid-sawn Southern pine at 12 % MC. Three-point and five-point bending tests with a constant L/d ratio of 5 were conducted and the full-size shear strength was compared with the results obtained from small, clear shear blocks. The shear failure percentage was raised from 35 % for seasoned full-size samples to 69 % for cut samples by the application of saw kerfs. In general, shear strength decreased with increasing member size and with ascending saw kerf length as shown in Table 2-2. The test results conformed well with previously stated relationship between shear area (Rammer and Soltis 1994) or shear volume (Asselin 1995) and shear strength. In

contrast, natural defects yielded no correlation to shear stress, since crack closure leading to contact, which might invoke frictional forces, was observed during loading. The five-point bending test constantly produced higher shear strength values than the three-point test did, with τ_5/τ_3 ranging from 1.24 to 1.79 as presented in the fourth column. Most τ/τ_{ASTM} ratios were smaller than unity except for 38 mm wide beams tested under five-point loading. The final three columns document the effects of saw kerfs of different lengths on shear strength, stating (τ_3/τ_{ASTM}) ratios. The ratios were based on full-size member shear strengths and only those members that failed in shear were considered.

Table 2-2: Shear Strength Ratios obtained by Peterson (1995) on Pine

Size [mm^2]	τ_5/τ_{ASTM}	τ_3/τ_{ASTM}	τ_5/τ_3	0.5d kerf	1.0d kerf	1.5d kerf
38 x 89	1.45	0.99	1.24	1.08	0.72	0.73
38 x 184	1.27	0.50	1.79	0.48	0.38	
89 x 184	1.00	0.74	1.45			
89 x 286	0.72	0.55	1.25	0.54	0.35	
89 x 337	0.70	0.50	1.50	0.42	0.29	

Sanders (1996) investigated the effects of different bending test set ups, span lengths, and moisture contents on the shear strength of structural-size members. Three different sizes of coastal Douglas-fir (*Pseudotsuga menziesii*) were tested. Sanders obtained an average shear strength ratio (τ_5/τ_3) of approximately 1.35 for both, green and seasoned samples, when comparing five-point to three-point flexure tests and suggested that this might be due to a different state of stress in the specimens. The five-point set up induces higher compressive stresses perpendicular to the grain on the beam than the three-point test does. Furthermore, the bending moment/shear force ratios are different for the two setups. As expected, a lower moisture content resulted in a higher

value for shear strength (τ_{dry}/τ_{green} = 1.26), where MC was approximately 12 % for the dry samples and around 30 % for the green samples. Increase in span length not only resulted in inconclusive data, but it became also problematic to produce shear failure. In general, the empirical equations proposed by Rammer and Soltis (1994) and Asselin (1995) correlated well to the data Sanders obtained. The shear strength ratios obtained by Sanders are given in Table 2-3.

Table 2-3: Shear Strength Ratios obtained by Sanders (1996) on Douglas-fir

		Green – 30 % MC			Dry – 12 % MC		
Size [mm^2]	L/d	τ_5/τ_{ASTM}	τ_3/τ_{ASTM}	τ_5/τ_3	τ_5/τ_{ASTM}	τ_3/τ_{ASTM}	τ_5/τ_3
38 x 89	5	1.28	1.11	1.27	1.21	1.20	1.30
63 x 115	5	1.22	0.83	1.44	1.18	0.84	1.39
38 x 184	5	1.06	0.74	1.37	1.23	0.81	1.39
38 x 89	6				0.88	0.89	1.09
38 x 89	7				1.08	0.73	1.57

Two years after the study on glued laminated timber (Rammer and Soltis 1994) Rammer et al. (1996) applied the empirical equation on solid-sawn Douglas-fir (*Pseudotsuga menziesii*) beams. The results were very similar to those obtained earlier for glulam beams, but a higher variation (12 – 18 % vs 8 %) was observed for the solid-sawn beams. However, there was little correlation between shear strength and modulus of rupture (MOR) in matched solid-sawn beams, while no correlation existed in matched glued-laminated beams. The shear/bending strength ratio (τ/σ) of solid-sawn Douglas-fir varied between 20 and 30 %, as observed earlier by Breitinger et al. (1994) on Radiata pine. The MC of the samples was between 20 and 28 %. Shear strength values were based on the five-point bending test with a L/d ratio of 5 and only those specimens that failed in shear were considered. Bending strength was evaluated

by means of the third-point (four-point bending) test with a half shear span/depth ratio (a/d) of 5.

Table 2-4: Results obtained by Rammer et al. (1996) on Douglas-fir

Size [mm^2]	τ_5/τ_{ASTM}	τ/σ
40 x 90	1.32	0.23
40 x 191	1.06	0.29
90 x 191	0.90	0.19
90 x 292	0.72	0.21
90 x 343	0.74	0.18

Cofer et al. (1997) modeled different sized solid-sawn Southern pine beams by means of a finite element analysis and applied the Tsai-Hill failure criterion to predict shear strength. Three-point and five-point loading configurations were idealized using two-dimensional, eight-node, biquadratic plane stress elements and the results were compared to the study of Peterson (1995). The effects of the length of loading and support plates, span/depth ratio (L/d) and member size were investigated. The FEM results compared reasonably well with experimental results for both setups for small member sizes, whereas the reduction in shear strength with increasing beam size was not reproduced by the FE analysis. Therefore the authors concluded that the size effect might be caused by the higher probability of the presence of natural defects in larger members of wood, since the model did not account for any flaws. Different stress states were obvious between the two setups and the authors concluded that the beams subjected to three-point bending are at least as likely to fail in tension as in shear.

Leichti et al. (1996) investigated stress interactions occurring in the five-point bending specimen, modeling two different sized beams 38 x 89 and

38 x 240 [mm^2] with the finite element method (FEM). The problem was reduced to a plane stress problem since the changes in normal and shear stresses through the thickness were small. The authors remarked that the thickness of the bearing plates can have a substantial effect on the stress distribution within the specimen. The maximum shear stress (τ) and the maximum compressive stress perpendicular to the grain ($\sigma_{c\perp}$) occurred for both models at the same point, at the neutral axis, or mid depth, halfway between a load head and the center reaction point. The absolute value of ratio $\tau/\sigma_{c\perp}$ was 3.6 for the smaller and 5.8 for the deeper beam, indicating that the compressive stress perpendicular to grain in the denominator is higher relative to the shear stress for the smaller, or less deep beam. Mandery (1969) showed a linear relationship between apparent shear strength and concomitant compressive stress perpendicular to grain applying two different test methods. Therefore the authors concluded, that it appears to be that concomitant compressive stresses perpendicular to the grain and shear stresses do show a substantial interaction and that the effect of this interaction is more pronounced for smaller cross sections. This means that the apparent shear strength of smaller beams measured via five-point bending tests is artificially increased by simultaneously acting stresses perpendicular to the grain.

Leichti and Nakhata (1999) evaluated the role of bearing plates in the five-point bending test of structural-size lumber, using FEM. First, they reminded the reader that the five-point bending test was initially used to evaluate the shear strength of wood-based structural panels (OSB) having a very large thickness/depth ratio compared to structural lumber, although the length/depth ratio is the same. Furthermore, oriented strand board shows a higher density than structural lumber and a density gradient through the thickness, with the highest density on the outside. Besides, rounded load bearing plates were applied for the tests of structural panels, whereas later on in most cases flat bearing plates have been used for tests on structural-size lumber and engineered wood products. Leichti and Nakhata modeled 38 x 89 and 38 x 240 [mm^2]

Douglas-fir beams under five-point load configuration with a L/d ratio of 5 using two-dimensional, four-node plane stress elements. The model simulated the test setup used by Rammer et al. (1996). An additional model of the smaller beam with shorter load bearing and center support plates was used to determine the effects of bearing plate length. The effect of the flexural rigidity (EI) of the bearing plates was evaluated by applying two different bearing plate thicknesses of 25 mm and 13 mm, reducing EI by a factor of 8. The authors concluded that elementary beam theory did not accurately predict the complex state of shear and bending stresses within the specimen, but overestimated the FE solution for the shear stresses by about 30 – 40 %. The stress state was not influenced by the bearing plates, as long as the plates flexural rigidity counted for at least 2.9 times that of the specimen. The bearing plate geometry, i.e., rounded corners or sharp edges, was not believed to have a major impact, since it only affected the stress state in the very immediate vicinity of the plate perimeter, but dissipated rapidly. However, the stress state can be influenced if the clear plate edge to plate edge distance (PEPE) gets too small. In addition, the provision of sufficient bearing area to prevent crushing for smaller sizes of dimension lumber presents an immense problem. Consequently, the authors concluded that beams having smaller cross sections should not be tested in the five-point configuration or that a standard test method, which is applicable to all sizes of lumber should be introduced.

Riyanto (1996) compared different test methods to evaluate the shear strength of structural lumber. Standard 38 x 89 mm^2 (nominal 2 x 4 in^2) Douglas-fir (*Pseudotsuga menziesii*) beams were tested in edgewise bending as a joist using three-, four- and five-point bending test setups, as well as in torsion. The span/depth (L/d) ratio was maintained constant at 5 for all full-size tests. There was no linear relationship between modulus of elasticity (MOE) and shear strength. The author found a significant linear relationship between shear strengths from the three-, five-point bending, and torsion test and the shear strength from the ASTM shear block test. Despite, the four-point bending test

proved to be unsuitable to determine the shear strength of structural lumber, because only very few samples failed in shear and their coefficient of variation (COV) was very high, as shown by the following results of Riyanto in Table 2-5. Riyanto recommended the torsion test as a method to determine shear strength as a material property, since pure shear stresses are produced in the specimen, and the three-point bending test to determine the shear strength of structural lumber, since it best represents the real-life loading condition.

Table 2-5: Results obtained by Riyanto (1996) on Douglas-fir

Setup	Shear Failure [%]	τ [MPa]	COV [%]	τ/τ_{ASTM} [1]
Shear block	100	7.94	15	
Three-point	44	9.07	16	1.14
Four-point	8	6.44	28	0.81
Five-point	28	11.09	18	1.40
Torsion	100	12.64	17	1.59

Heck (1997) evaluated the torsion test as a method to determine shear strength of structural lumber. Solid-sawn Douglas-fir (*Pseudotsuga menziesii*) beams of five different depths and also five different lengths were tested to investigate a size effect on shear strength. There was no evidence of a length effect and no conclusive evidence of a depth effect on shear strength values obtained by the torsion test. Failure typically occurred at mid depth of the long side, or wide face, of the beam and propagated toward the ends of the sample. According to Heck, the shear stress causing failure in structural lumber is the same for bending and torsional loading conditions. The failure plane as well as the sliding direction, are both parallel to the grain. In contrast to flexure tests the torsion test induces a state of pure shear stress in the specimen and it yields

100 % shear failure. Based on the test results, Heck concluded, that "the torsion test is the best practical method to determine the pure shear strength of full-size structural lumber". The results reported by Heck are given in Table 2-6, where the subscript T indicates torsion and ASTM stands for small, clear shear blocks.

Table 2-6: Torsion Results obtained by Heck (1997) on Douglas-fir

		Torsion		Shear Block		Ratio
	Size [mm^2]	τ_T [MPa]	COV [%]	τ_{ASTM} [MPa]	COV [%]	τ_T/τ_{ASTM} [1]
Length Study	38x89	10.5	15.7	8.3	10.9	1.27
Depth Study	38x89-286	9.9	7-18	8.9	12.8	1.11

2.2 Engineered Wood Products (EWP)

Möhler and Hemmer (1977) evaluated the deformation and strength behavior of solid-sawn softwood lumber and glued-laminated timber subjected to torsion. The authors performed short and long-term tests and applied pure torsion as well as simultaneous bending and torsion loading. They tested small, clear wood samples of circular and rectangular cross section opposed to full-size lumber containing defects. Further, they investigated the influence of MC and density. The species considered was spruce (*Picea abies*). For practical reasons the authors applied isotropic theory, they emphasized however that wood behaves rhombic orthotropic and for this reason the calculated values for shear stresses and moduli are dependent on the aspect or side (h/b) ratio, the annual ring orientation and the growth conditions. Preliminary tests on small, clear samples indicated that the pure shear strength is more reliable when determined in torsion, whereas concomitant bending stresses lead to lower apparent shear

strengths. The results are displayed in Table 2-7, where the subscript 05 indicates the lower 5th-percentile tolerance limit (τ_{05}, G_{T05}). The significantly higher shear strength of rectangular torsion samples (1st row) compared to circular members (2nd row) might indicate a shape effect, though a higher density might be the more probable explanation. The tension shear test (last row) proved that shear strength is higher, if the orientation of the shear plane is perpendicular (τ_{LT}) than if it is parallel (τ_{LR}) to the annual rings. The results of the main test series in torsion that was conducted on 100 cm long beams are presented in Table 2-8. The area of the rectangular cross section was kept constant at 36 cm^2, but aspect, or depth/width, (h/b) ratio varied from 1 – 9. The mean torsional strength (τ_T) and modulus (G_T) increased with increasing aspect ratio for clear wood and glued-laminated timber, whereas this shape or size effect was weakened by wood texture for SSL. Clear wood offered markedly higher torsional values and significant lower variability compared to SSL, containing defects. Horizontally laminated glulams of 6 x 24 cm^2 cross section were subjected to torsion, as indicated in the last row of Table 2-9, as well as combined torsion and third-point bending. Generally failure was obvious over the entire length for the first group, whereas it initiated always from the first third of the span from the constrained end, if additional bending loads acted. A marked decrease in torsional strength (τ_T) occurred when the shear stresses (τ_Q) caused by shear forces surpassed 0.6 MPa, while the torsional moduli remained more or less constant. In long-term tests, torsional moduli (G_T) decreased practically independent of the value of the torsional moment; that means, the rotational deformation increased with longer duration of load. The loss of torsional rigidity with time, or creep, was more pronounced for SSL compared to glulams. As expected, torsional strength and moduli increased with increasing density. On the other, hand torsional moduli decreased with increasing MC between 6 and 28 %, that means below fiber saturation point, while the torsional strength surprisingly increased.

Table 2-7: Preliminary Results by Möhler and Hemmer (1977) on Spruce

Test Method	n	h/b [mm]	τ [MPa]	COV [%]	τ_{05} [MPa]	G_T [MPa]	COV [%]	G_{T05} [MPa]
Torsion	13	35/10	20.02	14.8	14.72	855.3	25.7	462.8
	10	Ø 25	10.31	7.4	8.91	563.5	3.2	530.4
Shear Cross (DIN 52187)			6.80	7.9	5.81		τ_{LT} [MPa]	τ_{LR} [MPa]
Tension							9.38	8.8

Table 2-8: Torsion Results by Möhler and Hemmer (1977) on Spruce

Material	n	h/b [cm]	c = h/b	τ_T [MPa]	COV [%]	τ_{05} [MPa]	G_T [MPa]	COV [%]	G_{T05} [MPa]
Clear Wood	20	6/6	1	12.58	11.6	10.05	556.4	13.1	430.6
	30	9/4	2.25	14.30	16.8	10.22	616.1	16.9	438.9
	30	12/3	4	15.53	15.7	11.40	724.0	15.4	533.9
	6	18/2	9	24.45	16.8	16.16	1002.6	5.3	894.6
SSL	43	6/6	1	7.46	23.5	4.50	410.5	19.4	276.7
	62	9/4	2.25	9.83	32.4	4.51	525.1	20.8	342.9
	68	12/3	4	8.14	34.2	3.52	499.9	28.2	265.6
	15	15/2.4	6.25	13.62	34.7	5.30	712.4	25.9	387.5
Glulam (Horizontal)	4	6/6	1	6.41	8.1	5.18	491.5	7.9	399.7
	5	9/4	2.25	6.14	6.0	5.36	532.9	5.7	468.3
	5	12/3	4	7.65	5.2	6.81	605.5	6.9	516.6
	5	15/2.4	6.25	8.00	8.1	6.61	646.4	5.6	569.8

Table 2-9: Comparison of Torsion Results on Spruce Glulam by Aicher (1990) and Möhler and Hemmer (1977)

Material Glulam	Grade	ρ [kg/m^3]	n	h/b [cm]	c = h/b	A [cm^2]	V [m^3]	τ_T [MPa]	G_T [MPa]
Vertical (Aicher)	S 13	450 – 470	2	65/10	6.5	650	0.085	7.50	912
			2	86/13	6.5	1118	0.145	6.66	788
Horizontal (Möhler)	S 10/ S 13	440 – 490	1	48/6	8.0	288	0.124	9.12	887
			1	36/6	6.0	216	0.073	7.24	700
			5	24/6	4.0	144	0.043	6.70	752

Aicher (1990) investigated the torsional properties of structural-size, vertically laminated glued-laminated timber (glulam) of European spruce (*Picea abies*). Focus of the study was the effect of not generally glued edge joints in the outer laminations. The laminations were 33 mm thick, of grade S 13 according to German standard DIN 4074, continuous over the entire length of 1.7 m and therefore not finger jointed. Altogether 18 specimens of two different sizes, with three or four laminations across the thickness, were tested in torsion. In addition, three different configurations, where the edge joints (a) remained unchanged, (b) every second, or (c) all edge joints were opened 3.5 mm wide by the application of saw kerfs to the whole depth of the outer laminations along member length, were considered. The aspect, or depth/width (h/b) ratio was kept constant at 6.5. Two equivalent cycles of loading to the allowable torque were applied before the samples were finally destructively tested. Failure occurred after about 11 to 15 minutes. The torque-twist curves were linear up to about twice the allowable torsional moment of equivalent horizontal glulams (6 kNm). Then, a slight loss in rigidity that was more distinct for specimens with sawn-up edge joints was observed before failure was reached between four to five times the allowable torque (13 - 14 kNm) at an ultimate twist of 9 - 15 degrees for the smaller specimens. The thicker beams, with one additional lamination, were able to

endure about double the torsional moment (28 - 31 kNm) and failed between 9 - 12 degrees of twist. For all samples, cracks initiated from edge joints of the outer laminations and reached almost along the whole beam. The torsional shear strength ranged between 6.2 and 7.5 MPa, based on St. Venant torsion (unrestrained warping) and isotropic material behavior. The author suggested that due to a partial warping restraint in the experimental setup the shear strength and the apparent torsional moduli might be 10 – 15 % too high. There was no distinct drop in torque at failure, since the displacements at the wide faces within the clamps were highly restricted due to frictional forces. The author argued that the applied torque was consequently equilibrated at a load level comparable to ultimate torque by the torsional rigidities of three to six sub cross-sections that developed from the original one due to cracking. There was a distinct size or volume effect. Torsional shear strength and modulus decreased with increasing size and increasing number of sawn-up edge joints. The latter was more pronounced for the smaller specimens with only 3 laminations across the width. Torsional rigidity is more susceptible to the application of saw kerfs than shear strength; shear strength decreased by roughly 10 %, while the drop in torsional rigidity counted for nearly 30 %. The results indicate that the effectiveness of edge glue lines is high and the author assumed an effective edge glue line percentage beyond 50 %. A comparison of torsion results on spruce glulams without saw kerfs is presented in Table 2-10, where the values for vertical glulams were taken from Aicher and those for horizontal ones from Möhler and Hemmer (1977).

Aicher also performed a finite element (FE) analysis, applying 3-dimensional, 8-node, prismatic elements and compared isotropic with orthotropic material behavior. In the second case, orthotropic elastic constants were used, however no differentiation was made between radial and tangential direction, i.e., $E_x = E_y$ and $G_{xz} = G_{yz}$ since for glulams the growth ring orientation of the individual laminations varies generally strongly over the cross-section of the beam. Two different models were evaluated, one simulating St. Venant

torsion (free warping), the other one considering warping torsion (restrained warping). Loading was applied by means of concentrated forces. The consideration of warping torsion resulted in significant differences between isotropic and orthotropic, squatty glulam beams, with the second exhibiting markedly higher normal stresses and an articulate increase in torsional rigidity.

Bateman, Hunt, and Sun (1990) first evaluated the five-point bending test on engineered wood products to determine the interlaminar shear strength of oriented strand board (OSB). The authors were looking for a more effective test method compared to the current standard test methods ASTM D 1037 and D 2718. The latter two test methods are labor-intensive and time-consuming; furthermore, they do not result in the same state of shear stress produced by transverse bending, which is the primary loading condition in structural applications. Bateman et al. concluded that the five-point bending test is suitable to determine the interlaminar shear strength of structural wood composites, but it might not be appropriate for bending critical, nonstructural composites. The main point of their results is that shear strength decreased with increasing span length, but at a decreasing rate, which complies with earlier studies.

Janowiak and Pellerin (1992) determined the orthotropic shear moduli for three reconstituted wood panel products using torsion. The torsion test offered the advantage of simultaneous evaluation of the three orthotropic shear moduli, both in-plane and transverse, and it provided a pure shear strain field. In contrast to standard test methods like the anticlastic plate bending test (ASTM D 3044), there was no limitation for the evaluation of transverse G, because of the small thickness. Hence, the authors commented that the torsion test might be a more efficient test method to determine the orthotropic shear moduli compared to flexure tests. The authors recommended the use of at least four different slenderness ratios and to apply correction for restrained warping deformation or grip effects. The in-plane shear moduli of particleboard, waferboard and oriented strand board (OSB) obtained by torsion tests were found to agree reasonably well with the values obtained by the standard method.

Rammer and Soltis (1994) evaluated the shear strength of unchecked glued-laminated (glulam) beams of Douglas-fir and Southern pine using the five-point bending test with a constant span/depth ratio (L/d) of 5. According to the authors, the five-point bending test setup resulted in higher shear forces within the specimen compared to the three-point bending test setup and was therefore used to maximize the amount of shear failures. They developed a relationship between shear strength and beam size, based on the shear strength obtained from the ASTM shear block test. A regression analysis was performed, based on beam depth, beam area, or beam volume versus shear strength using linear and nonlinear regression functions. It turned out that shear area best characterized the variation of shear strength. There was a strong decrease in shear strength for small shear areas, which turned then into an asymptotical decline for larger shear areas, similar to the results of Bateman et al. (1990) on OSB. Besides, the shape of the regression curve was independent of species. Altogether 272 of 330 specimens, or 82.4 %, failed in shear. Failure typically initiated at the most highly stressed region, i.e., at beam mid depth between one load point and the center support. Cracks usually occurred at the early/late wood border and propagated along the grain, but seldom passed the loading points, or, to put it another way, did not propagate to the end of the beam. As expected, the shear strength values for Southern pine were higher compared to those of Douglas-fir. In addition, the results indicated that for beams with larger cross sections the shear strengths obtained from ASTM shear block tests were higher than those obtained from full-size beam tests, resulting in τ_5/τ_{ASTM} smaller than unity. The authors recommended the five-point bending test as a standard method for determining shear strength of structural-size lumber. Bending strength was evaluated by means of the third-point (four-point bending) test with a half shear span/depth ratio (a/d) of 5. The results obtained by Rammer and Soltis are documented in Table 2-10, where LQ means low quality and HQ high quality.

Table 2-10: Results obtained by Rammer and Soltis (1994) on Glulam

L/d = 5	Douglas-fir glulam		L/d = 5	Southern pine glulam	
Size [mm^2]	τ_5/τ_{ASTM}	τ/σ	Size [mm^2]	τ_5/τ_{ASTM}	τ/σ
38 x 127 LQ	1.29	0.21	38 x 102	1.43	0.18
38 x 127 HQ	1.18	0.19			
64 x 165 LQ	1.01	0.23	64 x 140 LQ	1.21	0.21
64 x 165 HQ	0.98	0.16	64 x 140 HQ	1.17	0.15
76 x 305	0.90	0.14	76 x 279	0.94	0.15
111 x 292 LQ	0.60	0.19			
111 x 292 HQ	0.61	0.14			
127 x 610	0.80	0.14	127 x 559	0.72	0.13

Tingley and Kent (1996) investigated the effects of test setup on shear strength of full-size glued-laminated timber. The authors remarked that the current standard test method to evaluate the shear strength of full-size timber beams, ASTM D 198, does not consider compression perpendicular to the grain effects on shear strength. Despite the fact, that Mandery showed already in 1969 that shear strength increases to a higher value than predicted by conventional theory, when compressive stresses perpendicular to the shear plane act simultaneously. Based on their results, Tingley and Kent strongly recommended two additions to ASTM D 198. First, a minimum value for one half shear span/depth ratio (a/d) of approximately 3.0 and second an outer load head to inner reaction bearing plate, or plate edge to plate edge (PEPE), distance of at least two times the specimen depth. Otherwise, the measured shear strength might be artificially increased by concomitant compressive stresses perpendicular to the grain.

Tingley, Kent, and Leichti (1996) evaluated the effects of test configuration on the shear strain in fiber-reinforced glued-laminated timber. A 130 x 305 x 6400 mm^3 aramid-reinforced glulam beam was loaded under four-point bending up to 125 % of the allowable design load applying different load

point geometries, flat and curved load heads, PEPE distances, and half shear span/depth ratios a/d. In conclusion, the geometry of the load head did not influence the maximum shear strain, whereas both, the a/d and the PEPE ratio did have major effects on the maximum shear strain.

Tingley, Pooley, and Kent (1996) elucidated the shear strength of full-scale glulam beams, stating that the small clear shear block samples according to ASTM D 143 do not relate well to structural-size samples. Several factors like orientation of grain to load, size effects, anisotropy, defects in full-scale samples (homogeneity) and testing apparatus (ASTM D 143) effects, including the 3 mm offset and the sharp reentrant corner that lead to stress concentrations and interactions, are some of the reasons that shear strength obtained from small clear samples usually exceeds that of full-scale beams. According to the authors, the shear stress raiser appears to be close to two. Furthermore, the stresses perpendicular to grain are dramatically influenced by the offset that increases the bending moment acting in the specimen. Mandery (1969) found that the shear stress capacity increased up to 50 % when concomitant compression perpendicular to grain stresses were present. Tingley et al. measured the actual shear strains acting in an ASTM D 143 block and visualized the resulting stresses in the different directions. It turned out that all stresses, shear, compression parallel and compression perpendicular to grain showed their maximum value close to the very top of the block at the reentrant corner. Moreover, these stress concentrations increased heavily with increasing load. Tension perpendicular to the grain was present in the middle section of the height of the block, whereas it turned into compression perpendicular to the grain close to the top and bottom. The authors also commented on full-size testing of glulams and emphasized that the following factors, span/depth (L/d) ratio, bearing plate size and stiffness, and the distance between support plate edge and the closest load bearing plate edge (PEPE) are of special importance.

Yeh (1993) evaluated the shear strength of Douglas-fir structural glued-laminated timber via the center-point (three-point bending) test. Specimens of

different lay-ups and widths were tested with a low span/depth ratio (L/d) of 3.3 to ensure a high number of shear failures. Altogether, 97.4 % of the specimens ultimately failed in a pure shear mode. However, for some groups of specimens initial or intermediate failure occurred, which might, according to Yeh, have been located at different laminations and therefore be inconsistent with the ultimate failure.

Four years later, Yeh (1997) tested full-size glued-laminated beams of three different species and different net widths via a two-point load method (four-point bending test). The clear distance between the inner edge of the reaction bearing plate and the outer edge of the closest load head (PEPE) equaled at least two times the specimen depth. The considered species were Douglas-fir, Southern pine, and Spruce-Pine-Fir. Overall, 70.1 % of the specimens failed in shear ranging from 42.5 % for Spruce-Pine-Fir to 92.5 % for the smaller width Southern pine. Shear failure typically initiated at the end of the member near beam mid-depth or in the tension stressed part below the neutral axis. Shear cracks usually propagated along the late/early wood interface and sometimes jumped over to adjacent growth rings or laminations; nevertheless, a few samples failed across growth rings in the radial direction. Yeh concluded that the width effect on characteristic shear strength was negligible for Southern pine and Douglas-fir glued-laminated timber.

Hindman (1999) evaluated the elastic constants of selected engineered wood products. The author delivered elastic constant ratios for LSL, LVL, PSL, and OSB like those offered in Bodig and Jayne (1982) for solid wood. The results were obtained by torsion, bending, compression and tension tests. Hindman followed the torsion test method as introduced by Janowiak and Pellerin (1992) and the five-point bending test procedure that has been applied by Bateman et al. (1990) on OSB. In conclusion, it was evident that SCL showed a different elastic response than did solid wood. Lathe checks in LVL and PSL were found to decrease transverse elastic stiffness as well as the shear resistance through the thickness, whereas cross-ply lamination in OSB caused an increase in

exactly the same values. The variability was high for Poisson ratios obtained from tension and compression tests, but all values were higher than those for solid wood. Flatwise and edgewise longitudinal MOE did not show a corresponding relationship. It seemed that some shear moduli showed a correlation to wood species or the type of EWP. Hindman strongly recommended not to use the set of elastic constants of solid wood for EWPs manufactured of the same species, because of the obviously different elastic behavior.

2.3 Structural Composite Lumber (SCL)

Hunt, Shook, and Bradtmueller (1993) determined the longitudinal shear strength of laminated veneer lumber (LVL) via the five-point bending test. They tested nominal 38 x 58 mm^2 (1.5 x 2.3 in^2) Southern pine LVL in flatwise bending as a plank, i.e., the bending load was applied perpendicular to the gluelines. A comparison with the results of a modified ASTM D 143 shear block test, and a short beam (three-point, or center-point bending) test was drawn. The average SG of the tested LVL samples was 0.633 at 7.6 % MC. The test material was composed of 13 plies of average grade and a densification of 22 %, based on Loblolly pine (*Pinus taeda*) was observed; however, there was no evidence for a density gradient through the thickness. Under five-point bending, the shear strength decreased with increasing span/depth (L/d) ratio at a decreasing rate, like observed earlier on OSB by Bateman et al. (1990). The highest mean value for L/d = 8 counted for 1.33 times the average shear strength value of 4.76 MPa obtained for L/d between 14 and 18, where the shear strength seemed to be relatively constant. The percentage of shear failures dropped drastically for L/d larger than 18 and bending became the prevailing failure mode. The shear block test yielded the highest average values for shear strength, 6.34 MPa (920 psi), followed by the three-point bending test, 5.72 MPa (830 psi), and the five-point test, 4.76 MPa (690 psi). The authors recommended the use of the five-point

bending test as a quality control test to generate an extensive database for longitudinal shear strength values based on full-size members. Additionally, a third-point (four-point bending) test was performed to evaluate the bending strength. The average value for MOR was 74.5 MPa with a corresponding COV of 17 %. The results obtained by Hunt et al. (1993) in combination with the results of a follow up study (last row) by Bradtmueller et al. (1998), described in the next paragraph, are presented in Table 2-11.

Table 2-11: Results obtained by Hunt et al. (1993) on Southern pine LVL

Setup	Size [mm^2]	Orien-tation	L/d [1]	τ [MPa]	COV [%]	τ_T/τ_{ASTM} [1]	σ [MPa]	τ/σ [%]
Shear Block	44x58	Plank		6.34	18.0			
Center-Point	38x58	Plank	6.7	5.72	9.4	0.90	74.46	7.7
Five-Point	38x58	Plank	14-18	4.76	8.1	0.75	64.81	7.3
Five-Point	38x58	Joist	9.3-10.6	8.14	5.8		70.33	11.6

In 1998 Bradtmueller, Hunt, and Shook presented a second study on the mechanical properties of Southern pine LVL in the joist orientation. The average SG was 0.670, which was slightly higher compared to the first study, while the MC (7.7 %) and the cross sectional dimensions were the same. The authors remarked that it is inherently more difficult to induce shear failure in joist oriented LVL by means of a bending test compared to plank oriented LVL. The shear strength was found to be 8.14 MPa, which is 71 % higher than in the plank orientation, whereas the bending strength (70.3 MPa) nearly stayed the same. Shear strength of the joist oriented samples was based on a span/depth ratio L/d of 9.3 and 10.6, while the plank oriented values were evaluated with L/d ranging from 14 to 18. The authors did not perform shear block tests in the joist

orientation. The results of Bradtmueller et al. are shown in the last row of Table 2-11.

Craig and Lam (1996) investigated four different flexure test setups and compared the values of longitudinal shear strength of SCL with the results of ASTM shear block tests. The study was performed on nominal 44 x 184 mm^2 (1.75 x 7.25 in^2) laminated veneer lumber (LVL) and parallel strand lumber (PSL), both of Douglas-fir (*Pseudotsuga menziesii*). The structural-size samples were tested in edgewise bending as a joist, i.e., the bending load was applied parallel to the glue lines. The four-point bending test was proved to be inappropriate to determine the shear strength of SCL, since none of the LVL samples and only 18.8 % of the PSL specimens failed in a shear mode. The center-point configuration produced 37.5 % shear failure for both composites whereas all other tests resulted in shear failure only. MC was 10.3 % for LVL and between 8.8 and 9.3 % for PSL. SG was 0.57 for LVL and ranged from 0.64 to 0.66 for PSL. The shear plane for the ASTM shear block test was slightly smaller (44 x 51 mm^2) than stated in the standard as a result of the small width of the test material. The results obtained by Craig and Lam are summarized in Table 2-12.

Table 2-12: Results on Joist Oriented SCL by Craig and Lam (1996)

Setup	Material	Size [mm^2]	L/d [1]	τ [MPa]	COV [%]	τ/τ_{ASTM} [1]	σ [MPa]	τ/σ [%]
Shear Block	DF LVL	44x51		7.94	10.2			
Center-Point	DF LVL	44x184	6	5.60	7.0	0.71	63.12	8.9
Four-Point	DF LVL	44x184	6				50.54	
Shear Block	DF PSL	44x51		8.26	16.8			
Center-Point	DF PSL	44x184	6	5.49	1.6	0.66	64.90	8.5
Four-Point	DF PSL	44x184	6	4.81	4.0	0.58	52.76	9.1
Five-Point	DF PSL	44x184	6	6.75	8.0	0.82		
Five-Point	DF PSL	44x184	5	8.00	10.5	0.97		

The difference in average shear strength for PSL for the two five-point bending test setups, where the half test span equals 5 times or 6 times the specimen depth, is similar to the results of previous studies (Lam, Yee, and Barrett, 1995). The ratio of five-point(5d)/center-point shear strength τ_5/τ_3 equaled 1.46. In general, shear failure mainly occurred close to mid depth of the specimens; however, in contrast to earlier studies on solid-sawn and glued-laminated beams (Riyanto 1996, Rammer and Soltis 1994 & 1996), initial failure cracks propagated through the sample to the end. Furthermore, the failure surfaces were jagged for both composites.

Four years later, Craig and Lam (2000) conducted a second study on Douglas-fir LVL, as well as Douglas-fir and Southern pine PSL of two different sizes. The specimens were tested in five-point bending and center-point (three-point) bending. However, the cross-section of the samples supposed to center-point loading was remanufactured into an I-shape, as indicated by the (I) synonym in the size column in Table 2-10, to enforce shear failure rather than bending failure, since only 37.5 % of the beams failed in shear in a preliminary study. The cross section of the beams supposed to five-point bending was maintained rectangular. The MC was in a close range since most specimens were conditioned at 20 °C/65 % RH. SG was also very consistent for the different composites. The results of the structural-size beam tests were compared to those obtained by tests on small shear blocks having a shear plane of 44 x 51 mm^2. The ratios of full-size/small block shear strength (τ/τ_{ASTM}) ranged from 0.73 to 0.91 for center-point loading and from 1.03 to 1.39 for five-point loading and the ratios of five-/three-point shear strength varied between 1.34 and 1.53. It is obvious that all ratios decrease with increasing size, or member depth, indicating a distinct size effect. This trend is consistent with earlier studies on solid-sawn lumber as well as glued-laminated beams. The results obtained by Craig and Lam on specimens in the standard or joist configuration are presented in Table 2-13. The authors also tested PSL samples in plank orientation, those results are finally displayed in Table 2-14.

Table 2-13: Results on Joist Oriented SCL by Craig and Lam (2000)

Setup	Material	Size [mm^2]	L/d [1]	τ [MPa]	τ_{ASTM} [MPa]	τ/τ_{ASTM} [1]	σ [MPa]	τ/σ [%]
Center-Point	1.8E DF LVL	44x184 (I)	6	6.83	7.52	0.91	61.53	11.1
Center-Point	1.8E DF LVL	44x305 (I)	6	6.39	7.69	0.83	57.24	11.2
Five-Point	1.8E DF LVL	44x184	5	10.45	7.52	1.39		
Five-Point	1.8E DF LVL	44x305	5	9.15	7.49	1.22		
Center-Point	2.0E DF PSL	44x184 (I)	6	5.88	7.07	0.83	54.83	10.7
Center-Point	2.0E DF PSL	44x305 (I)	6	5.40	7.43	0.73		
Center-Point	2.0E SP PSL	44x184 (I)	6	6.87	7.92	0.86	64.29	10.7
Center-Point	2.0E SP PSL	44x305 (I)	6	6.89	9.01	0.76	59.14	11.7
Five-Point	2.0E DF PSL	44x184	5	9.00	7.07	1.27		
Five-Point	2.0E DF PSL	44x305	5	7.56	7.35	1.03		
Five-Point	2.0E SP PSL	44x184	5	10.45	7.92	1.32		
Five-Point	2.0E SP PSL	44x305	5	9.21	8.59	1.07		

Table 2-14: Results on Plank Oriented PSL by Craig and Lam (2000)

Setup	Material	Size [mm^2]	L/d [1]	τ [MPa]	τ_{ASTM} [MPa]	τ/τ_{ASTM} [1]	σ [MPa]	τ/σ [%]
Center-Point	2.0E DF PSL	44x184	6	4.14	5.69	0.73	59.50	7.0
Center-Point	2.0E DF PSL	44x280	6	3.93	5.52	0.71		
Center-Point	2.0E SP PSL	44x184	6	4.73	6.78	0.70	70.93	6.7
Center-Point	2.0E SP PSL	44x280	6	4.51	6.71	0.67	68.24	6.6

3. Materials and Methods

3.1 Materials

Eighty-five structural-size SCL beams (29 LSL, 30 LVL, and 26 PSL) with nominal dimensions of 44 x 140 x 1524 mm^3 (1.75 x 5.5 x 60 in^3) were obtained from Trus Joist – A Weyerhaeuser Company. The cross section is shown schematically for LSL in Figure 3-1. Each of the three composites was produced in a different plant. The beams were stacked in an uncontrolled room for about two months, before testing began, to allow them to come to equilibrium. No conditioning was applied to the specimens, since this only would have raised the moisture content.

Figure 3-1: Joist Orientation

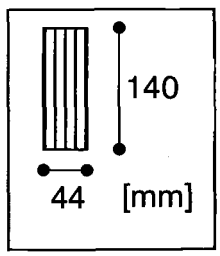

3.1.1 Laminated Strand Lumber (LSL)

Twenty-nine specimens of 1.5 E-rated LSL produced in Deerwood, Minnesota were obtained. The principal species was aspen (*Populus spp.*). Aspen is a fast growing, low density hardwood, or deciduous tree, which was formerly considered a lesser value species. The moisture content at time of production was between 6.0 and 7.0 % according to the manufacturer. For LSL, all strands are sliced directly from debarked logs. The length of LSL strands is two to four times that of oriented strand board (OSB), approximately 300 mm (12 in), but shorter than for PSL. LSL was first introduced to the market as PSL 300™ LSL, referring to its strand length and later renamed as LSL. The strand thickness before pressing ranges between 0.8 and 1.3 mm (0.03 and

0.05 in) and the width averages around 25 mm (1 in). Short strands and other waste are removed during the manufacturing process. The strands are dried and coated with a mixture of resin and a small amount of wax, which is added to enhance moisture resistance. Then the strands are aligned and bonded with high temperature cured polymeric diphenylmethane diisocyanate (MDI) through steam injection pressing. The mechanical properties of the end product can be controlled by strand alignment and mat densification.

3.1.2 Laminated Veneer Lumber (LVL)

Thirty specimens of 1.9 E-rated coastal Douglas-fir (*Pseudotsuga menziesii*) laminated veneer lumber manufactured at Eugene, Oregon were received. The moisture content at time of manufacture was between 6.0 and 7.0 %, like for LSL. All veneers were rotary peeled and the initial veneer thickness was approximately 2.5 or 3.2 mm (1/10 or 1/8 in). The number of plies depended on the veneer thickness and was either nineteen, for nineteen samples, or fifteen, for the remaining eleven samples. Four of the 30 samples received had wax seal on both narrow faces to reduce moisture uptake. All veneers were ultrasonically graded, curtain coated with adhesive, laid up in a certain sequence depending on veneer grade and lap-jointed. The resin used was high temperature cured phenol formaldehyde (PF). LVL is typically compressed by means of a continuous press although hot presses are also used.

3.1.3 Parallel Strand Lumber (PSL)

The species of the parallel strand lumber samples was again coastal Douglas-fir (*Pseudotsuga menziesii*). Twenty-six 2.0 E-rated specimens originating from Vancouver, British Columbia, Canada were tested. The moisture

content at manufacture for PSL was higher, compared to the other two composite materials, and ranged from 8.0 to 9.0 %. All veneers were rotary peeled and then clipped into strands. The veneer strand thickness before pressing was approximately 3.2 mm (1/8 in). The strands were up to 2.4 m (8 ft) long and about 2.5 mm (1 in) wide. Short strands are eliminated during the manufacturing process when the strands pass an adjustable gap on the conveyor belt. The resin used was high temperature cured phenol formaldehyde (PF), again combined with a small amount of wax. In PSL there was no significant density gradient across the thickness from microwave curing and pressing. The microwave curing works from inside out and is therefore applicable to bigger cross sections than usual methods since the temperature gradient throughout the cross section is less of a problem.

3.1.4 Material Characteristics

The major characteristics of the tested materials are summarized in Table 3-1. LVL and PSL were both made of Douglas-fir and bonded with PF resin. LSL, in contrast, was made of Aspen and bonded with MDI resin. All three materials are wood composites; however, the geometry of the wood constituents differs greatly. For LVL, the laminates are continuous over the width and beside occasional lap joints also over the length, whereas LSL with its short strands is discontinuous in both directions. The strands of PSL are much longer and thicker compared to LSL strands. Furthermore, it has to be mentioned that the strand or veneer orientation is not the same for the three products. LVL is generally unidirectional that means all veneers are aligned longitudinally. The strands within the PSL specimens were almost completely oriented in the longitudinal direction, whereas the alignment of the LSL strands was less controlled, compared to the other two products. It is hardly possible to express this difference in numbers, since these are proprietary products, but the degree of

strand or veneer alignment is highest for LVL, followed closely by PSL and much lower for LSL, where it might even vary through the thickness.

Note, that only LVL and PSL are rotary peeled and therefore susceptible to lathe checks, whereas LSL is not. The veneers of LVL cannot undergo much densification without fiber crushing (Hindman 1999). The ratio $sg = SG_{SCL}/SG_{SSL}$ is an expression of the degree of densification. Ratio sg is highest for LSL (1.84), followed by PSL (1.38) and LVL (1.19). The specific gravity SG of the three composites follows the same ranking.

LVL is different from the other two composites in that there might be a density gradient through the thickness due to hot pressing, while LSL and PSL are not designed to have a density gradient. In addition, the veneers of LVL are E-rated and were stacked according to their stiffness, causing a stiffness gradient through the thickness with the higher quality veneers towards the outside faces. The information on the test materials given in this chapter were either obtained directly from the manufacturer or taken from Smulski (1997). The design properties presented in Tables 3-2 and 3-3 were obtained from the National Evaluation Service, Inc. (NES), the homepage of the manufacturer (www.tjm.com), and the German Institute for Construction, Berlin.

Table 3-1: Major Characteristics of Test Materials

	LSL	LVL	PSL
Species & E-Rating	Aspen 1.5E	Douglas-fir 1.9E	Douglas-fir 2.0E
Veneers (V) or Strands (S)	S directly sliced	V rotary peeled	V rotary peeled & sliced into S
Initial Length [mm]	300	2400	< 2400
Thickness [mm]	S ~ 0.9	2.5 < V < 3.2	S ~ 3.2
Width [mm]	25	1200	19
$sg = SG_{SCL}/SG_{SSL}$	1.84	1.19	1.38
Resin	Isocyanate (MDI)	Phenol Formaldehyde (PF)	
Pressing & Curing	Steam injection	Hot press	Microwave (inside out)

Table 3-2: US Design Properties according to NER-481, March 1997

			Axial		Joist (Edgewise)				Plank (Flatwise)			
Material	**G**	E	$F_{t\parallel}$	$F_{c\parallel}$	F_b (5.5in)	F_b (12in)	**F_v**	$F_{c\perp}$	F_b (5.5in)	F_b (12in)	**F_v**	$F_{c\perp}$
	[GPa]		[MPa]									
1.5E A-LSL	**0.65**	10.3	10.3	13.4	16.7	15.5	**2.8**	5.3	18.7	17.4	**1.0**	2.4
1.9E DF-LVL	**0.82**	13.1		17.3	19.9	17.9	**2.0**	5.2			**1.3**	3.3
2.0E DF-LVL		13.8	12.4	18.8	22.4	20.2	**2.0**	5.2	26.5	23.8	**1.3**	3.3
2.0E DF-PSL	**0.86**	13.8	15.5	20.0	21.8	20.0	**2.0**	5.2	21.1	19.3	**1.4**	3.3

Table 3-3: German Design Properties according to Z-9.1-323/245/241

			Axial		Joist (Edgewise)				Plank (Flatwise)			
Material	**G**	$E_{B\parallel}$	$\sigma_{t\parallel}$	$\sigma_{c\parallel}$	$\sigma_{B\parallel}$ 14cm	$\sigma_{t\perp}$	τ_{yx}	$\sigma_{c\perp}$	$\sigma_{B\parallel}$ 14cm	$\sigma_{t\perp}$	τ_{zx}	$\sigma_{c\perp}$
	[GPa]		[MPa]									
1.5E A-LSL	**2.10**	10.5	12.0	13.0	15.7	1.5	**4.0**	3.2/ 6.5	12.5	1.5	**1.8**	1.5/ 2.0
2.0E DF-LVL	**0.75**	14.5	17.0	19.0	21.0	0.5	**2.5**	3.3/ 4.5	21.0	0.5	**1.3**	2.0/ 3.3
2.0E DF-PSL	**0.75**	14.5	18.0	20.0	21.0	0.2	**2.8**	2.6/ 4.1	21.0	0.2	**1.0**	1.6/ 2.9

3.2 Sample Size

The calculated sample size was determined according to ASTM D-2915 standard. The equation used to estimate the sample size was,

$$n = \left(\frac{t * COV}{\alpha} \right)^2 = \left(\frac{2 * 0.1}{0.05} \right)^2 = 16 \qquad (3\text{-}1)$$

where:

n : sample size

t : statistical constant (from Table 1 of ASTM D-2915)
t = 2, based on a 95 % confidence level

COV : coefficient of variation
(approximated by 10 %, according to the results of Craig and Lam, 1996)

α : precision of estimate, α = 0.05

However it was decided to test all the available material. The actual sample size was 29 pieces of LSL, 30 pieces of LVL, and 26 pieces of PSL, resulting in 85 samples in total, to increase the statistical significance and to account for problems that might occur during testing.

3.3 Measurements

The dimensions, weight, modulus of elasticity (MOE), moisture content (MC), specific gravity (SG), on an oven-dry basis, maximum torque and rotation angle at failure, as well as time to failure were recorded for each specimen. In addition, the failure mode was observed and sketched for each

sample and photographs were taken for representative samples. The dimensions and the weight of the specimens were measured first, where the width and depth were taken on both ends and in the middle of the samples and subsequently averaged. Next, the modulus of elasticity (MOE) was nondestructively determined via stress wave timer (Metriguard, 239 A) and the third-point (four-point bending) test. In bending tests, the specimens were loaded in flatwise orientation as planks. The applied load was well within the elastic range, resulting in a maximum flexural stress of approximately 10 MPa (1,500 psi). Deflections were measured at mid span on the neutral axis, or mid depth, of the beam using a string potentiometer. The load-deflection relation was linearly regressed over a range of 30 % to 90 % of the applied maximum load.

After bending tests, 76 mm (3 in) pieces were cut from each end of the specimens for ASTM shear block tests. The remaining length, 1372 mm (54 in), was about 9.8 times the larger cross-sectional dimension and still well exceeded the eight times the depth recommendation given in ASTM D 198 for torsion tests. This procedure was used to make sure that the measured MOE was applicable to the whole length of the specimen and was also necessary to be able to fit the specimen into the torsion machine that offered a maximum span of 1397 mm (55 in). Additionally, it ensured that the ASTM shear block samples, which were obtained from the specimens trim ends, originated from the untested portion of the beam. There was no need to take the shear block samples from close to the area were failure occurred, since for reconstituted SCL the MOE does not vary along the length. Also, there might be some delamination during tests. In general, the MOE was measured to make sure that all specimens were within a close range. MC and SG were determined from the shear block samples that were cut from the trim ends of the beams before the torsion test was conducted. MC was determined via the oven-drying and weighing method in accordance with ASTM D 4442, method A. SG was determined using the water immersion procedure following ASTM D 2395, method B. SG was derived on an oven-dry basis, i.e., dividing oven-dry weight by oven-dry volume. Both measurements, MC and SG,

took place directly after the shear block tests were finished. All tests and measurements were completed within about two weeks.

Data acquisition and handling was performed using a load cell, a string potentiometer, a datalogger and a small computer. The following testing machines, all manufactured by Tinius Olsen, were used. To measure maximum torque values at failure, a torsion machine of type SN 2800 with a capacity of 6779 Nm (60,000 lbf-in), to determine MOE via third-point bending test a universal testing machine having a capacity of 534 kN (120,000 lbf), and to evaluate maximum load for shear block testing a smaller test machine capable of a capacity of 267 kN (60,000 lbf).

3.4 Test Methods

All tests were conducted according to the ASTM standards. The third-point bending test as well as the torsion test followed the ASTM D 198 procedure applicable to structural-size lumber and ASTM D 4761 addressing lumber and wood-base structural material. The shear block tests on small, clear specimens were conducted in accordance with ASTM D 143 and ASTM D 5456 for the evaluation of SCL products.

3.4.1 Third-Point Test

The setup for the third-point, or four-point bending, test is shown schematically for LVL in Figure 3-2. It consisted of two 152 mm (6 in) wide support plates and two symmetrically placed load bearing plates of 203 mm (8 in) width at the third points. The load plates were rounded with a radius of 279 mm (11 in). There was no overhang. The end of the beam and the outer edge of the support plate coincided with each other. One support can be idealized as a pin,

allowing rotation only, while the other one, a roller support allowed translation as well as rotation. The specimens were loaded well within the elastic range in flatwise bending; therefore, no lateral support was necessary. The span L equaled 1372 mm (54 in), resulting in a span/depth (L/b) ratio of 31, which is very close to the recommendation of 32 given in ASTM D 4761 for 38 mm thick lumber. The total length of the samples was 1524 mm (60 in). The span length (L) of the samples was 1372 mm (54 in) with a half shear span (a) of 457 mm (18 in) resulting in an a/b ratio of 10.4, which is in the range of 5 to 12 as recommended in ASTM D 198.

Figure 3-2: Third-Point Test Setup – Flatwise Bending

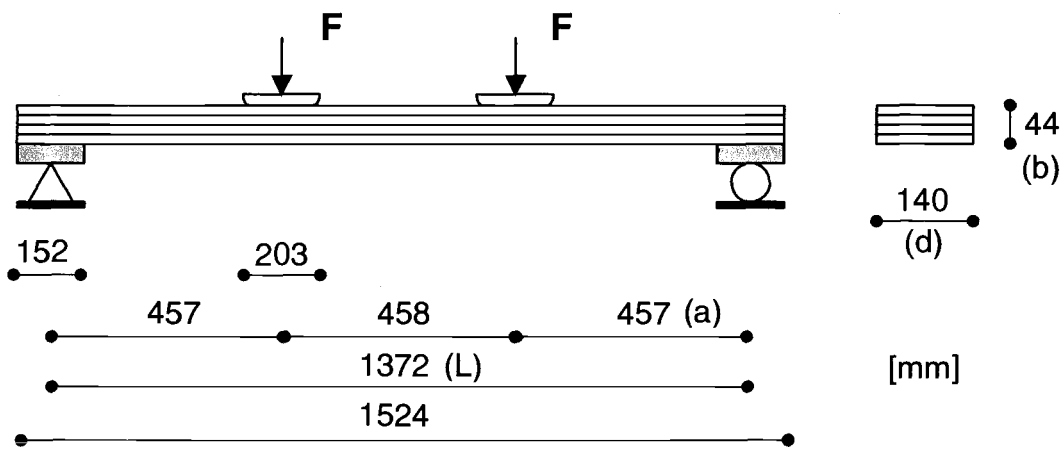

3.4.2 Shear Block Test

The shear block test was performed because it is the current standard test method to evaluate longitudinal shear strength, for SCL as well as for SSL, in the United States. According to ASTM D 5456 the tests were conducted in two different setups (Figure 3-3), to induce shear failure in the longitudinal-tangential (**LT**) plane, called the **plank** orientation, as well as in the longitudinal-radial

(**LR**) plane, called the **joist** orientation. Two shear blocks were manufactured from the trim ends of each beam to obtain one sample in each orientation per beam. Consequently two series of 85 samples each, or 170 samples in total were tested The dimensions of the small, clear shear blocks had to be modified from those given in ASTM D 143 since the width of the samples was only 44 mm (1.75 in) which is less than the required 51 mm (2 in). According to ASTM D 5456, the shear failure plane was kept constant at 2600 mm^2 (4 in^2). Therefore adjustments in the height of the samples were necessary for the joist specimens, i.e., the height had to be increased from 51 mm (2 in) to 58 mm (2.3 in). The different dimensions, orientations and failure planes are shown schematically for LVL in Figure 3-3.

Figure 3-3: Shear Block Dimensions

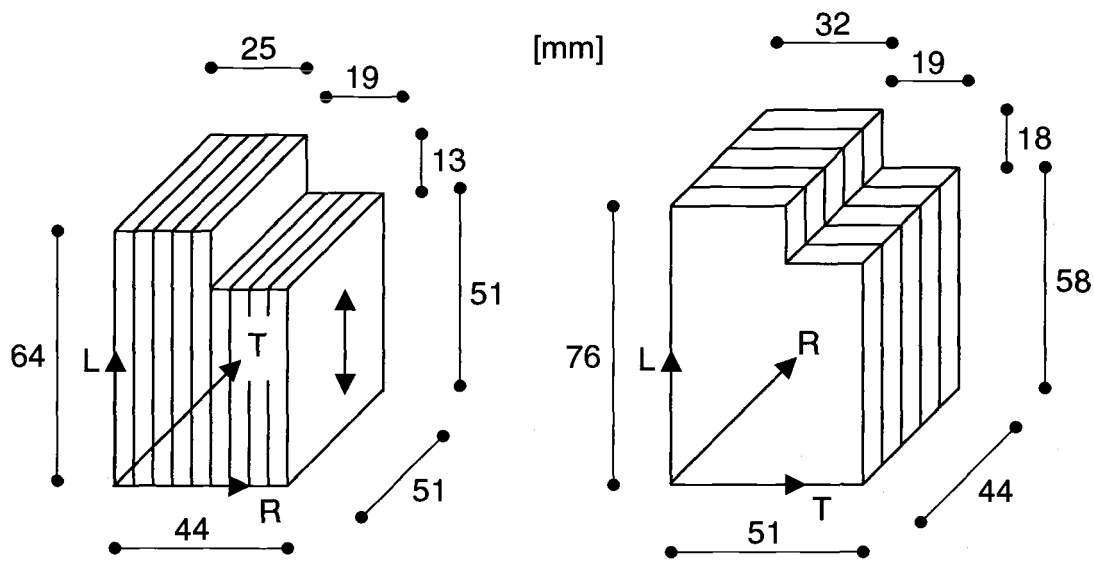

Plank Orientation
TL – Failure Plane
τ_{RL} – Shear Strength

Joist Orientation
RL – Failure Plane
τ_{TL} – Shear Strength

The actual dimensions for the samples in plank orientation were 44 x 51 x 64 (1.75 x 2 x 2.5) whereas the dimensions of the blocks in joist orientation were 51 x 44 x 76 (2 x 1.75 x 3). The failure plane was 51 x 51 (2 x 2) for the plank orientation and had to be modified to 44 x 58 (1.75 x 2.3) for the joist orientation. All values are in millimeters [mm], the values in parenthesis are in inches [in]. Otherwise the shear block tests followed ASTM D 143. A usual shear test jig, applying an offset of 3 mm (⅛ in) between the inner edge of the supporting surface and the plane of the adjacent edge of the loading surface was utilized. This offset permits the shear failure to occur in the plane of least resistance, however it simultaneously increases the bending moment, which is applied to the specimen. The load was applied on the end grain surface at the 19 mm (¾ in) deep reentrant corner. Data recorded for the shear block tests included only the maximum load at failure and the time to failure. The load was measured every second. No displacements were measured. The shear strength for this test method was derived as follows.

$$\tau_{ASTM} = \frac{F}{A} \tag{3-2}$$

where:

F : maximum force at failure

A : failure plane

τ_{ASTM} : shear strength

The objective for this test method was to compare the shear block based shear strength with the torsion based shear strength, which will be described in the next section.

3.4.3 Torsion Test

The torsion test followed ASTM D 198. The specimen length was again 1372 mm (54 in), which was 9.8 times the depth and therefore well above the eight times the larger cross-sectional dimension recommendation given in the standard. A gripping distance in longitudinal direction of 51 mm (2 in) was used. Furthermore, a distance of two times the depth (2d), 279 mm (11 in), was provided on each side to exclude end, or clamp effects. As shown by Heck (1997), it is assumed that shear stress distribution is constant within the shear span of 5d, 712 mm (28 in).

Each of the 85 full-size specimens was destructively tested in the same manner. The maximum torque and rotation angle at failure, as well as time to failure were recorded. Measurements were taken every second. The test setup is shown in Figure 3-4 followed by a schematic and a photograph of the torsion machine in Figures 3-5 and 3-6, respectively.

Figure 3-4: Torsion Test Setup

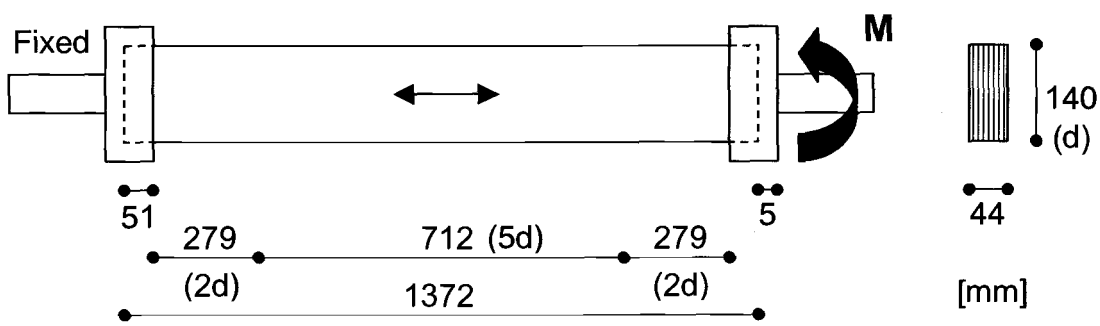

Figure 3-5: Schematic of Torsion Machine

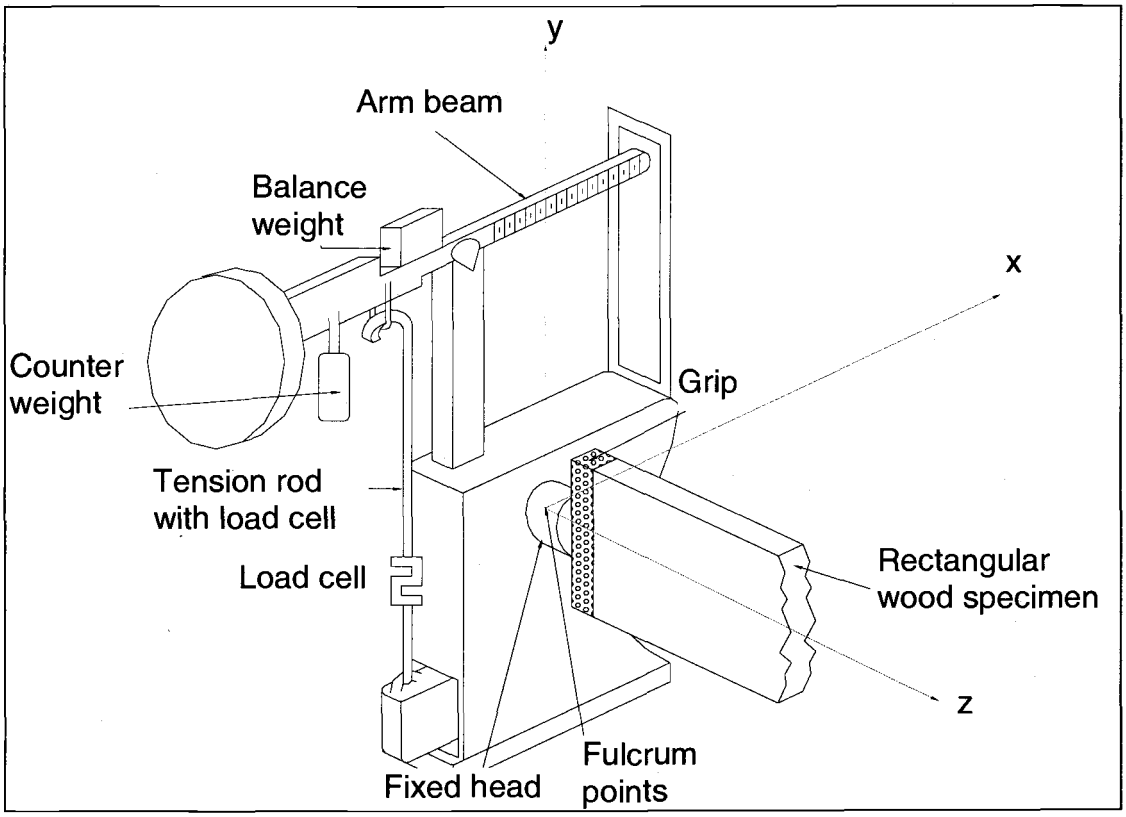

The schematic is taken from Heck (1997), who gave a very detailed description of the torsion machine that has been used and the modifications and calibrations that were applied to the testing equipment. Following is just a short summary on the most important points, but the interested reader is invited to consult the quoted reference to get a better understanding for the conducted torsion tests. The torsion machine was deformation driven and provided a constant rate of twist to the rotating head, while the head on the opposite beam end was fixed. The rotation of the specimen was set equal to the twist of the loading head that was measured by means of a string potentiometer. The applied torque was transferred to a load cell via the fixed head. Data acquisition was

performed using a datalogger and a small computer. A calibration of the test equipment was performed before testing started and the obtained relations were directly input, so that the values recorded by the datalogger were the final torque and twist values. Vise-like clamps securely clenched the beam over the entire depth and a grip length of 51 mm (2 in) in longitudinal direction. The grips were placed symmetrically about the center of the cross-section allowing the beam to rotate about its longitudinal axis. Both grips did not allow for longitudinal movement. The setup restricted longitudinal movement on the wide faces over the small contact area between specimen and clamps. Warping torsion was not considered. As compensation, a gap between the beam end face and the clamp end of about 5 mm (1/5 in) was provided to allow for free (unrestrained) warping. This procedure was taken to justify the assumption of St. Venant torsion.

Figure 3-6: Photograph of Torsion Machine

3.4.4 Determination of Shear Stresses

Two different approaches were taken for the evaluation of the shear stresses. First, isotropic material behavior was assumed and the equations by Trayer and March (1930), also given in ASTM D 198 standard were applied to calculate the shear stresses. Second, a more sophisticated approach was taken assuming orthotropic material behavior. This method followed Lekhnitskii's (1981) approach for an anisotropic body.

In the case of longitudinal torsion the shear stresses τ_{RL} and τ_{TL} in the two longitudinal planes (TL and RT) are both causing shear failure parallel to the grain. The difference between the two stresses is their location with respect to grain angle. The stress τ_{RL} with its maximum value acting on the center of the short side of the cross-section causes longitudinal shear failure with a grain angle of 0°, or along the annual rings, i.e., parallel to the depth, in tangential direction. On the other hand τ_{TL} with its maximum value located on the center of the long side causes longitudinal shear failure for a grain angle of 90°, or across the annual rings, i.e., parallel to the width, in radial direction. Orientations and shear stresses are shown in Figure 3-7. The possible shear planes are marked by the broken, red lines. The third shear stress τ_{RT}, acting in the transverse RT-plane causes rolling shear; however it is of no practical importance, since τ_{RT} theoretically equals zero in the case of axial torsion.

Figure 3-7: Shear Stresses

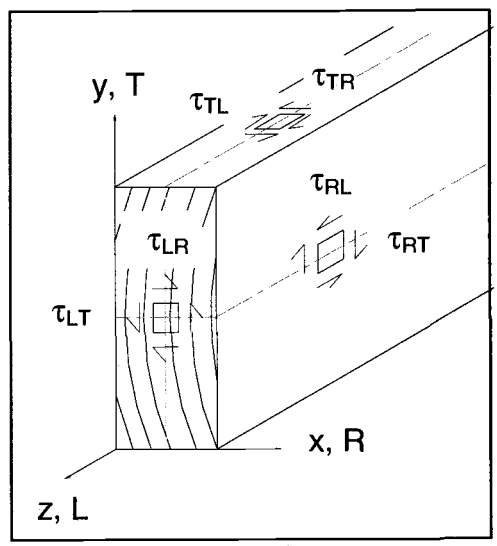

3.4.4.1 *Isotropic Material Behavior*

Materials that exhibit no internal symmetry and hence no directional properties are termed isotropic. Assuming an isotropic material behavior the following equations were used to ascertain the shear stresses that led to failure.

$$\tau_{LT-I} = \frac{8M\gamma}{hb^2\mu} \tag{3-3}$$

$$\tau_{LR-I} = \frac{8M\gamma_1}{b^3\mu} \tag{3-4}$$

where:

τ_{LT-I} : maximum isotropic shear stress on the center of the long side

τ_{LR-I} : maximum isotropic shear stress on the center of the short side

M : maximum torsional moment at failure

b : beam width

h : beam depth

γ, γ_1, μ : factors depending on the aspect or side ratio (see ASTM D 198)

The shear stresses obtained by isotropic equations are independent of material properties. Only three parameters influence the results and these are the cross sectional dimensions, namely depth and width, and the maximum torque at failure. For samples with rectangular cross section, τ_{LT-I} is always greater than τ_{LR-I}. The maximum shear stress according to the given equations always occurs on the center of the long side, or wide face. This approach was

taken by Riyanto (1996) and Heck (1997) in their studies on solid-sawn Douglas-fir lumber. In this study, all three evaluated composites showed a different failure behavior than the one observed by Riyanto (1996) and Heck (1997) on SSL, as will be described in the results section. Furthermore, one of the three composites tested here showed a different failure behavior than the other two. For this reason, an orthotropic torsion theory approach was used to describe the failure behavior.

3.4.4.2 *Orthotropic Material Behavior*

Orthotropic materials are anisotropic, but symmetric about three mutually perpendicular planes. Simultaneously, they are characterized by directional properties. Applying orthotropic theory to wooden beams of rectangular cross section under torsion is definitely more complex than just assuming isotropic behavior. However, it is more realistic since material properties are considered. Especially the two shear moduli in LR and LT plane have fundamental influence on the results for shear strength. The following equations are taken from Lekhnitskii (1981). He emphasized, that for an orthotropic beam the maximum shear stress might occur on the center of either the long ($\tau_{LT\text{-}O}$) or the short ($\tau_{LR\text{-}O}$) side. Shear stresses are therefore not only depending on the aspect, or side ratio, but also on the ratio of the two shear moduli in longitudinal direction. Shear stresses based on orthotropic material behavior are given by:

$$\tau_{LT-O} = \frac{k_1 M}{hb^2} \tag{3-5}$$

$$\tau_{LR-O} = \frac{k_2 M}{hb^2 \mu} \tag{3-6}$$

where:

$\tau_{LT\text{-}O}$: maximum orthotropic shear stress on the center of the long side

$\tau_{LR\text{-}O}$: maximum orthotropic shear stress on the center of the short side

M : maximum torsional moment at failure

b : width

h : depth

c : aspect or side ratio ($c = h/b > 1$)

G_{LT} : shear modulus in LT-plane

G_{LR} : shear modulus in LR-plane

g, μ : ratio of shear moduli and its square root ($g = G_{LT}/G_{LR}$; $\mu = \sqrt{g}$)

d : factor depending on the ratios of shear moduli and sides

k_1, k_2 : factors to be interpolated from Table 3-1, depending on c and d

d : factor depending on the ratios of shear moduli and sides ($d = c/\mu$)

Torsional rigidity, angle of twist per unit length and total twist are given by:

$$C = G_{LT} h b^3 \beta \tag{3-7}$$

$$\omega = \frac{M}{G_{LT} h b^3 \beta} = \frac{M}{C} \tag{3-8}$$

$$\theta = \omega l = \frac{Ml}{C} \tag{3-9}$$

where:

C : torsional rigidity

β : factor to be interpolated from Table 3-1, depending on c and d

ω : angle of twist per unit length [rad/m]

θ : total angle of twist at maximum torsional moment [rad]

l : length

Note the difference between the parameters in the two theories, especially μ is not defined in the same way, although the same variable has been used. Table 3-4 presents values for the factors that are needed to derive the orthotropic torsional shear stresses and is taken from Lekhnitskii (1981). The factors k_1, k_2, β were derived based on mathematical series and are valid for orthotropic, rectangular beams with one fixed end and the other end subjected to a torsional moment. No other loads were applied. Lekhnitskii solved a 2nd order differential equation for the stress function Ψ applying Fourier sine series.

Table 3-4: Orthotropic Factors

D	β	k_1	k_2	d	β	k_1	k_2
1	0.141	4.803	4.803	3	0.263	3.742	2.820
1.25	0.172	4.545	4.141	4	0.281	3.550	2.644
1.5	0.196	4.329	3.718	5	0.291	3.430	2.548
1.75	0.214	4.184	3.431	10	0.312	3.202	2.379
2	0.229	4.065	3.232	20	0.323	3.098	2.274
2.5	0.249	3.882	2.970	∞	0.333	3.000	-

3.5 Finite Element (FE) Modeling

The experimental torsion test configuration was modeled using the finite element method to illuminate the state of stress within the orthotropic specimen, to clarify the stress distribution and to investigate, if there are stress concentrations at the restrained contact areas between the specimen and clamps.

Figure 3-8: Orientations

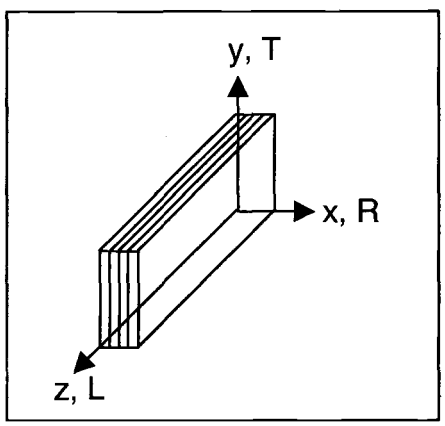

The commercial finite element program ANSYS 5.6® (Swanson 1999) was used to perform the analysis. A 3-dimensional, 8-node brick element was used to model the specimen. The SOLID45 element offered 6 degrees of freedom per node, allowing translations and rotations in the three major directions. The analysis focused on the full-size specimen with nominal dimensions of 44 x 140 x 1372 mm^3 (1.75 x 5.5 x 54 in^3) under torsion. The orientations were chosen as depicted in Figure 3-8. The x-axis represented the radial direction (R), the y-axis the tangential one (T) and the z-axis was oriented longitudinally (L).

3.5.1 Mesh

Initially, the idea was to apply elements with square cross section. Therefore, seven elements were used along the width and 22 along the depth. Care was taken not to exceed an aspect, or side ratio of two for the chosen elements. As a result, 108 elements were used along the length and no size factor, i.e., all elements had the same size, was employed. A ratio of 1:1:2 for the dimensions of an element in the x, y and z directions was applied. Heck, 1997 investigated the effects of different element lengths along specimen length (z-axis) on the model of a beam subjected to torsion. Heck concluded that changing the element length had no or negligible effect on the value of the maximum shear stress as well as on the location of the maximum shear stresses.

Finally, an even number of elements in each direction was preferred, because the chosen elements did not have nodes at mid side. Consequently, an even number of elements was more comfortable to analyze the stresses. A size factor, or mesh ratio, of outside edge element to middle inside element, of four was introduced to further refine the mesh at the center of the faces where the highest shear stresses were expected. This size factor was only applied along the depth and width, but not along the length following Heck's results. The mesh that finally served as basis for the FE model was composed of

6 x 22 x 108 = 14256 elements and 7 x 23 x 109 = 17549 nodes. An end view on the meshed cross section of the beam is depicted in Figure 3-10. This mesh is already very fine and further refinement would not be appropriate since the results are mainly influenced by the set of elastic constants.

Figure 3-9: Beam under Torsion, Loads and Boundary Conditions

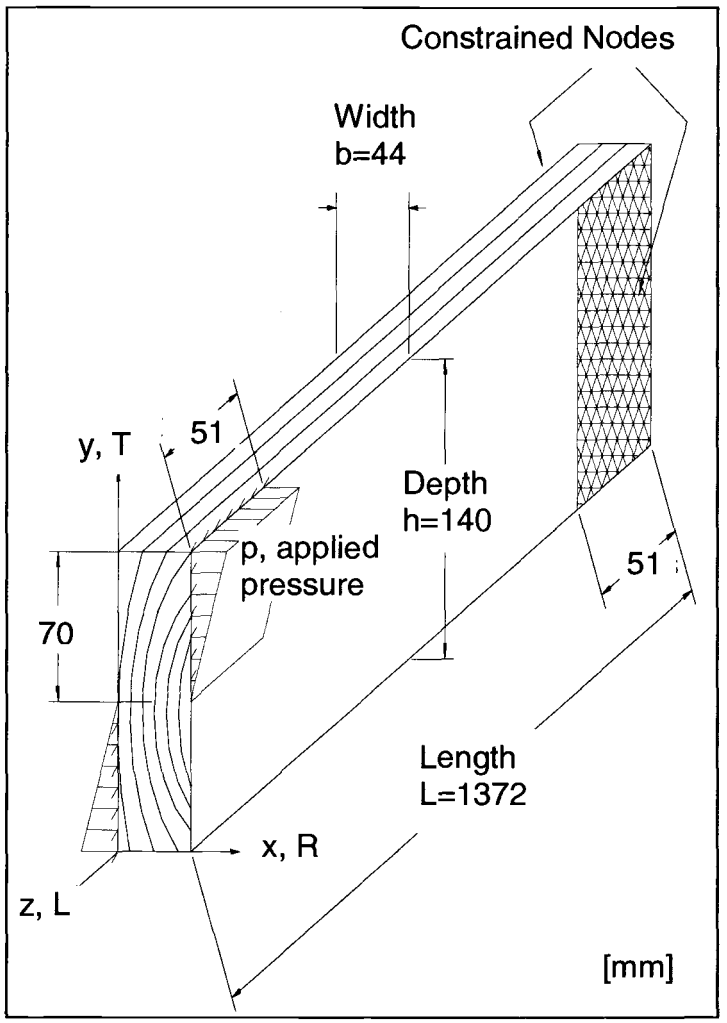

Figure 3-10:Cross Sectional Mesh, 6 x 22 Elements, Size Factor 4

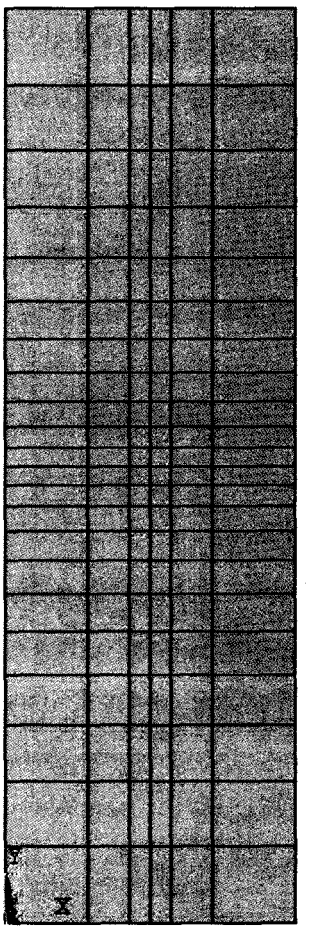

3.5.2 Boundary Conditions (BC)

One end of the beam was fixed while the opposite end had a twisting moment. The fixed end was modeled as follows. All nodes in longitudinal direction within the gripping distance of 51 mm (2 in) on the surface of both wide faces were fixed over the entire depth. All degrees of freedom were constrained for these nodes. The end face and both narrow faces were not restrained. Figure 3-9 is taken from Heck (1997), who applied the same torsion test on solid-sawn Douglas-fir beams, and shows the applied pressure and the constrained nodes. This procedure best described the actual test conditions and was as close as possible to pure St. Venant torsion, i.e., unrestrained warping, while still securely clenching the specimen. Unrestrained warping was possible for the entire end face and both narrow faces. The constraints at the wide faces were necessary to provide model stability. The twisted end of the model better reflects the real test conditions, since the restraints in longitudinal direction of the fixed end might slightly influence the state of stress.

3.5.3 Loads

The idea of modeling the applied torque was to use a force couple. It was decided to choose a triangular pressure distribution instead of a uniform one or just point loads to avoid high stress concentrations and to model the experimental tests more realistically. The tests consistently showed more impact on the corners of the wide faces compared to the center. Consequently, a triangular pressure distribution was applied to the gripping length of 51 mm (2 in) and one half of the pressure couple loaded the lower depth while the other one was imposed on the upper half on the opposite side as shown in Figure 3-9.

Two different load cases were investigated. For the first one, the applied torque was within the linear range of the moment – rotation angle distribution obtained by the tests. A torque of M = 300 Nm was chosen for this case. Second

the average ultimate torsional moment at failure for each of the three composites was applied. As will be shown later in the results section the following values were obtained from the torsion tests on SCL.

Mean torque values at failure:

LSL: $M_{Tmax} = 850$ Nm

LVL: $M_{Lmax} = 570$ Nm

PSL: $M_{Pmax} = 460$ Nm

The torque values were converted into equivalent force and pressure values using the following equations based on simple statics. The slope was determined since it was needed as an input variable for the finite element program. All necessary input values for the different load cases are summarized in Table 3-5.

Force: $$F = \frac{3M}{2d}$$

Pressure: $$p = \frac{4F}{dz}$$

Slope: $$s = \frac{2p}{d}$$

where:

M:	torsional moment
d = 140 mm	beam depth
z = 51 mm	gripping distance in longitudinal direction

Table 3-5: Input Values for FE Analysis to apply Torque

	Moment M [Nm]	Force F [N]	Pressure p [N/mm^2=MPa]	Slope s [N/mm^3]
Elastic Range	300	3221	1.82	0.0260
LSL	850	9123	5.14	0.0736
LVL	570	6117	3.45	0.0494
PSL	460	4937	2.78	0.0398

3.5.4 Orthotropic Material Properties

The finite element model used isotropic and orthotropic material properties. Heck (1997) concluded that for solid-sawn Douglas-fir it was not beneficial to perform an orthotropic analysis, since the results between an orthotropic finite element analysis and isotropic theory according to Trayer and March (1930) differed only by 1.3 %. However, it was believed that SCL might behave different from solid-sawn Douglas-fir and even for different wood species this trend might not be the same. Therefore this study investigated the orthotropic behavior of three different types of SCL. The assumption that the radial and the tangential moduli of elasticity (MOE) are equivalent had to be taken, since no source was found that offered more detailed values. However, this assumption was not restrictive since numerous calculations with varying transverse MOE values and even different values in radial and tangential direction did not have significant effects on the results. It turned out that the results were heavily

dependent on the two shear moduli in the longitudinal plane, G_{xz} and G_{yz}, whereas all other elastic constants, even the longitudinal MOE value E_z, where only of minor importance.

The longitudinal MOE values (E_z) were measured via third-point bending tests. The transverse MOE and all shear moduli values were calculated using elastic constant ratios for SCL given by Hindman (1999), based on the measured value for axial MOE. The Poisson Ratios are taken from the *Wood Handbook* (1999) for solid wood. The values for Douglas-fir are taken (1) from the *Wood Handbook* (1999) and for comparison also (2) from Bodig and Jayne (1982) as shown in the last row of Table 3-6 that shows all input values used.

Table 3-6: Orthotropic Material Properties

	MOE [MPa]		Shear Moduli [MPa]			Poisson Ratios [1]		
	$E_x=E_y$	E_z	G_{xy}	G_{xz}	G_{yz}	ν_{xy}	ν_{xz}	ν_{yz}
Material	$E_R=E_T$	E_L	G_{RT}	G_{RL}	G_{TL}	ν_{RT}	ν_{RL}	ν_{TL}
LSL	1207	11000	94.5	318	782	0.496	0.054	0.022
LVL	397	14600	44.4	407	593	0.390	0.036	0.029
PSL	404	15000	72.8	310	398	0.390	0.036	0.029
Douglas-fir-1	870	14740	103.0	943	1150	0.390	0.036	0.029
Douglas-fir-2	805	14762	85.1	800	743	0.432	0.022	0.017

4. Results and Discussion

The main goal of this study was to evaluate the torsion test as a method to determine the shear strength of structural composite lumber (SCL). The results of the torsion and ASTM shear block tests, and the finite element (FE) analysis are presented and discussed in this chapter. First, some general comments on the test materials are made. Second, the results obtained by torsion tests of full-size SCL are presented, accompanied by an evaluation of the observed failure modes. Third, results of the finite element modeling of the full-size SCL specimens subjected to torsion are discussed followed by a comparison with the experimental results. Next, the results obtained by tests on small shear blocks according to ASTM D 143 are documented. Finally, comparisons between test results on (a) full-size SCL versus small shear blocks, and (b) full-size SCL versus full-size solid-sawn lumber (SSL) are drawn.

4.1 Material

The MOE rating as given by the manufacturer, specimen size (n), actual dimensions, density (ρ), and the results of the modulus of elasticity (MOE) evaluation are presented in Table 4-1. MOE was determined in flatwise static bending (E_f) via the third-point test and by means of a stress wave timer (E_d).

Table 4-1: Properties of the Test Material

Rating Species Material	MOE Rating	n	b	h	L	Density (ρ)		Modulus of Elasticity			
								Third-Point Bending (E_f)		Stress Wave (E_d)	
	[GPa]		[mm]			Mean [g/cm^3]	COV [%]	Mean [GPa]	COV [%]	Mean [GPa]	COV [%]
1.5E A LSL	10.3	29	44.2	139.1	1371	0.711	3.3	11.0	11.0	11.7	4.5
1.9E DF LVL	13.1	30	44.3	140.4	1370	0.573	3.6	14.6	14.4	12.9	10.4
2.0E DF PSL	13.8	26	42.7	139.5	1371	0.660	2.8	15.0	7.1	14.8	8.1

The actual dimensions conformed well with the standard dimensions (44.5 x 139.7 mm^2), except for PSL that was almost 2 mm less wide. The density is based on the condition after the material was stacked in an uncontrolled room (test bay) for two months and allowed to come to equilibrium. The density is based on an air-dried condition and measurements on the full-size specimens. LSL showed the highest density and LVL the lowest one. The variability was very low for all three composites. MC was not measured before the tests were started, but was believed to conform well with the information given by the manufacturer (6 – 9 %), as documented in section 3-1.

MOE was evaluated by two different test methods. First, dynamic modulus of elasticity (E_d) was nondestructively determined via stress wave timer (Metriguard, 239 A) applying axial vibrations on the specimens. For LVL, E_d (12.9 GPa) turned out to be lower than the E-rating (13.1 GPa) given by the grade stamp. Therefore, MOE was additionally determined via flatwise bending (E_f). Except for E_d for LVL, all tested MOE values were higher than the E-ratings. For both test methods, PSL showed the highest stiffness and LSL the lowest, as expected by the E-ratings. The MOE values obtained by the two different test methods were within a close range. For LSL, a 6.4 % higher dynamic value (E_d)

was observed, compared to the static one (E_f), which is within the typical range of 5 – 15 %, as mentioned by Bodig and Jayne (1982). However, LVL showed a 12 % lower dynamic value. In addition, the variability was highest for LVL for both test methods, yet still within the expected range. The high variability of LVL might be due to the fact that within the manufacturing process the veneers are graded individually and sometimes laid up in a certain sequence according to their MOE values. The result is a stiffness gradient through the thickness, with higher rated veneer on the outside faces and lower quality veneer in the core. The stress wave method and especially the axial vibration approach that was applied in this case might be more susceptible to such a stiffness gradient. This topic will be further discussed in the following section. Another possible explanation for the high variability of LVL was the different veneer thickness, resulting in different number of plies within the tested LVL material, as mentioned earlier in section 3.1.2.

4.2 Torsion Test

4.2.1 Experimental Results

Sample size (n), maximum torque (T_{max}) and corresponding twist at failure (θ), as well as loading rate and time to failure (t) are listed in Table 4-2. The log file was not opened for one PSL sample, leaving 25 specimens. The complete torsion test data for all specimens is given in the appendix.

Table 4-2: Torsion Test Data

Material	n	Maximum Torque (T_{max})		Twist (θ)		Loading Rate [rad/m/min]		Time to Failure (t)	
		Mean [Nm]	COV [%]	Mean [deg]	COV [%]	Mean	COV [%]	Mean [s]	COV [%]
LSL	29	850	8.3	29.0	8.1	0.10	18.3	219	22.4
LVL	30	570	5.9	28.6	7.2	0.11	8.1	202	10.7
PSL	25	460	7.1	31.5	11.8	0.11	6.9	224	13.1

The maximum torque values were used to determine maximum shear stresses (Table 4-3) in the specimens. Maximum torque ranged between 744 - 963 Nm for LSL, 511 - 638 Nm for LVL, and 375 - 516 Nm for PSL. The mean value of maximum torque was highest for LSL (850 Nm), whereas LVL (570 Nm) and PSL (460 Nm) showed articulately lower values. LSL is therefore clearly the strongest of the three composites in torsion, followed by LVL and PSL. The COV related to torque was low (6 – 8 %). The measured twist at failure was within a narrow range of 25 - 32 degrees for LSL and LVL and up to 41 degrees for PSL. The mean twist at failure was almost equal for LSL (29.0 deg) and LVL (28.6 deg) and slightly higher for PSL (31.5 deg) that also showed the highest COV (12 %). The loading rate varied between 0.08 and 0.13 [rad/m/min] for all samples, averaging 0.10 for LSL, and 0.11 for LVL and PSL. These values of twist in radians per meter of length per minute were within the recommended range of 0.08 to 0.24, given in ASTM D 198. Shear failure generally took place within 3 to 5 minutes. The mean time to failure was 202 s for LVL, 219 s for LSL and 224 s for PSL.

The shear stresses listed in Table 4-3 are the maximum values on the middle of the long and short side of the rectangular cross-section, as explained in section 3.4.4. A summary of the mean torsion test results is presented in Table 4-3 and the cumulative density functions (CDF) of the orthotropic shear

stresses are given in Figure 4-1. The appendix contains the complete torsion test data.

Table 4-3: Torsion Test Results

Material	ISOtropic Shear Stress		ORTHOtropic Shear Stress		COV	Difference Ortho/Iso	
	Long ($\tau_{LT\text{-}I}$)	Short ($\tau_{LR\text{-}I}$)	Long ($\tau_{LT\text{-}O}$)	Short ($\tau_{LR\text{-}O}$)		Long Δ_{LT}	Short Δ_{LR}
	[MPa]				[%]	[%]	
LSL	11.59	8.83	12.69	**6.43**	8.3	+9.5	-27.2
LVL	7.66	5.83	**7.96**	4.90	6.3	+3.9	-16.0
PSL	6.65	5.02	**6.82**	4.55	7.1	+2.6	-9.4

The shear stresses given in Table 4-3 were obtained using Equations 3-3 to 3-6. The variability given in the sixth column is identical for both, isotropic and orthotropic, methods. The shear stresses stated in column two and three ($\tau_{LT\text{-}I}$ and $\tau_{LR\text{-}I}$) are based on isotropic material behavior (Equations 3-3 and 3-4), those in column four and five ($\tau_{LT\text{-}O}$ and $\tau_{LR\text{-}O}$) on orthotropic material behavior (Equations 3-5 and 3-6). The ranking of the materials according to shear stresses is the same than related to torque. Shear stresses are substantially higher in the LT-plane compared to the LR-plane for all three materials and both theories. Regarding isotropic shear stresses, the values in the LT-plane are about 30 % higher compared to those in the LR-plane ($\tau_{LT\text{-}I}/\tau_{LR\text{-}I} \cong 1.3$). This difference is independent of material and due to aspect, or side (h/b) ratio only. It is slightly higher for PSL tat was less wide. However, it looks different, if orthotropic shear stresses, where material properties are considered, are regarded. The different shear moduli ratios ($g = G_{TL}/G_{RL}$) cause a change in the state of stress. A shift from isotropic to orthotropic theory results in a slight increase (3 – 10 %) of the

shear stresses on the long side and a more distinct decrease (9 – 27 %) of the shear stresses on the short side, as shown by Δ_{LT} and Δ_{LR} in the last two columns of Table 4-3. This behavior can be explained by the fact that for all three composites the shear moduli ratio is larger than unity ($g > 1$). Difference Δ between the two theories is mainly dependent on the shear moduli ratio g. The further g from unity, the higher the difference Δ. Difference Δ is therefore highest for LSL ($g = 2.46$), lower for LVL ($g = 1.46$), and lowest for PSL ($g = 1.28$).

The most important columns in Table 4-3 are columns four and five that list the orthotropic shear stresses ($\tau_{LT\text{-}O}$ and $\tau_{LR\text{-}O}$). The three numbers in bold are the shear strengths of the materials, because that is where failure occurred, as will be shown in the next section. From here on, the focus of this study will lie on the orthotropic approach, since a different failure behavior proved the necessity of the consideration of material properties. The orthotropic shear stresses evaluated on the center of the long side ($\tau_{LT\text{-}O}$) are between 50 % (PSL) and almost 100 % (LSL) higher than those evaluated on the center of the short side ($\tau_{LR\text{-}O}$). LVL with a difference in shear stresses between the different locations of slightly more than 60 % disposes in between, but closer to PSL.

The assumption of isotropic material behavior is therefore only on the safe side ($\tau_{LT\text{-}I} < \tau_{LT\text{-}O}$), if failure occurs on the long side, or in joist orientation (LT-plane). However, the shear strength is overestimated and consequently on the unsafe side ($\tau_{LR\text{-}I} > \tau_{LR\text{-}O}$), as soon as failure initiates at the short side, or in plank orientation (LR-plane), as has been observed for LSL in the current study.

In comparison, the reverse is valid, if a material having a shear moduli ratio smaller than unity ($g < 1$) is considered. In such a case, a shift from isotropic to orthotropic theory results in an increase of shear stress (τ_{LR}) on the short side and a decrease of shear stress (τ_{LT}) on the long side. Consequently, the shear stress is overestimated and unsafe ($\tau_{LT\text{-}I} > \tau_{LT\text{-}O}$), if failure initiates at the long side, or in joist orientation (LT-plane), as has been observed for SSL before. This case occurs for most softwoods and all hardwoods, as will be shown later.

Figure 4-1: Cumulative Density Function of Shear Stress

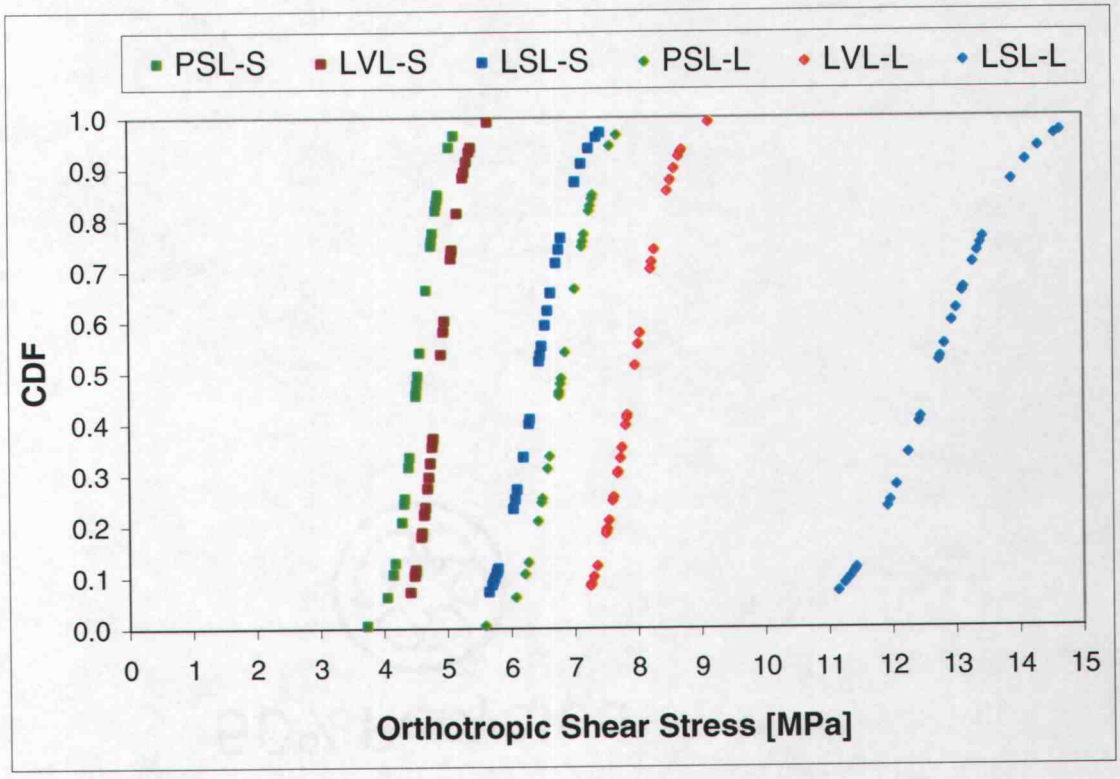

The cumulative density functions (CDF) of the orthotropic torsional shear stresses are visualized in Figure 4-1. The three curves to the left display the shear stresses ($\tau_{LR\text{-}O}$) on the center of the short (S) side, whereas the three curves to the right display the shear stresses ($\tau_{LT\text{-}O}$) on the center of the long (L) side. The graph clearly shows that the two Douglas-fir and veneer based composites LVL and PSL behave similar in torsion, while LSL is able to bear much higher torsional stresses. Note, the ability of LSL to bear higher shear stresses is especially pronounced on the long side (τ_{LT}). Furthermore, the range between LVL and PSL is higher for τ_{LT} on the long side. The graph also depicts that the scatter along the abscissa, that is COV related to shear stresses, is low for all three materials. To obtain the mean orthotropic shear stresses as listed in

Table 4-3 a horizontal line starting at 0.5 on the ordinate has to be drawn until the point of intersection with the curve of interest is reached and then followed by a vertical line to read the value on the abscissa.

4.2.2 Failure Modes

Failure typically initiated at mid span and propagated as a horizontal crack towards the ends of the beam. For some samples failure was more obvious towards one end of the beam compared to the other one. Failure occurred in longitudinal, or grain direction with the sliding direction also parallel to the grain for all specimens. This failure mode is known as shear parallel to grain, or simply longitudinal shear. LSL failed on the center of the short side, at mid width, only. LVL and PSL in contrast, failed mainly, on the center of the long side, at mid depth. The two different failure planes are depicted schematically in Figure 4-2. Failure took place in the LR-plane for PSL and LVL. Considering, for example, LVL, fracture occurred across the veneer thickness and the glue lines in radial direction. Heck (1997) observed the same behavior for solid-sawn Douglas-fir beams, where cracks propagated predominantly across the annual rings. Some LVL and PSL specimens also showed failure cracks on the center of the short side, that however did not seem to cross the entire depth. On the other hand the LT-plane acted as shear failure plane for LSL. In this case failure cracks were along strands and glue lines in tangential direction, as can be observed to the right in Figures 4-2 and 4-3. The end faces of representative samples that have been destructively tested under torsion and where failure cracks have been marked are depicted in Figure 4-3 from left to right for PSL, LVL and LSL.

Figure 4-2: Shear Failure Plane

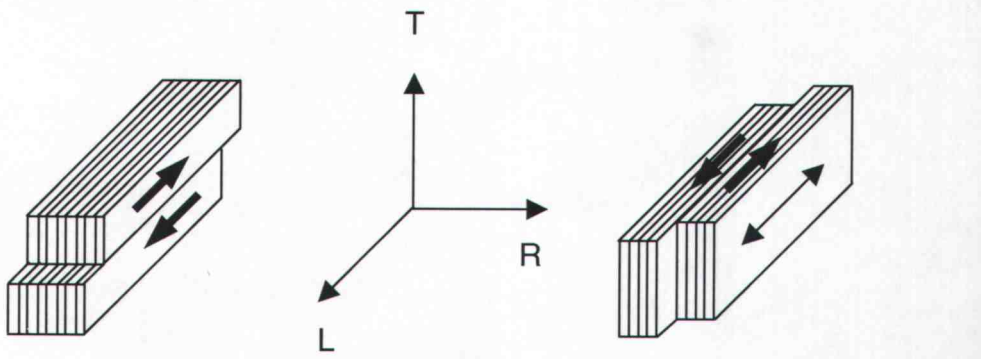

Longitudinal-**Radial** (LR)

Longitudinal-**Tangential** (LT)

Figure 4-3: End Faces of Representative Failed Torsion Samples

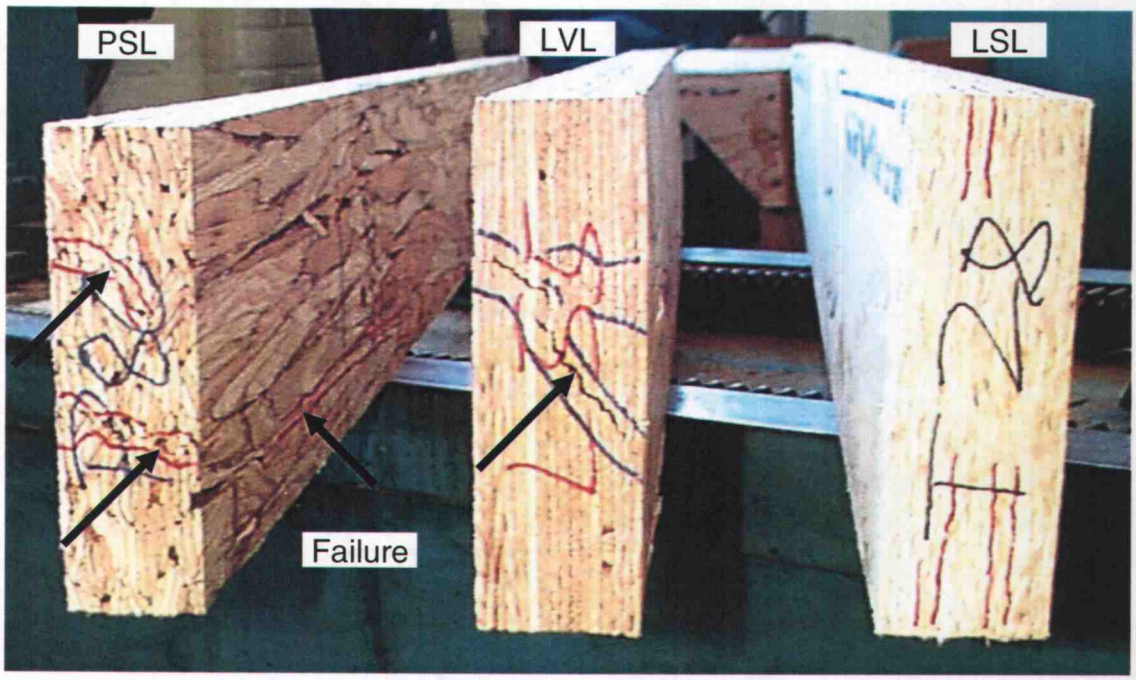

Generally, it is more difficult to detect failure cracks and follow their paths within SCL compared to SSL, because of the many strand or veneer boundaries. The more heterogeneous structure of the composites presents a challenge in this context, especially for PSL where there are numerous strand boundaries that are dark brown due to the PF resin. Photographs of destructively tested torsion samples with marked failure cracks are shown in Figure 4-4 for the different materials. The first two photographs (a, b) show top views on the short side of two different LSL specimens. The next three photographs (c-e) show side views on the long side of one LVL (c) and one PSL (d, e) specimen. There is a lap joint in the outer veneer of the LVL (c) specimen. Further, a longer horizontal crack at about mid depth and a shorter second crack close to the clamp are obvious.

During the testing phase of this study it turned out that the three composites showed a different failure behavior. LSL showed a very brittle failure behavior, i.e., it failed abruptly, in most cases accompanied by a loud bang and a distinct drop in applied torque, without any prior warning. In contrast, LVL and PSL failed more gradually, as can be observed in Figure 4-5. Sometimes the failure of individual veneers or strands was audible and even visible by dust falling down from the specimen, causing a slight drop in the applied torsional moment. Many specimens recovered from these slight drops in torque and were able to endure higher twisting moments, in some cases even more than once. This kind of failure behavior resembled more to a ductile failure type, which is preferred in structural applications and was more pronounced for PSL than for LVL. Moreover, PSL showed the lowest torsional modulus, which is represented by the slope in the torque – twist graph (Figure 4-5). The appendix contains graphs of all torsion samples.

Figure 4-4: Failed Torsion Samples

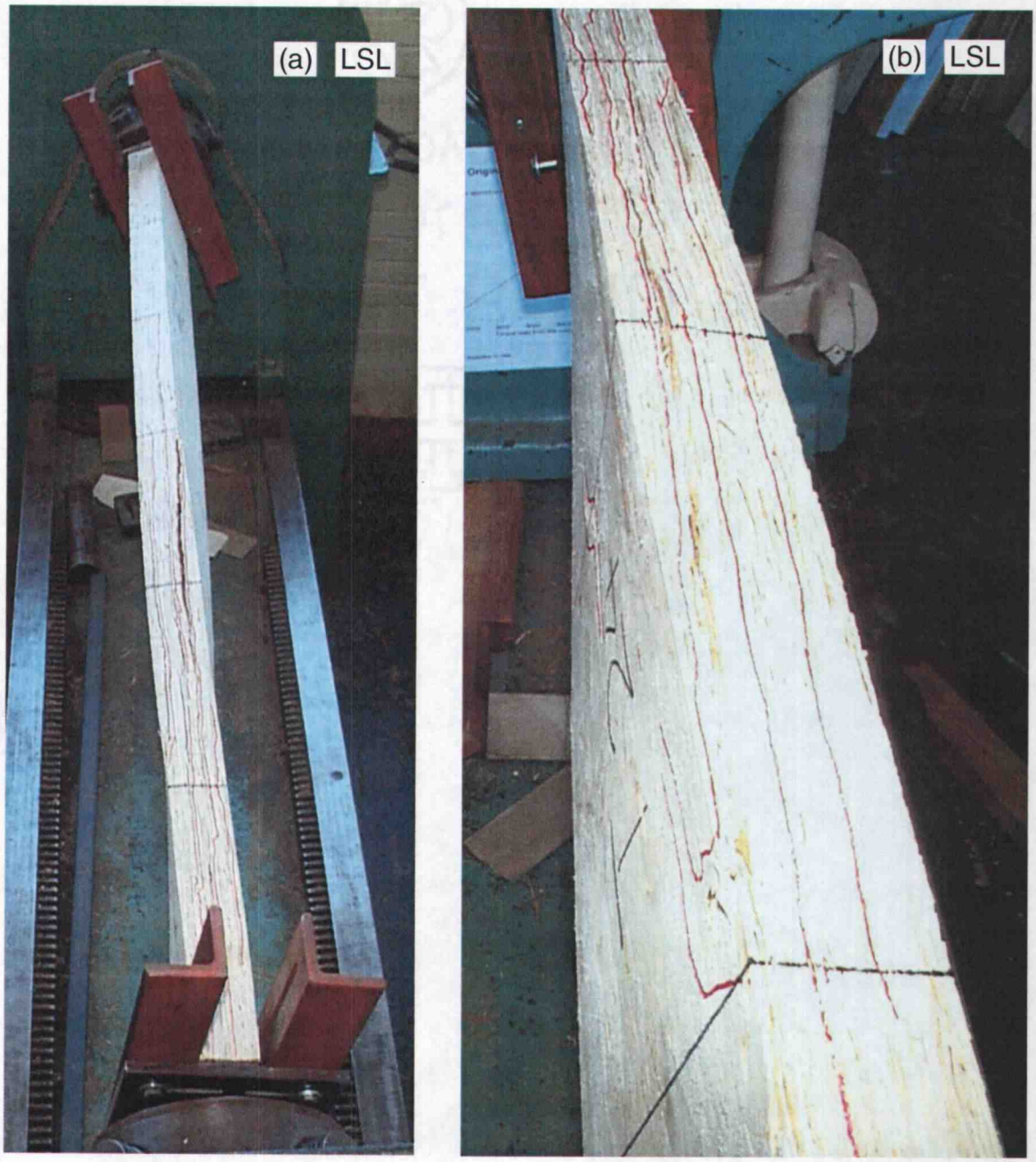

Figure 4-4: Failed Torsion Samples (Continued)

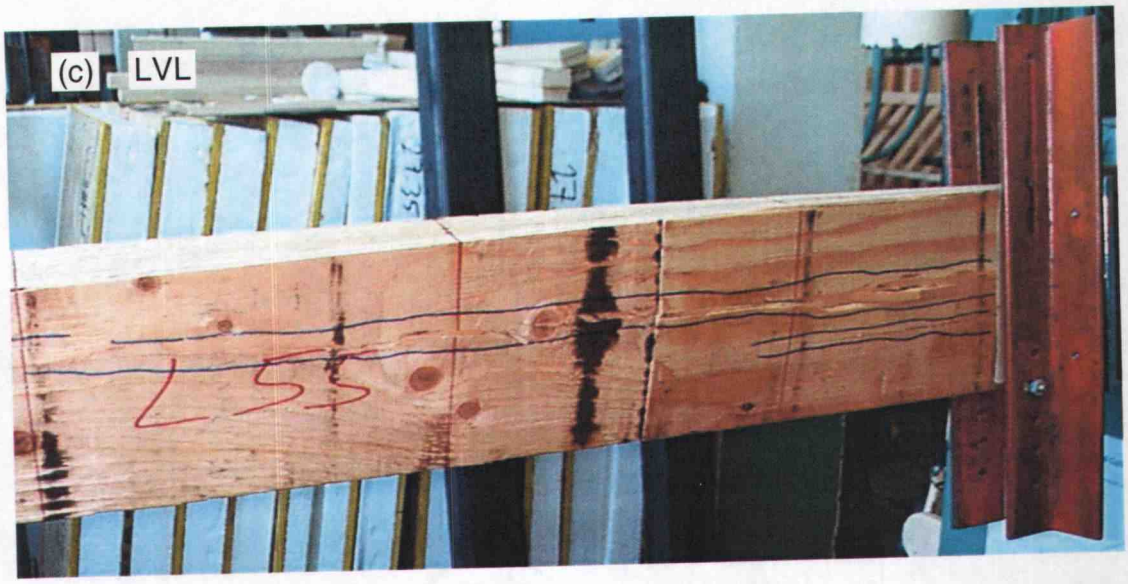

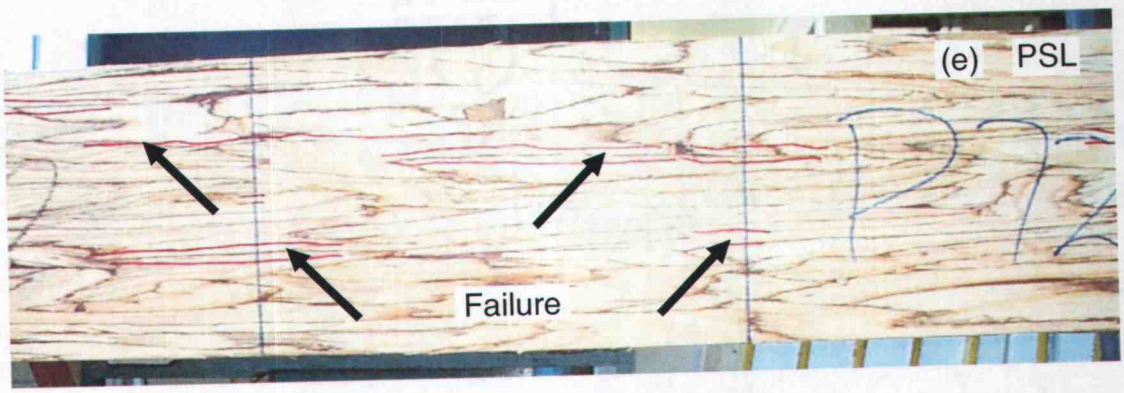

Figure 4-5: Torque – Twist Graph of Representative Samples

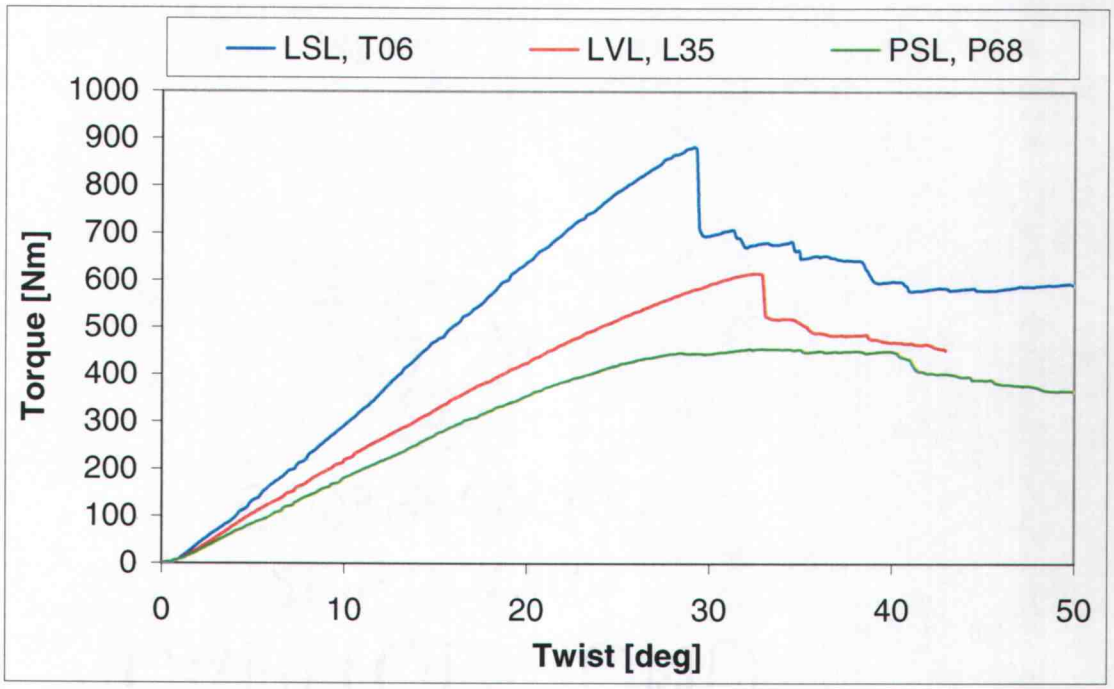

The torsional modulus (G_T) is entirely different from any shear modulus (G) for orthotropic materials, like wood. In the case of torsion parallel to grain, the torsional modulus depends on the two shear moduli G_{TL} and G_{RL} in the two longitudinal planes. According to (Hindman 1999), PSL showed the lowest G_{TL} (300 MPa) value determined via torsional stiffness measurement test compared to LVL (640 MPa), LSL (910 MPa), and OSB (1390 MPa). Since PSL has low G_{TL}, it is no surprise that it shows the lowest torsional modulus of the three composites. Therefore, the torsional modulus observed in this study confirmed Heimeshoff's (1982) conclusion, that the shear modulus on the longer side of the cross section (G_{TL}) has significant influence on the torsional modulus. In addition, G_{RL} is within a close range for the three tested materials. Besides, PSL showed typically no distinct drop in torque after reaching the ultimate value. The torque – twist curve leveled off for most PSL specimens, making it difficult to

detect, where exactly ultimate failure occurred. Although PSL failed at the lowest torque value (460 Nm), it took the longest to reach failure, because PSL was able to withstand the highest degree of twist (31.5 degrees). Some samples survived twist up to 50 degrees and more after reaching ultimate torque without catastrophic failure, i.e., a distinct drop in torque.

In contrast, LSL offered the highest torsional modulus, i.e., it showed the highest resistance to rotational deformation. What is more, LSL was able to bear a torsional moment of 850 Nm, 85 % more than PSL and almost 50 % more than LVL. LVL disposed in between the other two composites with a mean torque value of 570 Nm and a torsional modulus closer to PSL. Some LVL samples showed a less distinct drop in torque, compared to LSL, whereas the remaining specimens behaved more similar to the PSL samples and failed in a more ductile manner. As shown in Figure 4-5 the curves were linear up to approximately 300 Nm for PSL, 400 Nm for LVL and 600 Nm for LSL. Then, a slight loss in torsional modulus that was almost negligible for LSL, but more distinct for LVL and PSL can be observed from the graph. This behavior confirms the *Wood Handbook* (1999) in the estimate that the torsional shear stress at the proportional limit accounts for two-thirds of the value for torsional shear strength.

The morphology of the failure surfaces and the different failure behavior are discussed in more detail in section 4.3, where photographs of small shear blocks are presented. The small samples offer a better view on the failure surfaces and inside the composites, whereas it is rather difficult to document important details for full-size torsion samples.

4.2.3 Shear Strength

Since isotropic theory might overestimate shear strength and due to the different failure behavior, orthotropic material properties were considered, when analyzing the torsion test data. The shear stresses determined via orthotropic

theory are given in Table 4-3. The shear stresses were higher on the long side for all three composites. Considering the failure modes observed in the tests and the location where failure predominantly occurred, the mean shear stresses listed in Table 4-4 were defined as shear strength (τ_T) based on torsion.

Table 4-4: Mean Shear Strength of SCL in Torsion

Material	Failure in/at		Stress	Shear Strength τ_T [MPa]
	Orientation	Side		
LSL	Plank	Short	τ_{RL}	6.43
LVL	Joist	Long	τ_{TL}	7.96
PSL	Joist	Long	τ_{TL}	6.82

LSL is the strongest of the three materials, since it was able to bear the highest torque. Table 4-4 might however indicate the contrary, since the lowest value is presented for LSL. The different orientation, or failure behavior is the crux that has to be noticed here. The listed shear strength is valid for LSL that failed on the center of the short side, or in plank orientation (τ_{RL}). The shear strength of LSL in joist orientation (τ_{TL}) is at least double the value listed for the plank orientation. It must definitely be higher than the measured concomitant shear stress of 12.7 MPa, acting on the center of the long side, since all specimens failed on the short side only. A comparison of the three composites in the, for structural applications more important, joist orientation (τ_{TL}) proves that LSL is more than 60 % stronger in shear than LVL and even more than 86 % compared to PSL. The actual shear strength of joist oriented LSL could not be determined in this study and further torsion tests on less squatty beams, with

higher aspect ratio should be conducted. Nevertheless, it might be very difficult or almost impossible to fail LSL in joist orientation, i.e., on the center of the long side, as has been observed for ASTM shear blocks (see section 4.3).

LSL is also listed as the strongest of the three composites in edgewise shear within different evaluation reports. The design shear strength of LSL in joist orientation (τ_{TL}) is given as 4.0 MPa in Germany and 2.8 MPa in the US and Canada. However, in the US and Canada LVL (2.0 MPa) and PSL (2.0 MPa) offer the same design shear strength in joist orientation, whereas in Germany PSL (2.8 MPa) is considered to be slightly stronger than LVL (2.5 MPa). The torsion test in the current study provided a different ranking as the design values. In joist orientation, LVL (8.0 MPa) showed higher shear strength in torsion than PSL (6.8 MPa), and LSL proved to be significantly stronger. The design value of joist oriented LSL in the US and Canada LVL (2.8 MPa) might be conservative. Attention should be paid to the fact that design values are generally based on characteristic, or fifth percentile, values and additionally divided by safety factors. Design values are therefore well below average values. The material design values are given in section 3.1.4.

On the other hand, it looks different, if the failure behavior of specimens that failed on the center of the short side, or in plank orientation is addressed. According to design values, all three materials are remarkably weaker, if the shear failure plane coincides with the LT-plane. This tendency has also been observed for LSL in the current study. The true shear strength of plank oriented LVL and PSL could not be determined in this study, since all specimens failed on the long side, i.e., in joist orientation. It is however believed that the true shear strength in plank orientation is not much higher than the measured concomitant shear stresses on the short side, because for both materials some samples showed some signs of failure on the narrow face, too. The concomitant shear stresses evaluated on the center of the short side (τ_{RL}) are 4.9 MPa for LVL and 4.6 MPa for PSL. The shear strengths of the three laminated composites in plank orientation are in a narrower range compared to the other orientation. It is

therefore at this point not possible to rank the materials in order of their strength, since LVL and PSL might or might not surpass LSL (6.4 MPa). Even the design values of the materials according to evaluation reports of different countries do not present a clear picture in this case, if corresponding species and grades are compared. In Germany plank oriented materials are ranked in order beginning with LSL (1.8 MPa) as the strongest, followed by LVL (1.3 MPa) and PSL (1.0 MPa). In the US and Canada, on the contrary, it is exactly the other way round and the plank shear strength is highest for PSL (1.4 MPa), followed closely by LVL (1.3 MPa) and lowest for LSL (1.0 MPa). Again, the low design value of plank oriented LSL in the US and Canada might be conservative.

4.2.4 Finite Element Model

The focus of the FE analysis was to get a better idea of the stress distribution within the specimen and to compare the behavior of the three different SCL products. In addition, the analysis was performed to further verify the orthotropic theory that was applied to evaluate the torsion test results. The results of the FE analysis that are based on standard dimensions (44.5 x 139.7 mm^2) and orthotropic material properties are given in Table 4-5.

Table 4-5: FE Shear Stresses

Material	Input			FE Shear Stresses [MPa]			
	Shear Moduli [MPa]			Elastic Range		at Failure	
	G_{TL} G_{yz}	G_{RL} G_{xz}	g = G_{yz}/G_{xz}	Long τ_{yz}	Short τ_{xz}	Long τ_{yz}	Short τ_{xz}
LSL	782	318	2.46	4.35	2.22	12.33	6.28
LVL	593	407	1.46	4.13	2.61	7.84	4.96
PSL	398	310	1.28	4.05	2.73	6.21	4.19

The results of the FE analysis were heavily dependent on the two shear moduli in the longitudinal plane, G_{yz} and G_{xz} that are repeated in column two and three of Table 4-5. All other elastic constants, moduli of elasticity as well as Poisson Ratios and the third shear modulus, were only of very minor importance. This observation matches orthotropic theory, where the two shear moduli in the longitudinal planes are the only material constants that are considered. The ratio of shear moduli $g = G_{yz}/G_{xz}$, as listed in the fourth column, is the best indicator for the degree of orthotropicity in the axial torsion load case. The further g from unity, the more orthotropic is the material. Therefore, it is quite obvious that LSL behaves different from LVL and PSL, since g is almost twice the value. Columns five and six of Table 4-5 show the shear stresses within the elastic range based on a constant torque value of M = 300 Nm for all three composites. The final two columns present the values at failure, based on the different average ultimate torque values for each material that were listed in Table 4-2.

Note the fact that within the elastic range (constant torque) the least orthotropic material PSL ($g = 1.28$) shows the highest shear stress τ_{xz} (2.73 MPa) on the short side. Conversely, the most orthotropic composite LSL ($g = 2.46$) shows the highest shear stress τ_{yz} (4.35 MPa) on the long side. In other words, the higher g (if $g > 1$), the more probable is the material to fail at the long side. The shear stress τ_{yz} on the center of the long side increases with increasing g (if $g > 1$), while the shear stress τ_{xz} on the center of the short side decreases simultaneously. The observation that LSL still failed on the short side only, although it has the highest g, is thus even more astonishing. It might be due to the special design of the composite, for instance, the high degree of densification, the strand orientation, or the resin used.

At failure (different torque), LSL shows the highest shear stresses on both sides. In that case, the FE model was loaded according to the torsion test results, i.e., the highest torque load was applied for LSL. The shear stresses obtained from the FE analysis, as given in the final two columns of Table 4-5, match the

results evaluated according to orthotropic theory very well. They are within 2 % as will be shown in a comparison in the next section.

Moreover, this ratio g explains why solid Douglas-fir behaves almost isotropic. Heck (1997) reported of only 1.3 % difference between orthotropic and isotropic based shear strengths, considering a rectangular beam subjected to torsion. However, shear moduli vary between different sources. Bodig and Jayne reported shear moduli of coastal Douglas-fir as G_{LR} = 800 MPa and G_{LT} = 743 MPa leading to a ratio $g = G_{LT}/G_{LR} = 0.93$ which is very close to unity, i.e., isotropic behavior. The g ratios given by Bodig and Jayne are all smaller than unity and vary between 0.91 – 0.98 for softwoods and 0.70 – 0.76 for hardwoods. From the *Wood Handbook* (1999), on the contrary, one obtains the following moduli of rigidity for coastal Douglas-fir: G_{LR} = 943 MPa and G_{LT} = 1150 MPa, resulting in a ratio g = 1.22. Hereby, the listed MOE values have been multiplied by 1.1 to remove the effect of shear deflection and then been plugged in the elastic ratios (G/E_L). In general, the same tendencies are obvious for the shear moduli listed in the *Wood Handbook* (1999), i.e., higher ratios g for softwoods (0.83 - 0.99) compared to hardwoods (0.56 - 0.92). However, there are four exceptions. The hardwood True Mahogany as well as the softwoods Douglas-fir, Western Larch and Redwood have g values larger than unity. The opposite trend between the two sources for the two shear moduli in the longitudinal planes for coastal Douglas-fir is surprising, since all other elastic constants are relatively similar. On the other hand, Ylinen (1963) remarked that only for very few species of wood the ratio $g = G_{LT}/G_{LR}$ is about equal to unity and mentioned the following species as examples: Douglas-fir, spruce, Sitka spruce, yellow-poplar, yellow birch, and maple. This experience shows the need for further evaluation of the orthotropic material constants for EWPs, because of their orthotropic nature and the effect it might have on the material behavior and performance.

What is more, τ_{xz} might even outnumber τ_{yz} with decreasing g (if $g < 1$). For the given aspect ratio of 3.1, the shear stresses at the different locations were equal ($\tau_{xz} = \tau_{yz}$ = 3.8 MPa) for a shear moduli ratio g of 0.74 and the shear

stress τ_{xz} on the center of the short side was even higher than the shear stress τ_{yz} on the long side, if a shear moduli ratio smaller than the stated value ($g < 0.75$) would be assumed. As mentioned before, hardwoods possess such shear moduli ratios. Softwoods, however, have g ratios close to unity. SCL, in contrast, is proprietary and has, mainly due to densification during manufacture, g ratios well above unity. This example illustrates the importance of anisotropy in the case of axial torsion of specimens with rectangular cross section.

The shear stress distribution in the specimens is shown in Figure 4-6. The composites are subjected to the mean torque values at failure. All stresses are given in [MPa]. Two plots (a & b – LSL; c & d – LVL; e & f – PSL) are depicted for each material. The first plot for each material (a, c & e) shows the front view (or long side) of the specimen where the shear stress, S_{yz} ($= \tau_{TL}$), is maximum. The second plot for each material (b, d & f) shows an isometric top view (or short side) of the specimen where the shear stress, S_{xz} ($= \tau_{RL}$), is maximum. The constrained end is at the left end of the specimen. The loaded end, where the origin of the coordinate system lies, is at the specimens' right end. Maximum positive stresses are indicated in red, maximum negative stresses in dark blue, whereas smaller stresses are in yellow or light blue and areas where the shear stresses are close to zero are marked in green. There is a symmetric state of stress in the case of axial torsion, i.e., shear stresses on opposite sides (faces) of the specimen have same distribution and absolute values.

Figure 4-7 depicts the maximum shear stresses [MPa] along the specimen length [mm]. Note that the rotated end is now shown to the left and the constrained one to the right. The small kink in the plots of S_{yz} at the fixed end is similar to the kink Heck (1997) reported. It is due to the longitudinal direction constraint of the nodes at the fixed end that were required to provide model stability. The graphs for S_{yz} depict the shear stresses on the center of the wide face, or long side, and the graphs for S_{xz} show the shear stresses on the center of the narrow face, or short side. All graphs have same abscissa scale, but the

first one (a) has a different ordinate scale. For all specimens, shear stress is constant in the middle of the specimen (away from both ends) similar to Heck (1997). The values listed in Table 4-5 are taken at the center of the span at mid depth (τ_{yz}) or mid width (τ_{xz}).

The state of stress is the same for all materials. The FE plots (Figure 4-6) depict clearly that the maximum shear stresses act on the center of each side. In the case of axial torsion, there is a parabolic shear stress distribution along the width and the depth for specimens with rectangular cross-section. There is a constant state of stress within the specimens, except for a very short part of the span where end effects occur. The state of stress is more affected by the constrained end than by the loaded end. Shear stress (τ_{TL}) on the center of the long side shows its maximum value close to the loaded end and a distinct decline towards the constrained end. On the contrary, shear stress (τ_{RL}) on the center of the short side shows its maximum value close to the fixed end. However, the difference between maximum shear stresses and the values in the middle part of the span are in both cases negligible. For both, FE model and experimental tests the specimens were constrained by clamps only on the long side, as obvious in Figure 4-4.

Only the intensity of shear stresses varies. The FE model was subjected to different torque loads, as mentioned before in section 3.5.4, since the three composites were able to bear different torque loads in experimental testing. LSL shows the biggest difference in shear stress between the two faces. All three composites show markedly higher shear stresses on the long side.

Figure 4-6: FE Shear Stresses

(a) LSL – S_{yz} (= τ_{TL})

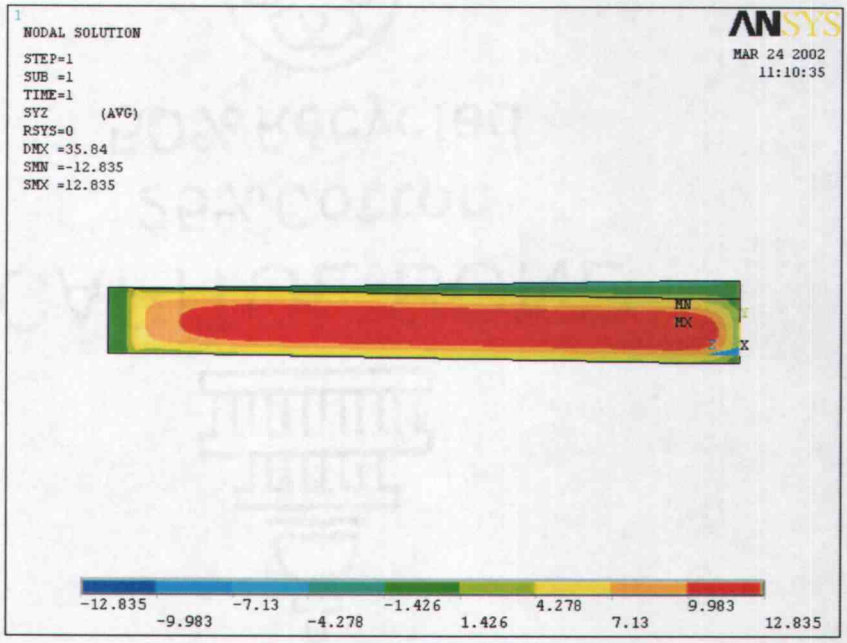

(b) LSL – S_{xz} (= τ_{RL})

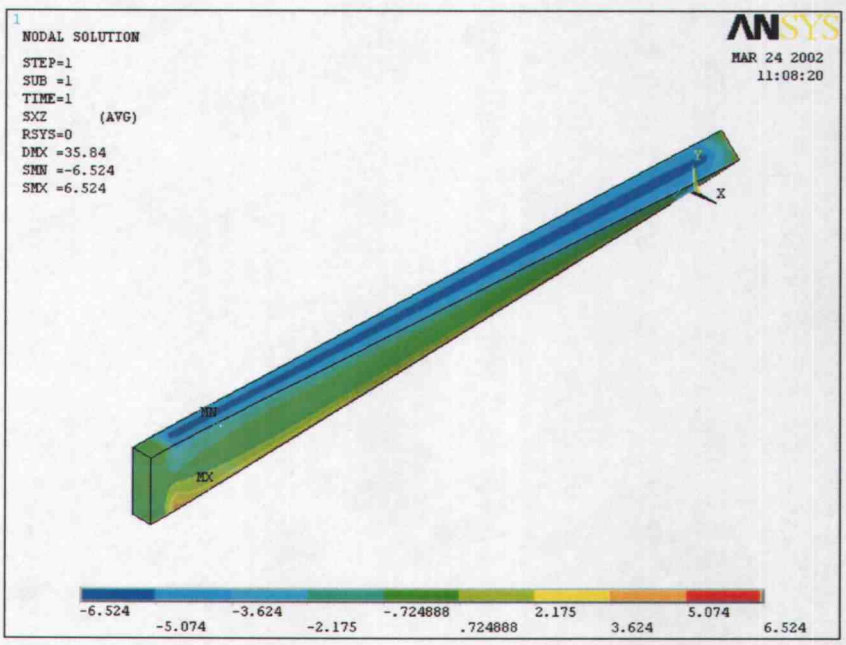

Figure 4-6: FE Shear Stresses (Continued)

(c) LVL – S_{yz} (= τ_{TL})

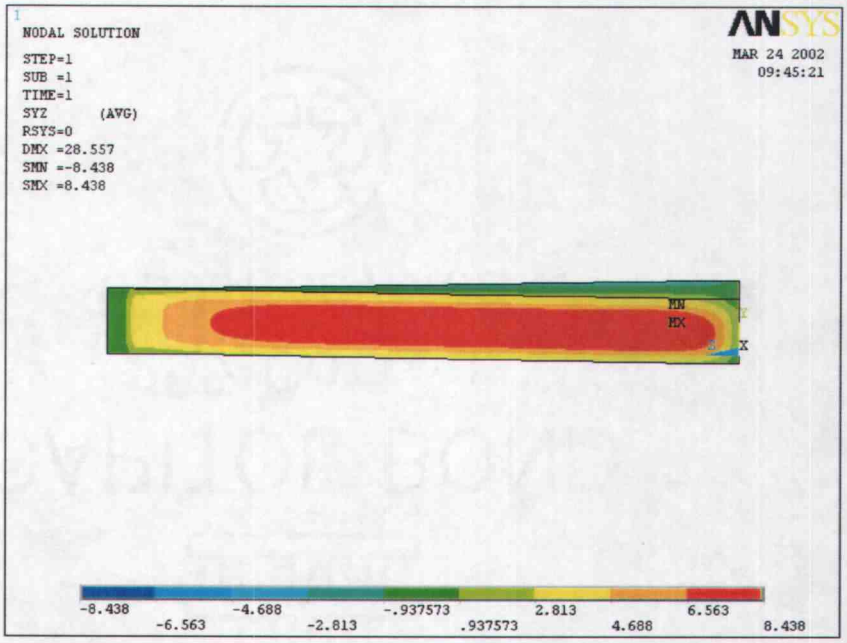

(d) LVL – S_{xz} (= τ_{RL})

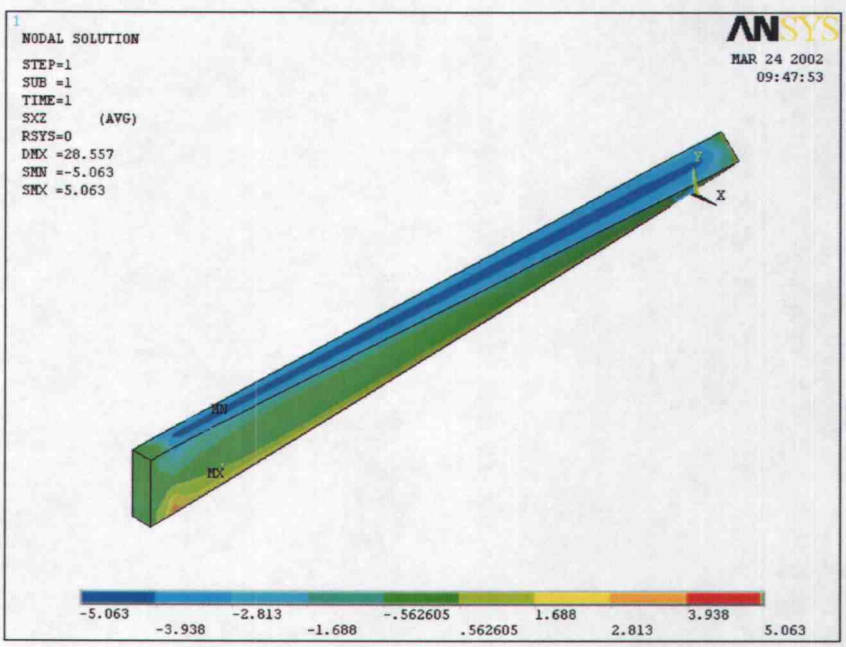

Figure 4-6: FE Shear Stresses (Continued)

(e) PSL – S_{yz} (= τ_{TL})

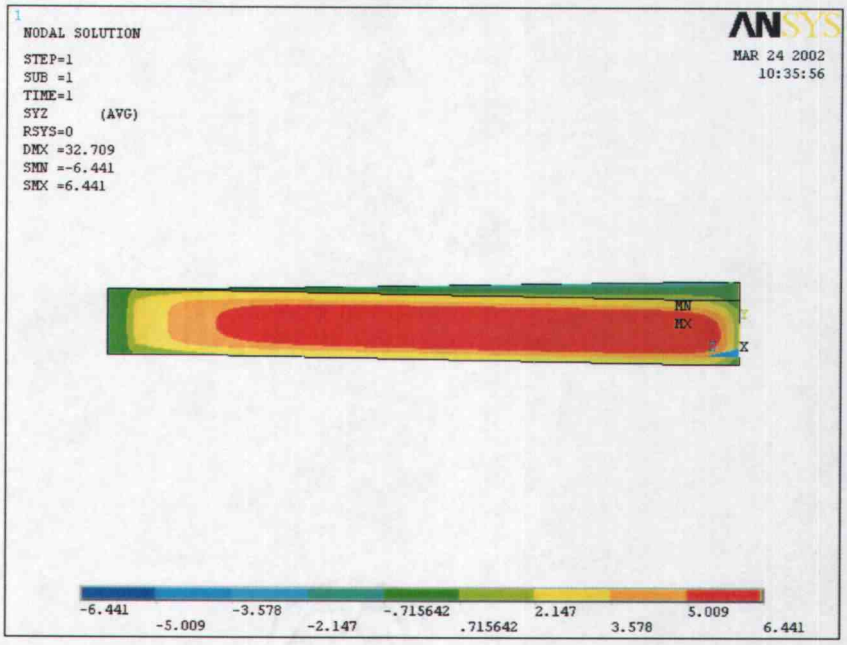

(f) PSL – S_{xz} (= τ_{RL})

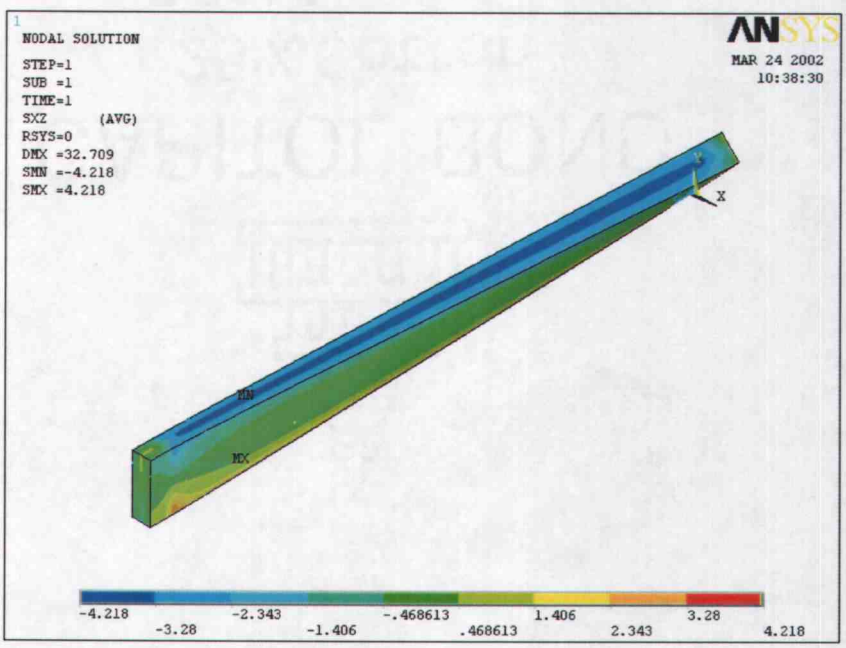

Figure 4-7: FE Maximum Shear Stresses along Beam Length

(a) LSL – S_{yz} (= τ_{TL})

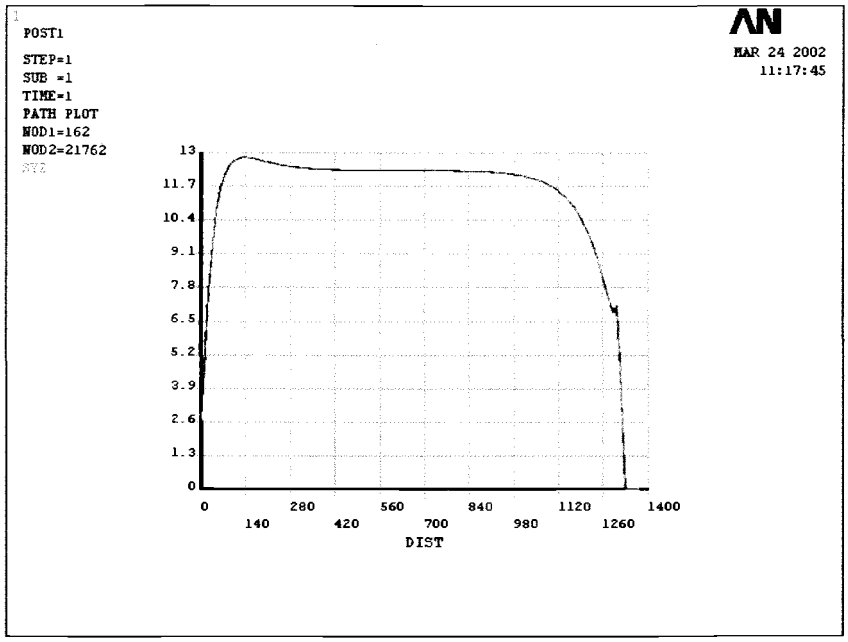

(b) LSL – S_{xz} (= τ_{RL})

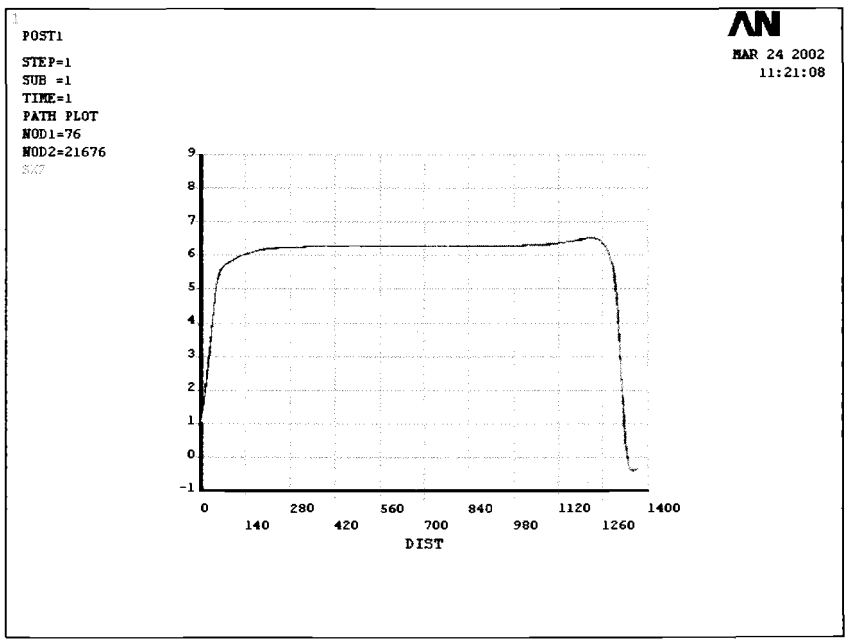

Figure 4-7: FE Maximum Shear Stresses along Beam Length (Continued)

(c) LVL – S_{yz} (= τ_{TL})

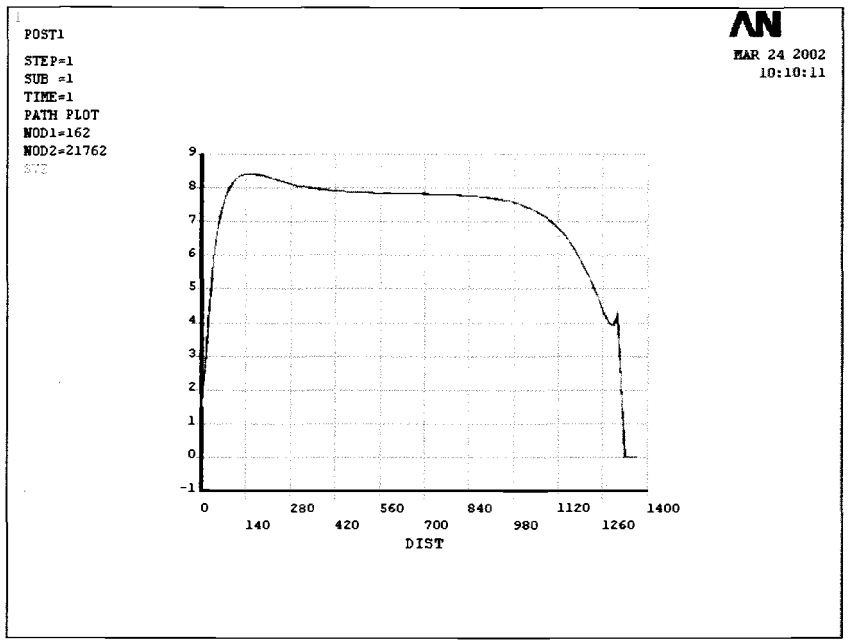

(d) LVL – S_{xz} (= τ_{RL})

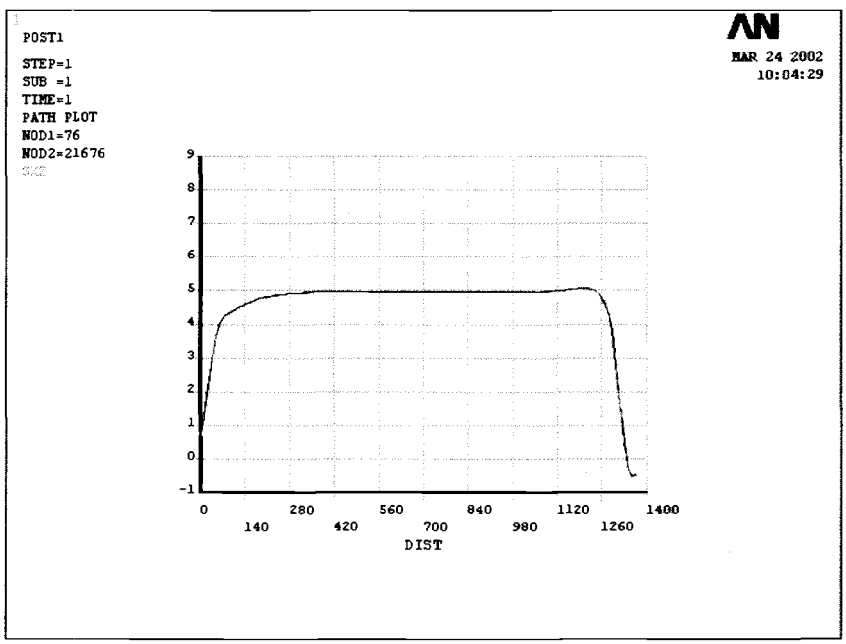

Figure 4-7: FE Maximum Shear Stresses along Beam Length (Continued)

(e) PSL – S_{yz} (= τ_{TL})

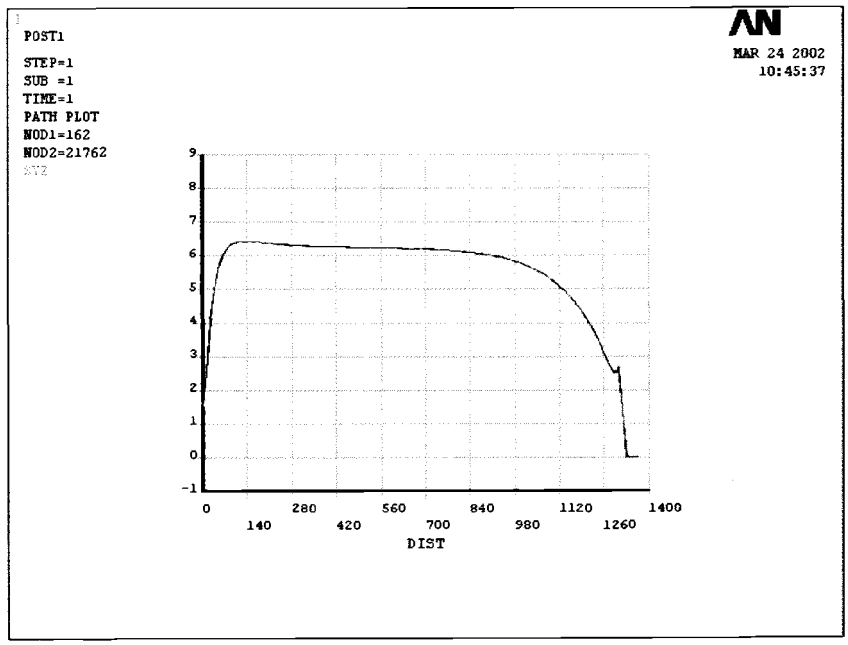

(f) PSL – S_{xz} (= τ_{RL})

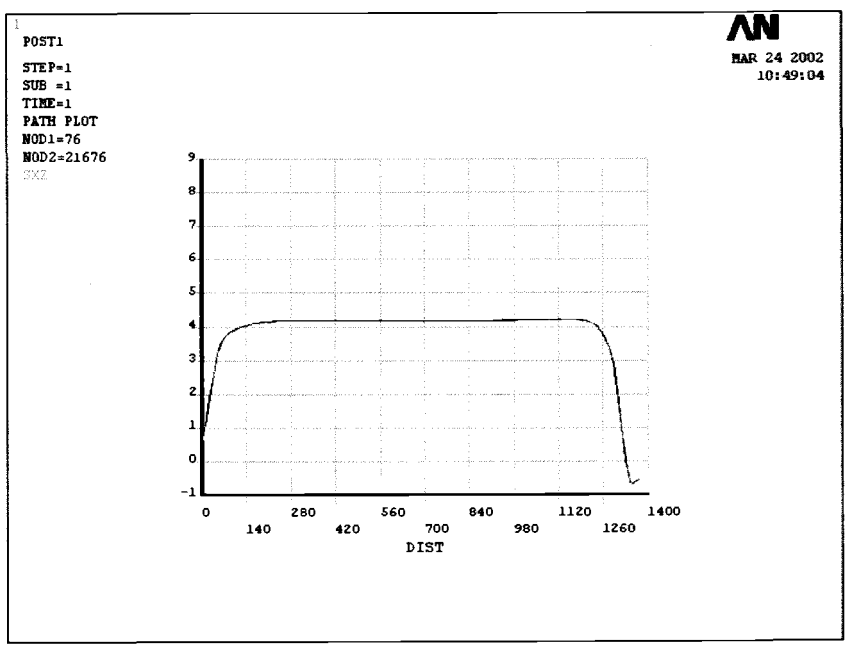

4.2.5 Comparison between Torsion Test and Finite Element Model

For a better comparison, all shear stresses listed in Table 4-6 are based on standard dimensions (44.5 x 139.7 mm^2). The shear stresses listed in columns two to five (Table 4-6) differ therefore slightly from the values given in Table 4-3, where actual dimensions were used to calculate stresses. PSL showed the highest deviation between actual and standard dimensions, e.g. about 1.7 mm in width. The deviation in orthotropic shear stresses that are inversely proportional to the square of the width (Equations 3-5 and 3-6) is yet highest for PSL. The difference between test and model results was also highest for PSL. The orthotropic approach according to Lekhnitskii is slightly closer to the FE solution than the one by Kollmann. The shear stresses according to Lekhnitskii are within 2 % of the ones derived by FEM. Therefore, this study focused on Lekhnitskii.

Table 4-6: Summary – Shear Stresses

	ISOtropic (ASTM)		ORTHOtropic (Lekhnitskii)		ORTHOtropic (Kollmann)		ORTHOtropic (FE)	
	Long τ_{LT-I}	Short τ_{LR-I}	Long τ_{LT-O}	Short τ_{LR-O}	Long τ_{LT-O}	Short τ_{LR-O}	Long τ_{LT-O}	Short τ_{LR-O}
Material	**Shear Stress [MPa]**							
LSL	11.42	8.70	12.51	6.34	12.00	6.47	12.33	6.28
LVL	7.66	5.83	7.95	4.88	7.62	5.05	7.84	4.96
PSL	6.18	4.71	6.34	4.25	6.08	4.24	6.21	4.19

The FE model confirms the test results and simultaneously proves the distinct orthotropic nature of the composites. The maximum shear stresses are on the center of the long side for LSL, LVL and PSL. In general, the difference between the stresses at the two locations (center of long and short side) is

highest for LSL and much lower for LVL and PSL. This difference in shear stresses [MPa] is 6.1 (96 %) for LSL, 2.9 (58 %) for LVL and 2.0 (48 %) for PSL, using FE analysis. The trend is the same for experimental results.

4.3 Shear Block Test

The ASTM shear block test results are summarized in Table 4-7. The complete test data are given in the appendix.

Table 4-7: Shear Block Test Results

Material	Orien-tation	Stress	Sample Size (n)	Moisture Content (MC)		Specific Gravity (SG)		Shear Strength (τ_{ASTM})	
				Mean [%]	COV [%]	Mean	COV [%]	Mean [MPa]	COV [%]
LSL	Joist	τ_{LT}	8/29	6.6	8.9	0.70	6.3	16.91	13.9
LVL	Joist	τ_{LT}	29	7.6	3.9	0.56	5.0	9.27	8.2
PSL	Joist	τ_{LT}	26	8.2	9.2	0.65	4.5	9.43	16.9
LSL	Plank	τ_{LR}	28	6.5	5.1	0.70	6.0	7.28	12.0
LVL	Plank	τ_{LR}	30	6.9	4.7	0.57	7.7	6.99	19.2
PSL	Plank	τ_{LR}	26	7.6	8.0	0.66	4.3	7.49	15.0

As shown in Table 4-7 only 8 out of 29 joist oriented LSL blocks failed in a typical shear mode. The remaining 21 samples failed either in a combined failure mode of shear and compression parallel to grain (crushing), or in crushing alone. The difference in sample size for LSL and LVL between the two orientations occurred because the maximum load was not recorded for one specimen of each material since the log file was not opened. The average moisture content (MC)

and specific gravity (SG) values were evaluated separately for each test series. MC was in a narrow range between 6.5 % and 8.2 % for all six test series, as expected. The coefficient of variation (COV) was lowest for LVL and highest for PSL. PSL might be more susceptible to moisture uptake due to its structure, whereas within LVL the continuous glue lines between the individual veneer layers might act as barrier for moisture transfer.

The specific gravity (SG) of all three SCL products is higher than solid wood SG, because of the densification during the manufacturing process. SG of LSL is 0.70 compared to the SG of 0.38 (*Wood Handbook* 1999) of Quaking aspen (*Populus tremuloides*). SG of LVL and PSL are 0.57 and 0.66, respectively, compared to the SG of 0.48 (*Wood Handbook* 1999) of coastal Douglas-fir (*Pseudotsuga menziesii*). Note that SG is highest for LSL, even though Aspen has low density. In addition, PSL has higher SG compared to LVL despite the fact that they both are made from same species and there are void areas within PSL. The veneers of LVL cannot undergo much densification without fiber crushing (Hindman 1999), whereas the strands of PSL and LSL can be compressed to a higher level. The ratio $sg = SG_{SCL}/SG_{SSL}$ is an expression of the degree of densification. Ratio sg is highest for LSL (1.84), followed by PSL (1.38) and LVL (1.19). These ratios indicate that LSL undergoes the highest amount of densification – roughly four times as much as LVL and twice as much as PSL – and LVL the least. The COV values for SG are very low, ranging from 4.3 % to 7.7 %, as expected. Void areas within some of the PSL specimens affected the volume measurements using the water immersion method.

Photographs of failed samples are presented in Figure 4-8 for the joist orientation and Figure 4-9 for the plank orientation. Two different views are shown for LSL (a, d), LVL (b, e) and PSL (c, f): first, the inside view (a - c) on the shear plane and second, the top view (d - f) of the failed shear blocks.

Figure 4-8: Failed Shear Block Samples – JOIST Orientation

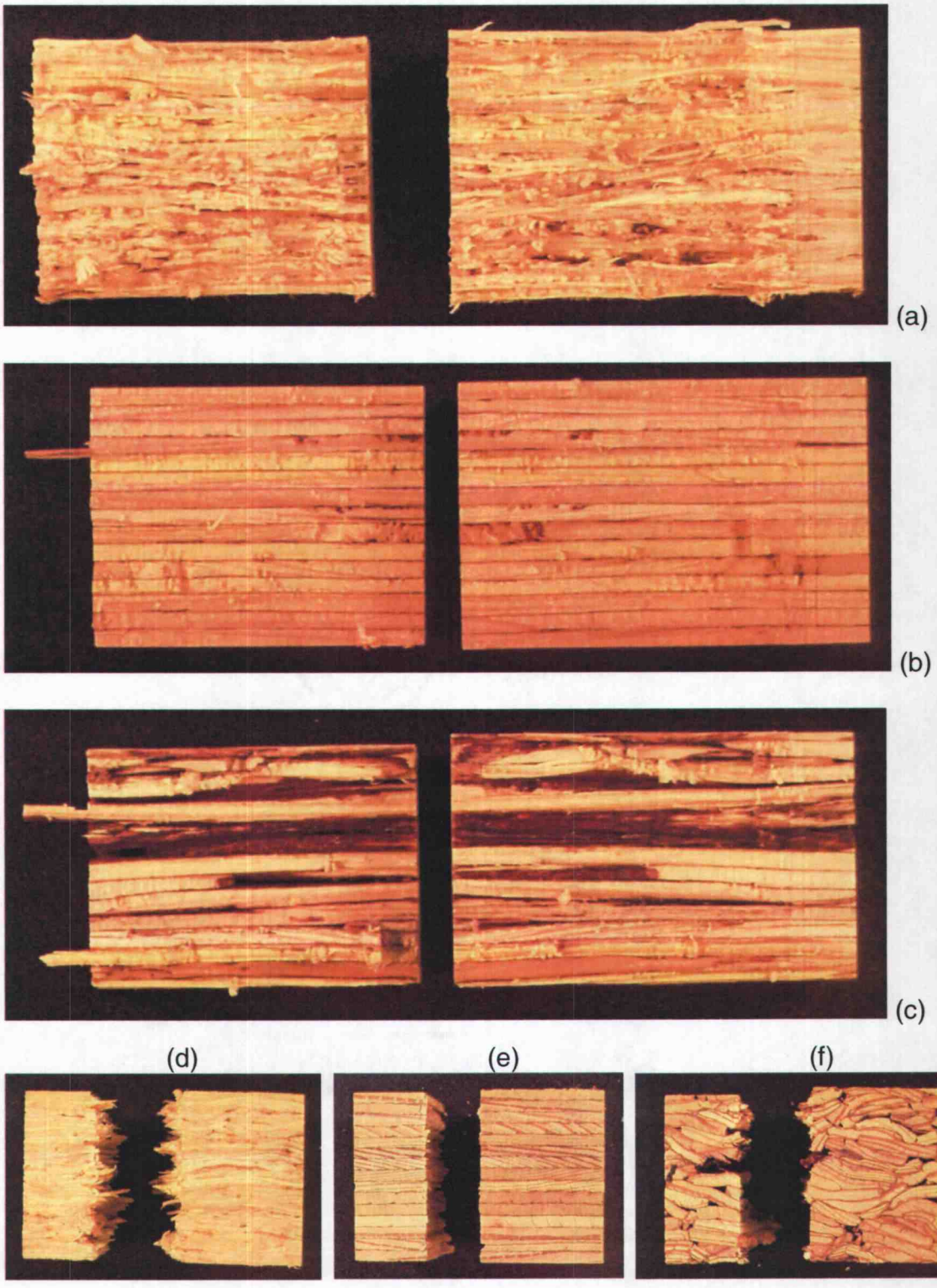

Figure 4-9: Failed Shear Block Samples – PLANK Orientation

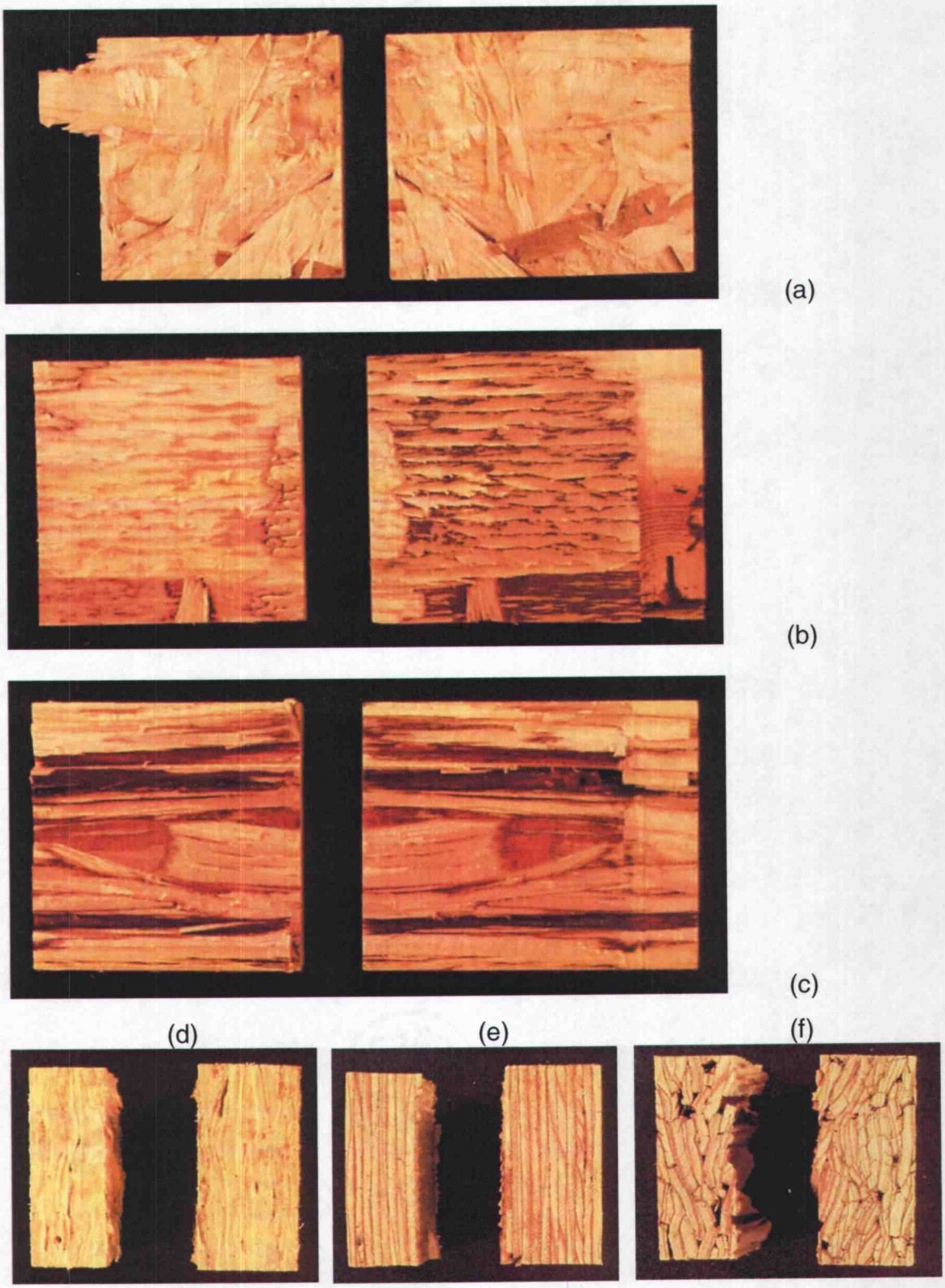

The fracture surface is rather rough or jagged for samples in the joist orientation (Figure 4-8), whereas it is generally pretty smooth for plank oriented specimens (Figure 4-9). This phenomenon is most pronounced for LSL and still evident for PSL. In the plank orientation, the two strand based composites LSL and PSL show delamination, i.e., adhesive failure at the interface between strands and adhesive. The longitudinal alignment of the strands is much better for PSL as opposed to LSL, since PSL strands are longer. However, it is the other way round regarding the tangential alignment, as can be observed in Figure 4-9 (d, f). PSL shows some cohesive failure of the wood strands, since the individual strands are thicker and not always as accurately parallel aligned with the shear plane compared to LSL.

The last column in Table 4-7 shows the shear strength (τ_{ASTM}). As expected, the values in joist orientation (τ_{TL}) were consistently higher compared to those obtained in plank orientation (τ_{RL}). This is due to the fact that, in joist orientation, the shear plane is oriented across veneer or strands, i.e., it coincides with the LR-plane (see Figure 3-3). The numerous strand or veneer boundaries, in other words interfaces between wood and adhesive, that cross the shear plane for joist oriented samples might act as crack arrestors. The difference in shear strength between the two orientations was about 2 MPa, or 30 % for PSL and LVL, whereas a very high difference of almost 10 MPa, or more than 130 % was observed for LSL. PSL showed slightly higher shear strength in both orientations compared to LVL, which might be attributed to the higher SG. This result agreed well with the results of Craig and Lam (1996). In the plank orientation the shear strengths of all three materials were within a very close range (7 - 7.5 MPa). The same was valid in joist orientation for LVL (9.3 MPa) and PSL (9.4 MPa), whereas the value for LSL was extraordinary high, which will be discussed later.

Craig and Lam (2000) reported shear strength values for 1.8E-rated Douglas-fir LVL shear blocks in the joist orientation between 7.49 and 7.69 MPa with corresponding COV values of 11 to 12 %. The lower shear strength in the referenced study in comparison to the shear strength obtained in this study might

partly be due to slightly lower stiffness rating and a higher MC (8.6 - 10 %) of their specimens. Another possible factor is the difference in shear area (44 x 51 mm) that at the same time might cause the higher variability in the referenced study, due to the smaller shear plane. Craig and Lam (2000) also tested 2.0E Douglas-fir PSL shear blocks in the joist orientation, reporting shear strength (τ_{TL}) values between 7.07 and 7.43 MPa (COV 18-22 %). Again, the lower shear strength might partly be due to roughly 2 % higher MC (9.0 - 10.2 %) for their study, and the smaller shear failure plane that simultaneously explains the slightly higher COV. The smaller the specimens are, the higher is the percentage void areas might compose of the shear plane, therefore causing higher variability. In an earlier study Craig and Lam (1996) reported higher values for shear strength (τ_{TL}) of 7.94 MPa (COV = 10 %, MC = 10.3 %) for Douglas-fir LVL and 8.26 MPa (COV 17 %, MC = 9.1 %) for Douglas-fir PSL with a slightly lower variability that are closer to the values obtained in this study. These two shear strengths are in between the values obtained for the different orientations in the current study, nevertheless they are still 14 % lower for LVL and 12 % lower for PSL compared to the corresponding joist oriented samples. At least the tendency that PSL shows a slightly higher shear strength, based on ASTM blocks, than LVL is consistent for all studies. The specific gravity was very consistent between the two referenced studies and the current study and is therefore not believed to play a major role in this context. The author recommends therefore that, if the shear block test is applied on SCL, the size should be predefined in ASTM D 5456 more clearly, for instance, a shear area of 38 x 38 mm^2 (1.5 x 1.5 in^2) for a better comparison of test results. Since SCL products are available in widths smaller than 51 mm (2 in) the requirement of a constant shear area of 2600 mm^2 (4 in^2) results in an adjustment of the depth. This however, might change the state of stress in the specimen and caused problems as will be described in the following paragraph.

The very high stress of LSL (16.9 MPa) in joist orientation might be the compression parallel to the grain strength rather than shear strength, because

LSL in joist orientation hardly ever fails in shear. As shown in Table 4-7 only 8 out of 29 specimens failed in a typical shear mode. The majority however, failed either in a combined failure mode of shear and compression parallel to the grain (crushing) or in crushing, alone. But it was difficult to differentiate these two failure modes in some cases. Delamination, separation of strands and crushing of strands at or close to the contact areas marked the samples that failed in modes other than shear only. The specimen shown in Figure 4-10 shows typical signs of compression parallel to grain failure. But, some samples did not show any obvious signs of failure along the intended shear plane at all. Although the strength value listed in Table 4-7 was based on only those eight samples that failed in shear, the value might still be deceptive, because the average shear strength of all specimens, irrespective of failure mode, is very close to the average shear strength of those eight specimens that failed in shear.

Figure 4-10: Typical Compression Failure in Joist-Oriented LSL Block

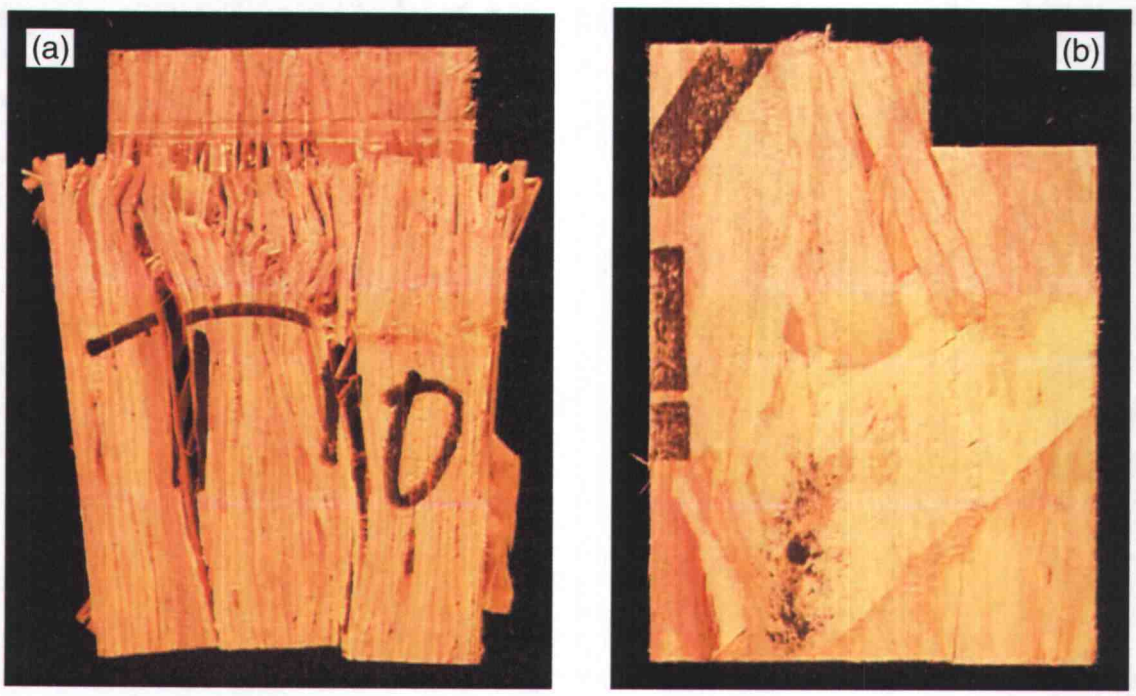

The different failure behavior for LSL in the joist orientation can be explained by its design, namely the geometry or size and the alignment of the strands, as well as the high degree of densification. LSL strands are only about 1 mm (0.04 in) thick, roughly a third of the thickness of PSL strands or LVL veneers. It is therefore easier to align LSL strands parallel to the tangential direction than for PSL, as obvious in Figure 4-8 (d, f). The higher degree of densification compared to the other two composites further improves the tangential alignment. LSL strands are also remarkably shorter and a little wider compared to PSL. Furthermore, LVL and PSL are more or less fully aligned longitudinally, whereas within LSL there is definitely less than 100 % strand alignment in the longitudinal direction. In addition, the strand alignment might vary through the thickness in LSL. There are many inclined strands that deviate from the longitudinal axis as shown in Figure 4-9 (a), or Figure 4-10 (b). These inclined strands might transfer the compressive load within the sample from the load bearing plate to the base plate past the offset and mainly be stressed in compression parallel to the grain. This however, leads to a change in the state of stress within the specimens. LSL might be more similar to a solid wood shear block showing a certain degree of slope of grain than to a straight-grained one. Therefore, the ASTM shear block test does not seem to be suitable for LSL.

Moses (2000) studied the influence of strand alignment on mechanical properties of LSL and reported the same problem. Shear blocks with the failure plane across the strands (joist orientation) did not fail in shear, but rather in crushing or separation of the strands, with no visible signs of failure along the intended shear plane. The author presented a shear strength value for the plank orientation of laboratory-made, fully aligned LSL of 6.07 MPa, which is lower than the value obtained in this study. For shear blocks with completely randomized strand orientation, i.e., no alignment, the strength was even lower and a value of 4.92 MPa was obtained. However, it has to be considered that commercially available LSL classifies somewhere in between these two laboratory-made LSL versions. Moses predicted shear strength values for LSL with 50 % strand

alignment, using laminate theory and the first order reliability method based on the tested specimens, of 7.56 MPa, which is very close to, or more precisely within 4 % of the value obtained by tests in the plank orientation in this study (7.28 MPa). Moses concluded that the quantity of oriented strands markedly influenced the material properties.

The COV of shear strength is for LSL and PSL about 2 % higher in joist orientation compared to plank oriented samples. In joist orientation, PSL has the highest COV and LVL the lowest. LVL shows a very low COV of 8 % in the joist orientation and a high variability of 19 % in plank orientation. The high COV of LVL in plank orientation may be due to the fact that the ASTM shear block test forces shear failure within a very small area, which is about the width of the offset of the test jig (3 mm or ⅛ in). The veneer thickness of LVL is generally around 3 mm and for plank oriented LVL the veneer layers are aligned parallel with the shear plane. The shear strength is therefore heavily dependent on only one or at the most two veneers and the adjacent interfaces. Hunt, et al. (1993) tested Southern pine (*Pinus spp.*) LVL shear blocks in the plank orientation and had a COV of 18 %, which is very close to the value obtained in the current study (19 %). The variability in shear strength of solid wood is around 14 % (*Wood Handbook* 1999). In comparison, LSL and joist oriented LVL show lower COV, while void areas in PSL result in an increased variability.

Void areas within PSL contribute to an increased variability as can be observed in Figure 4-8 (f). Ellis and Dubois (1994) reported values of percentage macro-voids for Douglas-fir Parallam® PSL ranging from 2.35 to 3.45 using video, and varying between 1.29 and 2.24 applying line scan analysis. The average values were 2.90 for video and 1.66 for line scan camera. The authors concluded that the higher percentage macro-void value obtained by the video analysis gave the better estimate, i.e., almost 3 % void area.

According to Ehart et al. (1998), who evaluated the fracture characteristics of PSL, cracking preferentially occurs parallel to the longer side of the strand

cross section, i.e., in tangential direction. Consequently, a smooth fracture surface is obtained for plank oriented samples, since in this case the shear plane coincides with the LT-plane. Furthermore, they argue that the boundaries of single strands act as crack arrestors. A rough fracture surface favors friction and crack bridging, therefore increasing the resistance against crack propagation. As a consequence, joist oriented PSL shows a ductile failure behavior compared to solid wood or LVL, because of its heterogeneous structure. LSL shows the roughest fracture surface and behaves even more extreme than PSL in this context. There are much more strand boundaries within LSL compared to PSL, since LSL strands are thinner and more compressed. Friction and crack bridging effects are most pronounced for LSL resulting in a completely ductile failure behavior. Ductile failure modes are welcome within structural applications, but not within tests conducted to determine the strength of materials.

The veneer based composite LVL is, compared to the two strand based composites, a more homogenous material with less interfaces and behaves therefore differently. The shear plane of joist oriented LVL is smoother and not jagged (Figure 4-8 b, e and Figure 4-11). The fracture surface of LVL might be influenced by lathe checks within the individual veneers. Lathe checks are also existent within PSL strands, but they might not play the same role as within LVL, since PSL is more compressed. Many lathe checks are, for instance, detectable in the light colored fourth or seventh veneer layer from the bottom in the sample that is shown in Figure 4-11 and the small kink at the shear plane in the second layer might also be attributed to a lathe check. The crack path follows the lathe check until it stops at an earlywood/latewood interface and continues in tangential direction towards the predefined shear plane and from there on traverses the remaining portion of the veneer layer again in radial direction. This is just one example that illustrates how lathe checks might affect shear failure of joist oriented LVL. It is not possible to make a general comment on plank oriented LVL, since the variability for this setup is very high and it is not appropriate to speak of a representative sample in this case. The specimen that

is chosen as an example in Figure 4-9 shows mainly cohesive failure of the wood veneer. Though, others showed mainly adhesive failure, or delamination.

Figure 4-11: Lathe Checks in Failed LVL Shear Block

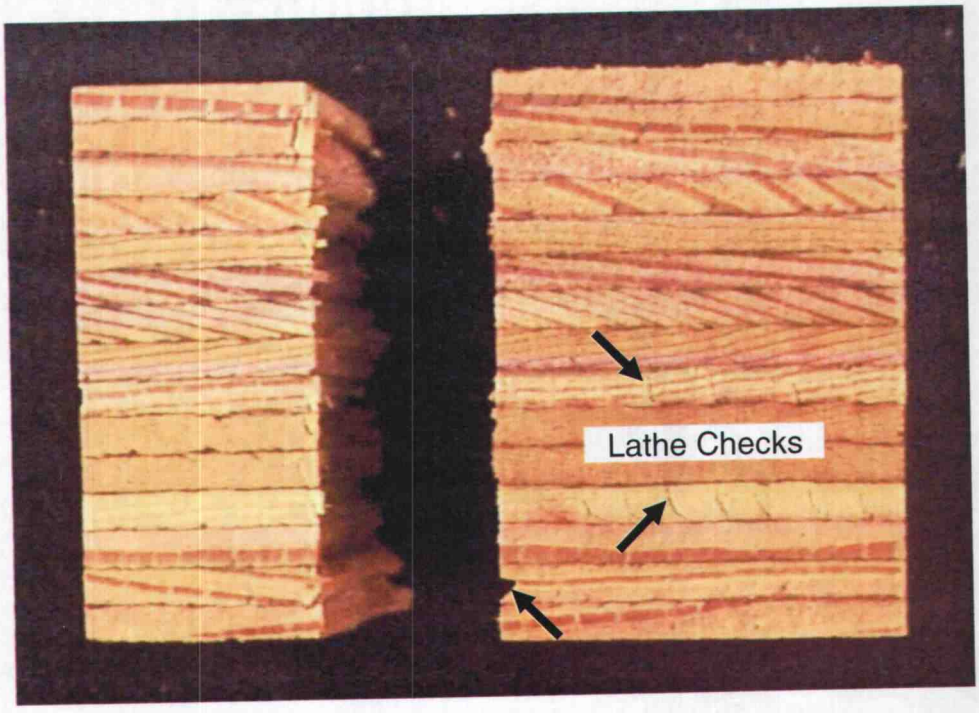

The author recommends the use of another shear test as standard test method for several, well known reasons. The ASTM shear block is unsymmetric and a bending moment is exerted on the specimen that results in a complex state of stress with superimposed tensile and compressive stresses. What is more, a high stress concentration acts at the sharp reentrant corner close to the top of the specimen. In addition, there are the following problems that occur specifically for SCL.

First, it is almost impossible to fail joist oriented LSL ASTM blocks in shear. The usual failure behavior of joist oriented LSL ASTM shear blocks is

rather compression parallel to grain, or a combination of crushing and shear, than shear only, as shown in Figure 4-10. Especially the front view (a) to the left shows crushing and delamination of strands. Second, joist oriented LSL specimens cannot be regarded as straight-grained, or fully longitudinally aligned. Oblique strands, as shown in the side view presented in Figure 4-10 (b), may cause a change in the state of stress within the specimen, since they might transfer the exerted stress past the offset and rather be stressed in compression parallel than shear. Third, since SCL is produced in widths smaller than 51 mm (2 in) the requirement of a 2600 mm^2 (4 in^2) shear plane results in an increase of the specimens' depth in some cases. A different shape of the shear failure plane makes it difficult to compare test results. Specifically a smaller width and a higher depth might increase the probability of crushing failure rather than shear failure, as has been observed for joist oriented LSL blocks in the current study. Fourth, the fact that the shear failure plane is predefined within the 3 mm offset causes high variability for plank oriented LVL, since failure is primarily dependent on only one veneer and the adjacent interfaces, as discussed before. Finally, defects like void areas or lathe checks might cause high variability in small samples, too.

In conclusion, the author would like to emphasize that shear strength based on tests of small ASTM shear blocks is not representative of the shear strength of full-size specimens.

4.4 SCL – Full-Size Specimens versus Small Shear Blocks

A comparison of the mean shear test results on full-size specimens under torsion and small ASTM shear blocks is presented in Table 4-8. Ratio (τ_T/τ_{ASTM}), expressing the relationship between shear stresses obtained by full-size torsion tests (τ_T), applying orthotropic behavior, and ASTM shear block tests (τ_{ASTM}), is introduced to discuss the results. Care was taken to compare only corresponding stresses and failure modes. That means, torsion based stresses on the center of

the long side of the cross section were divided by shear block stresses in joist orientation, since in both cases failure was supposed to occur across the plies in the LR-plane (τ_{LT}). Accordingly, torsion based stresses on the center of the short side were compared to shear block based stresses in plank orientation, because in both cases the failure plane coincided with the LT-plane (τ_{LR}), i.e., failure was supposed to occur along the strands or veneers. Shear strength in torsion, i.e., the orientation where failure took place, is marked in bold.

In general, as shown in the last three columns of Table 4-8, the full-size torsion test resulted in lower shear stresses than the shear block test did. The average τ_T/τ_{ASTM} ratios obtained in this study on LSL, LVL, and PSL ranged from 0.61 for PSL to 0.88 for LSL, both in plank orientation. In other words, the shear stresses based on torsion counted for roughly 60 to 90 % of the small shear block values. Shear stresses obtained in torsion (τ_T) are plotted over ASTM block shear stresses (τ_{ASTM}) for individual samples in Figure 4-12.

Table 4-8: SCL Shear Test Comparison

Material	Orientation	Stress	Shear Stresses [MPa]		Ratio τ_T/τ_{ASTM}
			Torsion τ_T	ASTM Block τ_{ASTM}	
LSL	Long/Joist	τ_{LT}	12.69	16.91	0.75
LVL	Long/Joist	τ_{LT}	**7.96**	9.27	0.86
PSL	Long/Joist	τ_{LT}	**6.82**	9.43	0.72
LSL	Short/Plank	τ_{LR}	**6.43**	7.28	0.88
LVL	Short/Plank	τ_{LR}	4.90	6.99	0.70
PSL	Short/Plank	τ_{LR}	4.55	7.49	0.61

Figure 4-12: Orthotropic Torsion versus ASTM Block Shear Stresses

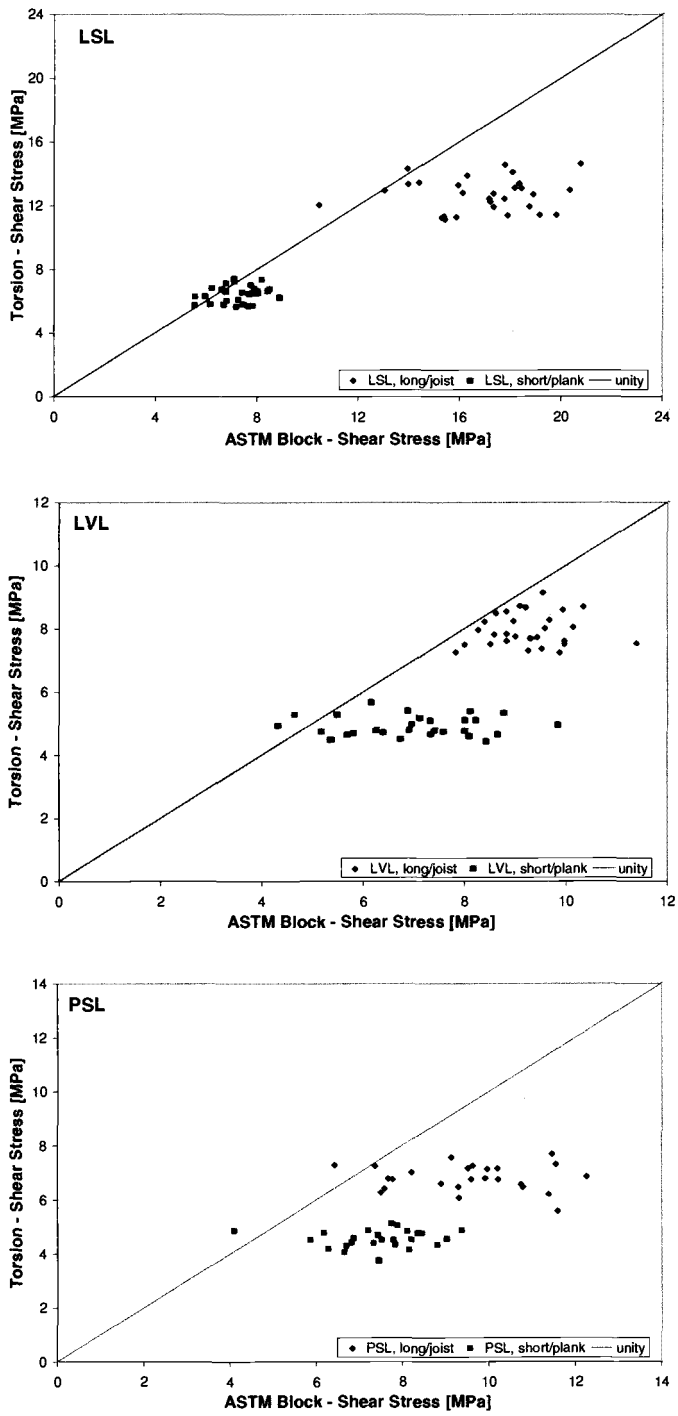

The τ_T/τ_{ASTM} ratio of 0.75 for LSL in the joist orientation is again questionable, since it is based on the very high block shear stress (τ_{TL}) as mentioned in section 4.2. Except for LSL, the ratios are higher in the long/joist orientation (τ_{TL}), where failure occurred across the strands or veneers. That means, the ratios are higher in the orientation, where failure occurred in torsion, as marked in bold. The ratios are low for PSL and LVL in plank orientation since the shear stresses obtained in torsion are not ultimate stresses. LVL and PSL failed in joist orientation. Thus, the short/plank ratios are based on concomitant shear stresses in torsion rather than shear strength and might accordingly be conservative. PSL shows smaller ratios compared to LVL. But, there is a different ranking between the two test methods, that is consistent in both orientations. The full-size torsion test results in higher shear stresses for LVL compared to PSL. Small LVL blocks, on the contrary, show lower shear strengths than PSL blocks.

Both test methods constantly resulted in lower shear strength for plank oriented samples. The relationship between full-size torsional and small block based shear stress is visualized in Figure 4-10 for each specimen. The diagonal marks unity, squares the long/joist (τ_{TL}) stresses, and diamonds the short/plank (τ_{RL}) stresses. LSL is shown first, LVL second and PSL third. Note the different scale in the graphs. It is apparent that almost all ratios are smaller than unity, i.e., located to the right of the diagonal. The scatter along the abscissa is markedly higher than along the ordinate, indicating the high variability of the shear block test compared to the low COV obtained in torsion. LSL shows the least scatter within the short/plank test series, what might be an indication for the very brittle failure behavior in that case.

Hunt et al. (1993) also observed lower shear strength values via full-size tests on Southern pine LVL in the plank orientation in three-point ($\tau_3/\tau_{ASTM} = 0.90$) and five-point ($\tau_5/\tau_{ASTM} = 0.75$) bending compared to shear block tests. They showed that the shear strength (τ_{RL}) of LVL obtained via five-point tests decreased with increasing span/depth ratio (L/d), but at a decreasing rate. In a

follow up study, Bradtmueller et al. (1998) tested joist oriented Southern yellow pine LVL in five-point bending. The material showed a slightly higher density compared to the first study by Hunt et al. (1993). Bradtmueller et al. (1998) evaluated a mean shear strength (τ_{TL}) of 8.14 MPa. This value was 1.71 times the strength obtained in the plank (τ_{RL}) orientation. Bradtmueller et al. concluded that it was inherently more difficult to induce shear failure in the joist orientation than in the plank orientation using flexure tests. Bending strength (σ), or modulus of rupture (MOR), were nearly the same in the different orientations, whereas the shear strength was much higher in the joist orientation.

Craig and Lam (1996) also observed lower shear strength values for joist oriented Douglas-fir LVL and PSL based on three-point and five-point bending tests, compared to shear block tests. The resulting τ/τ_{ASTM} ratios from their first study (1996) were: PSL – 0.66 three-point; 0.82 five-point; 0.97 five-point (L/d = 5); and LVL – 0.71 three-point. All tests were performed using L/d ratio of 6, except for one series of five-point loading, where a lower L/d ratio of 5 was applied that resulted in the highest τ/τ_{ASTM} ratio. Craig and Lam (2000) performed a second study on Douglas-fir LVL, as well as Douglas-fir and Southern pine PSL, proving the same tendency ($\tau_3/\tau_{ASTM} = 0.73 - 0.91$) to be valid for three-point tests conducted on beams with I-shaped cross-sections in joist orientation (L/d = 6). However, the same composites with rectangular cross-section behaved different when subjected to five-point bending in the joist orientation with a lower L/d ratio of 5, leading to τ_5/τ_{ASTM} ratios between 1.03 and 1.39.

A comparison of different full-size SCL test results of various studies, proves that the torsion test generally results in the highest values for shear strength and the lowest variability, as shown in Table 4-10. First, shear stresses obtained under torsion (τ_T) and center-point, or three-point, bending (τ_3) – the first two rows in each section of Table 4-9 – are compared. The results are the following ratios (τ_T/τ_3), where J indicates joist orientation and P plank orientation: 1.165 LVL-J; 1.160 PSL-J; 0.857 LVL-P; 1.099 PSL-P. That means, torsion

based shear stresses are 10 – 17 % higher than shear stresses based on three-point bending. Only plank oriented LVL with a 14 % lower shear stress in torsion does not follow the general trend. Though, LVL tested under three-point bending was Southern pine and showed a higher SG (0.63) than the Douglas-fir LVL (0.58) tested under torsion. All other specimens tested were Douglas-fir and had similar SG. However, the two joist oriented composites tested under three-point bending had I-shaped cross-section, carved out of rectangular beams. This specimen preparation possibly affects the state of stress, in case it may cause some checks. That might partly explain the 16 % and 17 % lower shear stresses for PSL and LVL based on three-point bending.

The τ_T/τ_3 ratios are markedly higher, 1.421 LVL-J and 1.242 PSL-J, if specimens of rectangular cross-section are considered – the second last row in the first and third section of Table 4-9. This is yet no surprise, since the three-point bending test of joist oriented SCL results in low shear failure percentage. Therefore, the evaluated shear strength always marks the lower tail of the shear stress distribution, since not all specimens fail in shear, but many rather in bending. The shear stresses based on rectangular specimens subjected to three-point bending are hence even less comparable to torsion based shear stresses than the ones with I-shaped cross section, dealt with before. These ratios indicate how complex the shear phenomenon is and how many factors might influence shear strength. It is therefore rather difficult to compare different shear test results. In bending, there are always tensile and compressive stresses superimposed. The state of stress is even more complex within small shear blocks where stresses perpendicular to grain further cloud the issue. It is therefore not possible to determine the true shear strength using bending or small block tests and each approach has to be considered as an approximation.

Table 4-9: SCL – Comparison of different full-size Test Results

LVL – Joist Orientation								
Study	Setup	Species Material	Size [mm^2]	MC [%]	SG [1]	τ_{LT} [MPa]	COV [%]	Ratio τ_T/τ_B
Siller 2002	torsion	DF LVL	44x140	7.6	0.58	**7.96**	6.3	
Craig/Lam 2000	three-pt	DF LVL	44x184 (I)	9.3	0.57	**6.83**	10.0	1.165
Craig/Lam 1996	three-pt	DF LVL	44x184	10	0.57	**5.60**	7.0	1.421
Hunt et al. 1998	five-pt	SP LVL	38x58	7.7	0.67	**8.14**	5.8	0.978
LVL – Plank Orientation								
Study	Setup	Species Material	Size [mm^2]	MC [%]	SG [1]	τ_{LR} [Mpa]	COV [%]	Ratio τ_T/τ_B
Siller, 2002	torsion	DF LVL	44x140	7.6	0.575	**4.90**	6.3	
Hunt et al. 1993	three-pt	SP LVL	38x58	7.6	0.633	**5.72**	9.4	0.857
Hunt et al. 1993	five-pt	SP LVL	38x58	7.6	0.633	**4.76**	8.1	1.029
PSL – Joist Orientation								
Study	Setup	Species Material	Size [mm^2]	MC [%]	SG [1]	τ_{LT} [MPa]	COV [%]	Ratio τ_T/τ_B
Siller 2002	torsion	DF PSL	44x140	8.2	0.67	**6.82**	7.1	
Craig/Lam 2000	three-pt	DF PSL	44x184 (I)	10	0.66	**5.88**	12.4	1.160
Craig/Lam 2000	three-pt	SP PSL	44x184 (I)	9.4	0.69	**6.87**	11.3	0.993
Craig/Lam 1996	three-pt	DF PSL	44x184	9.2	0.64	**5.49**	7.0	1.242
Craig/Lam 1996	five-pt	DF PSL	44x184	8.8	0.65	**6.75**	8.0	1.010
PSL – Plank Orientation								
Study	Setup	Species Material	Size [mm^2]	MC [%]	SG [1]	τ_{LT} [Mpa]	COV [%]	Ratio τ_T/τ_B
Siller 2002	torsion	DF PSL	44x140	8.2	0.67	**4.55**	7.1	
Craig/Lam 2000	three-pt	DF PSL	44x184	9.3	0.63	**4.14**	13.0	1.099
Craig/Lam 2000	three-pt	SP PSL	44x184	7.8	0.69	**4.73**	14.2	0.962

A comparison of shear stresses obtained under torsion (τ_T) and five-point bending (τ_5) – the first and the last row in the first three sections of Table 4-9 –

results in the following ratios (τ_T/τ_5): 0.978 LVL-J; 1.029 PSL-J; 1.010 LVL-P. In other words, torsion based shear stresses are within 3 % of the shear stresses based on five-point bending. Only joist oriented LVL shows a 2 % lower shear stress in torsion. Yet, LVL tested under five-point bending was Southern pine and showed a higher SG (0.67) than the Douglas-fir LVL (0.58) tested under torsion. Plank oriented LVL tested under five-point bending was also Southern pine with a lower SG (0.63) compared to joist oriented Southern pine LVL (0.67), but still higher than the Douglas-fir LVL (0.58) tested under torsion. Therefore, the 3 % higher shear stress based on torsion is surprising. Joist oriented PSL was Douglas-fir and had almost identical SG in both studies. Shear stress based on torsion is, as a consequence, only 1 % higher than shear stress evaluated under five-point bending. All ratios between torsion and bending agree very well.

The shear strength (τ_{LR}) of plank oriented LVL and PSL in torsion might even be higher, since the specimens failed on the long side (joist) and the shear stresses listed here (plank) are the concomitant stresses on the short side, where only some beams showed some signs of failure. Further tests are recommended on more squatty LVL and PSL beams with lower aspect, or depth/width, ratio to induce failure on the short side to obtain the true shear strength in torsion in the plank orientation.

The lower variation of shear stresses based on torsion compared to bending and especially block tests and the fact that all torsion samples do fail in shear, owing to a state of pure shear stress are further arguments in favor of torsion. Low variation means more reliability, resulting in higher characteristic, or 5^{th}-percentile tolerance, values and finally in higher design values.

The comparison given here is focused on samples of similar size, since a size effect has been observed in bending and in torsion, too. Craig and Lam (2000) performed further tests on bigger SCL members subjected to five-point bending that are omitted here, but are given in section 2.3, since the low span/depth ratio of 5 is believed to result in artificially increased shear strengths. Hunt et al. (1993) performed their five-point bending tests with L/d ratios of 9 – 11

(joist) and even 14 – 18 (plank), where the shear strength seemed to become constant, while there was a marked, nonlinear increase in shear strength with decreasing L/d ratios. The discussion on a size effect in shear will be further elucidated in the next section.

No other source reporting of full-size shear tests on LSL was found. Further torsion tests on less squatty LSL beams with higher aspect, or depth/width, ratio are recommended to obtain failure on the long side thereby evaluating the true shear strength in torsion in the joist orientation. It might however be difficult, or almost impossible, to fail joist oriented LSL in shear since LSL in joist orientation hardly ever fails in shear. Small, joist oriented ASTM blocks of LSL failed, either in a combined failure mode of shear and compression parallel to the grain (crushing), or in crushing, alone (see section 4.3).

4.5 Torsion – Structural Composite Lumber versus Solid-Sawn Lumber

A comparison of different studies on shear strength, focusing on torsion, is presented in Table 4-9. All three studies used the same torsion machine. However, Heck (1997) and Riyanto (1996) evaluated the shear strength of SSL, using isotropic theory. The current study on SCL was based on orthotropic theory, i.e., material properties were considered, since the different failure behavior of the three wood composites proved the necessity for that approach. All shear stresses in torsion are τ_{TL}, except for LSL, where τ_{RL} is listed.

For SCL, the shear strength based on full-size specimens in torsion is lower than that of small ASTM blocks ($\tau_T/\tau_{TASTM} < 1$), as shown in the last column of Table 4-9. For SSL, on the contrary, the reversed has been observed earlier. Ylinen (1963) reported that, for SSL (Finnish pine, *Pinus silvestris*), the torsion test resulted in a higher shear strength in comparison to cube or block shear tests ($\tau_T/\tau_{TASTM} > 1$), since a non-uniform shear stress distribution for the latter

two test methods as well as stress interactions, especially with tensile stresses might decrease their apparent shear strengths.

Table 4-10: Comparison of Torsion and ASTM Block Shear Strength of SCL and SSL taken from different Studies

Study	Species Material	Size [mm^2]	MC [%]	SG	τ_T [MPa]	COV [%]	τ_{ASTM} [MPa]	COV [%]	τ_T/τ_{ASTM}
Siller	A **LSL**	44x140	6.8	0.67	**6.43**	8.3	**7.28**	12.0	**0.88**
Siller	DF **LVL**	44x140	7.6	0.58	**7.96**	6.3	**9.27**	8.2	**0.86**
Siller	DF **PSL**	44x140	8.2	0.67	**6.82**	7.1	**9.43**	16.9	**0.72**
Heck (Length)	DF **SSL**	38x89	12	0.49	**10.5**	15.7	**8.3**	10.9	**1.27**
Heck (Depth)	DF **SSL**	38x89 -286	12	0.52	**9.9**	7-18	**8.9**	12.8	**1.11**
Riyanto	DF **SSL**	38x89	13	0.49	**12.64**	17	**7.94**	15	**1.59**

The shear strength (τ_{TL}) of full-size LVL and PSL obtained via torsion was significantly lower compared to full-size Douglas-fir SSL, even though, the two composites had higher SG and lower MC. Manufacturing defects, or checks, such as, lathe checks, resulting from rotary peeling, internal checks from drying of veneers, or simply checks due to not properly glued strand or veneer boundaries, and void areas, are the most plausible explanation for this phenomenon. Hindman (1999) concluded that the shear resistance through the thickness, as well as the transverse elastic stiffness, is decreased in LVL and PSL by the presence of lathe checks.

Jagged failure surfaces have been observed for full-size, joist oriented SCL that failed in shear. For LVL and PSL, failure occurred across the width, in the LR-plane, with the failure path preferentially progressing in the weaker tangential direction in both, torsion and edgewise (joist) bending tests. Lathe checks occur across the veneer thickness, in radial direction for joist oriented specimens. LVL and PSL are therefore more susceptible to shear failure than

solid wood, because discontinuities like lathe checks, or void areas in PSL, can weaken the stronger radial plane of the fibers, thereby reducing the effective shear plane. Not properly glued strand or veneer interfaces might have the same effect. Consequently, LSL is, due to the thinner strands and much higher densification during manufacturing, not as severely affected by checks than LVL and PSL are. The absence of lathe checks in LSL, since LSL strands are sliced directly from debarked logs and not rotary peeled, should be mentioned, too.

These checks, or manufacturing defects, might even attract peak stresses, similar to kerfs, and initiate failure. Respectively, assist in propagating failure, if one or more veneers at or close to mid depth of the beam have such checks. This phenomenon might cause the significant decrease in torsional rigidity which is most pronounced for PSL, that simultaneously has the lowest shear strength.

Aicher (1990) reported a distinct decrease in torsional strength (10 %) and torsional rigidity (30 %) for vertical glulams, when the edge joints of the outer laminations are forcibly opened by saw kerfs. Accordingly, lathe checks, void areas, or not perfectly laminated strands, specifically in the outer laminations of the specimens, might cause a similar decrease in torsional strength and rigidity for SCL. As a consequence, shear failure does not necessarily occur directly at mid depth, where theoretically the highest shear stresses are present. There is no predefined failure plane in full-size torsion or bending tests, as opposed to tests on small shear blocks. The shear failure plane is rather free to follow the path of least resistance to shear within the highest stressed region, close to mid depth of the specimen. In reality, however, higher shear stresses might occur somewhat further up or down than mid depth, due to a reduced effective shear area across the width, if checks are present. LVL and PSL have discontinuities that are much more severe than rays are in solid wood. In addition, it is not surprising that LVL offers higher shear strength compared to PSL, because void areas are a problem that is restricted to PSL. Moreover, PSL has much more interfaces between strands and resin. These interfaces are possible locations of microscopic checks. Consequently, the loss in torsional rigidity with increasing

torque, that was observed for LVL, but to a much higher degree for PSL (see Figure 4-5) can be attributed to such checks.

LSL, in comparison, offers very high shear strength in joist orientation (τ_{TL} > 12.7 MPa), whereas the shear strength in plank orientation (τ_{RL} = 6.4 MPa) is rather low. The high degree of mat densification, during manufacture results in a high SG. Shear strength of SSL is, as other strength properties, proportional to density or SG (Kollmann 1951). Möhler and Hemmer (1977) found the same relationship to be valid in torsion of clear wood, SSL and glulam. The more than 80 % higher SG of LSL compared to solid-sawn Aspen is definitively a major cause for the high shear strength in joist orientation (τ_{TL}). Other factors like the different strand geometry and orientation, or the different resin (MDI versus PF), are further possible explanations for the more than 60 % higher shear strength compared to LVL and even more than 86 % higher shear strength than PSL.

Nevertheless, the shear strength (τ_{RL} = 6.4 MPa) of LSL in plank orientation based on torsion is hardly higher than the shear strength (5.9 MPa) of Quaking aspen (*Populus tremuloides*) and even lower than the shear strength (7.4 MPa) of Bigtooth aspen (*Populus grandidentata*) based on small, clear ASTM block, as given in the (*Wood Handbook* 1999). The low plank shear strength of LSL strongly disagrees with the effort and cost that are put into the manufacture of the composite, especially since aspen is considered as a low density hardwood. For this reason, it is strongly recommended to avoid LSL in structural applications, where shear failure in plank orientation might occur. This example shows, that the shear phenomenon is much more complex, if SCL is considered, where the orientation of the material seems to play the key role, in comparison to SSL, where the variation in shear strength between the different orientations is rather negligible. In addition, the relationship between SG and shear strength is not valid in general for SCL.

The large difference between shear strength in the different orientations for LSL is due to the different fracture morphology as addressed in section 4.3. The low shear strength of LSL in plank orientation, where failure occurred in the

LT-plane, along the strands, can be attributed to the resin (isocyanate, MDI) that served as matrix. As shown in Figure 4-9 the failure plane showed delamination, i.e., adhesive failure only, but no cohesive failure of the thin wood strands. In other words, the high degree of densification only contributes to an increased shear strength (τ_{TL}) in joist orientation. The plank shear strength (τ_{RL}), on the contrary, does not take any benefit at all out of the high SG of LSL.

SCL behaves different from SSL, where tests on structural-size samples led to higher shear strength values than tests on small, clear shear blocks, resulting in τ/τ_{ASTM} ratios ranging from 1.14 for center-point bending, to 1.40 for five-point bending, and 1.59 for torsion (Riyanto 1996). One exception of 0.81 for four-point bending (third-point test) did not follow the general trend. However, Riyanto concluded that four-point bending was not an appropriate test method to determine shear strength of solid-sawn Douglas-fir lumber, since only 6 out of 76 samples failed in the targeted shear mode. Hence, the reported value for four-point bending might only represent the lower tail of the shear strength distribution. The same conclusion was drawn by Craig and Lam (1996), who tested LVL and PSL in four-point bending.

Heck (1997) presented shear strength values obtained by tests performed on solid-sawn Douglas-fir in torsion and in the ASTM shear block standard method, leading to τ_T/τ_{ASTM} ratios of 1.11 for a depth study and 1.27 for a length study.

4.6 Discussion of Different Shear Test Methods

First, some general comments that illustrate the complexity of the shear phenomenon with focus on the state of stress within test specimens and the possible presence of a size, or shape effect in shear, are made. Then, a discussion on the three most common shear test methods, namely the ASTM shear block test, different bending tests, and the torsion test, follows.

It is extremely difficult to produce a state of pure shear stress in wood experimentally. Actually, torsion is the only load configuration that provides a state of pure shear stress. All other shear tests result in a complex state of stress and are consequently problematic due to the superposition of mostly bending stresses. Compressive and tensile stresses, stress concentrations and material inhomogeneity, like checks, result in complex stress interactions. In addition, the shear stress distribution is not uniform over the shear plane for most shear test methods. As a consequence of the different states of stress, special care has to be taken for the comparison of the results of different types of shear tests.

As with other strength properties, there might be a size or shape effect on shear strength. Therefore, the results obtained on small specimens are not necessarily similar to the results obtained from full-size tests. The following factors are frequently cited as possible reasons for a size, or shape effect: probability of defects, stress concentrations, material inhomogeneity, and test setup.

The first one sounds plausible, is however weakened by the fact that a size effect in shear is not only evident for SSL (Rammer et al. 1996), but also for EWPs, like OSB (Bateman et al. 1990), LVL (Hunt et al. 1993), and horizontal glulam (Rammer and Soltis 1994) under five-point bending. Likewise, a size, or shape effect was observed in torsion for vertical glulam (Aicher 1990) and for horizontal glulam and clear wood (Möhler and Hemmer 1977). However, it seemed to be covered by wood texture for SSL of spruce (*Picea abies*), according to Möhler and Hemmer (1977). Heck (1997) found no size effect in torsion for SSL of Douglas fir (*Pseudotsuga menziesii*). Consequently, it appears like the probability of natural defects might be excluded as cause for a size effect, since no size effect was observed for SSL, containing natural defects like knots; but, there was a size effect for clear wood, not containing natural defects, and engineered wood products, where natural defects are dispersed and variability is thereby reduced.

Stress concentration might be closer related to a shape than to a size effect. Stress concentrations are peak stresses that usually occur only within very restricted areas and dissipate rapidly. They are more severe for small specimens. Especially, ASTM shear blocks with the sharp, reentrant corner, acting like a notch, are subjected to stress concentrations. This kerf might result in conservative design values due to high stress concentrations. In full-size specimens, stress concentrations might only occur at the supports or load bearing areas, if not sufficient area is provided, in other words for small width or depth. Stress concentrations might be responsible for an aspect, or side ratio effect on shear strength.

Material inhomogeneity, on the other hand, contributes to stress concentrations and again the effect increases with decreasing size. Even within clear wood samples the porous earlywood does not bear the same stresses as the dense latewood. Species like Douglas-fir, that exhibit abrupt changes in the growth zones, or materials that contain internal checks and shakes, which can act as planes of weakness for shear failure to develop, appear to be more inclined to this type of failure behavior, according to Bodig and Jayne (1982). Therefore, material inhomogeneity is of special interest in wood composites, where internal or lathe checks, void areas, variation in strand orientation, density or stiffness gradients through the thickness, as well as wood/adhesive interfaces are the most critical examples.

Finally, test setup is illuminated, starting with the ASTM shear block test that was presented in detail in section 4-3 and not recommended as standard test method in the future. Tingley, Pooley, and Kent (1996) reported that the shear strength obtained from small, clear samples usually exceeds that of full-size specimens ($\tau/\tau_{TASTM} < 1$). The same behavior was observed in the current study on torsion of SCL. Tingley et al. measured strains in Douglas-fir shear blocks and reported that the highest shear stresses were present near the sharp reentrant corner. They also observed a disproportionate increase in shear stresses with increasing load. Simultaneously, the same observations were made

for compressive stresses parallel and perpendicular to the grain. Shear stresses and compressive stresses parallel to grain decreased significantly from top to bottom. Stresses perpendicular to grain turned from maximum compressive values near the top into tension close to mid height and with increasing load again into compression at the lower end. This complex stress distribution is not at all uniform over the shear plane. Furthermore, the maximum shear stresses at the top are suppressed by the maximum compressive stresses perpendicular to grain, while the shear stresses at mid height are supported by tensile stresses perpendicular to the grain. It is therefore almost impossible to make general statements on, where failure might be initiated and, if shear or tension perpendicular to grain might act as sparkplug, what might even change with different shear/tension perpendicular to grain strength ratios ($\tau/\sigma_{\perp\perp}$) of the tested materials. If failure initiation takes place at the top, the apparent shear strength might be on the unsafe side, since concomitant compressive stresses perpendicular to grain were proved to increase the shear capacity (Mandery 1969). If, on the other hand, failure might be initiated close to mid height the reverse is true and the apparent shear strength might be conservative. The different full-size/small, clear shear strength ratio statements from Ylinen ($\tau_T/\tau_{TASTM} > 1$) for torsion, respectively Tingley et al. ($\tau_B/\tau_{TASTM} < 1$) regarding bending, where a distinct size effect is well known, are therefore not contradictory, especially since the latter mainly tested glulams of bigger dimensions.

More important for the current study, the different trend between SCL (LSL, LVL and PSL), where $\tau_T/\tau_{TASTM} < 1$ on one side, and SSL (Douglas-fir (*Pseudotsuga menziesii*), where $\tau_T/\tau_{TASTM} > 1$ on the other side, might be explained by the complex state of stress within the small shear blocks and different shear/tension perpendicular to grain strength ratios for the different materials. The brittle failure behavior of LSL that failed in the LT-plane resembled more to a tension perpendicular to grain failure mode. For some specimens a

loud bang accompanied catastrophic failure and many specimens showed wide, open cracks. This observation might indicate that the low shear strength of LSL that failed in plank orientation might be due to the limited internal bond capacity of the diphenylmethane diisocyanate (MDI) resin that served as matrix in LSL.

Only one source was found that delivered values for tensile strength perpendicular to grain for SCL. If the German design values, as given in Table 3-3, for flatwise shear strength (τ_{RL}) are set into relation with the tensile strength perpendicular to grain ($\sigma_{t\perp}$), one obtains the following ratios ($\tau_{RL}/\sigma_{t\perp}$) for the different SCL products: 1.2 for LSL, 2.6 for LVL, and 5.0 for PSL. To put it another way, LSL shows the highest capacity regarding tension perpendicular to grain. As a consequence, tension perpendicular to grain might be excluded as controlling strength, since LVL and PSL, having higher $\tau_{RL}/\sigma_{t\perp}$ ratios failed in LR-plane and not in LT-plane.

Another possibility to induce shear failure within a specimen is to subject it to bending. Bending is the primary loading condition in structures. Bending tests are therefore widely applied. The obtained failure mode is then typically either bending or shear, where the probability of shear failure increases with decreasing span/depth (L/d) ratio, i.e., it is high for short, deep beams and materials with low shear/bending strength ratio (τ/σ). Various test configurations are possible, most commonly used to obtain shear failure are however three-point bending, also called center-point, and the statically indeterminate five-point bending setup. Sometimes specimens are notched, saw kerfs are applied, or specimens with I-shaped cross-sections are used to reduce the shear area, while the moment of inertia (I) is hardly reduced. Thus, the percentage of shear failure is increased, especially for three-point bending tests of materials with high shear/bending strength ratio. The shear/bending stress ratio (τ/σ) is according to elementary beam theory more than 80 % higher for the five-point setup (11d/12L) compared to the three-point configuration (d/2L). Therefore, the probability for the occurrence of shear failure should be higher for the five-point bending test when

regarding a constant span/depth ratio. However, Riyanto (1996) and Sanders (1996) observed a different trend during their test series on Douglas-fir SSL beams. In both cases, shear failure percentage was higher for the three-point loading configuration. This difference between theory and practice might indicate that elementary beam theory is rather not capable of describing the complex state of stress within a specimen under five-point bending.

Several studies that focused on bending tests to determine the shear strength are presented in the *Literature Review* in chapter 2. A short summary of the most important observations is following here. First, bending introduces a complex interaction of three-dimensional tension, compression and shear strains. Second, the type of loading configuration (three-, four-, or five-point bending) and the span/depth ratio (L/d) mainly affect the measured shear strength. Third, there is no significant relationship between bending and shear strength on one hand, as well as between MOE and shear strength on the other hand. Fourth, the measured shear stress at failure usually represents a lower bound to the true shear strength, since a certain percentage, often times more than half, of the samples, fails in bending. Fifth, the five-point setup usually results in markedly higher shear strengths than the three-point configuration does. Sixth, there is a substantial interaction between shear stresses and concomitant compressive stresses perpendicular to the grain that is more pronounced for smaller beams. Seventh, bending tests are problematic for small, narrow samples, since crushing might occur at the load or support plates. Finally, there is a distinct size effect on shear strength obtained via flexure tests, especially in the five-point setup, as mentioned before.

The torsion test, on the other hand, has been presented in section 4.2. Its biggest advantage is a state of pure shear stress. Consequently, all specimens fail in shear. No other failure modes are observed. Thus, it is possible to evaluate the true shear strength. Other advantages are the possibility of the consideration of orthotropic material properties, a uniform shear stress distribution along member length and applicability to all sizes. Last, but not least, torsion results

show very low variation, leading to high characteristic, or 5^{th}-percentile tolerance, values and, more important for structural applications, to high design values.

5. Conclusions and Recommendations

The following conclusions are drawn based on the results of the study on the longitudinal shear strength of structural composite lumber (SCL) and finally some recommendations are suggested for future projects.

5.1 Conclusions

- Since torsion provides a state of pure shear stress and torsion theory is capable of taking into account the orthotropic nature of SCL, torsion tests do provide pure shear strength of SCL, which is similar to other pure strength properties (bending, tension, compression).
- Shear strength based on torsion is highly dependent on the ratio of the shear moduli in the two longitudinal planes, G_{LT} and G_{LR}.
- In torsion, LSL failed abruptly, in a brittle manner, on the short side, along the strands (LT-plane), whereas LVL and PSL failed gradually, in a more ductile manner, mostly on the long side, across the strands or veneers (LR-plane).
- LVL and PSL displayed a distinct decrease in torsional rigidity with increasing torque, while LSL showed a much more linear torque-twist relation.
- Void areas and checks, like lathe checks, resulting from rotary peeling and internal checks, resulting from drying of veneers, or not properly glued interfaces, possibly decrease the shear resistance of LVL and PSL.
- The finite element analysis confirmed the shear stresses as given by orthotropic theory.

- Shear strength of SCL based on torsion was obtained as follows: LSL in plank orientation τ_{LR} = 6.43 MPa; LVL in joist orientation τ_{LT} = 7.96 MPa; PSL in joist orientation τ_{LT} = 6.82 MPa.
- Shear strength of SCL is significantly higher in joist orientation, where failure occurs across the strands or veneers (RL-plane), compared to plank orientation, where failure occurs along the strands or veneers (TL-plane), for both test methods, torsion and ASTM block (i.e., $\tau_{TL} > \tau_{RL}$).
- In joist orientation, LSL shows much higher shear strength (τ_{TL}) than LVL and PSL for both test methods, whereas in plank orientation all three composites show similar shear strengths (τ_{RL}).
- Based on the failure modes of three composites observed in this study, the shear strength of SCL may not be as strongly influenced by density as in SSL, but rather by the design of the composite.
- ASTM blocks of joist oriented LSL failed rather in compression parallel to grain (crushing), or a combined failure mode of crushing and shear than in pure shear.
- Shear strength of SCL based on shear block is higher than shear strength based on full-size torsion ($\tau_T/\tau_{ASTM} < 1$) as opposed to what has been observed earlier for SSL.
- Variation of shear stresses is significantly lower in full-size torsion (6 – 8 %) than for ASTM blocks (8 – 19 %). As a consequence, design values based on torsion might be more reliable.
- The design shear strength of LSL in the US and Canada might be conservative in both orientations.

5.2 Recommendations

- Torsion is recommended as standard test method to determine shear strength of SCL, because of the possibility to consider orthotropic material properties and its applicability to all sizes. Torsion shows low COV and is the only test method that imposes a state of pure shear stress on the specimen. This will complement the way other design stresses are determined, i.e., pure tensile, compressive and bending strength.
- ASTM shear block test is unsuitable for the evaluation of shear strength of SCL, since in joist orientation LSL rather fails in crushing than in shear. Besides, COV is generally high, specific for LVL in plank orientation. In addition, a size effect is present in shear, as has been observed earlier in bending as well as in torsion. Thus, ASTM shear block test should not be used as standard test method in the future.
- A follow up torsion study on SCL specimens with different aspect ratios should be performed to obtain shear failure in the other planes. Specific, shear strength of plank oriented SCL needs further evaluation, since the design values show a reversed ranking in the US and Canada compared to Germany.
- Teflon sheets are recommended to reduce the frictional forces at the clamps to further justify the consideration of St. Venant torsion only.
- Duration of load effects on torsion test results of SCL should be investigated.
- Further research is necessary on the orthotropic material properties of SCL and the effects of certain design factors – like strand geometry and orientation, wood/adhesive interfaces, stiffness or density gradient through the thickness, lathe checks, internal checks from drying, lap joints and void areas – on them.

Bibliography

Aicher, S. 1990. Investigation on the torsion properties of vertical glulam including warping torsion of orthotropic materials. Otto Graf Journal Vol. 1 1990 pp. 9-35. Forschungs- und Materialpruefungsanstalt Baden-Wuerttemberg, Otto Graf Institut, Stuttgart, Germany.

American Forest and Paper Association. 1997. ANSI/NFPA NDS-1997 National design specification for wood construction. AFPA, Washington, DC.

American Society for Testing and Materials. 2001. Test methods for small clear specimens of timber ASTM D 143. Annual Book of ASTM Standards. Vol. 04.10. West Conshohocken, PA.

American Society for Testing and Materials. 2001. Test methods of static tests of lumber in structural sizes ASTM D 198. Annual Book of ASTM Standards. Vol. 04.10. West Conshohocken, PA.

American Society for Testing and Materials. 2001. Specific gravity of wood and wood-base materials ASTM D 2395. Annual Book of ASTM Standards. Vol. 04.10. West Conshohocken, PA.

American Society for Testing and Materials. 2001. Evaluating allowable properties for grades of structural lumber ASTM D 2915. Annual Book of ASTM Standards. Vol. 04.10. West Conshohocken, PA.

American Society for Testing and Materials. 2001. Direct moisture content measurements of wood and wood-base materials ASTM D 4442. Annual Book of ASTM Standards. Vol. 04.10. West Conshohocken, PA.

American Society for Testing and Materials. 2001. Mechanical properties of lumber and wood-base structural material ASTM D 4761. Annual Book of ASTM Standards. Vol. 04.10. West Conshohocken, PA.

American Society for Testing and Materials. 2001. Specification for evaluation of structural composite lumber products ASTM D 5456. Annual Book of ASTM Standards. Vol. 04.10. West Conshohocken, PA.

Asselin, S. 1995. Effects of member size on the shear strength of sawn lumber beams. MS Thesis. Department of Civil and Environmental Engineering, Washington State University. Pullman, WA.

Bateman, J., M. Hunt, and C. Sun. 1990. New interlaminar shear test for structural wood composites. Forest Products Journal. 40(3):9-14.

Bodig, J. and B. Jayne. 1982. Mechanics of wood and wood composites. Van Nostrand Reinhold Company, New York.

Bradtmueller, J., M. Hunt, and S. M. Shook. 1998. Mechanical properties of laminated veneer lumber via five-point bending test. Journal of Testing and Evaluation. 26(2):132-137.

Breitinger, H., R. Leicester, C.Seath, and P. Walsh. 1994. In-grade wood beam shear strength. Proceedings of Pacific Timber Engineering Conference. Gold Coast, Australia.

Cofer, W., F. Proctor, Jr., and D. McLean. 1997. Prediction of the shear strength of wood beams using finite element analysis. Mechanics of Cellulosic Materials. ASME 1997. New York, NY.

Craig, B. and F. Lam. 2000. Shear strength in structural composite lumber. Draft paper received from the authors.

Craig, B. and F. Lam. 1996. Preliminary investigation of shear strength in structural composite lumber. Proceedings of the International Wood Engineering Conference. New Orleans, LA.

Ehart, R., S. Stanzl-Tschegg, and E. Tschegg. 1998. Fracture characteristics of PARALLAM® PSL in comparison to solid wood and particleboard. Wood Science and Technology. 32(1):43-55.

Ellis, S. and J. Dubois. 1994. Determination of Parallam® macroporosity by two optical techniques. Wood and Fiber Science. 26(1):70-77.

Ethington, R., W. Galligan, H. Montrey, and A. Freas. 1979. Evolution of allowable stresses in shear for lumber. FPL-23. U.S. Department of Agriculture, Forest Service, Forest Products Laboratory. Madison, WI.

Heck, L.R. 1997. Evaluation of the torsion test for determining the shear strength of structural lumber. MS Thesis. Department of Forest Products, Oregon State University. Corvallis, OR.

Heimeshoff, B. 1982. Ueber den Einfluss der Anisotropie auf den Spannungs- und Verformungszustand von Staeben mit Rechteckquerschnitt bei Torsionsbeanspruchung. Ingenieurholzbau in Forschung und Praxis. pp.9-16. Bruderverlag Karlsruhe, Germany. (in German).

Hindman, D. 1999. Elastic constants of selected engineered wood products. MS thesis. Department of Forest Resources, Pennsylvania State University. University Park, PA.

Hunt, M., S. R. Shook, and J. Bradtmueller. 1993. Longitudinal shear strength of LVL via the five-point bending test. Forest Products Journal. 43(7/8):39-44.

Janowiak, J. and R. Pellerin. 1992. Shear moduli determination using torsional stiffness measurements. Wood and Fiber Science. 24(4):392-400.

Kollmann, F. 1951. Technologie des Holzes und der Holzwerkstoffe. Springer-Verlag, Berlin, Germany. (in German).

Lam, F., H. Yee, and J. Barrett. 1995. Shear strength of Canadian softwood structural lumber. CIB-W18/28-6-1. Presented at International Council for Building Research Studies and Documentation Conference. Copenhagen, Denmark.

Leicester, R. and H. Breitinger. 1992. Measurement of beam shear strength. Proceedings of IUFRO S.05.02 Timber Engineering Meeting, Bordeaux, France.

Leichti, R. and T. Nakhata. 1999. The role of bearing plates in the five-point bending tests of structural-size lumber. Journal of Testing and Evaluation. 27(3):183-190.

Leichti, R., M. Vatovec, and P. Cheng. 1996. An appraisal of stress interactions in the five-point bending specimen. Presented at ASTM D07 Working Group Meeting. Madison, WI.

Lekhnitskii, S. G. 1981. Theory of elasticity of an anisotropic body. MIR Publishers, Moscow, Russia.

Mandery, W. 1969. Relationship between perpendicular compressive stress and shear strength of wood. Wood Science. 1(3):177-182.

Möhler, K. and K. Hemmer. 1977. Verformungs- und Festigkeitsverhalten von Nadelvoll- und Brettschichtholz bei Torsionsbeanspruchung. Holz als Roh- und Werkstoff 35(1977)473-478. Springer-Verlag, Berlin, Germany. (in German).

Moses, D. 2000. Constitutive and analytical models for structural composite lumber with applications to bolted connections. PhD Thesis. Department of Civil Engineering, University of British Columbia. Vancouver, BC, Canada.

Peterson, J. 1995. Shear strength of checked and split Southern pine lumber. MS Thesis. Department of Civil and Environmental Engineering, Washington State University. Pullman, WA.

Rammer, D. and L. Soltis. 1994. Experimental shear strength of glued-laminated beams. FPL-RP-527. U.S. Department of Agriculture, Forest Service, Forest Products Laboratory. Madison, WI.

Rammer, D., L. Soltis, and P. Lebow. 1996. Experimental shear strength of unchecked solid-sawn Douglas-fir. FPL-RP-553. U.S. Department of Agriculture, Forest Service, Forest Products Laboratory. Madison, WI.

Riyanto, D. 1996. A comparison of test methods for evaluating shear strength of structural lumber. MS Thesis. Department of Forest Products, Oregon State University. Corvallis, OR.

Sanders, C. 1996. The effects of testing conditions on the measured shear strength of wood beams. MS Thesis. Department of Civil and Environmental Engineering, Washington State University. Pullman, WA.

Smulski, S. 1997. Engineered wood products, a guide for specifiers, designers and users. PFS Research Foundation. Madison, WI.

Tingley, D. and S. Kent. 1996. The effects of test setup and apparatus on full-scale glued laminated timber beam shear strength. Draft paper received from the authors.

Tingley, D., S. Kent, and R. Leichti. 1996. The effects of test configuration on the shear strain in glue-laminated timber. Presented at Forest Products Society Annual Meeting. Minneapolis, MN.

Tingley, D., B. Pooley, and S. Kent. 1996. Shear strength of full-scale glulam beams. Draft paper received from the authors.

Trayer, G. and H. March. 1930. The torsion of members having sections common in aircraft construction. FPL Report No. 334. U.S. Department of Agriculture, Forest Service, Forest Products Laboratory. Madison, WI.

U.S. Forest Products Laboratory. 1999. Wood handbook: Wood as an engineering material. General Technical Report. FPL-GTR-113. U.S. Department of Agriculture, Forest Service, Forest Products Laboratory. Madison, WI.

Tsoumis, G. 1991. Science and technology of wood: Structure, properties, utilisation. Chapman & Hall, New York.

Wangaard, F. 1979. Wood: its structure and properties. Clark C. Heritage memorial series on wood. Volume 1. Forest Products Laboratory. Madison, WI.

Yeh, B. 1997. Shear strength of structural glued-laminated timber based on full-size flexure tests. APA Rep. T97-25. American Plywood Association – The Engineered Wood Association. Tacoma, WA.

Yeh, B. 1993. Shear strength of Douglas-fir structural glued-laminated timber. AWS Rep. T93-2. American Wood Systems – American Plywood Association. Tacoma, WA.

Ylinen, A. 1963. A comparative study of different types of shear test for wood. The State Institute for Technical Research. Helsinki, Finland.

APPENDICES

Appendix A

Abbreviations and Notations

Abbreviations:

A	Aspen
ASTM	American Society for Testing and Materials
BC	Boundary Conditions
CDF	Cumulative Density Function
COV	Coefficient of Variation
DF	Douglas-Fir
EWP	Engineered Wood Products
FE	Finite Element
GLULAM	Glued-Laminated Timber
J	Joist
L	Longitudinal
LR	Longitudinal-Radial
LT	Longitudinal-Tangential
LSL	Laminated Strand Lumber
LVL	Laminated Veneer Lumber
MC	Moisture Content
MOE	Modulus of Elasticity
MOR	Modulus of Rupture
OSB	Oriented Strand Board
P	Plank
PEPE	Plate Edge to Plate Edge
PSL	Parallel Strand Lumber
R	Radial
RH	Relative Humidity
SCL	Structural Composite Lumber
SG	Specific Gravity
SP	Southern Pine
SSL	Solid-Sawn Lumber
T	Tangential
	Torsion

Notations:

A	Area
C	Torsional Rigidity
E	Modulus of Elasticity
E_d	Dynamic Modulus of Elasticity determined via Stress Wave Timer
E_f	Static Modulus of Elasticity determined via flatwise Bending Test
E_L	Modulus of Elasticity in Longitudinal Direction
E_R	Modulus of Elasticity in Radial Direction
E_T	Modulus of Elasticity in Tangential Direction
G	Shear Modulus, or Modulus of Rigidity

G_{RL}	Shear Modulus in RL-Plane
G_T	Torsional Modulus
G_{TL}	Shear Modulus in TL-Plane
G_{05}	Lower 5th-percentile Tolerance Limit for Shear Modulus
M	Torsional Moment, or Torque
b	Width
c	Aspect Ratio, or Side Ratio, or Depth/Width Ratio (c = h/b)
d	Ratio, relating aspect ratio to shear moduli ratio (d = c/μ)
g	Ratio of Shear Moduli in Longitudinal Planes ($g = G_{TL}/G_{RL}$)
h	Depth
l	Length
n	Sample Size
x	Co-ordinate Axis in Radial Direction (ASTM defined x as Tangential)
y	Co-ordinate Axis in Tangential Direction (ASTM defined y as Radial)
z	Co-ordinate Axis in Longitudinal Direction
μ	Ratio ($\mu = \sqrt{g}$)
ν	Poisson Ratio
θ	Total Angle of Twist (at maximum Torque)
ρ	Density
σ	Normal Stress
$\sigma_{c\parallel}$	Compressive Stress parallel to Grain
$\sigma_{c\perp}$	Compressive Stress perpendicular to Grain
$\sigma_{t\parallel}$	Tensile Stress parallel to Grain
$\sigma_{t\perp}$	Tensile Stress perpendicular to Grain
τ	Shear Stress
τ_{ASTM}	Shear Stress based on ASTM Shear Block Test
τ_B	Shear Stress based on Bending Test
τ_{dry}	Shear Stress at 12 % MC
τ_{green}	Shear Stress at 30 % MC
τ_{RL}	Shear Stress (Shear Failure in TL-Plane)
$\tau_{RL\text{-}I}$	Isotropic Shear Stress (Shear Failure in TL-Plane)
$\tau_{RL\text{-}O}$	Orthotropic Shear Stress (Shear Failure in TL-Plane)
τ_T	Shear Stress based on Torsion Test
τ_{TL}	Shear Stress (Shear Failure in RL-Plane)
$\tau_{TL\text{-}I}$	Isotropic Shear Stress (Shear Failure in RL-Plane)
$\tau_{TL\text{-}O}$	Orthotropic Shear Stress (Shear Failure in RL-Plane)
τ_{05}	Lower 5th-percentile Tolerance Limit for Shear Stress
τ_3	Shear Stress based on Three-Point Bending Test
τ_5	Shear Stress based on Five-Point Bending Test
τ_{45}	Shear Stress at an Angle of 45 degrees to the Annual Rings
ω	Angle of Twist per unit Length

Appendix B

Elastic Constants

Modulus of Elasticity via Stress Wave Timer

LSL	Volume [ccm]	Density [g/ccm]	Time [1E-06 s]	E_d [GPa]	LVL	Volume [ccm]	Density [g/ccm]	Time [1E-06 s]	E_d [GPa]	PSL	Volume [ccm]	Density [g/ccm]	Time [1E-06 s]	E_d [GPa]
					L30	8422	0.558	292	12.27	P60	8148	0.675	280	16.18
T01	8489	0.716	348	11.15	L31	8393	0.570	301	11.79	P61	8188	0.677	276	16.68
T02	8378	0.747	337	12.37	L32	8497	0.567	301	11.77	P62	8148	0.679	278	16.53
T03	8427	0.678	341	10.98	L33	8451	0.550	296	11.77	P63	8221	0.636	285	14.72
T04	8473	0.721	347	11.26	L34	8378	0.553	302	11.38	P64	8186	0.665	292	14.62
T05	8424	0.732	333	12.41	L35	8532	0.616	297	13.16	P65	8161	0.642	295	13.84
T06	8456	0.697	333	11.80	L36	8454	0.560	295	12.11	P66	8146	0.663	296	14.17
T07	8441	0.722	334	12.20	L37	8439	0.582	301	12.06	P67	8243	0.631	277	15.49
T08	8469	0.686	338	11.30	L38	8551	0.597	289	13.40	P68	8157	0.664	297	14.16
T09	8436	0.687	339	11.26	L39	8478	0.546	318	10.15	P69	8162	0.672	303	13.72
T10	8418	0.727	342	11.72	L40	8437	0.575	322	10.41	P70	8195	0.621	298	13.14
T11	8416	0.731	343	11.72	L41	8659	0.553	283	12.97	P71	8163	0.637	295	13.75
T12	8477	0.730	336	12.19	L42	8384	0.572	300	11.89	P72	8162	0.656	308	13.03
T13	8413	0.715	334	12.03	L43	8473	0.597	283	13.97	P73	8177	0.652	289	14.70
T14	8465	0.716	337	11.86	L44	8425	0.572	302	11.78	P74	8164	0.640	309	12.62
T15	8425	0.688	335	11.52	L45	8675	0.588	278	14.30	P75	8183	0.671	278	16.34
T16	8402	0.737	331	12.67	L46	8699	0.552	280	13.28	P76	8135	0.676	309	13.30
T17	8422	0.699	333	11.84	L47	8514	0.565	303	11.59	P77	8146	0.673	285	15.56
T18	8450	0.719	331	12.32	L48	8657	0.554	278	13.47	P78	8193	0.675	297	14.41
T19	8363	0.682	342	10.95	L49	8397	0.567	296	12.14	P79	8172	0.676	292	14.92
T20	8430	0.719	341	11.63	L50	8633	0.580	272	14.71	P80	8161	0.673	297	14.38
T21	8402	0.682	346	10.69	L51	8439	0.550	312	10.59	P81	8136	0.692	278	16.82
T22	8449	0.711	339	11.64	L52	8429	0.566	336	9.40	P82	8161	0.669	285	15.46
T23	8403	0.737	342	11.84	L53	8627	0.576	288	13.01	P83	8141	0.640	284	14.87
T24	8453	0.695	339	11.38	L54	8532	0.613	281	14.55	P84	8186	0.655	276	16.14
T25	8444	0.684	337	11.34	L55	8596	0.578	306	11.58	P85	8142	0.649	282	15.32
T26	8387	0.701	339	11.44	L56	8498	0.623	286	14.30					
T27	8504	0.753	341	12.17	L57	8624	0.560	282	13.23					
T28	8501	0.741	341	11.99	L58	8667	0.554	290	12.40					
T29	8401	0.666	342	10.69	L59	8666	0.579	283	13.60					
mean	8435	0.711	339	**11.67**	mean	8521	0.573	295	**12.86**	mean	8168	0.660	290	**14.80**
stdev	35.5	0.023	4.6	0.52	stdev	103.4	0.020	14.4	1.34	stdev	26.0	0.018	10.6	1.20
COV [%]	0.4	3.3	1.3	4.5	COV [%]	1.2	3.6	4.9	10.4	COV [%]	0.3	2.8	3.6	8.1

Modulus of Elasticity in Flatwise Bending Ef via Third-Point Test

LSL TimberStrand				LVL Microllam						PSL Parallam			
Name	R^2	# Obs	E_f [GPa]	Name		# Plies	R^2	# Obs	E_f [GPa]	Name	R^2	# Obs	E_f [GPa]
				L30		19	0.99	46	11.62	P60	1	30	15.93
T1	0.98	33	9.17	L31		19	0.99	41	14.22	P61	1	33	15.32
T2	1	27	13.29	L32		19	1	45	14.98	P62	1	35	16.45
T3	1	37	11.88	L33	x	19	1	48	13.93	P63	1	32	15.53
T4	0.98	40	10.62	L34		19	0.98	44	11.47	P64	1	31	16.71
T5	0.99	38	11.25	L35		19	1	17	14.48	P65	1	32	13.57
T6	0.98	49	9.26	L36	x	19	1	54	13.45	P66	1	33	14.43
T7	0.98	61	9.84	L37		19	0.98	41	13.41	P67	1	32	16.24
T8	0.99	68	9.15	L38	x	19	0.98	43	14.13	P68	1	34	15.40
T9	0.98	67	9.59	L39		19	1	50	13.47	P69	1	31	14.27
T10	0.99	37	10.60	L40		19	1	46	15.32	P70	1	34	13.16
T11	1	38	12.58	L41		15	0.99	51	12.52	P71	1	32	13.92
T12	0.99	42	10.33	L42		19	0.99	47	12.31	P72	1	31	14.88
T13	0.98	51	10.61	L43	x	19	0.99	41	13.88	P73	1	31	15.14
T14	0.98	48	10.76	L44		19	1	30	14.96	P74	1	32	14.27
T15	0.99	52	9.81	L45		15	1	20	19.90	P75	1	32	14.57
T16	0.99	43	11.26	L46		15	0.99	33	15.79	P76	1	34	13.90
T17	1	47	12.26	L47		19	1	31	16.06	P77	1	37	14.55
T18	0.99	45	10.28	L48		15	1	29	17.07	P78	1	31	15.25
T19	0.99	46	10.35	L49		19	1	35	12.84	P79	1	32	14.63
T20	0.98	48	10.29	L50		15	0.99	32	18.49	P80	1	33	13.99
T21	1	42	11.82	L51		19	1	38	12.97	P81	1	28	17.73
T22	1	42	11.36	L52		19	1	35	13.27	P82	1	33	15.51
T23	0.98	39	10.83	L53		15	0.98	31	13.62	P83	1	32	14.00
T24	0.99	41	10.30	L54		15	1	29	17.62	P84	1	32	14.34
T25	0.99	43	10.38	L55		15	1	34	13.62	P85	1	30	15.84
T26	1	45	12.25	L56		19	1	29	18.42				
T27	1	40	13.53	L57		15	0.98	32	13.08		x: both narrow side faces		
T28	0.99	42	13.03	L58		15	1	34	15.70				
T29	1	48	11.39	L59		15	1	31	16.77				
mean			**10.97**	mean					**14.64**	mean			**14.98**
stdev			1.21	stdev		19 x 19 plies			2.11	stdev			1.07
COV [%]			11.0	COV [%]		11 x 15 plies			14.4	COV [%]			7.1

Elastic Constants - LSL & LVL

all values for E and G in **[MPa]**
values found on page (Hindman 1999):
E: 99, 69-70, 89, 93 m: 96
G: 109-110, 72, 82

FPBT: Five-Point Bending Test
TSMT: Torsional Stiffness Measurement Test
LVL: Laminated Veneer Lumber
LSL: Laminated Strand Lumber
PSL: Parallel Strand Lumber

colour definition: bold & bigger: used as input values in current study
black: values from Hindman 1999 (E1 and E2 are mean of
blue: values from my study tension & compression test)
red: values based on my E1 value using Hindmans ratios
brown: values calculated from Hindmans 1999 study
green: values from Wood Handbook 1999 for **solid** wood
plum: values from Bodig and Goodman 1973 for **solid** wood
(average of 3 measurements)

Douglas-fir LVL 2.0E

coastal

comment: LVL in current study was 1.9 E-rated

MC [%] SG [1] Moduli of Elasticity (MOE) Shear Moduli (G) Poisson Ratio
11.3 0.52
7.6 0.56 longitudinal transverse in-plane through-the-thickness Elastic Ratios
12 0.48

Test:	E1flat E_L	E1edge	E2flat E_T	G12 G_{LT}	G21	G13 G_{LR}	G23 G_{TR}	m12 ν_{LT}	E2/E1 E_T/E_L	G12/E1 G_{LT}/E_L	G21/E1 G_{TL}/E_L	G13/E1 G_{LR}/E_L	G23/E1 G_{TR}/E_L
FPBT	18300	16100	500	405		331	45.8						
TSMT				642	710	440	48			0.0406	0.0449	0.0278	0.0030
Tension	15900	E1**mean**	390					0.767	0.0272				
Compression	15700	15800	470					0.580					
stress wave	12900	E2**mean**	430				m12**mean**	0.674	36.7	24.6	22.3	35.9	329.2
4-pt bending (third-pt)	**14600**		**397**	**593**	656	**407**	**44.4**						
	13400		670	1045		858	94	0.449	0.050	0.078		0.064	0.007

Aspen LSL 1.5E

quaking

comment: LSL in current study was the same

MC [%] SG [1]
8.5 0.65 Moduli of Elasticity (MOE) Shear Moduli (G) Poisson Ratio Elastic Ratios
6.8 0.7
12 0.38 longitudinal transverse in-plane through-the-thickness
12 0.30

Test:	E1flat E_L	E1edge	E2flat E_T	G12 G_{LT}	G21	G13 G_{LR}	G23 G_{TR}	m12 ν_{LT}	E2/E1 E_T/E_L	G12/E1 G_{LT}/E_L	G21/E1 G_{TL}/E_L	G13/E1 G_{LR}/E_L	G23/E1 G_{TR}/E_L
FPBT	13400	10000	1490	681		251	104						
TSMT				910	1790	370	110			0.0711	0.1398	0.0289	0.0086
Tension	13000	E1**mean**	1420					0.556	0.1098				
Compression	12600	12800	1390					0.496					
stress wave	11700	E2**mean**	1405				m12**mean**	0.526	9.1	14.1	7.2	34.6	116.4
4-pt bending (third-pt)	**11000**		**1207**	**782**	1538	**318**	**94.5**						
	8100							0.374					
	8763		265	436		618	94.5	0.374	0.030	0.050		0.071	0.011

Elastic Constants - PSL

all values for E and G in **[MPa]**
values found on page (Hindman 1999):
E: 99, 69-70, 89, 93 m: 96
G: 109-110, 72, 82

FPBT: Five-Point Bending Test
TSMT: Torsional Stiffness Measurement Test
LVL: Laminated Veneer Lumber
LSL: Laminated Strand Lumber
PSL: Parallel Strand Lumber

colour definition: bold & bigger: used as input values in current study
black: values from Hindman 1999 (E1 and E2 are mean of
blue: values from my study tension & compression test)
red: values based on my E1 value using Hindmans ratios
brown: values calculated from Hindmans 1999 study
green: values from Wood Handbook 1999 for **solid** wood

Yellow poplar PSL 2.0E

comment: PSL in current study was Douglas-fir

MC [%]	SG [1]	Moduli of Elasticity (MOE)			Shear Moduli (G)				Poisson Ratio	Elastic Ratios				
10.1	0.59													
8.2	0.65	longitudinal		transverse	in-plane		through-the-thickness							
12	0.42													
Test:		E1flat	E1edge	E2flat	G12	G21	G13	G23	m12	E2/E1	G12/E1	G21/E1	G13/E1	G23/E1
		E_L		E_T	G_{LT}		G_{LR}	G_{TR}	ν_{LT}	E_T/E_L	G_{LT}/E_L	G_{TL}/E_L	G_{LR}/E_L	G_{TR}/E_L
FPBT		14500	18000	400	252		372	98.6					0.0248	
TSMT					300	298	---	120			0.0200	0.0199		0.0080
Tension		15000	E1**mean**	330					0.985	0.0240				
Compression		15000	15000	390					0.611					
4-pt bending (third-pt)		**15000**	E2**mean**	360				m12**mean**	0.798	41.7	50.0	50.3	40.3	125.0
stress wave		14800		360	300	298	372	120						
		10900		469	752		818	120	0.392	0.043	0.069		0.075	0.011

Southern pine PSL 2.0E

longleaf comment: PSL in current study was Douglas-fir

MC [%]	SG [1]	Moduli of Elasticity (MOE)			Shear Moduli (G)				Poisson Ratio	Elastic Ratios				
9.5	0.66													
8.2	0.65	longitudinal		transverse	in-plane		through-the-thickness							
12	0.59													
Test:		E1flat	E1edge	E2flat	G12	G21	G13	G23	m12	E2/E1	G12/E1	G21/E1	G13/E1	G23/E1
		E_L		E_T	G_{LT}		G_{LR}	G_{TR}	ν_{LT}	E_T/E_L	G_{LT}/E_L	G_{TL}/E_L	G_{LR}/E_L	G_{TR}/E_L
FPBT		15100	15000	480	501		251	84.8			0.0330		0.0165	
TSMT					---	56.4	---	26				0.0037		0.0017
Tension		15400	E1**mean**	450					0.762	0.0299				
Compression		15000	15200	460					0.894					
4-pt bending (third-pt)		**15000**	E2**mean**	455				m12**mean**	0.828	33.4	30.3	269.5	60.6	584.6
stress wave		14800		449	494	55.7	248	25.7						
		13700		670	822		973	94	0.365	0.055	0.060		0.071	0.012
mean values for PSL (YP & SP):				**404**	**398**		**310**	**72.8**		0.02695	0.0265		0.02065	0.00485

Appendix C

Torsion Test Data

Torsion Test Data

	max Torque	Twist	Time		max Torque	Twist	Time		max Torque	Twist	Time
LSL	T_{max}	θ	t	**LVL**	T_{max}	θ	t	**PSL**	T_{max}	θ	t
	[Nm]	[deg]	[s]		[Nm]	[deg]	[s]		[Nm]	[deg]	[s]
T01	860.8	28.8	197	L30	510.6	27.4	189	P60	480.8	30.5	221
T02	963.4	32.6	233	L31	638.1	28.0	184	P61	484.3	26.2	182
T03	796.7	28.1	248	L32	520.5	27.4	175	P62	454.3	27.5	186
T04	896.5	29.4	272	L33	533.4	27.2	180	P63	464.5	30.1	202
T05	981.4	33.4	314	L34	535.6	30.0	192	P64	447.1	27.8	184
T06	882.9	29.2	276	L35	615.6	32.4	203	P65	473.3	27.6	189
T07	758.4	26.6	260	L36	581.2	30.4	209	P66	457.2	41.2	275
T08	760.2	27.3	252	L37	565.0	25.8	149	P67	491.0	35.6	234
T09	871.0	33.7	302	L38	625.9	28.5	167	P68	455.4	32.9	207
T10	854.7	30.4	258	L39	545.4	27.8	199	P69	409.8	35.5	234
T11	871.8	28.5	255	L40	566.7	24.6	167	P70	493.9	32.9	218
T12	935.2	31.6	279	L41	579.5	27.3	203	P71	436.6	29.4	190
T13	939.6	31.9	284	L42	609.6	29.8	217	P72	490.2	34.7	284
T14	905.0	30.1	238	L43	565.6	29.7	214	P73	493.8	28.1	223
T15	752.5	28.7	241	L44	577.3	33.4	249	P74	421.4	31.5	244
T16	859.4	28.6	191	L45	537.1	26.7	201	P75	490.4	29.9	230
T17	831.3	28.1	162	L46	546.3	25.9	197	P76	374.9	30.1	234
T18	963.1	31.6	185	L47	543.7	29.1	220	P77	461.4	29.3	222
T19	796.5	29.7	175	L48	570.0	26.3	204	P78	439.6	34.3	260
T20	895.4	30.2	183	L49	523.6	30.3	217	P79			
T21	800.5	28.8	169	L50	575.9	29.8	226	P80	508.1	31.0	223
T22	768.7	25.6	154	L51	613.6	30.5	217	P81	515.6	27.6	198
T23	829.1	27.1	167	L52	600.9	31.7	233	P82	445.4	40.1	288
T24	766.9	26.0	163	L53	624.5	29.1	212	P83	417.5	30.9	222
T25	763.8	26.1	169	L54	541.1	27.2	215	P84	458.0	30.4	206
T26	812.7	27.9	171	L55	570.8	26.8	198	P85	431.1	33.3	231
T27	867.1	26.0	171	L56	590.3	30.5	225				
T28	912.0	29.5	214	L57	550.2	29.9	215				
T29	744.0	24.5	177	L58	571.8	26.8	184				
				L59	561.6	28.6	193				
mean	849.7	29.0	219.3	mean	569.7	28.6	201.8	mean	459.8	31.5	223.5
stdev	70.8	2.36	49.1	stdev	33.7	2.07	21.5	stdev	32.9	3.71	29.2
COV [%]	8.3	8.1	22.4	COV [%]	5.9	7.2	10.7	COV [%]	7.1	11.8	13.1

Torsion Test Results - LSL

LSL	Width b [mm]	Depth h [mm]	Length L [mm]	Weight m [g]	Density ρ [g/cm³]	MC u [%]	MOE E_f [GPa]	at Failure Torque T_{max} [Nm]	at Failure Twist θ [deg]	Time t [s]	Loading Rate [rad/m/min]	Isotropic Shear Stress τ_{LT-I} [MPa]	Isotropic Shear Stress τ_{LR-I} [MPa]	Orthotropic Theory (Lekhnitskii 1981) Orthotropic Shear Stress τ_{LT-O} [MPa]	Orthotropic Theory (Lekhnitskii 1981) Orthotropic Shear Stress τ_{LR-O} [MPa]	Torsional Rigidity C [kN/m2]	calculated Twist θ [deg]
T01	44.4	139.3	1373	6077	0.72	7.0	9.2	860.8	28.8	197	0.11	11.64	8.87	12.75	6.46	2.18	31.0
T02	43.9	139.3	1371	6261	0.75	6.9	13.3	963.4	32.6	233	0.11	13.31	10.11	14.57	7.38	2.12	35.8
T03	44.1	139.2	1372	5713	0.68	6.6	11.9	796.7	28.1	248	0.09	10.90	8.30	11.94	6.05	2.15	29.2
T04	44.4	139.2	1371	6111	0.72	7.1	10.6	896.5	29.4	272	0.08	12.13	9.25	13.28	6.74	2.18	32.3
T05	44.3	138.7	1371	6164	0.73	6.8	11.2	981.4	33.4	314	0.08	13.39	10.21	14.66	7.44	2.16	35.7
T06	44.3	139.3	1370	5894	0.70	6.2	9.3	882.9	29.2	276	0.08	11.98	9.13	13.12	6.65	2.17	31.9
T07	44.2	139.2	1373	6094	0.72	6.8	9.8	758.4	26.6	260	0.08	10.36	7.89	11.34	5.75	2.15	27.7
T08	44.2	139.6	1372	5806	0.69	6.6	9.1	760.2	27.3	252	0.08	10.33	7.86	11.31	5.73	2.17	27.6
T09	44.2	139.2	1372	5800	0.69	6.4	9.6	871.0	33.7	302	0.09	11.89	9.05	13.02	6.60	2.15	31.8
T10	44.1	138.9	1373	6118	0.73	7.0	10.6	854.7	30.4	258	0.09	11.72	8.92	12.83	6.50	2.14	31.4
T11	43.9	139.6	1373	6155	0.73	6.7	12.6	871.8	28.5	255	0.09	12.00	9.11	13.14	6.65	2.13	32.3
T12	44.3	139.5	1373	6187	0.73	6.9	10.3	935.2	31.6	279	0.09	12.69	9.66	13.90	7.04	2.17	33.9
T13	44.0	139.7	1370	6013	0.71	6.6	10.6	939.6	31.9	284	0.09	12.89	9.79	14.12	7.14	2.13	34.6
T14	44.4	139.1	1372	6057	0.72	6.5	10.8	905.0	30.1	238	0.10	12.28	9.36	13.44	6.82	2.17	32.7
T15	44.2	139.1	1371	5796	0.69	7.1	9.8	752.5	28.7	241	0.09	10.28	7.83	11.26	5.71	2.15	27.5
T16	44.0	139.3	1372	6192	0.74	6.8	11.3	859.4	28.6	191	0.11	11.83	8.99	12.95	6.56	2.13	31.8
T17	44.2	139.1	1370	5890	0.70	7.1	12.3	831.3	28.1	162	0.13	11.35	8.64	12.43	6.30	2.15	30.3
T18	44.3	139.2	1370	6077	0.72	6.5	10.3	963.1	31.6	185	0.13	13.08	9.96	14.32	7.26	2.17	34.8
T19	43.8	139.3	1370	5703	0.68	6.5	10.4	796.5	29.7	175	0.13	11.02	8.38	12.07	6.11	2.11	29.6
T20	44.4	138.6	1371	6062	0.72	6.7	10.3	895.4	30.2	183	0.13	12.19	9.30	13.35	6.78	2.16	32.5
T21	44.3	138.5	1369	5733	0.68	7.1	11.8	800.5	28.8	169	0.13	10.93	8.34	11.97	6.08	2.15	29.1
T22	44.4	139.0	1371	6009	0.71	7.1	11.4	768.7	25.6	154	0.13	10.44	7.96	11.44	5.80	2.17	27.8
T23	44.1	138.9	1371	6191	0.74	7.0	10.8	829.1	27.1	167	0.12	11.37	8.66	12.45	6.31	2.14	30.4
T24	44.3	139.1	1372	5872	0.69	7.1	10.3	766.9	26.0	163	0.12	10.43	7.95	11.42	5.79	2.17	27.8
T25	44.3	139.1	1372	5774	0.68	6.9	10.4	763.8	26.1	169	0.12	10.41	7.93	11.39	5.78	2.16	27.8
T26	43.9	139.4	1370	5875	0.70	6.6	12.2	812.7	27.9	171	0.12	11.20	8.51	12.26	6.21	2.12	30.0
T27	44.5	139.3	1371	6400	0.75	6.9	13.5	867.1	26.0	171	0.12	11.66	8.89	12.77	6.48	2.20	31.0
T28	44.7	138.6	1371	6302	0.74	7.2	13.0	912.0	29.5	214	0.11	12.23	9.35	13.40	6.82	2.21	32.4
T29	44.2	138.7	1370	5593	0.67	7.0	11.4	744.0	24.5	177	0.11	10.19	7.76	11.15	5.66	2.15	27.2
mean	44.2	139.1	1371	5997	0.71	6.8	11.0	849.7	29.0	219	0.10	11.59	8.83	12.69	**6.43**	2.16	31.0
stdev	0.204	0.311	1.131	204.083	0.023	0.250	1.212	70.783	2.358	49.146	0.019	0.957	0.729	1.049	0.532	0.023	2.559
COV [%]	0.5	0.2	0.08	3.40	3.27	3.7	11.0	8.3	8.1	22.4	18.3	8.3	8.3	8.3	8.3	1.1	8.3

Torsion Test Results - LVL

								at Failure				Isotropic		Orthotropic Theory (Lekhnitskii 1981) Orthotropic		Torsional calculated	
	Width	Depth	Length	Weight	Density	MC	MOE	Torque	Twist	Time	Loading	Shear Stress		Shear Stress		Rigidity	Twist
LVL	b	h	L	m	ρ	u	E_f	T_{max}	θ	t	Rate	τ_{LT-I}	τ_{LR-I}	τ_{LT-O}	τ_{LR-O}	C	θ
	[mm]	[mm]	[mm]	[g]	[g/cm^3]	[%]	[GPa]	[Nm]	[deg]	[s]	[rad/m/min]	[MPa]	[MPa]	[MPa]	[MPa]	[kN/m2]	[deg]
L30	43.8	140.4	1369	4699	0.56	7.7	11.6	510.6	27.4	189	0.11	7.00	5.31	7.27	4.50	1.77	22.6
L31	43.6	140.5	1369	4782	0.57	7.3	14.2	638.1	28.0	184	0.12	8.81	6.67	9.15	5.67	1.76	28.5
L32	44.1	140.4	1371	4820	0.57	7.7	15.0	520.5	27.4	175	0.12	7.04	5.35	7.31	4.51	1.81	22.6
L33	44.0	140.5	1369	4648	0.55	7.8	13.9	533.4	27.2	180	0.12	7.27	5.52	7.55	4.67	1.79	23.4
L34	43.6	140.4	1369	4637	0.55	7.5	11.5	535.6	30.0	192	0.12	7.42	5.61	7.70	4.78	1.75	24.0
L35	44.3	140.5	1372	5259	0.62	7.8	14.5	615.6	32.4	203	0.12	8.28	6.30	8.60	5.30	1.82	26.5
L36	43.9	140.5	1371	4737	0.56	7.3	13.5	581.2	30.4	209	0.11	7.94	6.02	8.25	5.10	1.78	25.6
L37	43.9	140.4	1370	4911	0.58	7.5	13.4	565.0	25.8	149	0.13	7.73	5.86	8.03	4.96	1.78	24.9
L38	44.4	140.6	1369	5106	0.60	7.3	14.1	625.9	28.5	167	0.13	8.36	6.36	8.68	5.34	1.85	26.6
L39	44.0	140.4	1371	4628	0.55	7.5	13.5	545.4	27.8	199	0.11	7.41	5.63	7.70	4.75	1.80	23.8
L40	43.9	140.4	1370	4852	0.58	7.1	15.3	566.7	24.6	167	0.11	7.76	5.88	8.05	4.98	1.78	25.0
L41	45.1	140.2	1370	4793	0.55	7.5	12.5	579.5	27.3	203	0.10	7.56	5.77	7.85	4.79	1.91	23.8
L42	43.7	140.3	1367	4800	0.57	7.5	12.3	609.6	29.8	217	0.11	8.40	6.37	8.73	5.40	1.76	27.1
L43	44.0	140.6	1369	5058	0.60	8.0	13.9	565.6	29.7	214	0.11	7.68	5.83	7.97	4.93	1.80	24.6
L44	43.8	140.4	1370	4822	0.57	8.2	15.0	577.3	33.4	249	0.10	7.92	6.01	8.23	5.09	1.77	25.6
L45	45.2	140.1	1371	5099	0.59	7.0	19.9	537.1	26.7	201	0.10	6.99	5.34	7.26	4.42	1.92	22.0
L46	45.2	140.2	1373	4804	0.55	7.6	15.8	546.3	25.9	197	0.10	7.10	5.42	7.37	4.49	1.93	22.3
L47	44.2	140.5	1372	4813	0.57	8.1	16.1	543.7	29.1	220	0.10	7.34	5.58	7.63	4.70	1.81	23.6
L48	45.0	140.2	1371	4794	0.55	7.5	17.1	570.0	26.3	204	0.10	7.45	5.69	7.74	4.72	1.91	23.5
L49	43.7	140.4	1370	4757	0.57	7.9	12.8	523.6	30.3	217	0.11	7.23	5.48	7.51	4.65	1.76	23.4
L50	45.0	140.2	1370	5006	0.58	7.1	18.5	575.9	29.8	226	0.10	7.55	5.76	7.84	4.79	1.90	23.8
L51	43.9	140.4	1369	4641	0.55	7.9	13.0	613.6	30.5	217	0.11	8.39	6.36	8.71	5.38	1.78	27.0
L52	43.9	140.3	1369	4772	0.57	7.8	13.3	600.9	31.7	233	0.10	8.23	6.24	8.54	5.28	1.78	26.5
L53	45.0	140.1	1368	4972	0.58	7.5	13.6	624.5	29.1	212	0.11	8.18	6.24	8.49	5.18	1.90	25.7
L54	44.5	140.1	1369	5229	0.61	7.4	17.6	541.1	27.2	215	0.10	7.24	5.51	7.52	4.61	1.84	23.0
L55	44.8	140.2	1369	4972	0.58	7.5	13.6	570.8	26.8	198	0.10	7.54	5.75	7.82	4.79	1.88	23.8
L56	44.2	140.4	1370	5293	0.62	7.5	18.4	590.3	30.5	225	0.10	7.98	6.06	8.28	5.11	1.81	25.5
L57	44.9	140.3	1371	4827	0.56	7.0	13.1	550.2	29.9	215	0.11	7.24	5.52	7.52	4.60	1.89	22.9
L58	45.0	140.5	1372	4801	0.55	7.4	15.7	571.8	26.8	184	0.11	7.48	5.70	7.77	4.75	1.90	23.6
L59	45.0	140.4	1371	5021	0.58	7.7	16.8	561.6	28.6	193	0.11	7.33	5.60	7.62	4.65	1.91	23.1
mean	44.3	140.4	1370	4878	0.57	7.6	14.6	569.7	28.6	201.8	0.11	7.66	5.83	**7.96**	4.90	1.83	24.5
stdev	0.544	0.148	1.326	184.921	0.020	0.296	2.106	33.683	2.073	21.520	0.009	0.486	0.363	0.504	0.322	0.060	1.654
COV [%]	1.2	0.1	0.10	3.8	3.55	3.9	14.4	5.9	7.2	10.7	8.1	6.3	6.2	6.3	6.6	3.3	6.8

Torsion Test Results - PSL

PSL	Width b	Depth h	Length L	Weight m	Density ρ	MC u	MOE E_f	at Failure Torque T_{max}	at Failure Twist θ	Time t	Loading Rate	Isotropic Shear Stress τ_{LT-I}	Isotropic Shear Stress τ_{LR-I}	Orthotropic Theory (Lekhnitskii 1981) Orthotropic Shear Stress τ_{LT-O}	Orthotropic Theory (Lekhnitskii 1981) Orthotropic Shear Stress τ_{LR-O}	Torsional calculated Rigidity C	Torsional calculated Twist θ
	[mm]	[mm]	[mm]	[g]	[g/cm³]	[%]	[GPa]	[Nm]	[deg]	[s]	[rad/m/min]	[MPa]	[MPa]	[MPa]	[MPa]	[kN/m2]	[deg]
P60	42.7	139.1	1371	5498	0.67	7.7	15.9	480.8	30.5	221	0.11	6.98	5.27	7.15	4.78	1.12	33.7
P61	42.9	139.3	1370	5542	0.68	7.3	15.3	484.3	26.2	182	0.11	6.96	5.26	7.14	4.77	1.14	33.5
P62	42.7	139.3	1371	5536	0.68	7.7	16.5	454.3	27.5	186	0.11	6.60	4.98	6.76	4.51	1.12	31.9
P63	43.1	139.2	1371	5228	0.64	8.0	15.5	464.5	30.1	202	0.11	6.64	5.02	6.80	4.55	1.15	31.8
P64	43.0	139.2	1369	5441	0.66	7.5	16.7	447.1	27.8	184	0.12	6.42	4.85	6.58	4.40	1.14	30.8
P65	42.7	139.7	1369	5242	0.64	8.1	13.6	473.3	27.6	189	0.11	6.85	5.16	7.02	4.69	1.12	33.1
P66	42.7	139.6	1368	5402	0.66	9.6	14.4	457.2	41.2	275	0.11	6.63	4.99	6.79	4.53	1.12	32.0
P67	43.1	139.4	1372	5202	0.63	8.1	16.2	491.0	35.6	234	0.12	7.00	5.29	7.17	4.79	1.15	33.6
P68	42.7	139.5	1371	5419	0.66	8.5	15.4	455.4	32.9	207	0.12	6.61	4.98	6.77	4.52	1.12	32.0
P69	42.7	139.6	1369	5483	0.67	9.4	14.3	409.8	35.5	234	0.12	5.93	4.47	6.07	4.05	1.12	28.6
P70	43.0	139.0	1371	5087	0.62	9.0	13.2	493.9	32.9	218	0.12	7.09	5.36	7.27	4.86	1.14	34.1
P71	42.6	139.8	1370	5203	0.64	7.9	13.9	436.6	29.4	190	0.12	6.33	4.76	6.49	4.33	1.12	30.6
P72	42.7	139.4	1373	5351	0.66	8.3	14.9	490.2	34.7	284	0.09	7.12	5.37	7.30	4.87	1.12	34.5
P73	42.8	139.2	1372	5333	0.65	7.7	15.1	493.8	28.1	223	0.10	7.14	5.39	7.31	4.88	1.13	34.4
P74	42.6	139.7	1372	5226	0.64	9.1	14.3	421.4	31.5	244	0.10	6.12	4.61	6.27	4.19	1.12	29.7
P75	42.8	139.2	1372	5489	0.67	7.7	14.6	490.4	29.9	230	0.10	7.08	5.34	7.25	4.84	1.13	34.1
P76	42.6	139.4	1370	5503	0.68	9.9	13.9	374.9	30.1	234	0.10	5.46	4.11	5.59	3.73	1.11	26.4
P77	42.7	139.3	1370	5482	0.67	7.5	14.5	461.4	29.3	222	0.10	6.70	5.05	6.86	4.58	1.12	32.4
P78	42.8	139.6	1372	5530	0.68	8.3	15.2	439.6	34.3	260	0.10	6.34	4.78	6.50	4.34	1.13	30.6
P79	42.7	139.7	1371	5528	0.68	7.7	14.6									1.12	
P80	42.5	139.8	1373	5490	0.67	8.5	14.0	508.1	31	223	0.11	7.40	5.56	7.58	5.06	1.11	35.9
P81	42.6	139.3	1370	5634	0.69	6.9	17.7	515.6	27.6	198	0.11	7.50	5.65	7.69	5.13	1.12	36.3
P82	42.7	139.6	1370	5459	0.67	9.2	15.5	445.4	40.1	288	0.11	6.45	4.86	6.61	4.41	1.12	31.2
P83	42.6	139.6	1369	5208	0.64	8.6	14.0	417.5	30.9	222	0.11	6.07	4.57	6.22	4.15	1.12	29.3
P84	42.7	139.8	1370	5362	0.66	7.6	14.3	458.0	30.4	206	0.11	6.61	4.98	6.77	4.52	1.13	31.9
P85	42.6	139.6	1370	5283	0.65	8.6	15.8	431.1	33.3	231	0.11	6.27	4.72	6.43	4.29	1.11	30.4
mean	42.7	139.5	1371	5391	0.66	8.2	15.0	459.8	31.5	223.5	0.11	6.65	5.02	**6.82**	4.55	1.12	32.1
stdev	0.158	0.242	1.299	141.446	0.018	0.755	1.070	32.874	3.711	29.249	0.008	0.469	0.356	0.49	0.33	0.01	2.3
COV [%]	0.4	0.2	0.09	2.62	2.75	9.2	7.1	7.1	11.8	13.1	6.9	7.1	7.1	7.20	7.21	0.88	7.2

Appendix D

ASTM Shear Block Test Data

ASTM Block Shear Test Results - LSL - Joist Orientation - LR-Failure Plane

LSL	Width1 w1	Width2 w2	Depth d	Height1 h1	Height2 h2	Shear Area A	Block Volume V	green m_g	Weight dry m_d	under Water m_i	Water Immersion SG m_d/V_d	Weighing Density m_d/V_g	MC u	Time t	Load F	Joist Shear Strength τ_{LT}	Failure Type
	[mm]	[mm]	[mm]	[mm]	[mm]	[mm^2]	[cm^3]	[g]	[g]	[g]	[1]	[g/cm^3]	[%]	[s]	[kN]	[MPa]	
T01	50.9	31.9	44.0	69.8	58.6	2578	147.0	107.6	102.0	-41.3	0.71	0.69	5.4		49.11	18.95	compr. par
T02	50.8	31.9	44.2	69.8	58.6	2590	147.4	110.4	105.0	-36.7	0.74	0.71	5.1	245	46.44	17.84	compr. par
T03	50.8	31.9	44.5	69.8	58.6	2608	148.4	96.9	91.4	-51.9	0.64	0.62	6.0		45.58	17.39	compr&shear
T04	50.9	32.0	44.5	69.8	58.6	2608	148.7	98.4	93.2	-50.3	0.65	0.63	5.6	220	41.88	15.98	compr&shear
T05	50.9	32.0	44.3	69.8	58.6	2596	148.0	110.9	105.5	-35.4	0.75	0.71	5.1	250	54.35	20.83	compr. par
T06	50.9	31.9	44.2	69.9	58.6	2590	147.8	110.8	104.3	-37.0	0.74	0.71	6.2	455	48.14	18.49	compr. par
T07	50.9	32.0	44.2	69.9	58.7	2595	147.9	105.8	99.0	-42.0	0.70	0.67	6.8	125	40.23	15.43	shear
T08	50.9	32.0	44.3	69.8	58.7	2600	148.1	107.3	100.7	-41.9	0.71	0.68	6.6	140	41.58	15.91	compr&shear
T09	50.8	31.9	44.3	70.0	58.7	2600	148.1	107.9	101.4	-39.9	0.72	0.68	6.4	220	53.31	20.39	shear
T10	50.9	32.1	44.3	69.9	58.7	2600	148.3	104.2	97.4	-43.5	0.69	0.66	7.0	190	42.26	16.17	compr. par
T11	50.8	32.0	44.0	69.9	58.7	2583	147.0	103.6	97.1	-43.6	0.69	0.66	6.7	220	47.29	18.21	shear
T12	50.8	31.9	44.2	69.9	58.6	2590	147.5	112.8	105.5	-35.6	0.75	0.72	6.9	180	42.55	16.34	shear
T13	50.8	32.0	44.1	69.9	58.6	2584	147.2	99.9	93.7	-47.4	0.66	0.64	6.6	195	47.12	18.14	shear
T14	50.8	31.9	44.4	69.9	58.6	2602	148.2	103.0	96.7	-44.7	0.68	0.65	6.5	200	37.79	14.45	compr&shear
T15	50.8	32.0	44.2	69.8	58.6	2590	147.4	103.1	96.3	-44.4	0.68	0.65	7.1	180	39.93	15.34	compr&shear
T16	50.9	32.0	44.1	69.9	58.6	2584	147.5	100.1	93.7	-46.5	0.67	0.64	6.8	170	33.97	13.08	compr&shear
T17	50.9	32.1	44.2	69.9	58.6	2590	147.9	103.1	96.3	-44.3	0.69	0.65	7.1		46.38	17.81	compr&shear
T18	50.9	32.0	44.4	69.9	58.6	2602	148.5	95.1	89.2	-52.8	0.63	0.60	6.5	170	36.56	13.98	shear
T19	50.9	32.1	43.9	69.9	58.7	2577	146.9	87.5	82.2	-58.1	0.59	0.56	6.5	150	27.20	10.50	compr&shear
T20	50.9	32.0	44.2	69.9	58.6	2590	147.8	100.0	93.8	-47.8	0.66	0.63	6.7	160	36.45	14.00	shear
T21	50.8	31.9	44.2	69.9	58.6	2590	147.5	103.1	96.3	-44.4	0.68	0.65	7.1	200	48.97	18.81	shear
T22	50.9	32.0	44.5	69.9	58.6	2608	148.8	103.3	96.5	-44.4	0.69	0.65	7.1	270	50.34	19.20	compr&shear
T23	50.9	32.1	44.0	69.9	58.6	2578	147.2	109.1	101.9	-38.2	0.73	0.69	7.0	230	44.61	17.21	compr. par
T24	50.8	32.0	44.3	69.9	58.6	2596	147.9	108.7	101.5	-38.8	0.72	0.69	7.1	235	51.80	19.85	compr. par
T25	50.9	32.1	44.3	69.9	58.6	2596	148.2	103.6	96.9	-44.4	0.69	0.65	6.9	180	46.84	17.95	compr. par
T26	50.9	32.0	43.9	69.9	58.7	2577	146.9	115.6	108.5	-31.7	0.77	0.74	6.6	165	44.67	17.25	compr. par
T27	50.9	32.0	44.4	69.9	58.7	2606	148.6	114.3	106.9	-34.3	0.76	0.72	6.9	180	45.52	17.37	compr. par
T28	50.9	32.0	44.5	69.9	58.6	2608	148.8	115.9	108.1	-33.2	0.76	0.73	7.2	170	48.23	18.40	compr&shear
T29	50.8	32.0	44.4	69.9	58.6	2602	148.2	99.4	92.9	-48.6	0.66	0.63	7.0	200	40.43	15.46	compr&shear
mean	50.9	32.0	44.2	69.9	58.6	2594	147.8	104.9	98.4	-42.9	0.70	0.67	6.6	204	44.12	**16.91**	
stdev	0.049	0.067	0.174	0.049	0.045	9.837	0.578	6.465	6.105	6.256	0.044	0.041	0.583	62.086	6.033	2.347	
COV [%]	0.1	0.2	0.4	0.1	0.1	0.4	0.4	6.2	6.2	-14.6	6.3	6.2	8.9	30.5	13.7	13.9	

ASTM Block Shear Test Results - LVL - Joist Orientation - LR-Failure Plane

LVL	Width1 w1 [mm]	Width2 w2 [mm]	Depth d [mm]	Height1 h1 [mm]	Height2 h2 [mm]	Shear Area A [mm^2]	Block Volume V [cm^3]	green m_g [g]	Weight dry m_d [g]	under Water m_i [g]	Water Immersion SG m_d/V_d [1]	Weighing Density m_d/V_g [g/cm^3]	MC u [%]	Time t [s]	Load F [kN]	Joist Shear Strength τ_{LT} [MPa]
L30	51.0	31.9	43.6	69.8	58.7	2559	146.0	82.6	76.7	-63.0	0.55	0.53	7.7		20.20	7.85
L31	50.8	32.0	43.6	69.9	58.6	2555	145.6	84.4	78.7	-61.6	0.56	0.54	7.3	130	24.59	9.58
L32	50.9	32.0	44.1	69.9	58.6	2584	147.5	87.0	80.8	-60.2	0.57	0.55	7.7	125	24.10	9.28
L33	50.7	31.9	44.0	69.9	58.6	2578	146.6	89.4	82.9	-56.5	0.59	0.57	7.8	125	29.60	11.42
L34	50.9	32.0	43.8	69.8	58.6	2567	146.3	84.1	78.3	-61.5	0.56	0.53	7.5	120	24.04	9.32
L35	50.8	31.9	44.2	69.9	58.6	2590	147.5	92.7	86.0	-54.4	0.61	0.58	7.8	115	25.95	9.97
L36	50.8	32.0	44.0	69.9	58.6	2578	146.9	80.9	75.4	-64.7	0.54	0.51	7.3	120	23.31	9.00
L37	50.7	31.9	43.5	69.9	58.6	2549	144.9	79.9	74.3	-65.3	0.53	0.51	7.5	120	24.61	9.61
L38	50.9	32.0	44.4	69.9	58.6	2602	148.5	92.2	85.9	-54.9	0.61	0.58	7.3	120	24.15	9.23
L39	50.8	32.0	44.1	69.9	58.6	2584	147.2	87.1	81.1	-59.4	0.58	0.55	7.5	120	24.23	9.33
L40	50.8	31.9	43.6	69.9	58.6	2555	145.5	88.0	82.1	-57.6	0.59	0.56	7.1	115	26.11	10.17
L41	50.8	32.0	44.7	69.9	58.6	2619	149.2	79.9	74.3	-68.2	0.52	0.50	7.5			
L42	50.8	32.0	43.9	69.8	58.6	2573	146.4	77.9	72.4	-66.7	0.52	0.49	7.5	120	23.58	9.12
L43	50.7	31.9	43.9	69.9	58.6	2573	146.3	83.9	77.7	-61.7	0.56	0.53	8.0	115	21.45	8.29
L44	50.8	32.0	43.5	69.9	58.6	2549	145.2	79.2	73.2	-66.1	0.53	0.50	8.2	120	21.60	8.43
L45	50.8	31.9	45.1	69.9	58.6	2643	150.5	92.3	86.3	-57.8	0.60	0.57	7.0	130	26.29	9.90
L46	50.8	31.9	45.2	69.9	58.6	2649	150.8	85.6	79.6	-64.6	0.55	0.53	7.6	125	25.41	9.54
L47	50.8	31.9	43.9	69.9	58.6	2573	146.5	89.7	82.9	-55.5	0.60	0.57	8.1	115	25.83	9.99
L48	50.8	31.9	45.3	69.9	58.6	2655	151.2	85.2	79.3	-65.3	0.55	0.52	7.5	120	25.24	9.46
L49	50.8	31.9	43.9	69.9	58.6	2573	146.5	80.5	74.6	-64.1	0.54	0.51	7.9	110	20.76	8.03
L50	50.9	32.0	44.7	69.9	58.6	2619	149.5	84.1	78.5	-64.1	0.55	0.52	7.1	115	23.32	8.86
L51	50.9	32.0	43.7	69.9	58.6	2561	146.1	78.7	72.9	-67.5	0.52	0.50	7.9	120	26.69	10.37
L52	50.7	31.9	43.7	69.9	58.6	2561	145.6	82.9	76.9	-63.0	0.55	0.53	7.8	110	22.78	8.85
L53	50.8	31.9	44.8	69.9	58.6	2625	149.5	86.7	80.7	-62.7	0.56	0.54	7.5	115	22.83	8.65
L54	50.8	32.0	44.3	69.9	58.6	2596	147.9	87.9	81.9	-59.7	0.58	0.55	7.4	120	26.08	9.99
L55	50.8	31.9	44.5	69.9	58.6	2608	148.5	80.7	75.1	-66.9	0.53	0.51	7.5	110	22.56	8.61
L56	50.8	31.9	44.1	69.9	58.5	2580	147.1	89.1	82.9	-56.6	0.59	0.56	7.5	120	25.14	9.69
L57	50.8	31.9	45.1	69.9	58.6	2643	150.5	83.7	78.2	-67.5	0.54	0.52	7.0	115	22.68	8.54
L58	50.8	32.0	45.1	69.9	58.5	2638	150.5	57.2	53.3	-47.3	0.53		7.4	115	23.96	9.03
L59	50.8	31.9	44.9	69.9	58.6	2631	149.8	57.5	53.4	-44.4	0.55		7.7	110	23.43	8.86
mean	50.8	31.9	44.2	69.9	58.6	2592	147.7	83.0	77.2	-61.0	0.56	0.53	7.6	118	24.16	**9.27**
stdev	0.066	0.050	0.565	0.031	0.032	32.794	1.898	8.116	7.574	5.770	0.028	0.026	0.296	5.452	1.983	0.763
COV [%]	0.1	0.2	1.3	0.0	0.1	1.3	1.3	9.8	9.8	-9.5	5.0	4.9	3.9	4.6	8.2	8.2

ASTM Block Shear Test Results - PSL - Joist Orientation - LR-Failure Plane

PSL	Width1 w1 [mm]	Width2 w2 [mm]	Depth d [mm]	Height1 h1 [mm]	Height2 h2 [mm]	Shear Area A [mm^2]	Block Volume V [cm^3]	green m_g [g]	Weight dry m_d [g]	under Water m_i [g]	Water Immersion SG m_d/V_d [1]	Weighing Density m_d/V_g [g/cm^3]	MC u [%]	Time t [s]	Load F [kN]	Joist Shear Strength τ_{LT} [MPa]
P60	51.0	31.8	42.7	69.9	58.6	2502	143.0	101.4	94.1	-40.3	0.70	0.66	7.7	250	25.67	10.20
P61	50.9	31.9	43.0	69.9	58.6	2520	143.8	93.7	87.3	-50.0	0.64	0.61	7.3	115	25.24	9.97
P62	50.8	32.0	42.3	69.9	58.6	2479	141.2	93.9	87.2	-47.0	0.65	0.62	7.7	120	23.91	9.60
P63	50.8	31.9	42.9	69.9	58.6	2514	143.2	90.9	84.2	-51.1	0.62	0.59	8.0	115	25.07	9.92
P64	50.8	31.9	43.1	69.9	58.6	2526	143.8	92.8	86.3	-50.5	0.63	0.60	7.5	120	27.30	10.75
P65	50.9	32.0	42.5	69.9	58.6	2491	142.1	90.5	83.7	-49.9	0.63	0.59	8.1	115	20.56	8.21
P66	50.8	31.9	42.2	69.9	58.5	2469	140.8	91.0	83.1	-46.5	0.64	0.59	9.6	115	19.04	7.67
P67	50.8	32.0	42.8	69.9	58.6	2508	142.9	89.5	82.8	-53.4	0.61	0.58	8.1	135	24.00	9.52
P68	50.8	31.9	42.3	69.9	58.6	2479	141.2	94.3	86.9	-46.7	0.65	0.62	8.5	125	25.47	10.22
P69	50.5	31.7	42.4	69.9	58.6	2485	140.7	97.8	89.4	-42.5	0.68	0.64	9.4	125	23.24	9.31
P70	50.8	32.0	42.7	69.9	58.6	2502	142.6	87.5	80.3	-54.1	0.60	0.56	9.0	125	24.23	9.63
P71	50.8	32.0	42.4	69.9	58.6	2485	141.6	94.6	87.7	-47.9	0.65	0.62	7.9	120	26.95	10.79
P72	50.7	31.9	42.5	69.9	58.6	2491	141.6	94.1	86.9	-45.6	0.66	0.61	8.3	105	16.08	6.42
P73	50.8	32.0	42.8	69.9	58.6	2508	142.9	95.3	88.4	-47.6	0.65	0.62	7.7	140	29.14	11.56
P74	50.6	31.8	42.4	69.9	58.6	2485	141.0	90.0	82.5	-48.5	0.63	0.59	9.1	100	18.73	7.50
P75	50.8	32.0	43.0	69.9	58.6	2520	143.6	99.4	92.2	-43.4	0.68	0.64	7.7	105	18.67	7.37
P76	50.8	32.0	43.3	69.9	58.6	2537	144.6	97.0	88.3	-41.1	0.68	0.61	9.9	145	29.56	11.59
P77	50.9	32.0	42.9	69.9	58.6	2514	143.5	102.7	95.6	-40.2	0.70	0.67	7.5	150	30.99	12.26
P78	50.9	31.9	42.7	69.9	58.6	2502	142.8	99.1	91.5	-42.8	0.68	0.64	8.3	115	23.39	9.30
P79	50.9	31.9	42.4	69.9	58.6	2485	141.8	96.4	89.5	-44.2	0.67	0.63	7.7	105	18.10	7.25
P80	50.8	31.9	42.5	69.9	58.6	2491	141.8	97.4	89.7	-43.4	0.67	0.63	8.5	130	22.87	9.14
P81	50.8	32.0	42.8	69.9	58.6	2508	142.9	100.2	93.7	-42.9	0.69	0.66	6.9	120	28.90	11.46
P82	50.7	31.9	42.9	69.9	58.6	2514	142.9	95.8	87.8	-44.9	0.66	0.61	9.2	110	22.46	8.89
P83	50.9	31.9	42.5	69.9	58.6	2491	142.1	98.7	90.9	-42.2	0.68	0.64	8.6	140	28.50	11.39
P84	50.9	32.0	42.8	69.9	58.5	2504	143.1	66.5	61.8	-31.0	0.67		7.6	110	19.57	7.78
P85	50.8	31.9	42.6	69.9	58.6	2496	142.2	59.0	54.4	-35.7	0.60		8.6	115	19.03	7.58
mean	50.8	31.9	42.7	69.9	58.6	2500	142.4	92.7	85.6	125.8	0.65	0.62	8.2	126	23.72	**9.43**
stdev	0.102	0.078	0.278	0.000	0.027	16.548	1.030	9.658	8.995	28.415	0.029	0.027	0.755	28.415	4.073	1.594
COV [%]	0.2	0.2	0.7	0.0	0.0	0.7	0.7	10.4	10.5	22.6	4.5	4.3	9.2	22.6	17.2	16.9

ASTM Block Shear Test Results - LSL - Plank Orientation - LT-Failure Plane

LSL	Width1 w1 [mm]	Width2 w2 [mm]	Depth d [mm]	Height1 h1 [mm]	Height2 h2 [mm]	Shear Area A [mm^2]	Block Volume V [cm^3]	green m_g [g]	Weight dry m_d [g]	under Water m_i [g]	Water Immersion SG m_d/V_d [1]	Weighing Density m_d/V_g [g/cm^3]	MC u [%]	Time t [s]	Load F [kN]	Plank Shear Strength τ_{LT} [MPa]
T01	51.1	44.6	25.2	63.6	51.3	2621	132.8	97.8	91.5	-34.2	0.73	0.69	6.9	210	20.33	7.72
T02	51.0	44.0	24.5	63.5	51.2	2611	130.3	96.6	90.7	-33.3	0.73	0.70	6.6	200	21.56	8.21
T03	51.2	44.3	24.8	63.6	51.3	2627	132.0	97.1	91.3	-34.1	0.73	0.69	6.3	175	18.00	6.82
T04	51.0	44.3	24.9	63.6	51.3	2616	131.5	90.7	85.3	-40.5	0.68	0.65	6.3	180	17.44	6.63
T05	50.9	44.3	24.9	63.6	51.3	2611	131.3	103.6	97.4	-28.2	0.78	0.74	6.4	160	18.71	7.13
T06	51.1	44.4	24.9	63.7	51.3	2621	132.2	90.0	84.8	-41.6	0.67	0.64	6.0	160	21.18	8.04
T07	50.9	44.3	24.9	63.6	51.3	2611	131.3	93.6	87.9	-36.9	0.70	0.67	6.5	140	14.60	5.56
T08	51.2	44.3	24.9	63.6	51.3	2627	132.0	96.1	90.4	-36.0	0.72	0.68	6.4	170	20.75	7.86
T09	51.1	44.3	24.8	63.6	51.3	2621	131.7	81.1	76.5	-49.4	0.61	0.58	6.0	180	17.91	6.80
T10	51.1	44.2	24.7	63.6	51.3	2621	131.4	94.1	88.0	-37.1	0.70	0.67	6.8	160	21.26	8.07
T11	51.0	44.0	24.6	63.7	51.3	2616	130.7	93.2	87.5	-36.9	0.70	0.67	6.4	165	22.21	8.45
T12	51.0	44.3	24.9	63.7	51.4	2621	131.7	93.7	88.1	-37.6	0.70	0.67	6.4	170	20.51	7.78
T13	51.0	44.2	24.7	63.6	51.3	2616	131.1	87.2	82.0	-42.7	0.66	0.63	6.3	140	17.87	6.80
T14	51.1	44.4	25.0	63.6	51.3	2621	132.1	85.1	80.2	-45.9	0.64	0.61	6.1	160	16.45	6.24
T15	50.8	44.6	25.0	63.6	51.2	2601	131.8	90.2	84.4	-42.2	0.67	0.64	6.8	170	20.13	7.70
T16	51.0	44.0	24.6	63.7	51.2	2611	130.6	101.1	95.0	-29.8	0.76	0.73	6.4	160	19.53	7.44
T17	51.1	44.4	25.3	63.6	51.3	2621	132.3	89.6	84.2	-42.2	0.67	0.64	6.5		15.75	5.98
T18	51.1	44.4	25.0	63.7	51.3	2621	132.2	95.4	89.9	-36.5	0.71	0.68	6.1	160	18.80	7.13
T19	51.0	43.9	24.4	63.6	51.3	2616	130.2	87.7	82.6	-42.4	0.66	0.63	6.1	160	19.14	7.28
T20	51.1	44.3	24.8	63.6	51.3	2621	131.7	100.6	94.6	-31.1	0.75	0.72	6.4	190	22.48	8.53
T21	51.1	44.7	24.9	63.7	51.3	2621	133.0	96.4	90.3	-35.6	0.72	0.68	6.8			
T22	51.1	44.4	25.3	63.6	51.3	2621	132.3	91.9	85.9	-40.4	0.68	0.65	6.9	140	16.27	6.18
T23	51.1	44.4	25.4	63.6	51.2	2616	132.3	89.0	83.3	-42.8	0.66	0.63	6.9	160	14.68	5.58
T24	51.1	44.7	25.0	63.7	51.4	2627	133.1	96.2	89.9	-36.7	0.71	0.68	7.0	220	19.74	7.48
T25	51.2	44.2	24.7	63.6	51.3	2627	131.6	83.2	78.1	-47.8	0.62	0.59	6.6	150	17.73	6.72
T26	51.1	44.0	24.6	63.6	51.3	2621	130.8	99.1	93.2	-31.9	0.74	0.71	6.4	175	23.45	8.90
T27	51.1	44.6	25.0	63.6	51.3	2621	132.6	93.1	87.0	-39.0	0.69	0.66	7.0	170	20.58	7.81
T28	51.1	45.3	25.6	63.6	51.3	2621	134.8	103.0	96.1	-30.8	0.76	0.71	7.3	190	20.87	7.92
T29	51.2	44.6	24.9	63.6	51.4	2632	132.9	92.9	87.0	-39.1	0.69	0.65	6.7	175	19.06	7.20
mean	51.1	44.4	24.9	63.6	51.3	2619	131.9	93.4	87.7	-38.0	0.70	0.66	6.5	170	19.18	**7.28**
stdev	0.094	0.280	0.269	0.049	0.050	6.184	0.970	5.589	5.169	5.288	0.042	0.039	0.332	19.612	2.303	0.874
COV [%]	0.2	0.6	1.1	0.1	0.1	0.2	0.7	6.0	5.9	-13.9	6.0	5.9	5.1	11.5	12.0	12.0

ASTM Block Shear Test Results - LVL - Plank Orientation - LT-Failure Plane

LVL	Width1 w1 [mm]	Width2 w2 [mm]	Depth d [mm]	Height1 h1 [mm]	Height2 h2 [mm]	Shear Area A [mm^2]	Block Volume V [ccm]	green m_g [g]	Weight dry m_d [g]	under Water m_i [g]	Water Immersion SG m_d/V_d [1]	Weighing Density m_d/V_g [g/ccm]	MC u [%]	Time t [s]	Load F [kN]	Plank Shear Strength τ_{LT} [MPa]
L30	51.0	44.1	24.4	63.6	51.4	2621	130.8	70.7	65.7	-56.8	0.54	0.50	7.6	100	14.21	5.39
L31	51.1	43.8	24.6	63.6	51.3	2621	130.3	73.5	68.9	-54.4	0.56	0.53	6.8	110	16.29	6.18
L32	51.1	44.1	24.6	63.6	51.3	2621	131.1	71.5	66.5	-55.9	0.54	0.51	7.5	110	17.80	6.76
L33	51.0	44.0	24.6	63.6	51.3	2616	130.5	68.8	64.1	-59.0	0.52	0.49	7.3	150	19.34	7.35
L34	51.1	44.0	24.7	63.6	51.3	2621	130.9	66.5	61.8	-61.5	0.50	0.47	7.6	185	21.13	8.02
L35	51.2	44.1	24.6	63.6	51.2	2621	131.2	75.7	70.6	-51.7	0.58	0.54	7.3	150	12.27	4.66
L36	51.0	44.3	24.8	63.6	51.3	2616	131.5	79.1	73.8	-49.7	0.60	0.56	7.2	200	21.63	8.23
L37	51.0	43.9	24.3	63.6	51.3	2616	130.1	72.1	67.6	-55.5	0.55	0.52	6.8	190	25.88	9.84
L38	51.2	44.0	24.5	63.6	51.3	2627	131.0	75.2	70.3	-53.3	0.57	0.54	7.0		23.20	8.79
L39	51.1	43.8	24.6	63.6	51.3	2621	130.3	69.5	65.0	-58.4	0.53	0.50	6.8	180	13.70	5.20
L40	51.2	43.8	24.4	63.6	51.4	2632	130.5	69.7	65.2	-57.7	0.53	0.50	6.9	125	18.42	6.96
L41	51.2	44.7	25.2	63.6	51.3	2627	133.3	74.5	69.8	-56.6	0.55	0.52	6.8	100	18.29	6.93
L42	51.2	44.2	24.5	63.6	51.3	2627	131.5	77.9	72.8	-50.3	0.59	0.55	6.9	120	18.20	6.89
L43	51.2	44.7	24.9	63.6	51.3	2627	133.1	84.6	79.1	-45.9	0.63	0.59	6.9	120	11.41	4.32
L44	51.1	44.1	24.8	63.5	51.3	2621	131.1	77.5	72.6	-52.0	0.58	0.55	6.7	135	19.30	7.33
L45	51.2	44.9	25.3	63.5	51.3	2627	133.7	79.9	75.0	-51.9	0.59	0.56	6.6	160	22.30	8.45
L46	51.3	45.2	25.8	63.7	51.3	2632	135.4	74.6	70.0	-57.4	0.55	0.52	6.6	165	14.21	5.37
L47	51.1	44.1	24.7	63.6	51.3	2621	131.1	74.4	69.6	-53.2	0.57	0.53	6.9	200	15.35	5.83
L48	51.2	45.2	25.7	63.7	51.4	2632	135.1	71.2	66.7	-61.7	0.52	0.49	6.8	155	16.97	6.42
L49	51.3	43.8	24.3	63.7	51.4	2637	130.8	77.1	72.3	-49.7	0.59	0.55	6.7	165	15.12	5.70
L50	51.2	45.4	25.8	63.6	51.3	2627	135.5	81.3	76.6	-50.9	0.60	0.56	6.3	160	16.56	6.27
L51	51.1	43.7	24.2	63.7	51.3	2621	129.9	78.3	73.0	-48.5	0.60	0.56	7.2	140	21.40	8.12
L52	51.1	43.8	24.6	63.6	51.3	2621	130.3	77.4	72.6	-51.0	0.59	0.56	6.7	125	14.50	5.50
L53	51.1	44.9	25.4	63.6	51.4	2627	133.8	75.5	70.8	-56.2	0.56	0.53	6.5	140	18.81	7.12
L54	51.2	44.7	25.1	63.6	51.4	2632	133.3	84.3	78.9	-46.6	0.63	0.59	6.9	155	21.45	8.11
L55	51.2	44.8	25.4	63.6	51.3	2627	133.7	76.7	71.9	-54.9	0.57	0.54	6.7	180	19.60	7.43
L56	51.1	44.6	25.1	63.6	51.3	2621	132.7	96.6	90.4	-33.4	0.73	0.68	6.8	175	21.13	8.02
L57	51.1	45.2	25.6	63.5	51.3	2621	134.4	72.6	68.2	-59.3	0.53	0.51	6.5	150	21.38	8.11
L58	51.2	44.8	25.2	63.4	51.2	2621	133.2	79.7	74.7	-50.3	0.60	0.56	6.7	155	20.03	7.60
L59	51.0	44.8	25.3	63.5	51.3	2616	133.0	76.5	71.5	-53.7	0.57	0.54	6.9	170	22.82	8.68
mean	51.1	44.4	24.9	63.6	51.3	2624	132.1	76.1	71.2	-53.2	0.57	0.54	6.9	151	18.42	**6.99**
stdev	0.085	0.516	0.473	0.064	0.051	5.172	1.715	5.826	5.522	5.555	0.044	0.040	0.324	28.683	3.531	1.343
COV [%]	0.2	1.2	1.9	0.1	0.1	0.2	1.3	7.7	7.8	-10.4	7.7	7.4	4.7	19.0	19.2	19.2

ASTM Block Shear Test Results - PSL - Plank Orientation - LT-Failure Plane

PSL	Width1 w1 [mm]	Width2 w2 [mm]	Depth d [mm]	Height1 h1 [mm]	Height2 h2 [mm]	Shear Area A [mm^2]	Block Volume V [cm^3]	green m_g [g]	Weight dry m_d [g]	under Water m_i [g]	Water Immersion SG m_d/V_d [1]	Weighing Density m_d/V_g [g/cm^3]	MC u [%]	Time t [s]	Load F [kN]	Plank Shear Strength τ_{LT} [MPa]
P60	51.0	42.8	23.3	63.5	51.3	2616	126.5	86.5	80.8	-38.4	0.68	0.64	7.1	160	21.96	8.35
P61	51.0	43.0	23.5	63.6	51.2	2611	127.1	92.6	86.9	-32.5	0.73	0.68	6.6	165	22.18	8.45
P62	51.1	42.9	23.4	63.6	51.3	2621	127.2	88.9	83.4	-35.4	0.70	0.66	6.6	160	19.81	7.52
P63	50.9	42.7	23.3	63.6	51.3	2611	126.1	75.0	69.8	-46.0	0.60	0.55	7.5	190	23.70	9.03
P64	50.9	42.9	23.4	63.6	51.3	2611	126.7	83.7	78.1	-39.3	0.67	0.62	7.2	140	19.24	7.33
P65	51.0	42.5	23.0	63.6	51.3	2616	125.6	83.0	76.7	-36.6	0.68	0.61	8.3	140	19.54	7.43
P66	51.2	42.8	23.2	63.6	51.3	2627	127.0	83.3	77.2	-40.1	0.66	0.61	7.9	150	21.68	8.21
P67	51.2	43.2	23.7	63.5	51.3	2627	128.3	82.7	77.2	-42.5	0.64	0.60	7.1	140	16.33	6.18
P68	51.1	42.6	23.1	63.6	51.3	2621	126.2	80.3	74.3	-39.5	0.65	0.59	8.0	180	15.47	5.87
P69	51.2	42.7	23.3	63.6	51.4	2632	126.9	80.4	74.4	-41.2	0.64	0.59	8.1	170	17.60	6.65
P70	51.1	42.8	23.3	63.6	51.3	2621	126.8	76.3	70.8	-44.9	0.61	0.56	7.7	120	10.80	4.10
P71	51.0	42.8	23.3	63.6	51.3	2616	126.6	83.5	77.7	-40.2	0.66	0.61	7.5	140	23.16	8.81
P72	51.0	42.5	23.0	63.6	51.3	2616	125.6	84.0	77.8	-38.7	0.67	0.62	8.0	155	18.95	7.20
P73	51.2	43.0	23.4	63.7	51.3	2627	127.8	77.8	72.3	-46.2	0.61	0.57	7.6	150	24.77	9.38
P74	51.1	42.2	22.8	63.5	51.3	2621	124.8	81.7	75.4	-39.6	0.66	0.60	8.3	140	16.58	6.29
P75	50.9	42.8	23.5	63.5	51.2	2606	126.3	83.7	78.5	-39.8	0.66	0.62	6.7	200	21.26	8.12
P76	51.0	42.5	23.1	63.5	51.2	2611	125.5	84.7	77.9	-37.1	0.68	0.62	8.7	160	19.58	7.46
P77	51.1	42.8	23.3	63.6	51.3	2621	126.8	80.0	75.0	-43.5	0.63	0.59	6.7	160	18.09	6.87
P78	51.1	42.7	23.3	63.6	51.3	2621	126.6	86.2	79.8	-36.9	0.68	0.63	8.1	165	20.63	7.83
P79	51.1	43.0	23.3	63.6	51.3	2621	127.4	85.3	79.0	-37.9	0.68	0.62	8.0	145	22.38	8.49
P80	51.1	42.4	23.1	63.6	51.3	2621	125.7	84.1	78.1	-37.4	0.68	0.62	7.7		20.78	7.89
P81	51.0	42.7	23.3	63.6	51.2	2611	126.2	88.6	82.9	-36.4	0.70	0.66	6.8	160	20.33	7.74
P82	51.1	42.7	23.3	63.6	51.3	2621	126.6	84.2	78.0	-39.8	0.66	0.62	8.0	150	17.99	6.83
P83	51.2	42.7	23.2	63.6	51.3	2627	126.8	77.7	72.4	-43.6	0.62	0.57	7.4	140	21.53	8.15
P84	50.9	42.7	23.3	63.6	51.2	2606	126.0	81.4	76.1	-41.4	0.65	0.60	6.9	150	20.42	7.79
P85	51.1	42.4	23.0	63.5	51.3	2621	125.5	82.5	76.3	-39.5	0.66	0.61	8.1	135	17.65	6.70
mean	51.1	42.7	23.3	63.6	51.3	2619	126.5	83.0	77.2	-39.8	0.66	0.61	7.6	155	19.71	**7.49**
stdev	0.098	0.220	0.188	0.049	0.046	6.675	0.774	3.935	3.807	3.275	0.029	0.030	0.607	17.790	2.952	1.125
COV [%]	0.2	0.5	0.8	0.1	0.1	0.3	0.6	4.7	4.9	-8.2	4.3	4.9	8.0	11.5	15.0	15.0

Appendix E

Torque – Twist Graphs

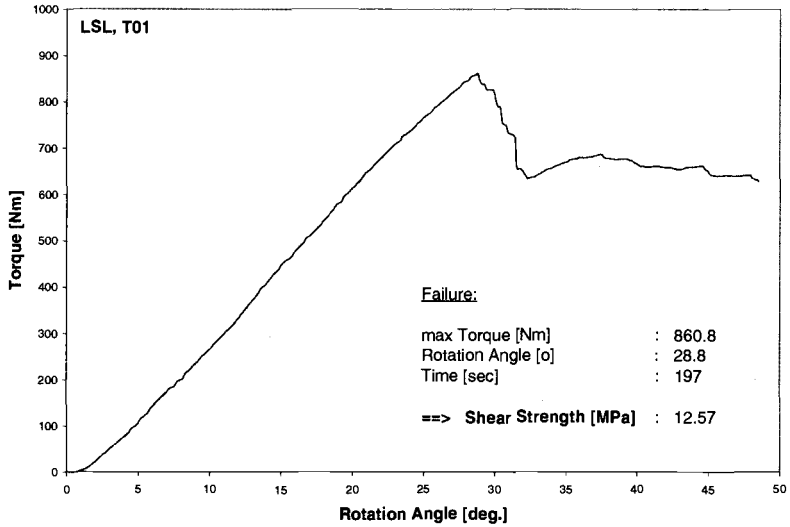
LSL, T01
Torque [Nm]
Rotation Angle [deg.]
Failure:
max Torque [Nm] : 860.8
Rotation Angle [o] : 28.8
Time [sec] : 197
==> Shear Strength [MPa] : 12.57

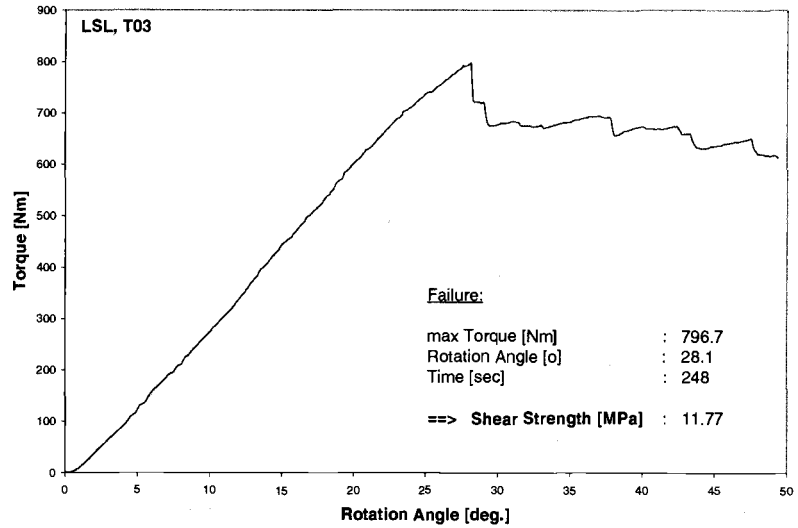
LSL, T03
Torque [Nm]
Rotation Angle [deg.]
Failure:
max Torque [Nm] : 796.7
Rotation Angle [o] : 28.1
Time [sec] : 248
==> Shear Strength [MPa] : 11.77

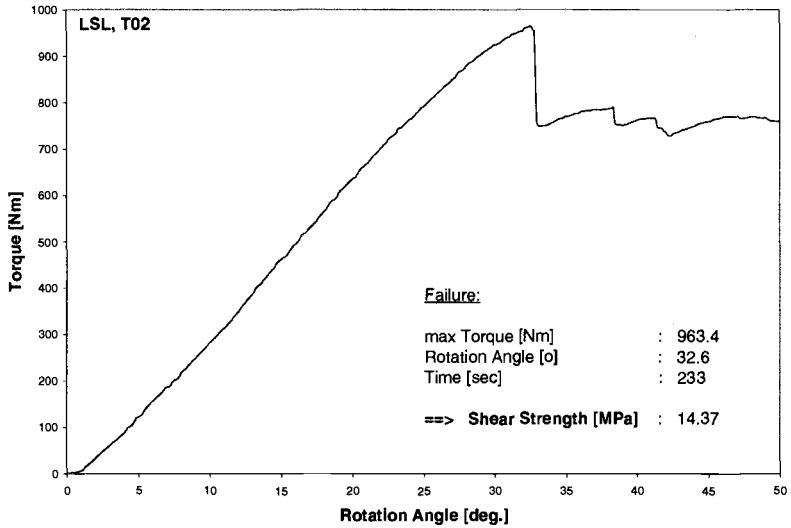
LSL, T02
Torque [Nm]
Rotation Angle [deg.]
Failure:
max Torque [Nm] : 963.4
Rotation Angle [o] : 32.6
Time [sec] : 233
==> Shear Strength [MPa] : 14.37

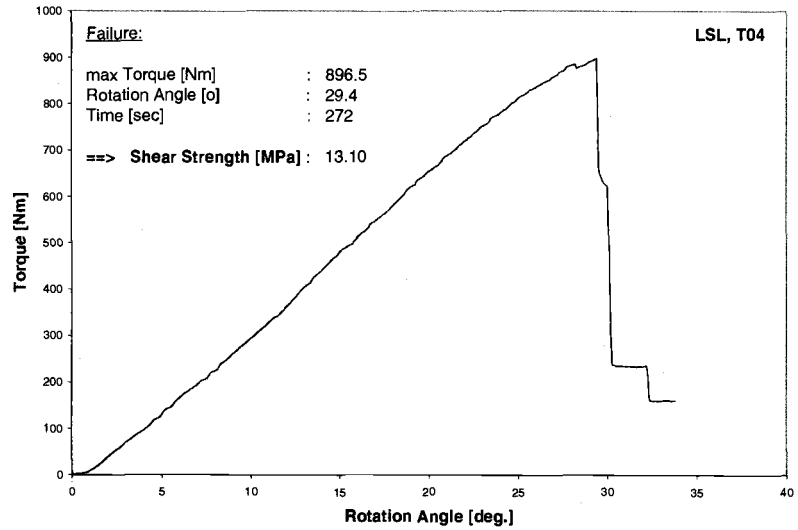
LSL, T04
Failure:
max Torque [Nm] : 896.5
Rotation Angle [o] : 29.4
Time [sec] : 272
==> Shear Strength [MPa] : 13.10
Torque [Nm]
Rotation Angle [deg.]

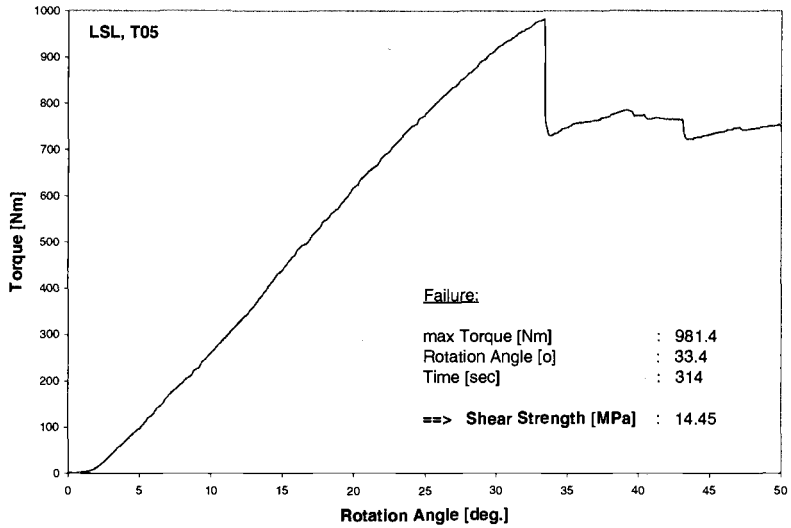
LSL, T05
Torque [Nm]
Rotation Angle [deg.]
Failure:
max Torque [Nm] : 981.4
Rotation Angle [o] : 33.4
Time [sec] : 314
==> Shear Strength [MPa] : 14.45

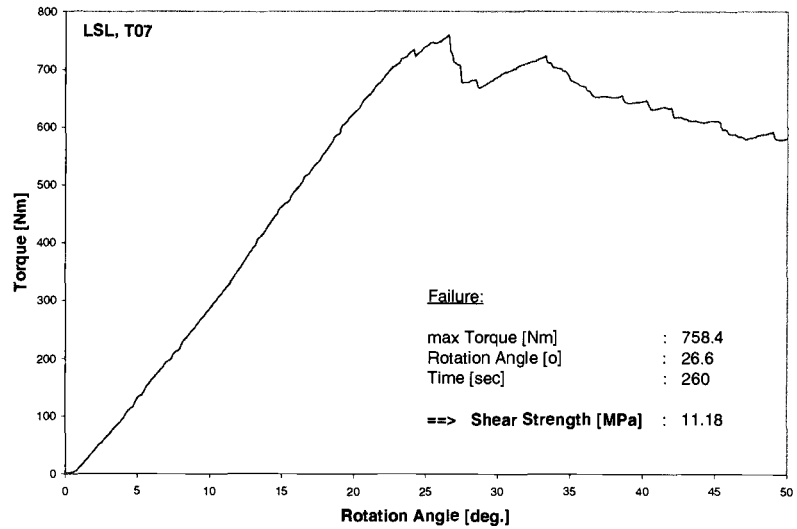
LSL, T07
Torque [Nm]
Rotation Angle [deg.]
Failure:
max Torque [Nm] : 758.4
Rotation Angle [o] : 26.6
Time [sec] : 260
==> Shear Strength [MPa] : 11.18

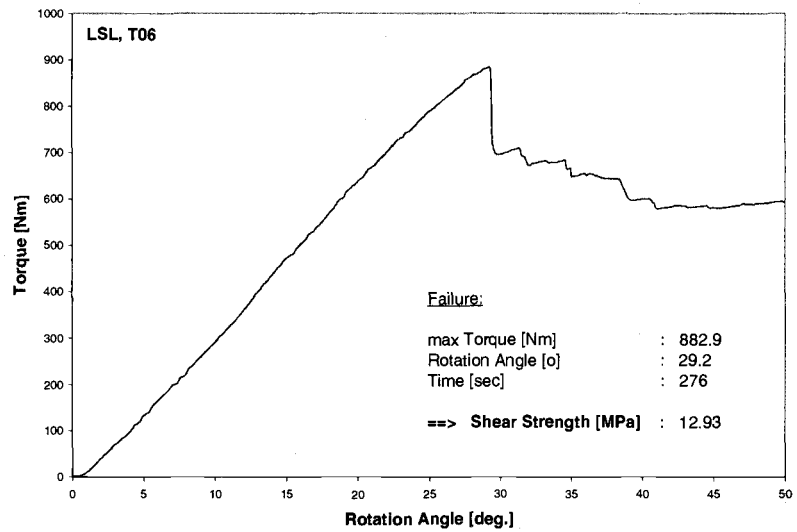
LSL, T06
Torque [Nm]
Rotation Angle [deg.]
Failure:
max Torque [Nm] : 882.9
Rotation Angle [o] : 29.2
Time [sec] : 276
==> Shear Strength [MPa] : 12.93

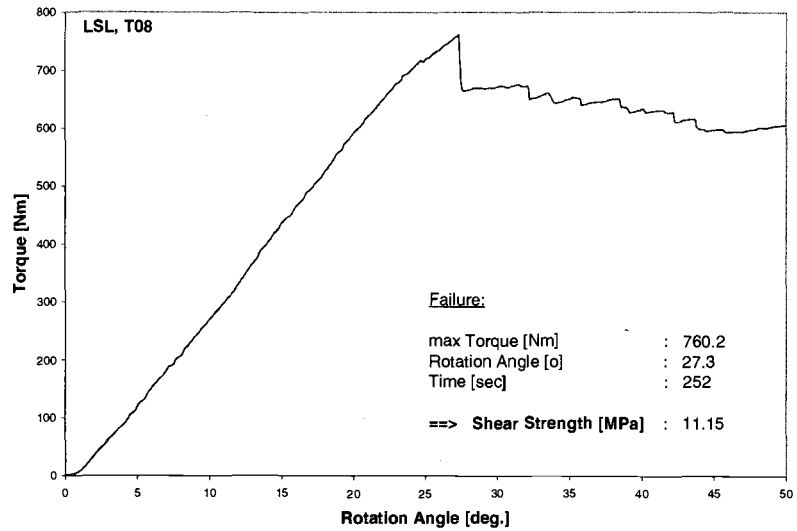
LSL, T08
Torque [Nm]
Rotation Angle [deg.]
Failure:
max Torque [Nm] : 760.2
Rotation Angle [o] : 27.3
Time [sec] : 252
==> Shear Strength [MPa] : 11.15

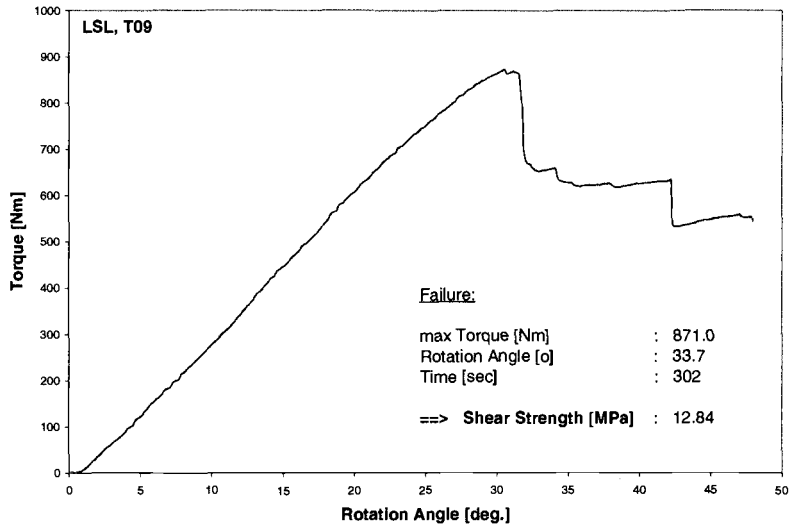
LSL, T09
Torque [Nm]
Rotation Angle [deg.]
Failure:
max Torque [Nm] : 871.0
Rotation Angle [o] : 33.7
Time [sec] : 302
==> Shear Strength [MPa] : 12.84

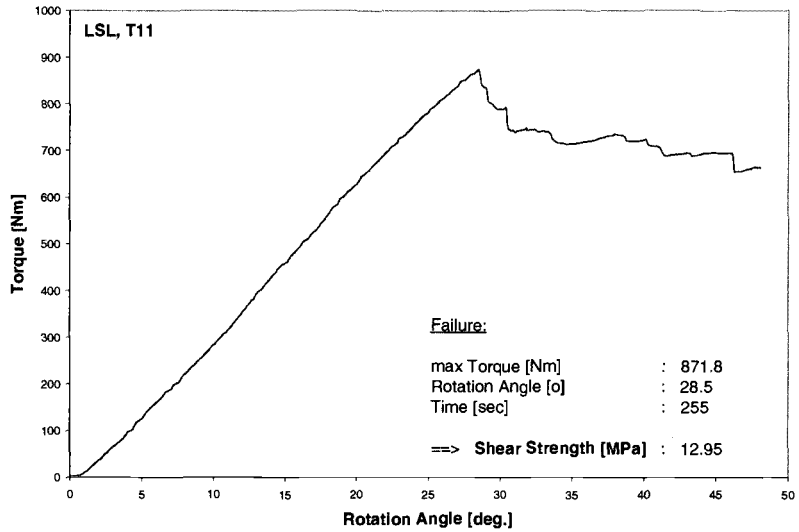
LSL, T11
Torque [Nm]
Rotation Angle [deg.]
Failure:
max Torque [Nm] : 871.8
Rotation Angle [o] : 28.5
Time [sec] : 255
==> Shear Strength [MPa] : 12.95

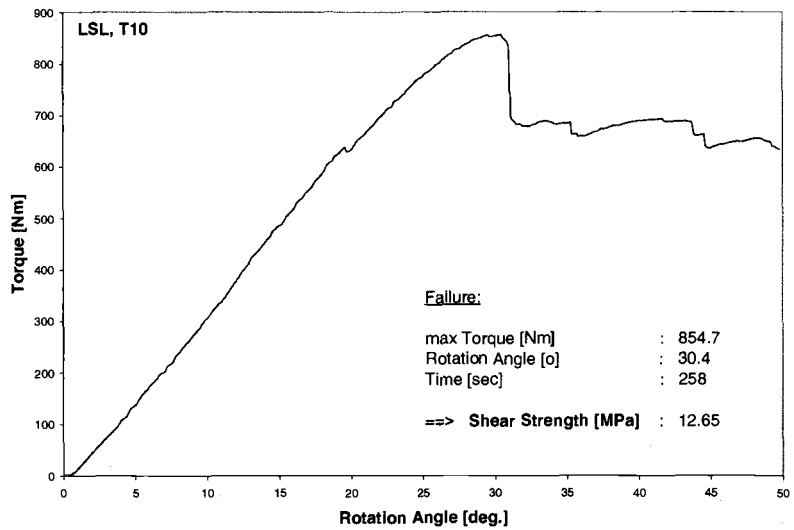
LSL, T10
Torque [Nm]
Rotation Angle [deg.]
Failure:
max Torque [Nm] : 854.7
Rotation Angle [o] : 30.4
Time [sec] : 258
==> Shear Strength [MPa] : 12.65

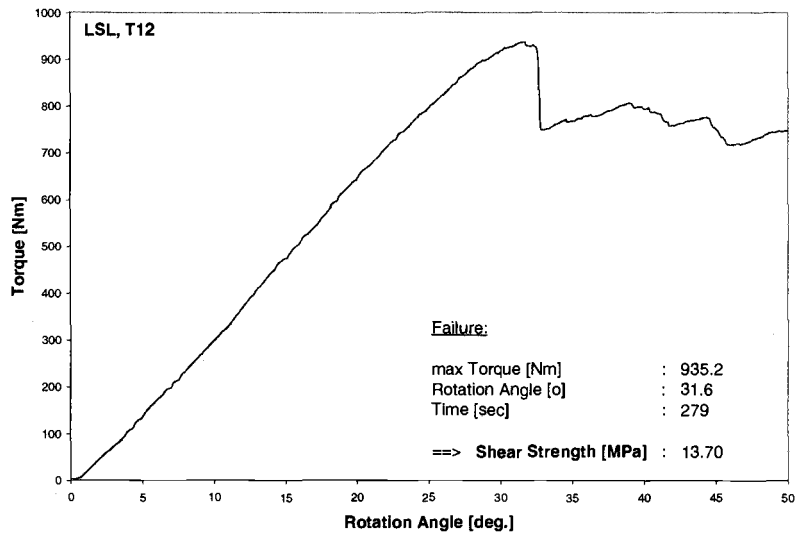
LSL, T12
Torque [Nm]
Rotation Angle [deg.]
Failure:
max Torque [Nm] : 935.2
Rotation Angle [o] : 31.6
Time [sec] : 279
==> Shear Strength [MPa] : 13.70

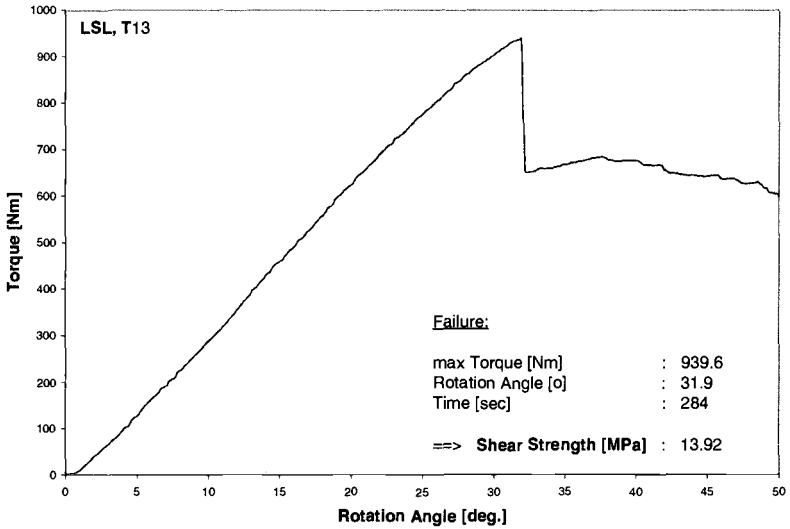
LSL, T13
Torque [Nm]
Rotation Angle [deg.]
Failure:
max Torque [Nm] : 939.6
Rotation Angle [o] : 31.9
Time [sec] : 284
==> Shear Strength [MPa] : 13.92

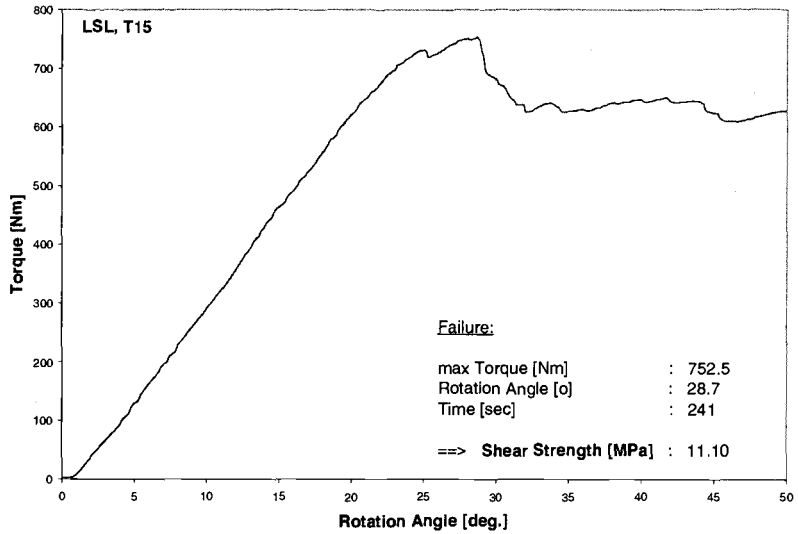
LSL, T15
Torque [Nm]
Rotation Angle [deg.]
Failure:
max Torque [Nm] : 752.5
Rotation Angle [o] : 28.7
Time [sec] : 241
==> Shear Strength [MPa] : 11.10

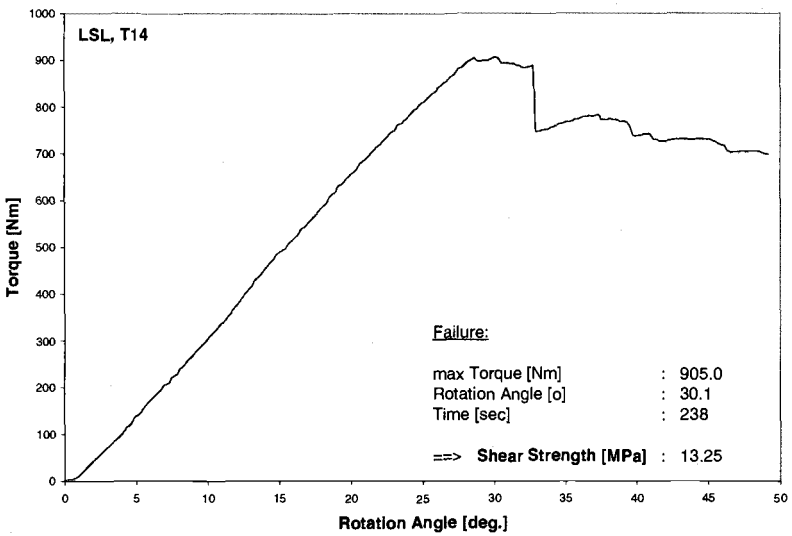
LSL, T14
Torque [Nm]
Rotation Angle [deg.]
Failure:
max Torque [Nm] : 905.0
Rotation Angle [o] : 30.1
Time [sec] : 238
==> Shear Strength [MPa] : 13.25

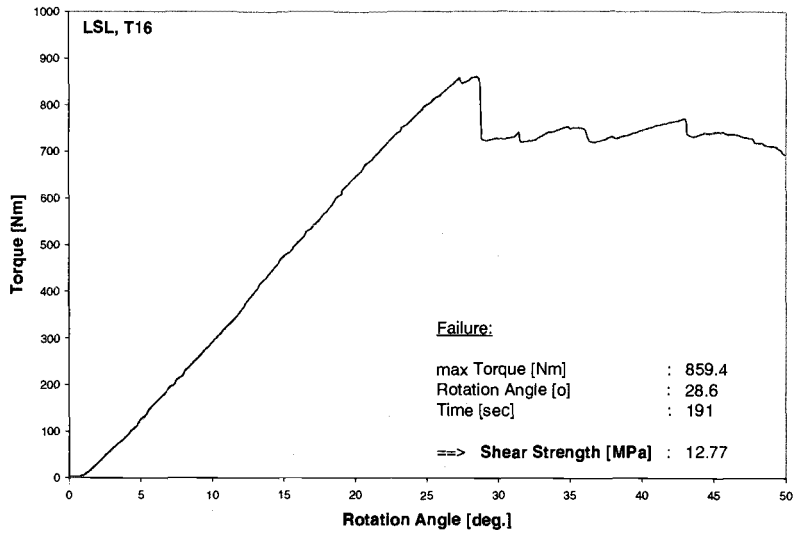
LSL, T16
Torque [Nm]
Rotation Angle [deg.]
Failure:
max Torque [Nm] : 859.4
Rotation Angle [o] : 28.6
Time [sec] : 191
==> Shear Strength [MPa] : 12.77

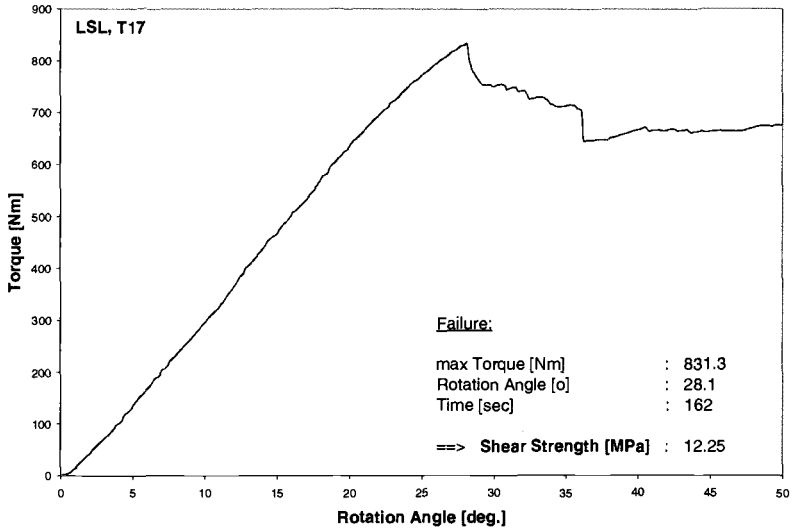
LSL, T17
Torque [Nm]
Rotation Angle [deg.]
Failure:
max Torque [Nm] : 831.3
Rotation Angle [o] : 28.1
Time [sec] : 162
==> Shear Strength [MPa] : 12.25

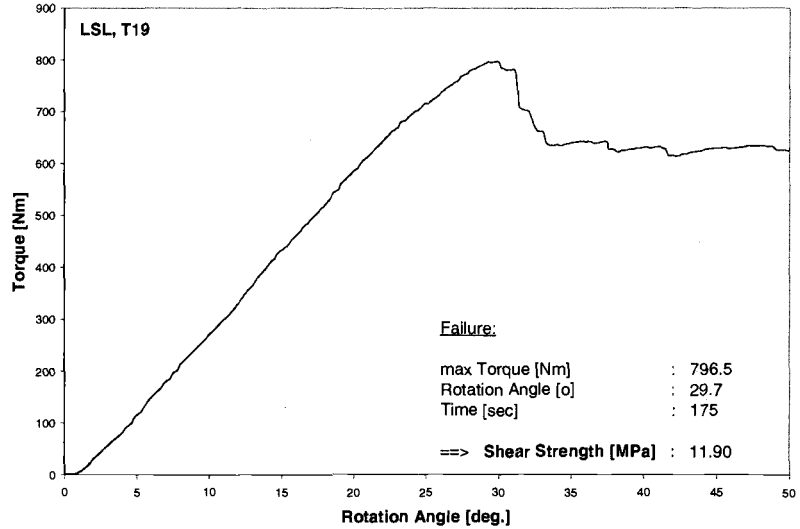
LSL, T19
Torque [Nm]
Rotation Angle [deg.]
Failure:
max Torque [Nm] : 796.5
Rotation Angle [o] : 29.7
Time [sec] : 175
==> Shear Strength [MPa] : 11.90

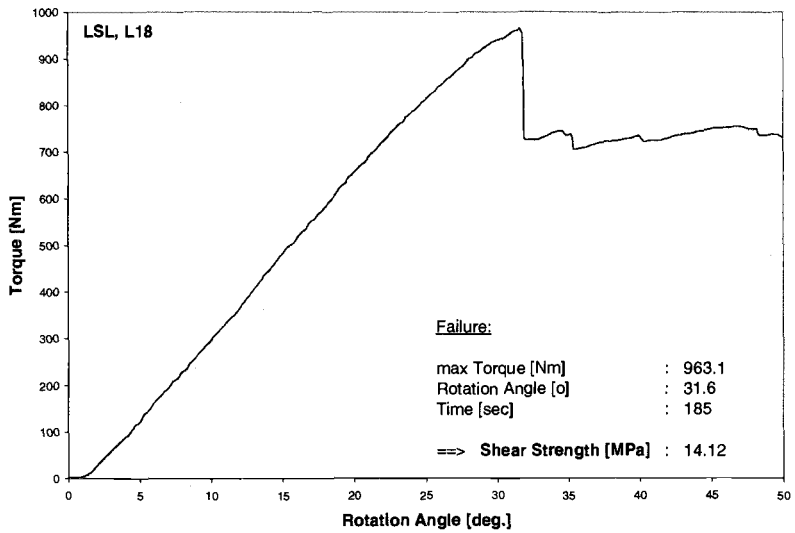
LSL, L18
Torque [Nm]
Rotation Angle [deg.]
Failure:
max Torque [Nm] : 963.1
Rotation Angle [o] : 31.6
Time [sec] : 185
==> Shear Strength [MPa] : 14.12

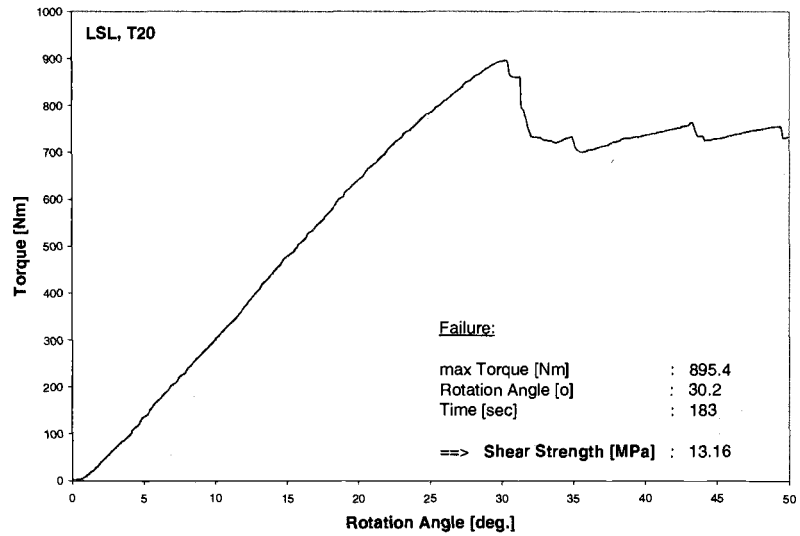
LSL, T20
Torque [Nm]
Rotation Angle [deg.]
Failure:
max Torque [Nm] : 895.4
Rotation Angle [o] : 30.2
Time [sec] : 183
==> Shear Strength [MPa] : 13.16

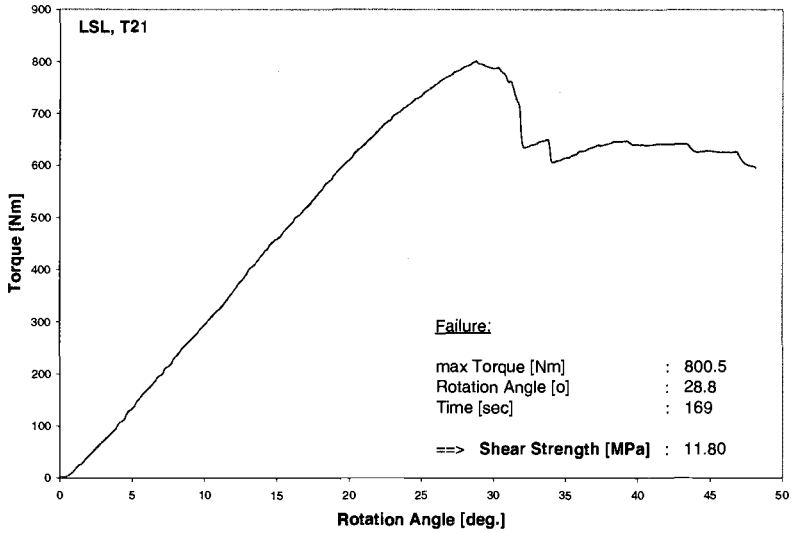
LSL, T21
Torque [Nm]
Rotation Angle [deg.]
Failure:
max Torque [Nm] : 800.5
Rotation Angle [o] : 28.8
Time [sec] : 169
==> Shear Strength [MPa] : 11.80

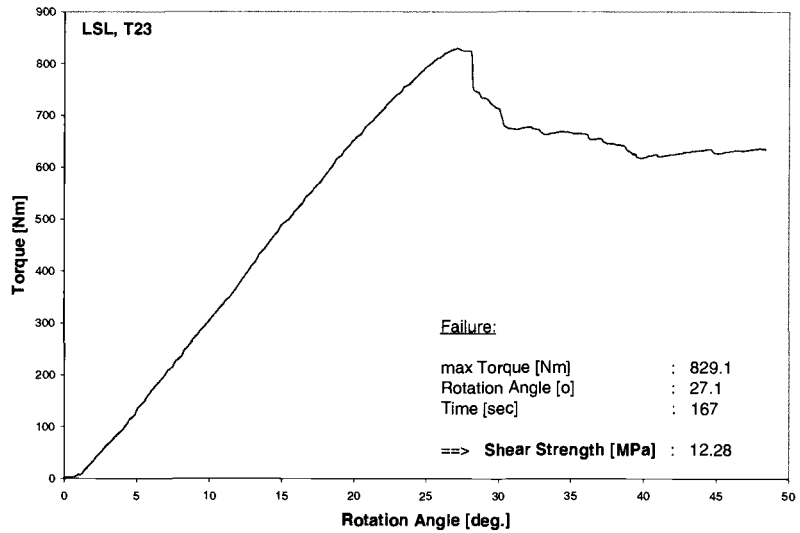
LSL, T23
Torque [Nm]
Rotation Angle [deg.]
Failure:
max Torque [Nm] : 829.1
Rotation Angle [o] : 27.1
Time [sec] : 167
==> Shear Strength [MPa] : 12.28

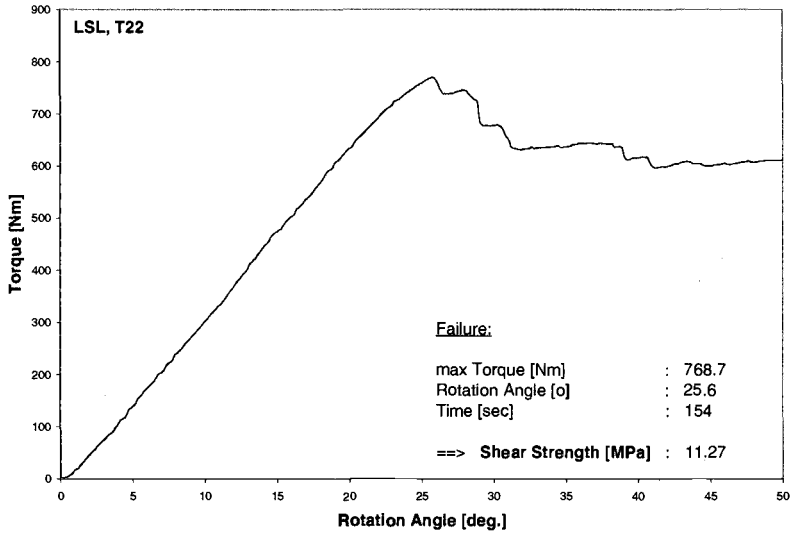
LSL, T22
Torque [Nm]
Rotation Angle [deg.]
Failure:
max Torque [Nm] : 768.7
Rotation Angle [o] : 25.6
Time [sec] : 154
==> Shear Strength [MPa] : 11.27

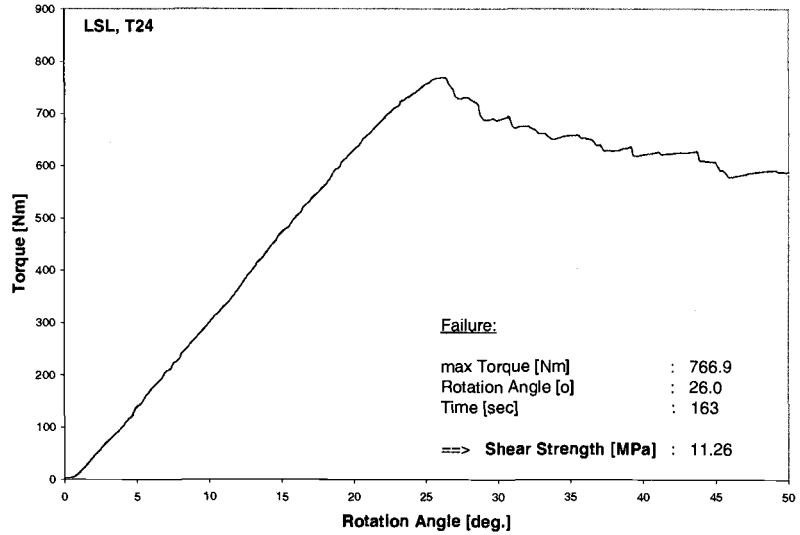
LSL, T24
Torque [Nm]
Rotation Angle [deg.]
Failure:
max Torque [Nm] : 766.9
Rotation Angle [o] : 26.0
Time [sec] : 163
==> Shear Strength [MPa] : 11.26

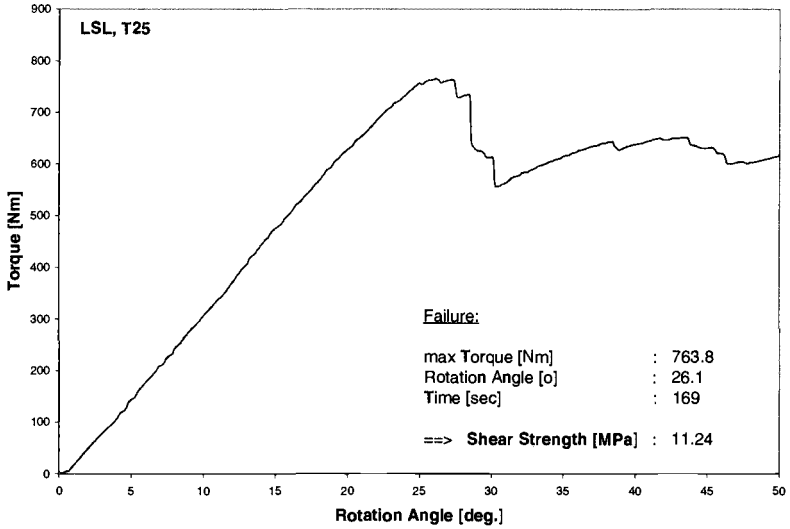
LSL, T25
Torque [Nm]
Rotation Angle [deg.]
Failure:
max Torque [Nm] : 763.8
Rotation Angle [o] : 26.1
Time [sec] : 169
==> Shear Strength [MPa] : 11.24

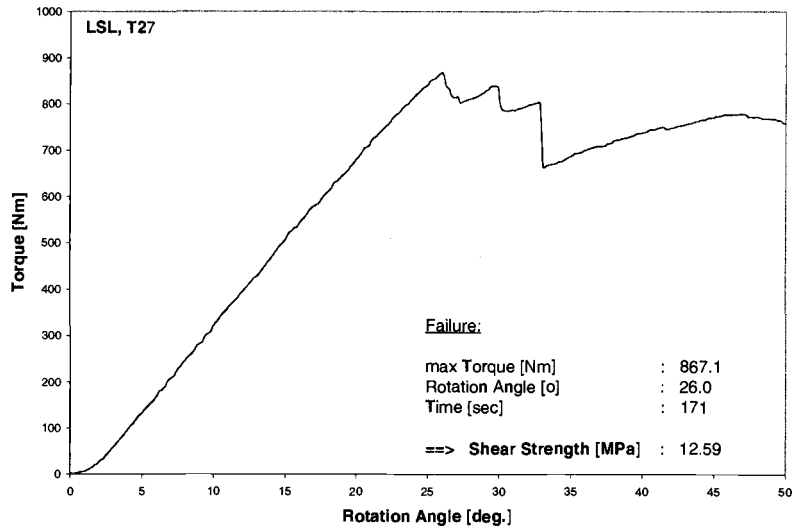
LSL, T27
Torque [Nm]
Rotation Angle [deg.]
Failure:
max Torque [Nm] : 867.1
Rotation Angle [o] : 26.0
Time [sec] : 171
==> Shear Strength [MPa] : 12.59

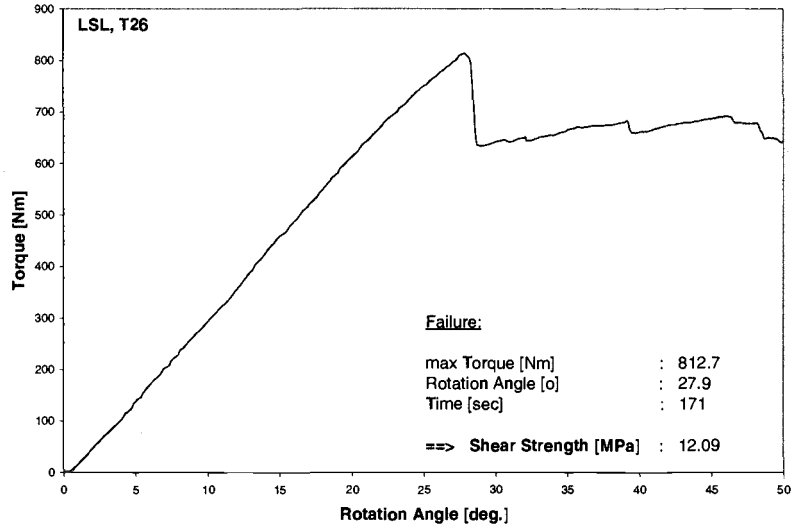
LSL, T26
Torque [Nm]
Rotation Angle [deg.]
Failure:
max Torque [Nm] : 812.7
Rotation Angle [o] : 27.9
Time [sec] : 171
==> Shear Strength [MPa] : 12.09

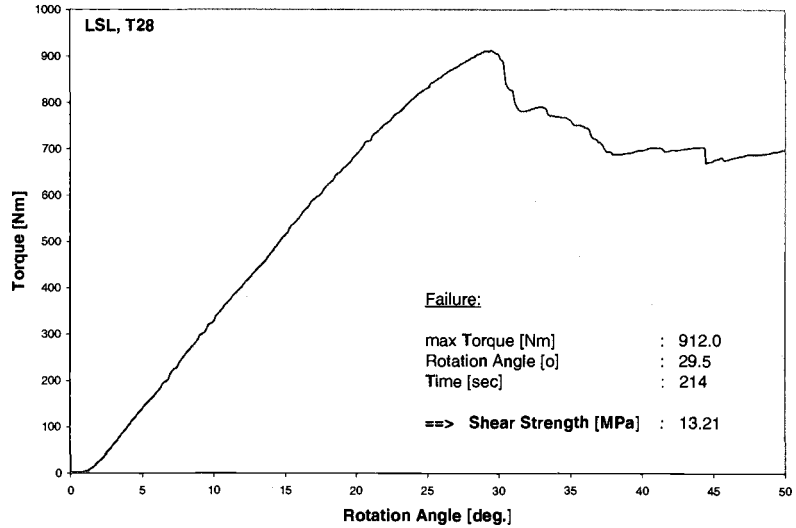
LSL, T28
Torque [Nm]
Rotation Angle [deg.]
Failure:
max Torque [Nm] : 912.0
Rotation Angle [o] : 29.5
Time [sec] : 214
==> Shear Strength [MPa] : 13.21

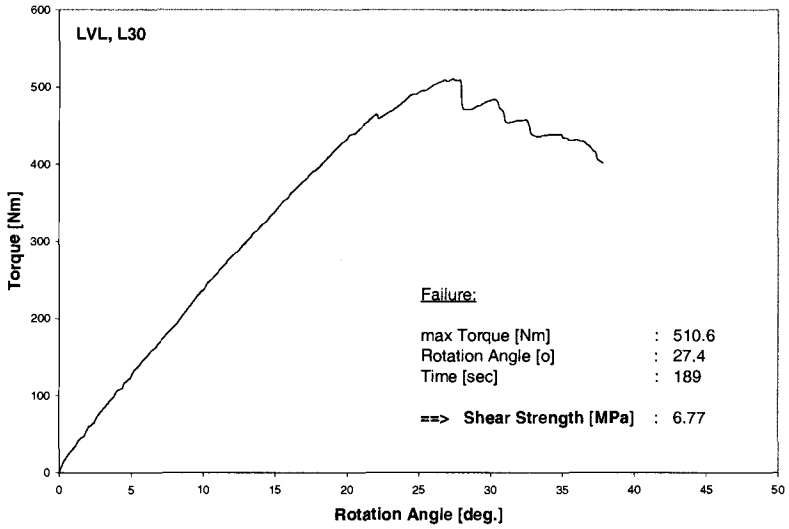
LVL, L30
Torque [Nm]
Rotation Angle [deg.]
Failure:
max Torque [Nm] : 510.6
Rotation Angle [o] : 27.4
Time [sec] : 189
==> Shear Strength [MPa] : 6.77

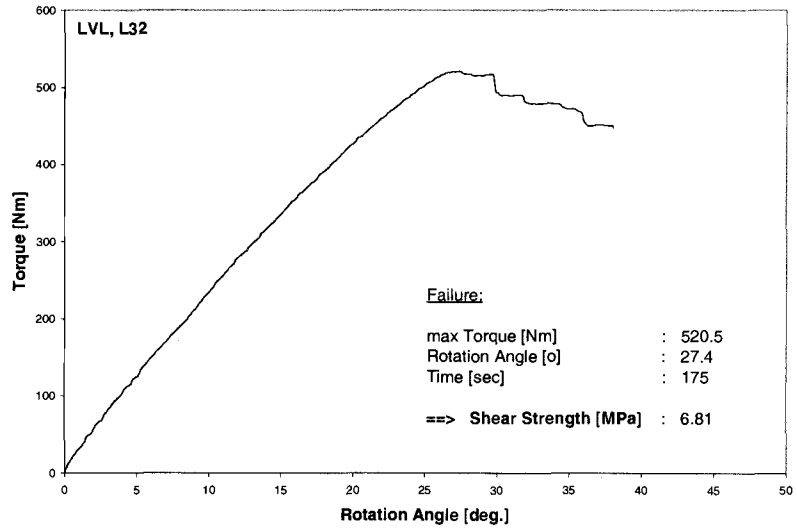
LVL, L32
Torque [Nm]
Rotation Angle [deg.]
Failure:
max Torque [Nm] : 520.5
Rotation Angle [o] : 27.4
Time [sec] : 175
==> Shear Strength [MPa] : 6.81

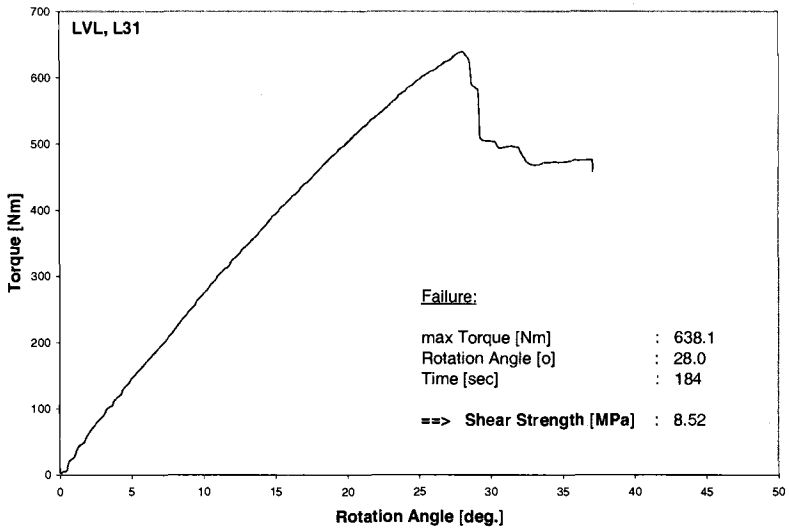
LVL, L31
Torque [Nm]
Rotation Angle [deg.]
Failure:
max Torque [Nm] : 638.1
Rotation Angle [o] : 28.0
Time [sec] : 184
==> Shear Strength [MPa] : 8.52

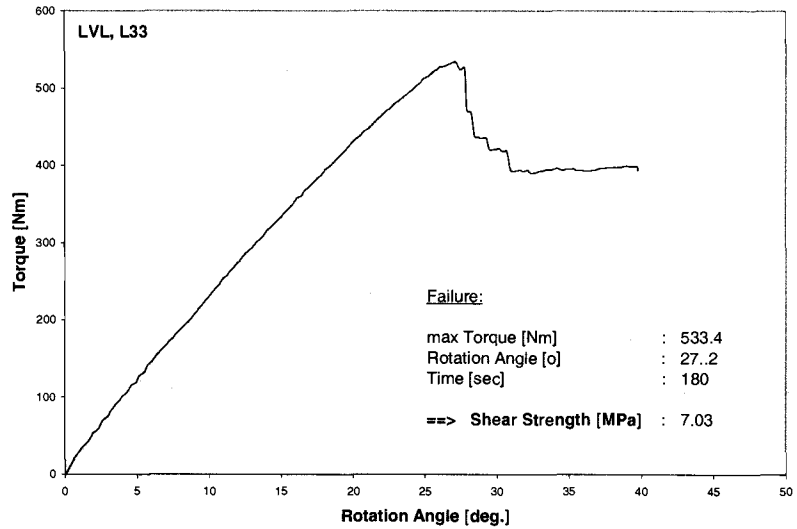
LVL, L33
Torque [Nm]
Rotation Angle [deg.]
Failure:
max Torque [Nm] : 533.4
Rotation Angle [o] : 27..2
Time [sec] : 180
==> Shear Strength [MPa] : 7.03

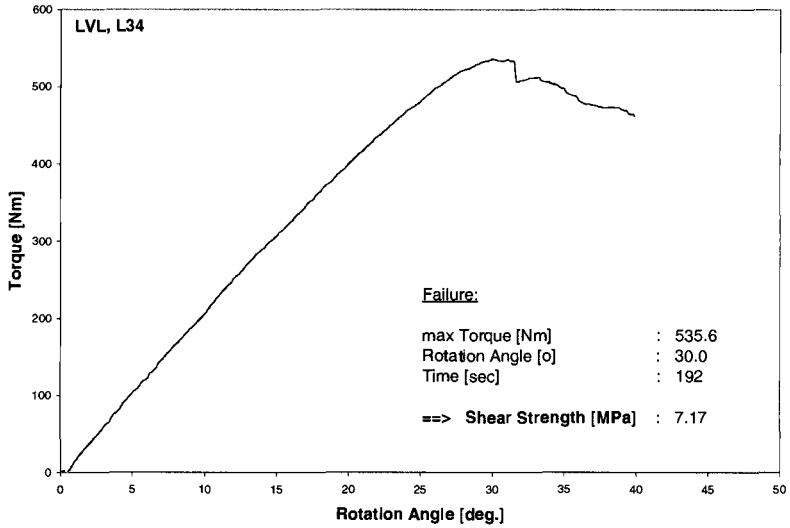
LVL, L34
Torque [Nm]
Rotation Angle [deg.]
Failure:
max Torque [Nm] : 535.6
Rotation Angle [o] : 30.0
Time [sec] : 192
==> Shear Strength [MPa] : 7.17

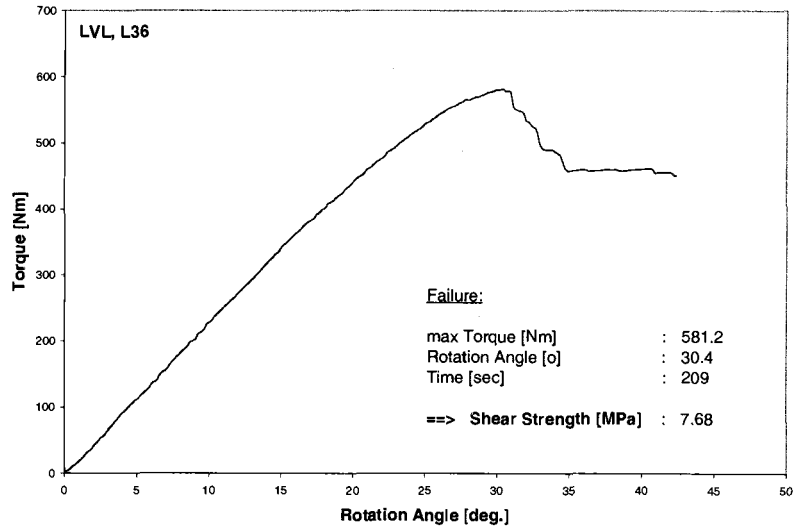
LVL, L36
Torque [Nm]
Rotation Angle [deg.]
Failure:
max Torque [Nm] : 581.2
Rotation Angle [o] : 30.4
Time [sec] : 209
==> Shear Strength [MPa] : 7.68

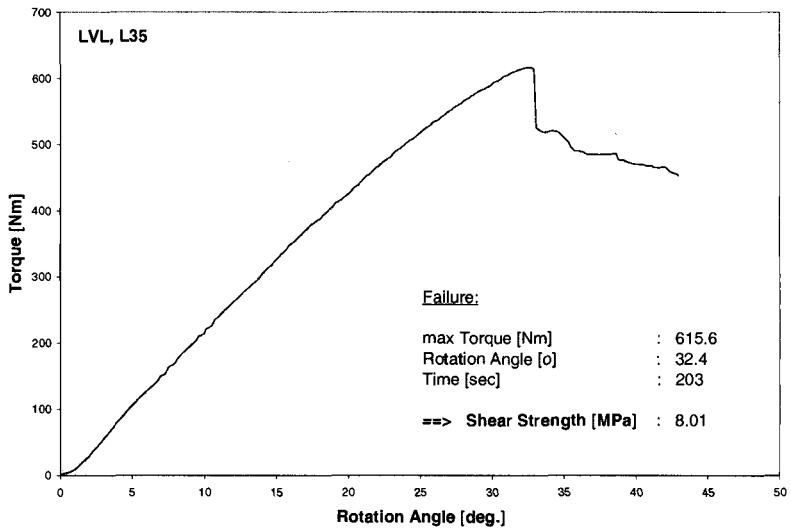
LVL, L35
Torque [Nm]
Rotation Angle [deg.]
Failure:
max Torque [Nm] : 615.6
Rotation Angle [o] : 32.4
Time [sec] : 203
==> Shear Strength [MPa] : 8.01

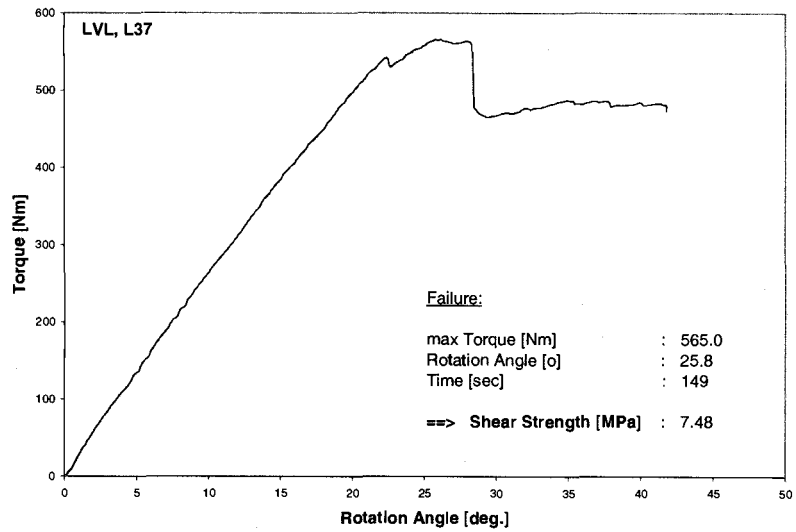
LVL, L37
Torque [Nm]
Rotation Angle [deg.]
Failure:
max Torque [Nm] : 565.0
Rotation Angle [o] : 25.8
Time [sec] : 149
==> Shear Strength [MPa] : 7.48

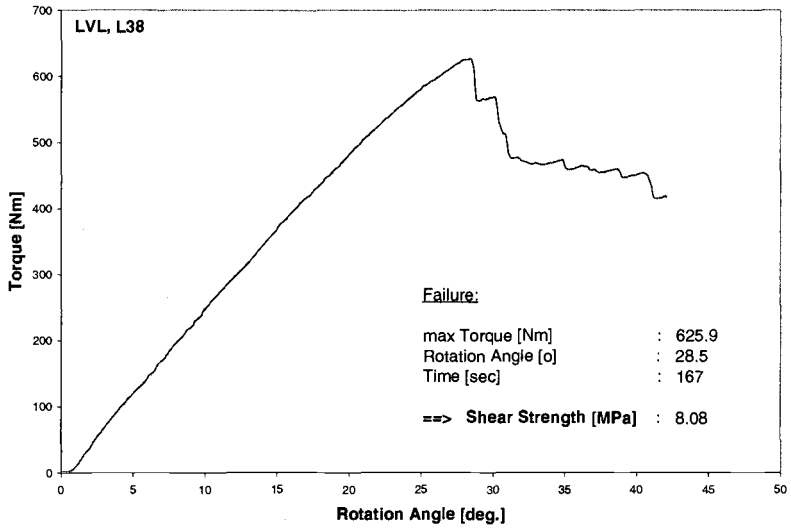
LVL, L38
Torque [Nm]
Rotation Angle [deg.]
Failure:
max Torque [Nm] : 625.9
Rotation Angle [o] : 28.5
Time [sec] : 167
==> Shear Strength [MPa] : 8.08

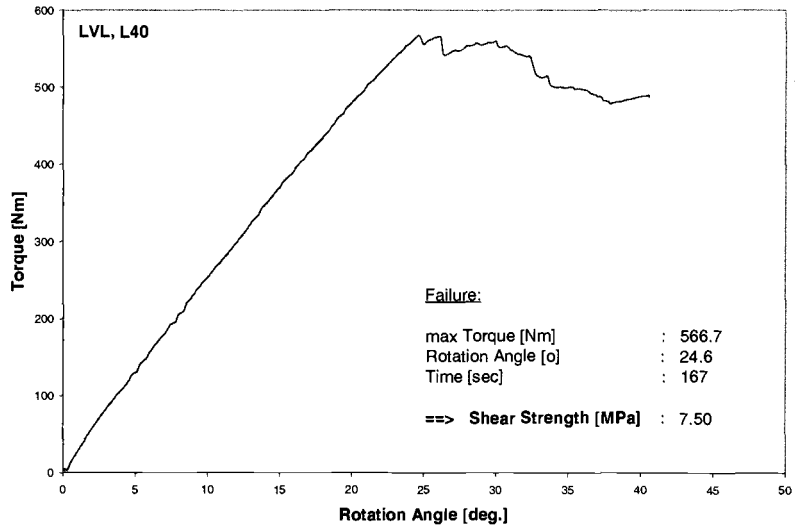
LVL, L40
Torque [Nm]
Rotation Angle [deg.]
Failure:
max Torque [Nm] : 566.7
Rotation Angle [o] : 24.6
Time [sec] : 167
==> Shear Strength [MPa] : 7.50

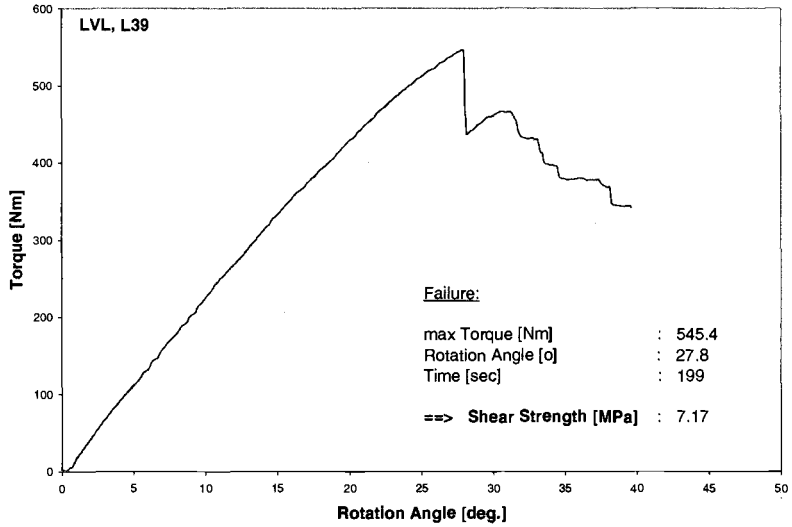
LVL, L39
Torque [Nm]
Rotation Angle [deg.]
Failure:
max Torque [Nm] : 545.4
Rotation Angle [o] : 27.8
Time [sec] : 199
==> Shear Strength [MPa] : 7.17

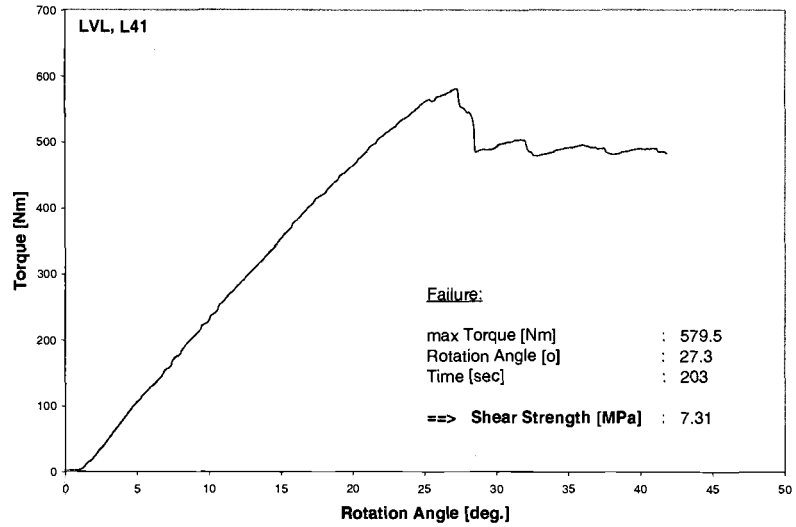
LVL, L41
Torque [Nm]
Rotation Angle [deg.]
Failure:
max Torque [Nm] : 579.5
Rotation Angle [o] : 27.3
Time [sec] : 203
==> Shear Strength [MPa] : 7.31

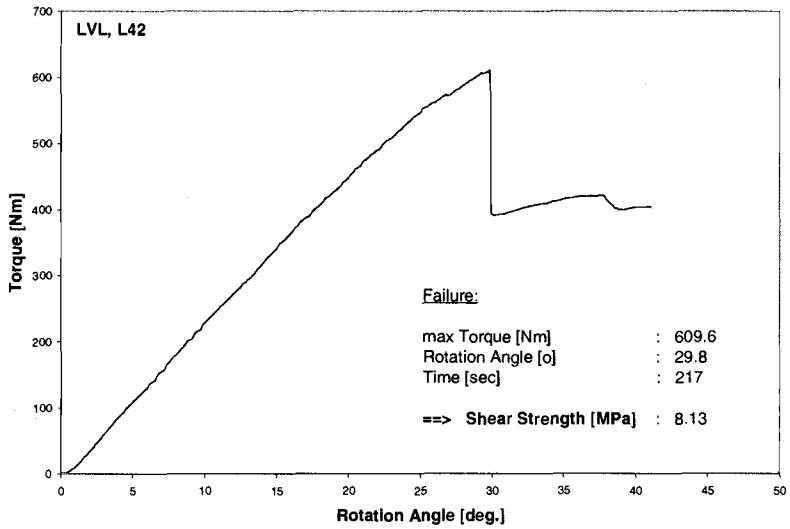
LVL, L42
Torque [Nm]
Rotation Angle [deg.]
Failure:
max Torque [Nm] : 609.6
Rotation Angle [o] : 29.8
Time [sec] : 217
==> Shear Strength [MPa] : 8.13

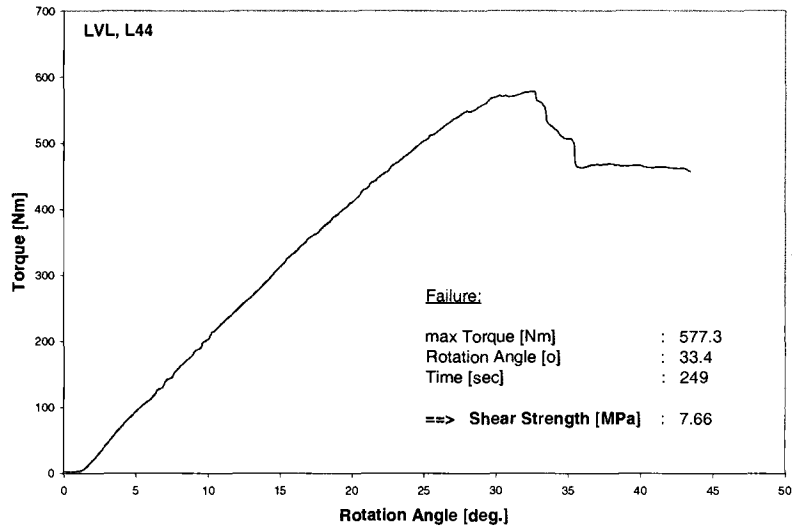
LVL, L44
Torque [Nm]
Rotation Angle [deg.]
Failure:
max Torque [Nm] : 577.3
Rotation Angle [o] : 33.4
Time [sec] : 249
==> Shear Strength [MPa] : 7.66

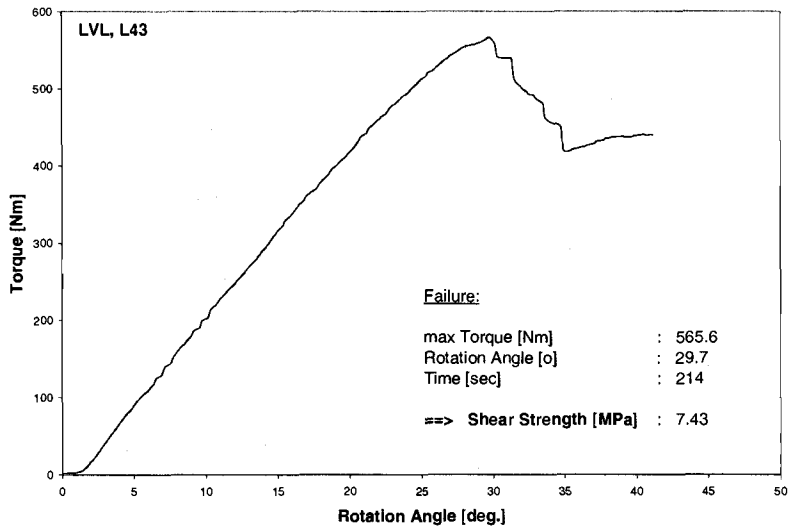
LVL, L43
Torque [Nm]
Rotation Angle [deg.]
Failure:
max Torque [Nm] : 565.6
Rotation Angle [o] : 29.7
Time [sec] : 214
==> Shear Strength [MPa] : 7.43

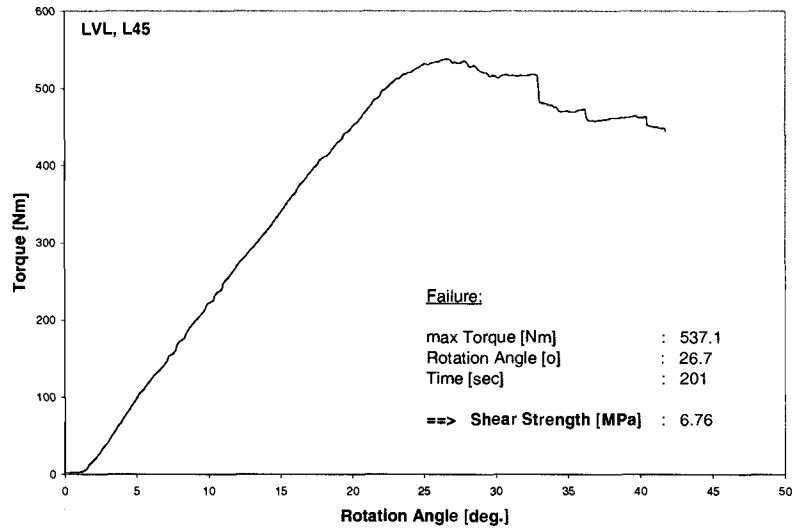
LVL, L45
Torque [Nm]
Rotation Angle [deg.]
Failure:
max Torque [Nm] : 537.1
Rotation Angle [o] : 26.7
Time [sec] : 201
==> Shear Strength [MPa] : 6.76

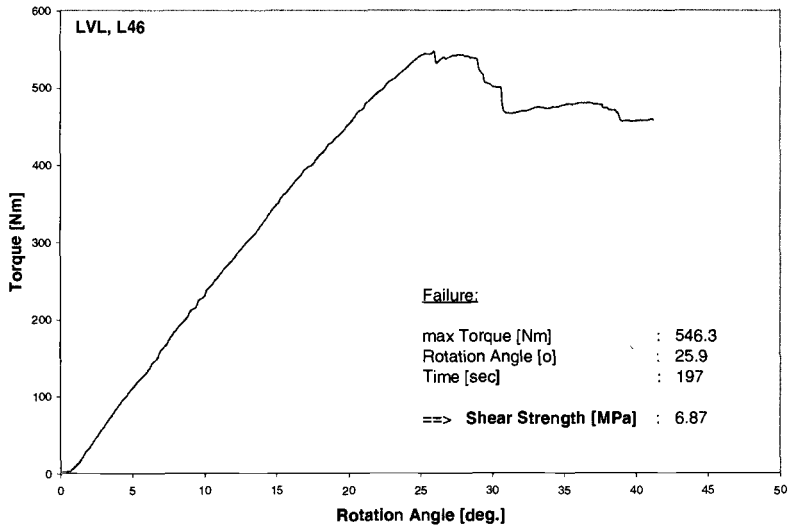
LVL, L46
Torque [Nm]
Rotation Angle [deg.]
Failure:
max Torque [Nm] : 546.3
Rotation Angle [o] : 25.9
Time [sec] : 197
==> Shear Strength [MPa] : 6.87

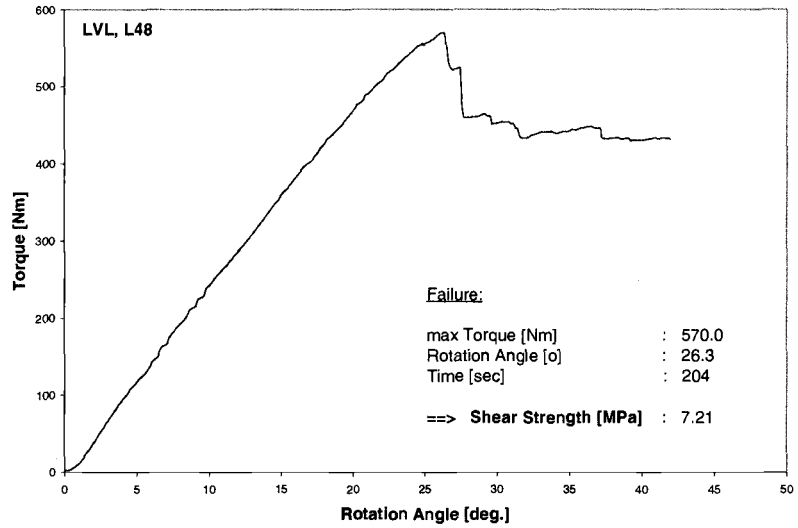
LVL, L48
Torque [Nm]
Rotation Angle [deg.]
Failure:
max Torque [Nm] : 570.0
Rotation Angle [o] : 26.3
Time [sec] : 204
==> Shear Strength [MPa] : 7.21

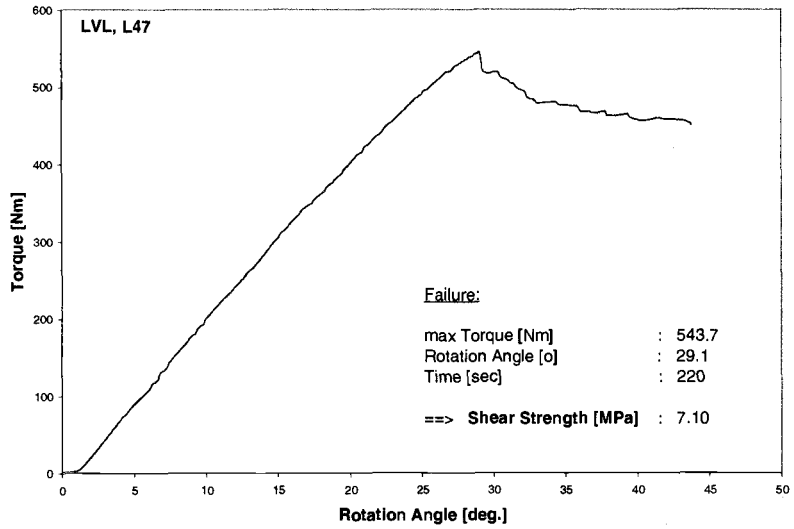
LVL, L47
Torque [Nm]
Rotation Angle [deg.]
Failure:
max Torque [Nm] : 543.7
Rotation Angle [o] : 29.1
Time [sec] : 220
==> Shear Strength [MPa] : 7.10

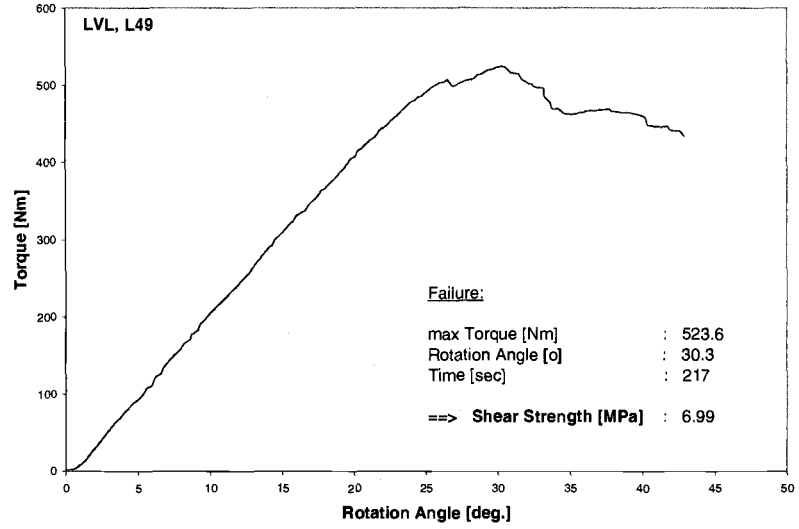
LVL, L49
Torque [Nm]
Rotation Angle [deg.]
Failure:
max Torque [Nm] : 523.6
Rotation Angle [o] : 30.3
Time [sec] : 217
==> Shear Strength [MPa] : 6.99

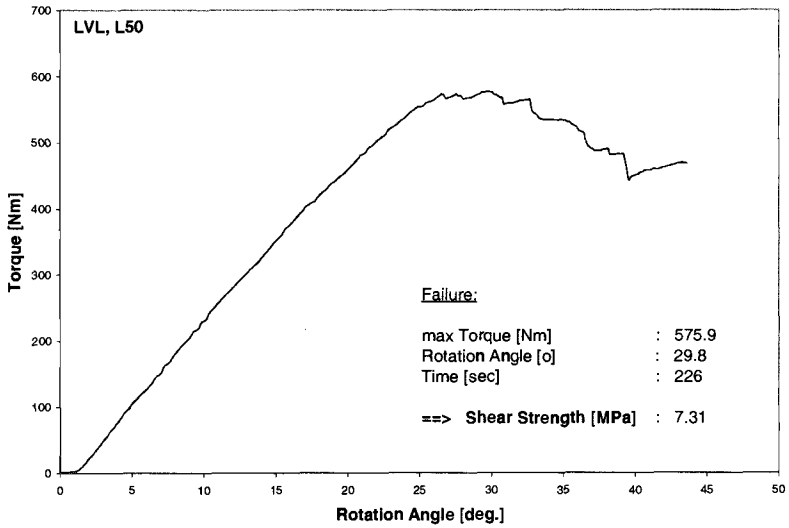
LVL, L50
Torque [Nm]
Rotation Angle [deg.]
Failure:
max Torque [Nm] : 575.9
Rotation Angle [o] : 29.8
Time [sec] : 226
==> Shear Strength [MPa] : 7.31

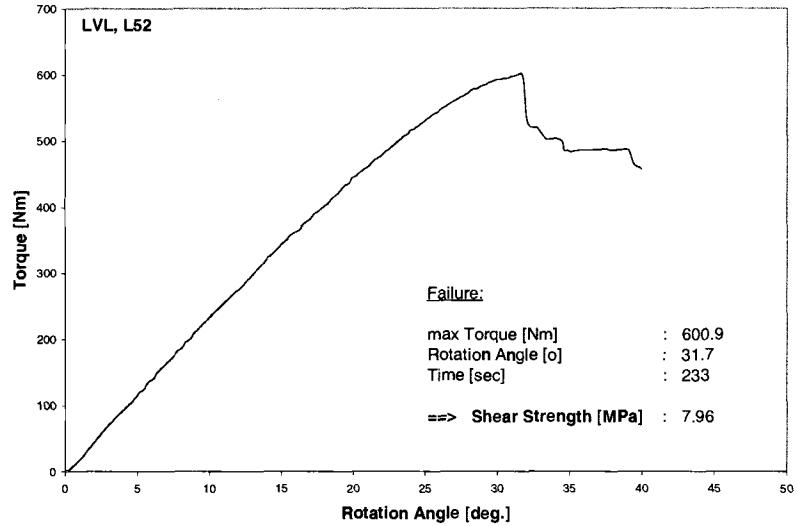
LVL, L52
Torque [Nm]
Rotation Angle [deg.]
Failure:
max Torque [Nm] : 600.9
Rotation Angle [o] : 31.7
Time [sec] : 233
==> Shear Strength [MPa] : 7.96

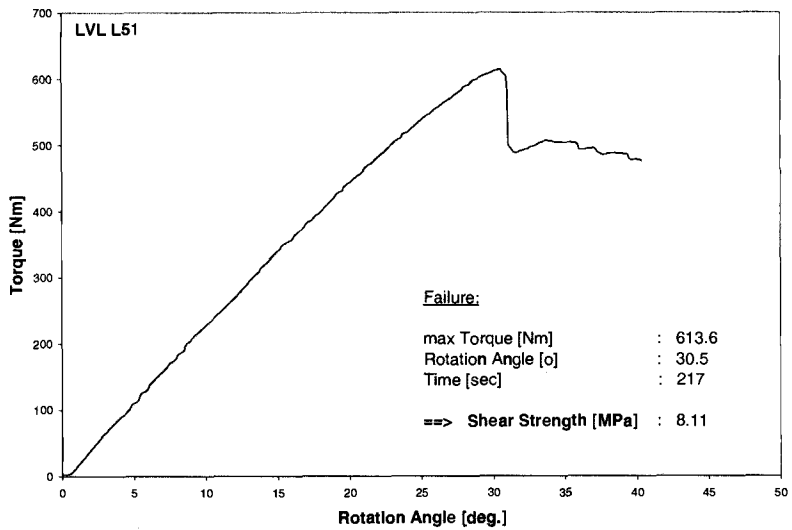
LVL L51
Torque [Nm]
Rotation Angle [deg.]
Failure:
max Torque [Nm] : 613.6
Rotation Angle [o] : 30.5
Time [sec] : 217
==> Shear Strength [MPa] : 8.11

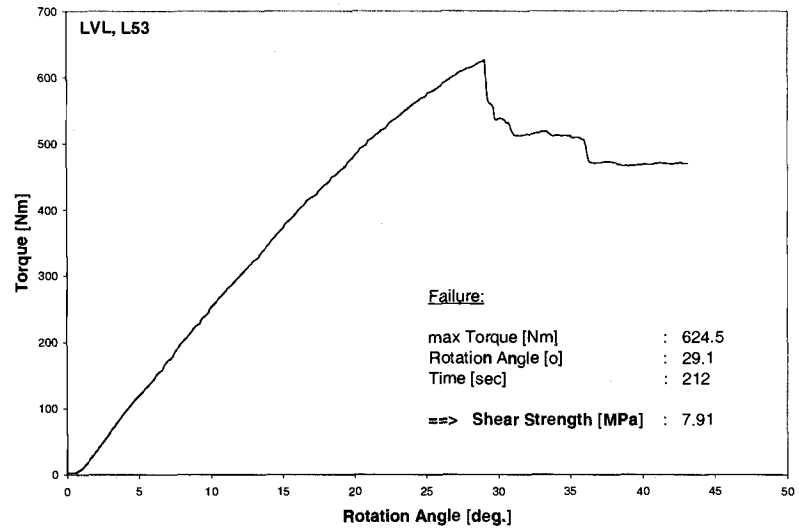
LVL, L53
Torque [Nm]
Rotation Angle [deg.]
Failure:
max Torque [Nm] : 624.5
Rotation Angle [o] : 29.1
Time [sec] : 212
==> Shear Strength [MPa] : 7.91

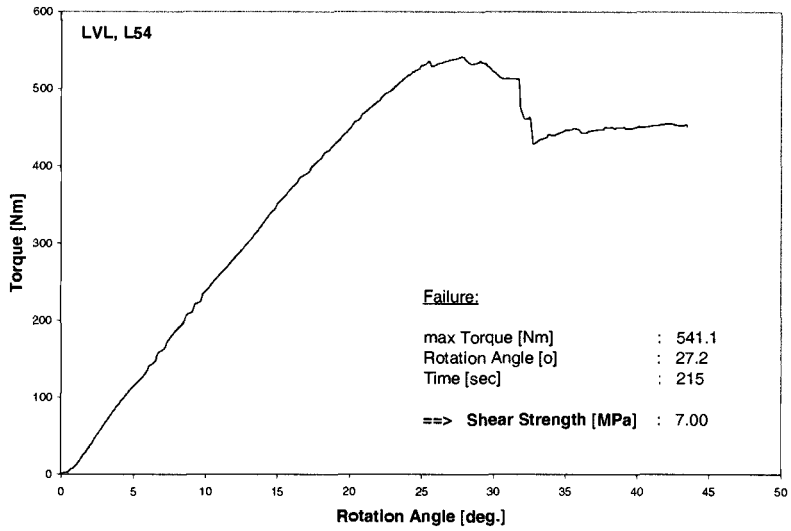
LVL, L54
Torque [Nm]
Rotation Angle [deg.]
Failure:
max Torque [Nm] : 541.1
Rotation Angle [o] : 27.2
Time [sec] : 215
==> Shear Strength [MPa] : 7.00

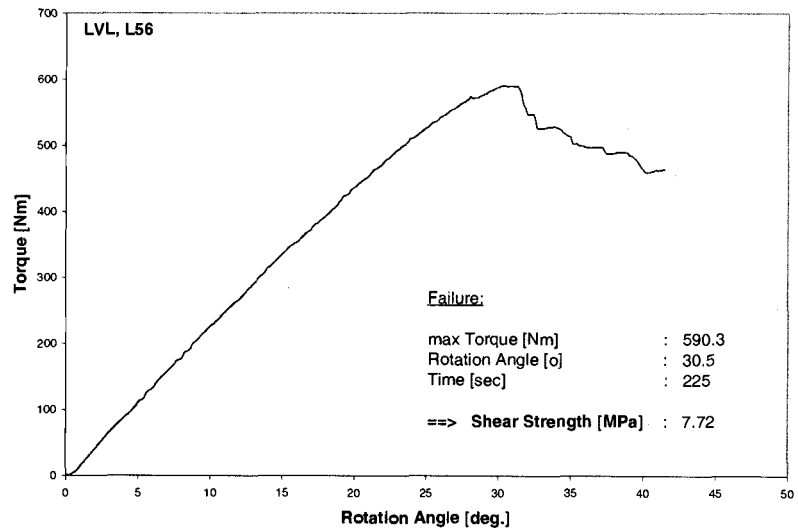
LVL, L56
Torque [Nm]
Rotation Angle [deg.]
Failure:
max Torque [Nm] : 590.3
Rotation Angle [o] : 30.5
Time [sec] : 225
==> Shear Strength [MPa] : 7.72

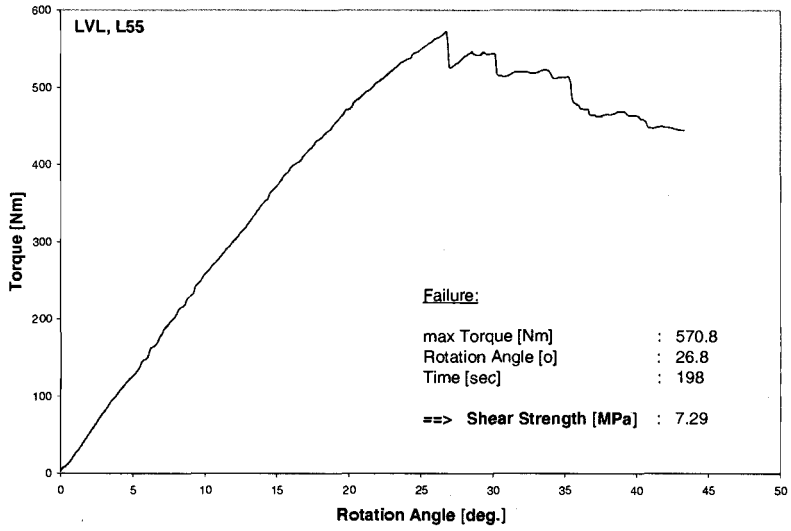
LVL, L55
Torque [Nm]
Rotation Angle [deg.]
Failure:
max Torque [Nm] : 570.8
Rotation Angle [o] : 26.8
Time [sec] : 198
==> Shear Strength [MPa] : 7.29

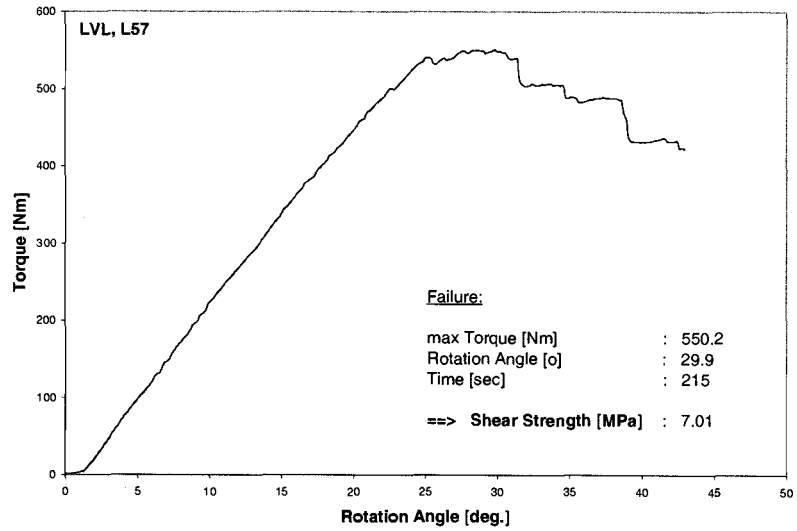
LVL, L57
Torque [Nm]
Rotation Angle [deg.]
Failure:
max Torque [Nm] : 550.2
Rotation Angle [o] : 29.9
Time [sec] : 215
==> Shear Strength [MPa] : 7.01

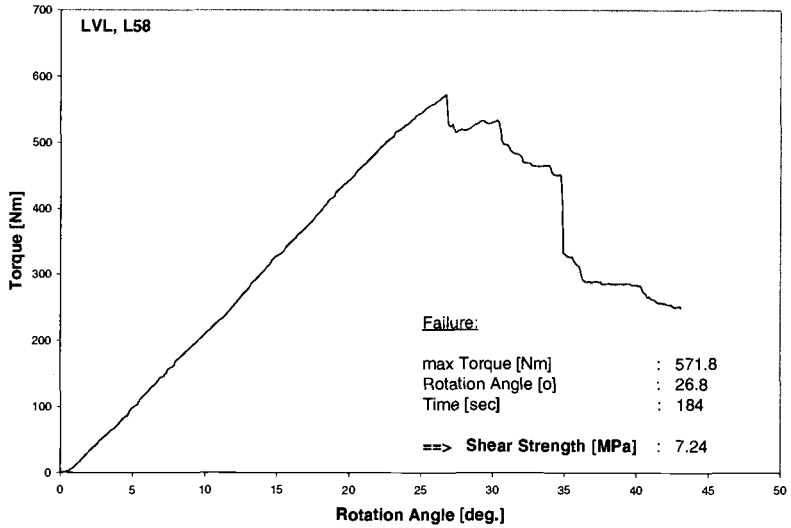
LVL, L58
Torque [Nm]
Rotation Angle [deg.]
Failure:
max Torque [Nm] : 571.8
Rotation Angle [o] : 26.8
Time [sec] : 184
==> Shear Strength [MPa] : 7.24

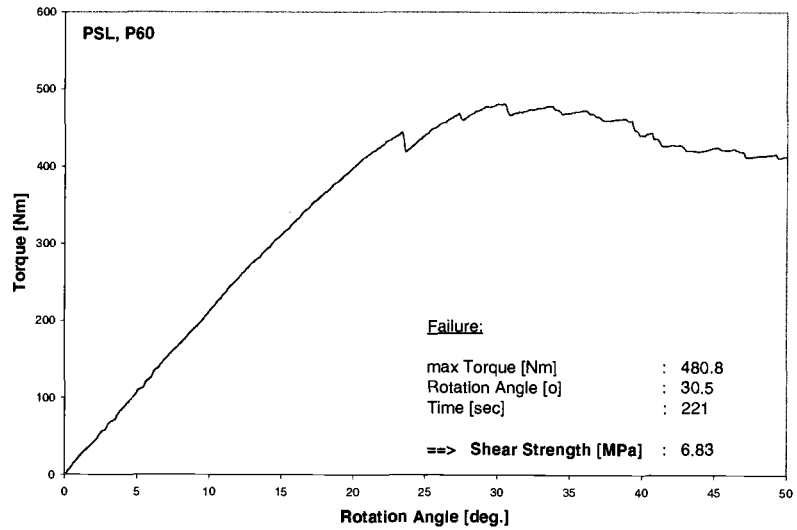
PSL, P60
Torque [Nm]
Rotation Angle [deg.]
Failure:
max Torque [Nm] : 480.8
Rotation Angle [o] : 30.5
Time [sec] : 221
==> Shear Strength [MPa] : 6.83

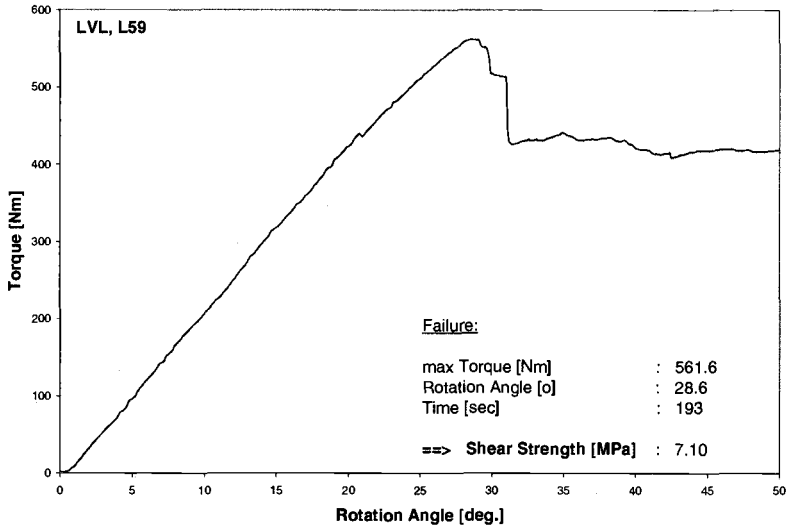
LVL, L59
Torque [Nm]
Rotation Angle [deg.]
Failure:
max Torque [Nm] : 561.6
Rotation Angle [o] : 28.6
Time [sec] : 193
==> Shear Strength [MPa] : 7.10

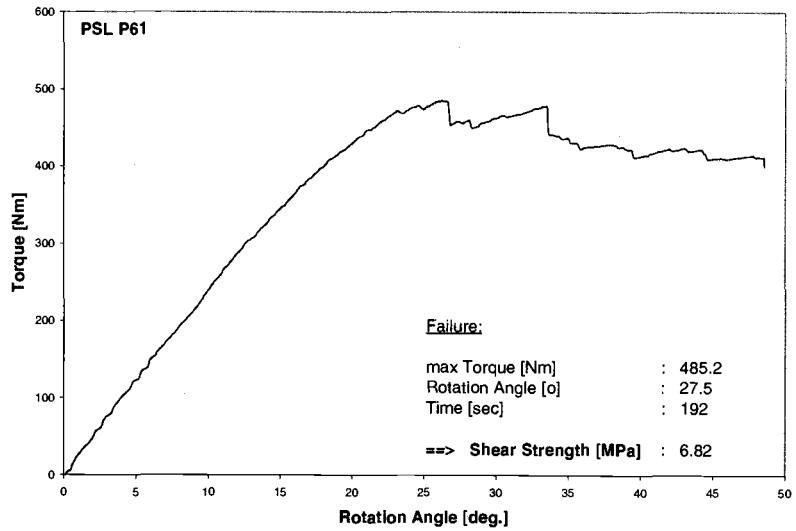
PSL P61
Torque [Nm]
Rotation Angle [deg.]
Failure:
max Torque [Nm] : 485.2
Rotation Angle [o] : 27.5
Time [sec] : 192
==> Shear Strength [MPa] : 6.82

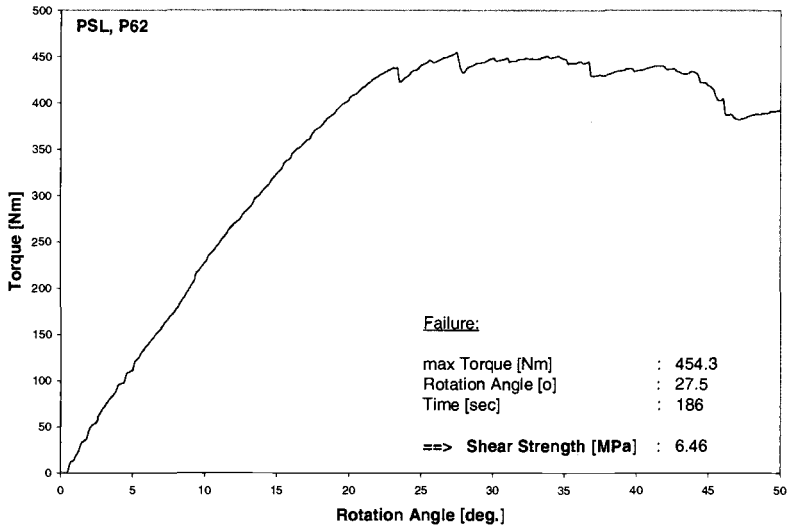
PSL, P62
Torque [Nm]
Rotation Angle [deg.]
Failure:
max Torque [Nm] : 454.3
Rotation Angle [o] : 27.5
Time [sec] : 186
==> Shear Strength [MPa] : 6.46

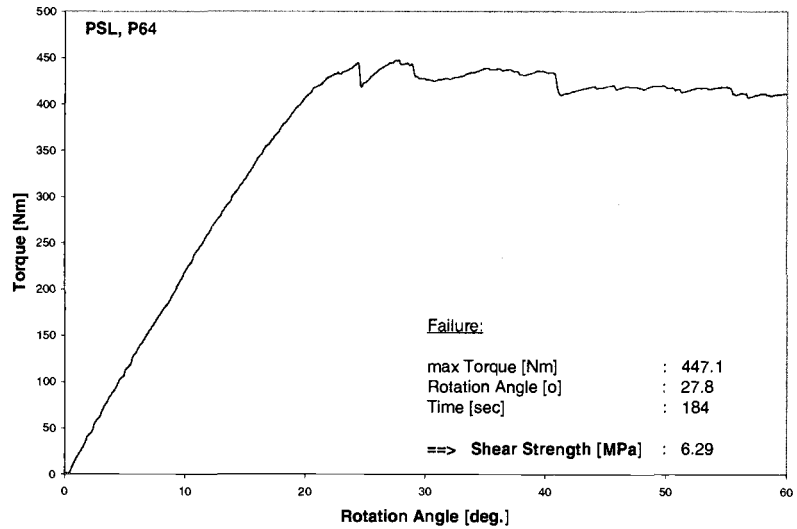
PSL, P64
Torque [Nm]
Rotation Angle [deg.]
Failure:
max Torque [Nm] : 447.1
Rotation Angle [o] : 27.8
Time [sec] : 184
==> Shear Strength [MPa] : 6.29

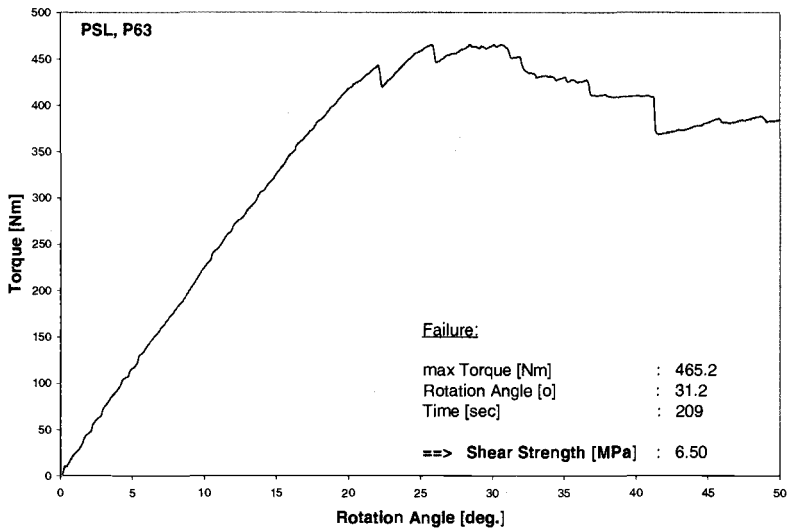
PSL, P63
Torque [Nm]
Rotation Angle [deg.]
Failure:
max Torque [Nm] : 465.2
Rotation Angle [o] : 31.2
Time [sec] : 209
==> Shear Strength [MPa] : 6.50

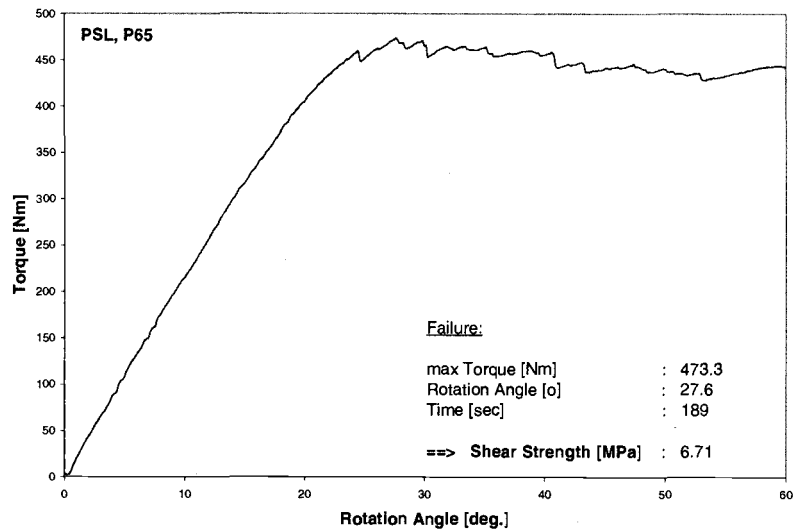
PSL, P65
Torque [Nm]
Rotation Angle [deg.]
Failure:
max Torque [Nm] : 473.3
Rotation Angle [o] : 27.6
Time [sec] : 189
==> Shear Strength [MPa] : 6.71

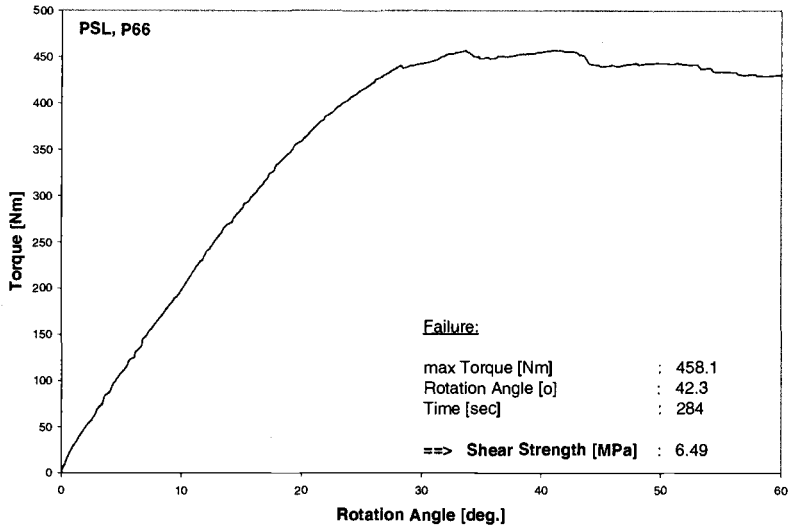
PSL, P66
Torque [Nm]
Rotation Angle [deg.]
Failure:
max Torque [Nm] : 458.1
Rotation Angle [o] : 42.3
Time [sec] : 284
==> Shear Strength [MPa] : 6.49

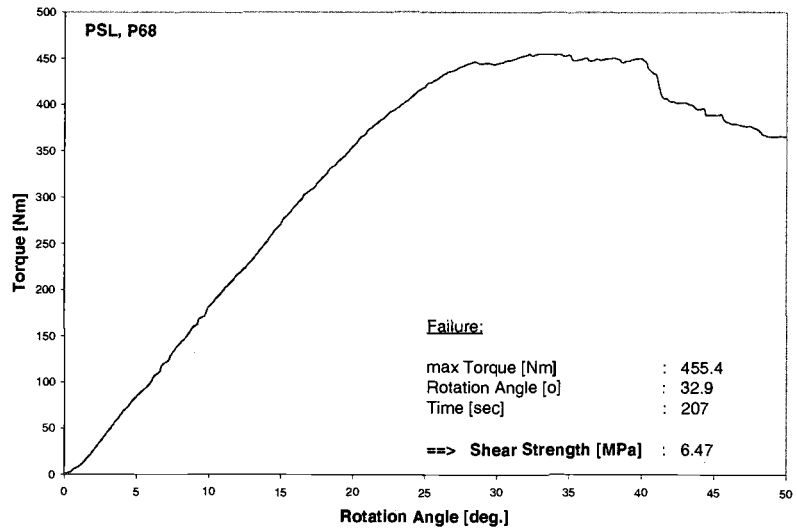
PSL, P68
Torque [Nm]
Rotation Angle [deg.]
Failure:
max Torque [Nm] : 455.4
Rotation Angle [o] : 32.9
Time [sec] : 207
==> Shear Strength [MPa] : 6.47

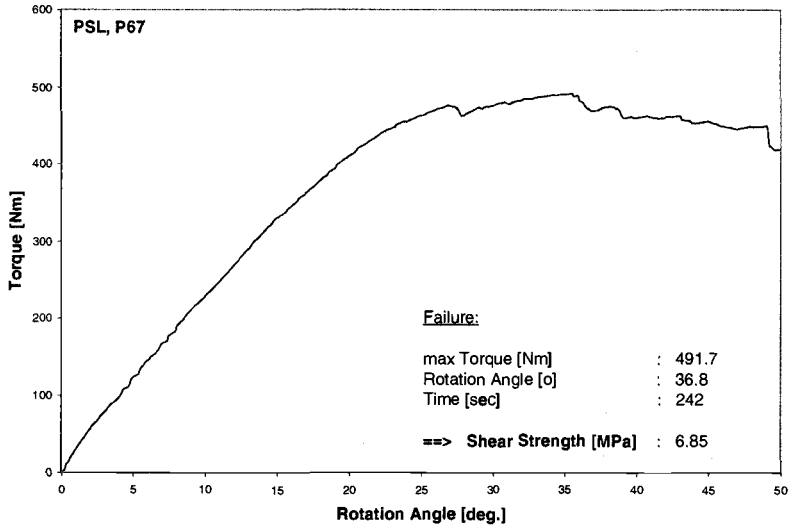
PSL, P67
Torque [Nm]
Rotation Angle [deg.]
Failure:
max Torque [Nm] : 491.7
Rotation Angle [o] : 36.8
Time [sec] : 242
==> Shear Strength [MPa] : 6.85

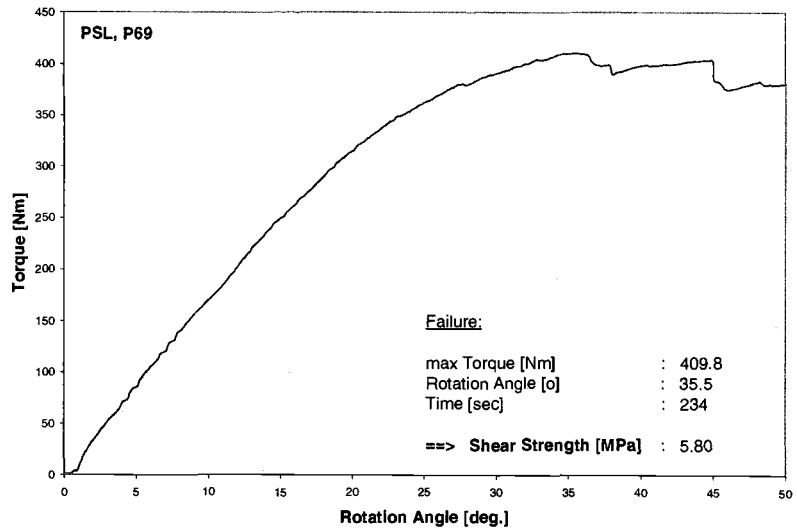
PSL, P69
Torque [Nm]
Rotation Angle [deg.]
Failure:
max Torque [Nm] : 409.8
Rotation Angle [o] : 35.5
Time [sec] : 234
==> Shear Strength [MPa] : 5.80

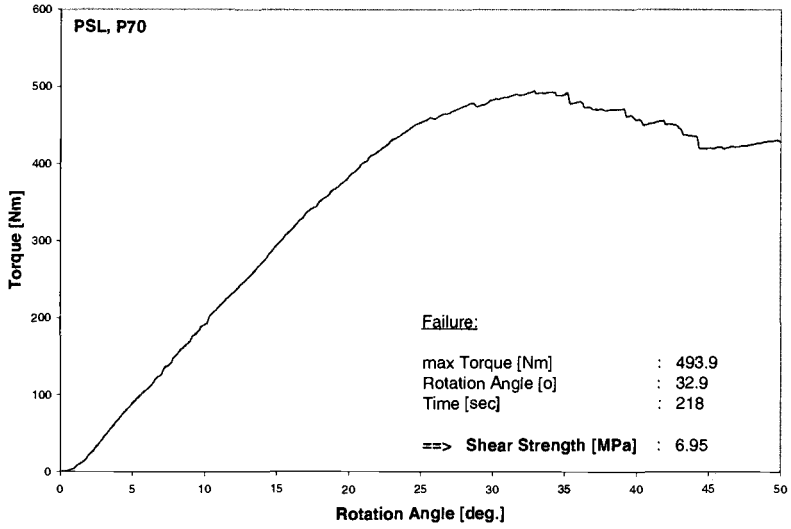
PSL, P70
Torque [Nm]
Rotation Angle [deg.]
Failure:
max Torque [Nm] : 493.9
Rotation Angle [o] : 32.9
Time [sec] : 218
==> Shear Strength [MPa] : 6.95

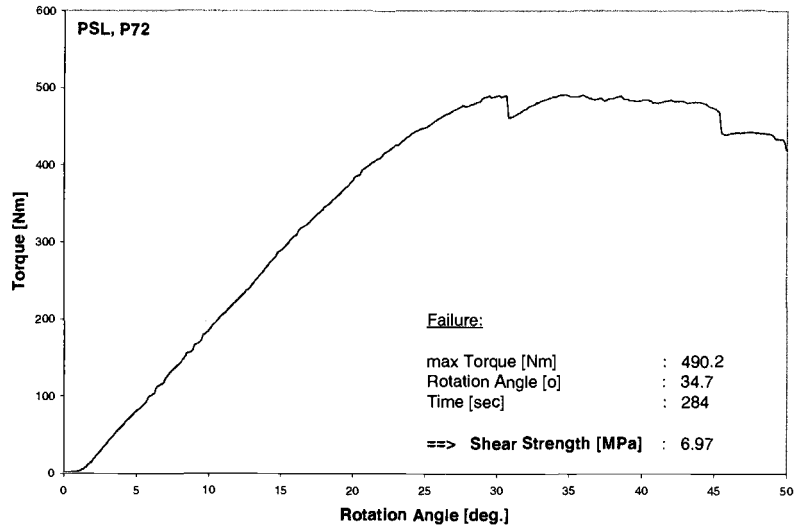
PSL, P72
Torque [Nm]
Rotation Angle [deg.]
Failure:
max Torque [Nm] : 490.2
Rotation Angle [o] : 34.7
Time [sec] : 284
==> Shear Strength [MPa] : 6.97

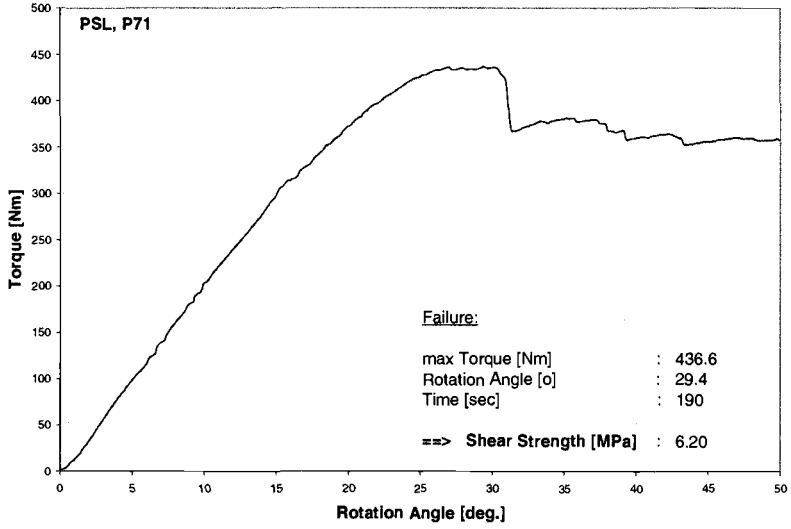
PSL, P71
Torque [Nm]
Rotation Angle [deg.]
Failure:
max Torque [Nm] : 436.6
Rotation Angle [o] : 29.4
Time [sec] : 190
==> Shear Strength [MPa] : 6.20

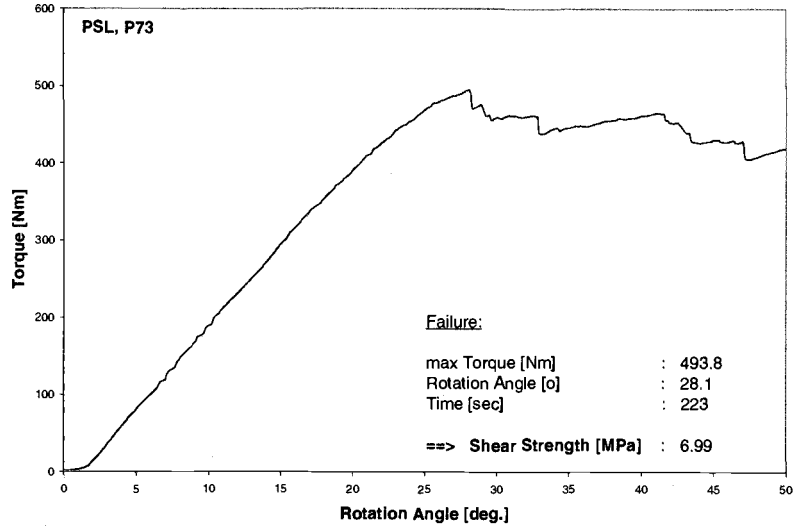
PSL, P73
Torque [Nm]
Rotation Angle [deg.]
Failure:
max Torque [Nm] : 493.8
Rotation Angle [o] : 28.1
Time [sec] : 223
==> Shear Strength [MPa] : 6.99

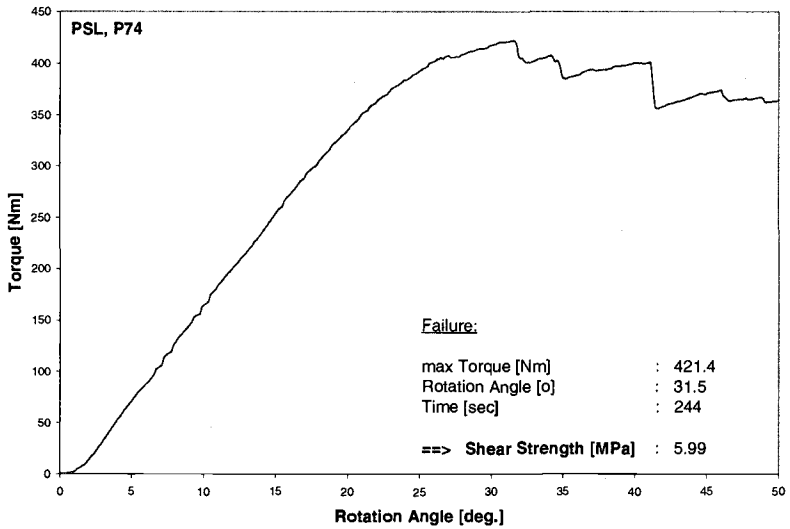
PSL, P74
Torque [Nm]
Rotation Angle [deg.]
Failure:
max Torque [Nm] : 421.4
Rotation Angle [o] : 31.5
Time [sec] : 244
==> Shear Strength [MPa] : 5.99

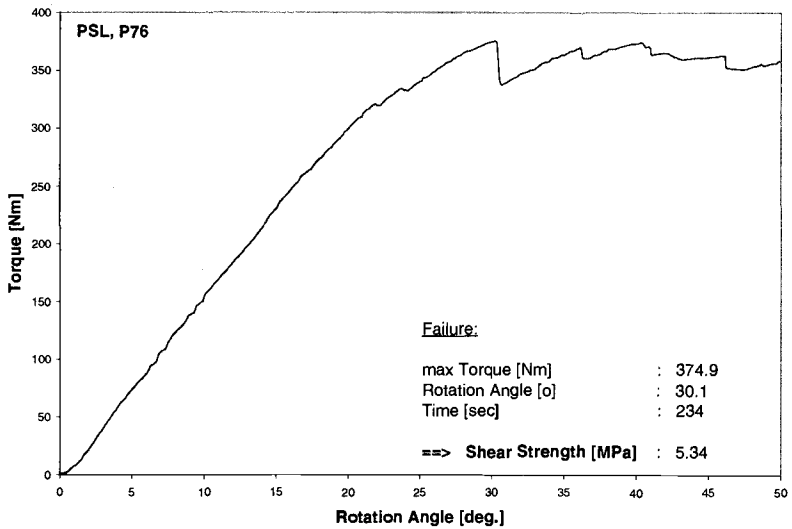
PSL, P76
Torque [Nm]
Rotation Angle [deg.]
Failure:
max Torque [Nm] : 374.9
Rotation Angle [o] : 30.1
Time [sec] : 234
==> Shear Strength [MPa] : 5.34

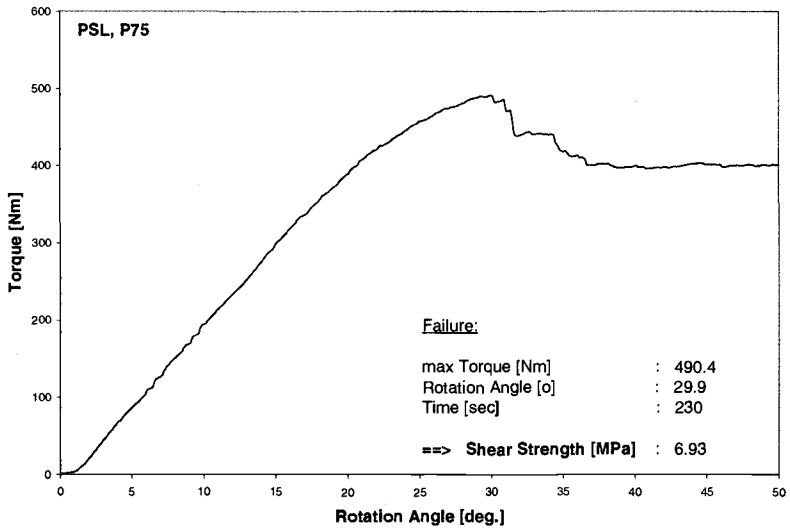
PSL, P75
Torque [Nm]
Rotation Angle [deg.]
Failure:
max Torque [Nm] : 490.4
Rotation Angle [o] : 29.9
Time [sec] : 230
==> Shear Strength [MPa] : 6.93

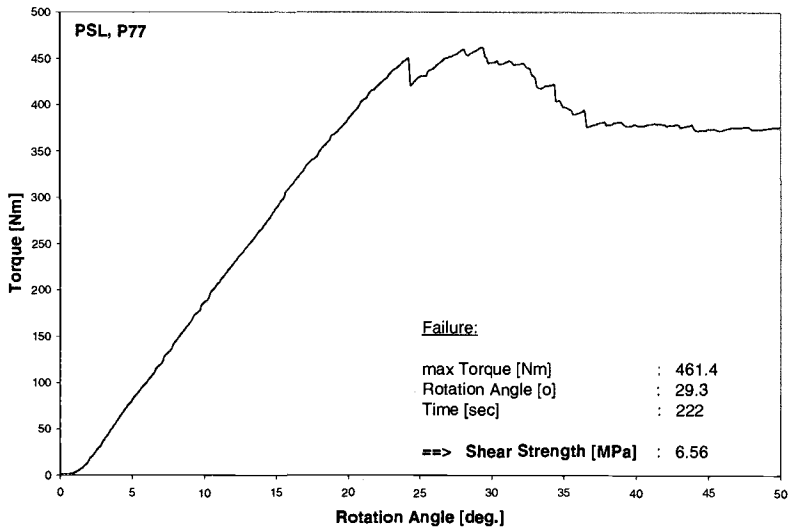
PSL, P77
Torque [Nm]
Rotation Angle [deg.]
Failure:
max Torque [Nm] : 461.4
Rotation Angle [o] : 29.3
Time [sec] : 222
==> Shear Strength [MPa] : 6.56

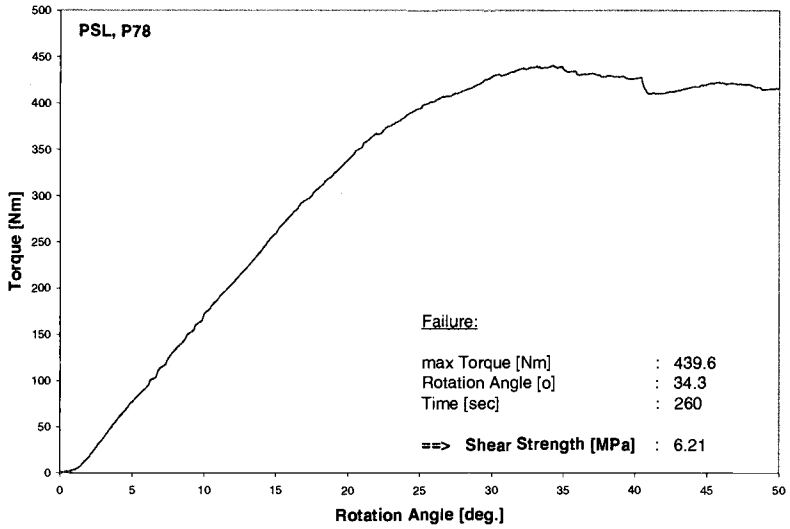
PSL, P78
Torque [Nm]
Rotation Angle [deg.]
Failure:
max Torque [Nm] : 439.6
Rotation Angle [o] : 34.3
Time [sec] : 260
==> Shear Strength [MPa] : 6.21

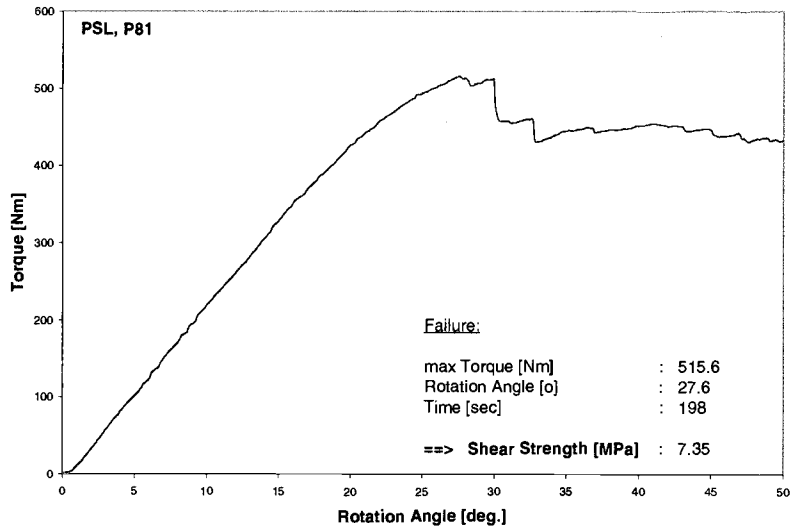
PSL, P81
Torque [Nm]
Rotation Angle [deg.]
Failure:
max Torque [Nm] : 515.6
Rotation Angle [o] : 27.6
Time [sec] : 198
==> Shear Strength [MPa] : 7.35

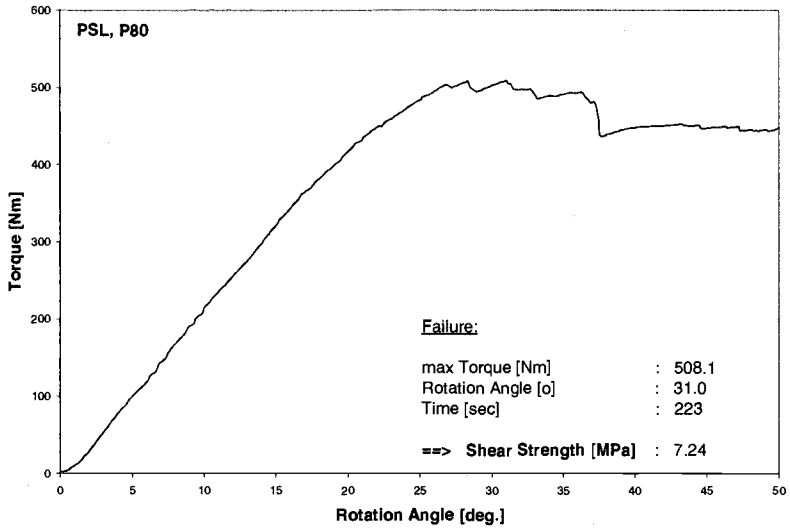
PSL, P80
Torque [Nm]
Rotation Angle [deg.]
Failure:
max Torque [Nm] : 508.1
Rotation Angle [o] : 31.0
Time [sec] : 223
==> Shear Strength [MPa] : 7.24

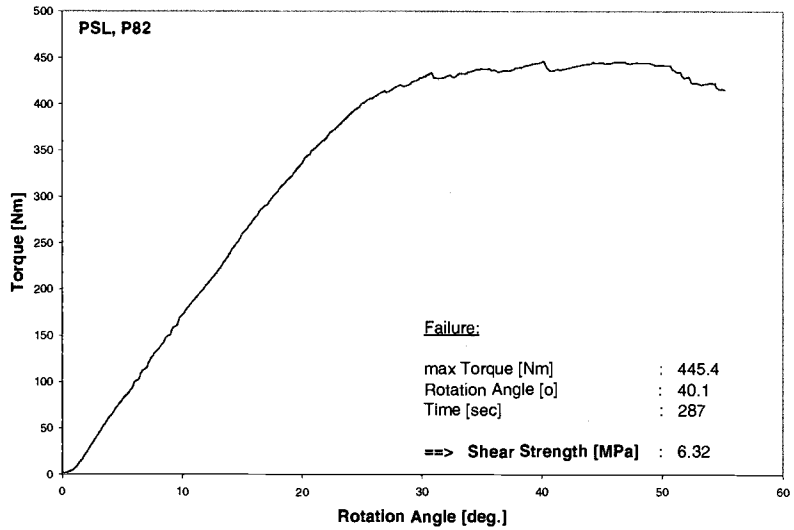
PSL, P82
Torque [Nm]
Rotation Angle [deg.]
Failure:
max Torque [Nm] : 445.4
Rotation Angle [o] : 40.1
Time [sec] : 287
==> Shear Strength [MPa] : 6.32

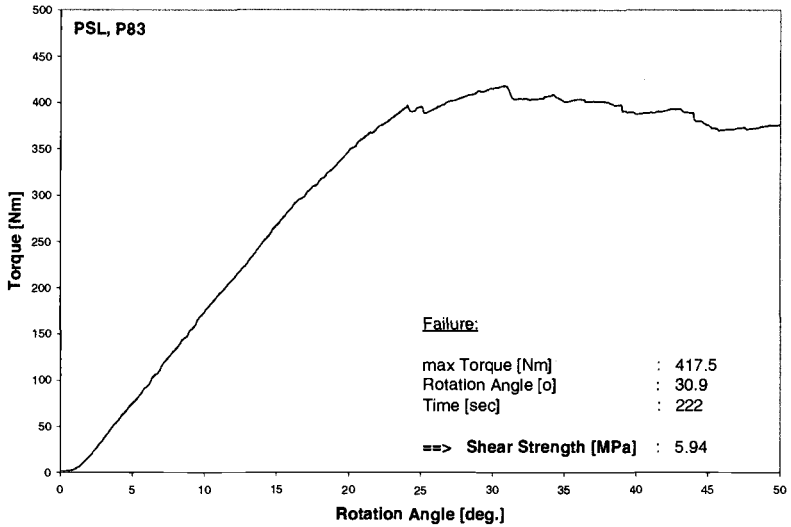
PSL, P83
Torque [Nm]
Rotation Angle [deg.]
Failure:
max Torque [Nm] : 417.5
Rotation Angle [o] : 30.9
Time [sec] : 222
==> Shear Strength [MPa] : 5.94

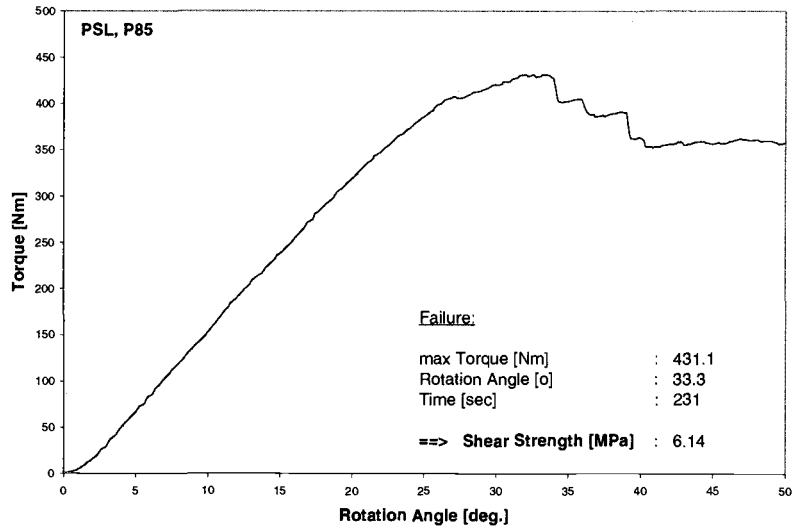
PSL, P85
Torque [Nm]
Rotation Angle [deg.]
Failure:
max Torque [Nm] : 431.1
Rotation Angle [o] : 33.3
Time [sec] : 231
==> Shear Strength [MPa] : 6.14

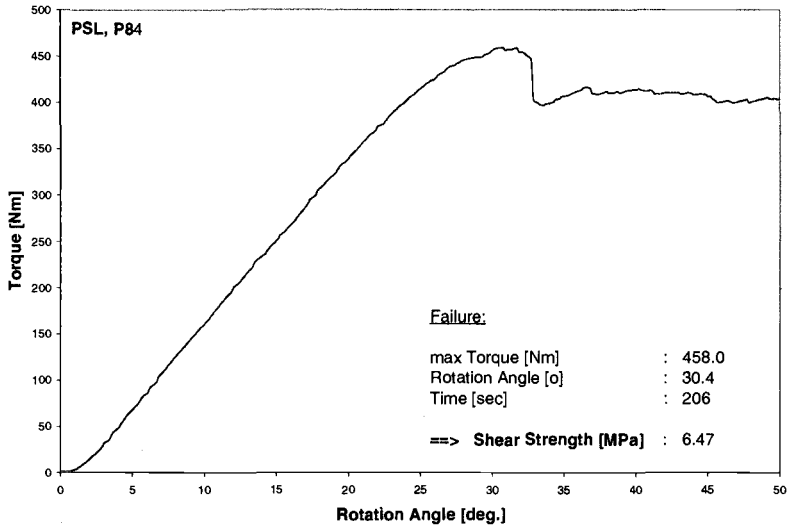
PSL, P84
Torque [Nm]
Rotation Angle [deg.]
Failure:
max Torque [Nm] : 458.0
Rotation Angle [o] : 30.4
Time [sec] : 206
==> Shear Strength [MPa] : 6.47

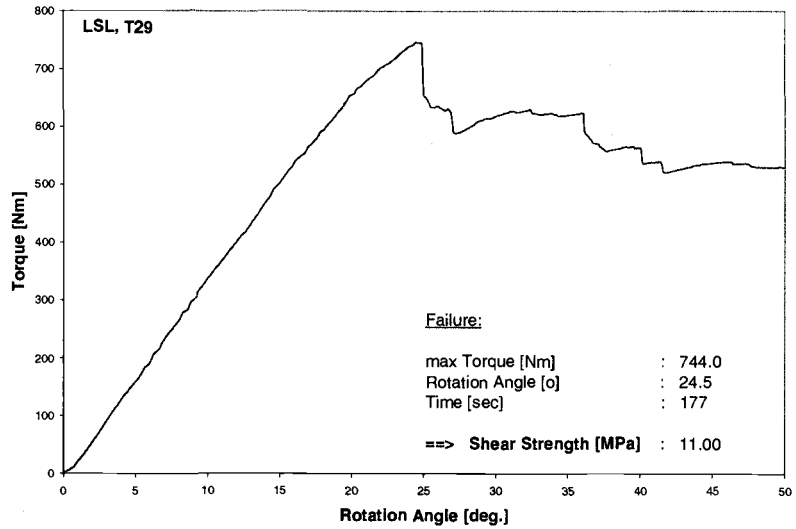
LSL, T29
Torque [Nm]
Rotation Angle [deg.]
Failure:
max Torque [Nm] : 744.0
Rotation Angle [o] : 24.5
Time [sec] : 177
==> Shear Strength [MPa] : 11.00